UCL SCHOOL OF PHARMACY
BRUNSWICK SQUARE

The application of 3D-printing in batch and flow chemistry for the synthesis of heterocycles

Zenobia X Rao

Supervisor: Dr. Stephen Hilton

April 2019

This research project is submitted in part fulfilment of the requirements for the PhD degree, UCL School of Pharmacy

Department of Pharmaceutical and Biological Chemistry

Abstract

The work described in this thesis focusses on 3D-printing as a novel technology and its use in both batch and flow chemistry. As such, fused deposition modelling and stereolithography printing were explored for their ability to affect organic synthesis. Initially, FDM printed column reactors for flow chemistry were developed and their scope in simple S_NAr chemistry explored. This work was further expanded into the synthesis of quinoxalinones, wherein a two-step flow sequence using this S_NAr step and an intramolecular acylal cyclisation step was able to generate the core structure in a single process from amino acids and environmentally benign solvents.

The next phase of the project focussed on the development of devices for batch chemistry using SLA printing. A catalytic stirrer bead device that would improve the efficiency of batch reactions was developed. The initial formulation incorporated tosic acid and these stirrer bead devices were used in the synthesis of Hantzsch dihydropyridines. This formulation was then further improved so as to make it chemically inert and palladium(0) tetrakis(triphenylphosphine) containing devices were prepared. Their scope was explored through their use in Suzuki couplings under both thermal and microwave conditions. A third catalytic stirrer bead device containing yttrium triflate was also developed and its use in the protection of carbonyl groups in aldehydes with thiols was investigated using microwave conditions.

In the last phase of the project, an SLA printed circular disc reactor was designed and fabricated using this new inert formulation. Its use in flow photochemistry has been explored shortly though C-H functionalisation chemistry and its limits have been explored. Last of all, the decarboxylation reaction in a synthetic sequence for Praziquantel was studied. It was found that a flow photo-decarboxylation using these newly developed reactors would be sufficient to carry out this key step in the synthetic sequence. The thesis closes with a description of the experimental conditions and full detail of the compounds produced in this thesis.

Impact Statement

This present thesis is concerned with the synergistic combination of chemical synthesis and 3D-printing with an emphasis on its linking up with continuous flow synthesis. As such, this is a novel area, but is rapidly growing in importance. The ability to combine the low-cost and unique structural architectures that can be created with 3D-printing with chemical synthesis, mean that this research described in this thesis is of particular high impact.

In this thesis, I have designed and developed various reactors made from inert printable materials that could potentially be used in external laboratories (both pharmaceutical and academic) that have access to continuous flow equipment. These reactors are also easily modifiable so as to suit the end user. The development of catalytically active stirrer beads can, as such, also be used in research laboratories ranging from teaching levels for graduate and undergraduate students to demonstrate simple chemistry, or at a higher level (pharmaceutical and academic) where similar reactions produce greater structural complexity in the final products.

The stirrer beads that were developed as part of my PhD have been evaluated by a range of pharmaceutical companies worldwide and these are currently under development for market realisation.

The work in this thesis has resulted in three publications so far with a further three in preparation.

Acknowledgements

To my parents, who have not only shaped me to be the person that I am today but also supported me throughout these years, I humbly thank you. None of this would be possible if it weren't for you. A very special thanks goes out to my supervisor Dr. Stephen Hilton who has guided me through the course of this PhD and allowed me to reach my true potential- Steve, I am forever grateful!

I would like to thank my old colleagues Bhaven, Bruno, Marta, Alessandra and Raiza for I have learnt so much from each one of you. Matthew, a special thanks goes out to you for putting up with my silly questions and for taking the time and effort with everything that you do. I couldn't have asked for a better postdoc and am very greatful. To all my other lab colleagues, Ash, Zi, Ben, Queenie, Marpin and Rumintha, thank you for making what has to be the best team of students anyone has the pleasure to work with! To Zaid, for all his tech support during the formatting of this thesis- I owe you one!

I would like to thank all the staff of the School of Pharmacy especially Dr. Colin James for his assistance with using the NMR facility. To my old school teacher Mrs. Pratibha Shettigar, this journey began many years ago when you introduced me to the field of science. I cannot thank you more! To Dr. Hamied, for his support throughout this PhD, you have been truly inspirational. To all my other friends and family who have been vital in making these years wonderful Zubin, Lauren, Nilza, Javi and Rom I thank you so much.

Last but certainly not least, to my late grandparents, I dedicate this thesis to you.

Plagiarism Statement

I, Zenobia Rao, hereby confirm that the work submitted in the thesis is my own. Any ideas submitted in this thesis are my own. Any ideas, quotations, and paraphrasing from other peoples work and publications have been appropriately referenced. I have not violated the School of Pharmacy's policy on plagiarism.

Signature ..... Date .....

Abbreviations

°C	Degree Celcius
µL	Microlitre
µM	Micrometer
3D	Three Dimensional
ABS	Acrylonitrile Butadiene Styrene
AFCT	Addition-Fragmentation Chain Transfer
AM	Additive Manufacturing
AMPA	α-Amino-3-hydroxy-5-methyl-4-isoxazolepropionic Acid
API	Active Pharmaceutical Ingredient
ATR	Attenuated Total Reflectance
BAPO	Phenyl*bis*(2,4,6-trimethylbenzoyl)phosphine Oxide
BBT	2,5-*Bis*-(5-*tert*-butyl-benzoxazole-2-yl)thiophene
BDMA	Benzyl *N*,*N'* Dimethyl Amine
BHT	Butylated Hydroxyl Toluene
BMSB	(1,4-*Bis*(2-dimethylstyryl)benzene
Bn	Benzyl
BOC	*tert*-Butoxycarbonyl
BPR	Back Pressure Regulator
br	Broad
Bu	Butyl

CAD	Computer Aided Design
Cat	Catalytic
CDVE	1,4-Cyclohexane Dimethanol Divinyl Ether
CHR	Circular Hotplate Reactor
CLIP	Continuous Liquid Interface Production
CSM	Catalytic Static Mixer
d	Doublet
Da	Damköhler Number
DAD	Diode Array Detector
DAS	Difunctional β-Allyl Sulfone
DAST	Diethylamoniosulfur trifluoride
DBU	1,8-Diazabicyclo[*5.4.0*]undec-7-ene
DCB	1,4-Dicyanoebenzene
DCC	*N*,*N'*-Dicyclohexylcarbodiimide
DCE	Dichloroethane
DCM	Dichloromethane
DDDS	*Bis*(4-chlorophenyl)disulfide
DGEBA	Bisphenol A Diglycidyl Ether
DHP	Dihydropyridine
DIEA	Diisopropylethylamine
DLP	Digital Light Processing
DLS	Dynamic Light Scattering

DMA	Dimethacrylate
DMAP	4-Dimethylaminopyridine
DMC	Dimethyl carbonate
DMD	Digital Micromirror Device
DMF	Dimethylformamide
DMF	*N,N*-Dimethylformamide
DMLS	Direct Metal Laser Sintering
DMSO	Dimethylsulfoxide
DOD	Drop On Demand
DPDGA	Dipropylene Glycol Diacrylate
DSPR	Designed Porous Structure Reactor
EBM	Electron Beam Melting
ECC	3,4-Epoxycyclohexylmethyl-3,4-epoxycyclohexanecarboxylate
EDMA	2-Ethyl-9,10-dimethoxy Anthracene
ee	Enantiomeric Excess
equiv.	Equivalent
ESI	Electrospray Ionisation
Et	Ethyl
EtOAc	Ethyl Acetate
FDM	Fused Deposition Modelling
FEP	Fluorinated Ethylene Polymer
FFF	Fused Filament Fabrication

FOSS	Free and Open-Source Software
g	Grammes
GABA	Gamma-aminobutyric Acid
h	Hours
HIPS	High Impact Polystyrene
HIV	Human Immunodeficiency Virus
HPLC	High Performance Liquid Chromatography
HSV	Herpes Simplex Virus
IAC	Intramolecular Acylal Cyclisation
ID	Internal Diameter
IPA	Isopropyl Alcohol
IR	Infrared Spectroscopy
LED	Liquid Crystal Display
M	Molar
m	Multiplet
m/z	Mass to charge ratio
MAS	Monofunctional β-Allyl Sulfone
MBE	2-Methyl-3-buten-2-ol
MBHA	*p*-Methylbenzhydrylamine
MBY	2-Methyl-3-butyn-2-ol
Me	Methyl
MEHQ	Methoxy Hydroquinone

mg	Milligrammes
MHz	Mega Hertz
mL	Millilitre
mmol	Millimoles
MOF	Metal Organic Framework
mp	Melting Point
MRI	Magnetic Resonance Imaging
MW	Microwave Irradiation
NCS	*N*-Chlorosuccinimide
NMP	*N*-Methyl-2-pyrrolidone
NMR	Nuclear Magnetic Resonance
NSI	Nanospray Ionisation
p	Pressure
PBN	Prussian Blue Nanoparticles
PEEK	Polyether Ether Ketone
PEG	Poly(ethylene) Glycol
PEGDA	Poly(ethylene glycol) Diacrylate
PET	Polyethylene Terephthalate
PETA	Pentaerythriol Tetraacrylate
PETG	Polyethylene Terephthalate Glycol
PFA	Perfluoroalkoxy Alkane
Ph	Phenyl

PLA	Polylactic Acid
PMP	*p*-Methoxyphenyl
PP	Polypropelene
ppm	Parts Per Million
PTFE	Polytetrafluoroethylene
PVA	Polyvinyl Alcohol
PVC	Polyvinyl Chloride
q	Quartet
quin	Quintet
RBF	Round Bottom Flask
RD	Reactor Design
Re	Reynolds Number
RT	Reverse Transcriptase
rt	Room temperature
s	Singlet
SAR	Structure Activity Relationship
SB	Stirrer Bead
SLA	Stereolithography
SLM	Selective Laser Melting
SLS	Selective Laser Sintering
S_NAr	Substitution Nucleophilic Aromatic
SST	Stainless Steel

STL	Standard Tessellation Language
t	Tertiary
t	Triplet
TBAA	Tetrabutylammonium Acetate
TES	Triethylsilane
THF	Tetrahydrofuran
TLC	Thin Layer Chromatography
TPO	2,4,6-Trimethylbenzoyl Diphenylphosphine Oxide
TTVE	Trimethyloyl Propane Trivinyl Ether
UV	Ultra violet
VSE	Vinyl Sulfone Ester
W	Watt

List of Schemes

List of Figures

List of Tables

List of Graphs

Contents

1.0 Introduction

1.1 General Introduction

The work presented in this thesis is concerned with two emerging technologies that are and will impact chemical synthesis, namely 3D-printing and continuous flow synthesis. In order to better understand the applications of such techniques in organic synthesis, the introduction has been divided into four parts. The first section gives an account of the parameters related to continuous flow chemistry with regards to the equipment used, key components of such equipment and the justification and advantages of reactions performed using this technique. The second part explains the use of 3D-printing as an emerging technology and gives a broader outlook on the various methods that fall under this method of fabrication. The third section describes previous approaches where 3D-printing is used in organic synthesis and focusses on catalysis, the design of reactors for batch chemistry and flow chemistry. To conclude the introduction, the importance of certain heterocyclic targets that have been synthesised in this thesis are also described so as to highlight the relevance of the techniques used in this research and their respective advantages.

1.2 Flow Chemistry

Flow chemistry has gained a significant amount of interest over the past decade and the various enabling technologies it comprises have given synthetic chemists a variety of tools to carry out their research in a streamlined and efficient manner. Peristaltic pumps, inert tubing, reactor modules and separating channels replace round bottom flasks, reflux condensers and closed vessels in modern day continuous flow methodologies. The complexity and diversity of equipment plays an important role in the ability to carry out the necessary transformation reactions required. There are now commercially available flow systems such as Uniqsis FlowSyn, Vapourtec R-Series and E-Series, Syrris Asia, FutureChemistry FlowStart Evo, Chemitrix Labtrix, Accendo Propel, Advion NanoTek, ThalesNano H-Cube Pro, Sigma-Aldrich Microreactor Explorer, etc., a few of which have been shown below (**Figure 1**).

Figure 1: Types of flow system machines available on the market shown from left to right: Uniqsis FlowSyn [1], Vapourtec R-Series [2], Syrris Asia [3].

A simple representation of how reactors work in flow is shown below (**Scheme 1**). Stock solutions of reagents (A and B) are made to pass through pumps or injected into their respective sample loops. Flow rates are determined prior to starting the experiment based on the stoichiometry required in the reaction. The solutions meet (commonly at a T-piece junction) and the combined flow passes through a reactor unit. This can either be a chip reactor, a coil reactor, a column reactor with a flow path built inside it or a packed bed reactor. Streams exiting this unit can be further reacted or quenched, or by-products scavenged by using columns or cartridges fitted with solid-supported reagents (with immobilized functional moieties) [4]. It is also possible to incorporate in line purification, reagent recycling, selective product capture and release, all of which help in minimising waste and manual handling of materials [5] [6]. The ability to incorporate in line data processing such as IR analysis and mass spectrometry gives real time structural information on reactions carried out in this manner and enables rapid optimisation of reaction conditions [7] [8] [9].

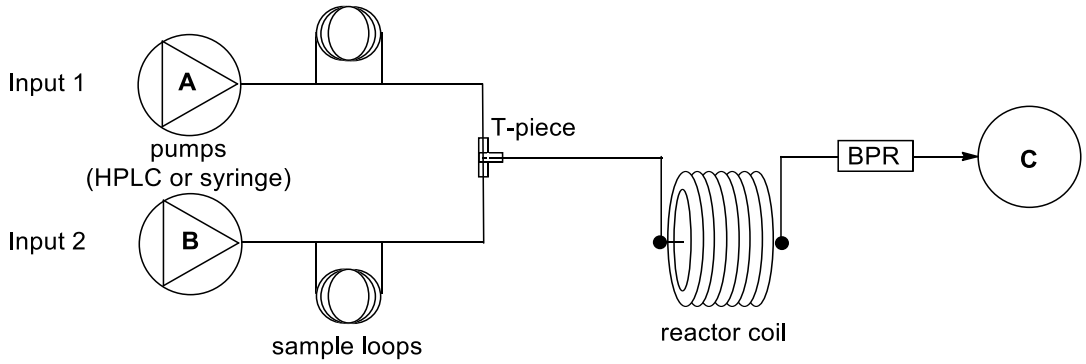

Scheme 1: Simple configuration of a flow reaction setup where reagents A and B give product C.

The parameters that affect flow chemistry are quite different to those related to batch synthesis. The size of the channels in the flow paths of reactors (10-500 µm i.d. ranging to several mm i.d.) and their ability to transfer heat; the relationship between residence time and flow rate; the relationship between flow rate, heat and pressure; all play an important role in the synthesis of compounds in continuous flow. The ability to work with reactive intermediates in flow owing to the small reaction volumes gives chemists the ability to explore the scope of such reactions in greater depth [10]. Functionalized polymers or inorganic supports such as scavengers and other solid supported reagents such as Merrifield-type azide monoliths (**Scheme 2**) can widen the applicability of flow reactors. This can be very advantageous in reaction planning. More importantly, flow and supported catalysis becomes possible as it can decrease wasteful isolation and purification procedures. This will be discussed in detail in the latter portion of this thesis (Page 123). Multicomponent reactions and multistep synthesis become more conceivable by connecting individual flow modules together. Photochemistry in flow is an altogether more promising alternative in industrial applications and the potential to scale up in flow too, becomes feasible [10].

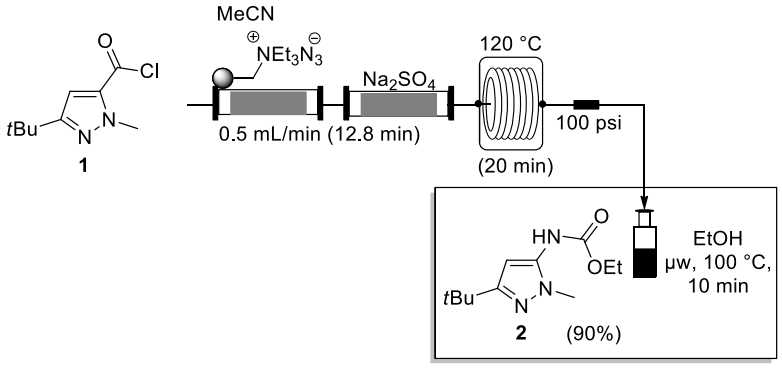

Scheme 2: Carbonyl isocyanate (**2**) prepared from acyl chloride (**1**) using Merrifield-type azide monoliths [11].

Flow chemistry is widely applied and used in the petrochemical and food processing industries. However, the pharmaceutical industry is still dominated by batch processes, but there is an ever growing interest from 'big pharma' to switch to flow as it offers the possibility to keep production high and costs low and numerous companies are investigating new techniques to scale up

syntheses in both research and production scale synthesis [12] [13]. API's such as efaproxiral **3** a small molecule with radiosensitising activity and rimonabant **4**, a anorectic antiobesity drug are some of the early molecules that were synthesised in flow [14]. The antimalarial drug artemisinin **6** was also synthesised in the same manner using a continuous flow route [15]. The crucial step in this sequence was the generation of a singlet oxygen ($^1O_2$) species *in situ*. This was achieved photochemically by wrapping the fluorinated ethylene propylene (FEP) tubing around the light source. This key step in the process was perfectly suited for a flow-based approach as the technique is safer, procedurally simpler and the reaction by-product ($^1O_2$) could be easily contained in the system within the tubes making it further available for its incorporation into the structure of the final molecule [15] [16]. Complex molecules such as the anti-cancer drug Imatinib **5** or Gleevec, were synthesised by utilising tubular flow coils packed with scavengers and reagents in a sequential manner [5]. This is another unique property that can be attributed to flow to allow for cleaner product formation. Simpler small molecules such as ibuprofen **7** have also been synthesised using a three-step flow based approach [17] [18] [19]. This work comprised of a Friedel-Crafts acylation, followed by an 1,2-aryl migration and finally a hydrolysis or saponification step all conducted in a series of flow reactors. This afforded the product in 51% yield over three steps in only ten minutes.

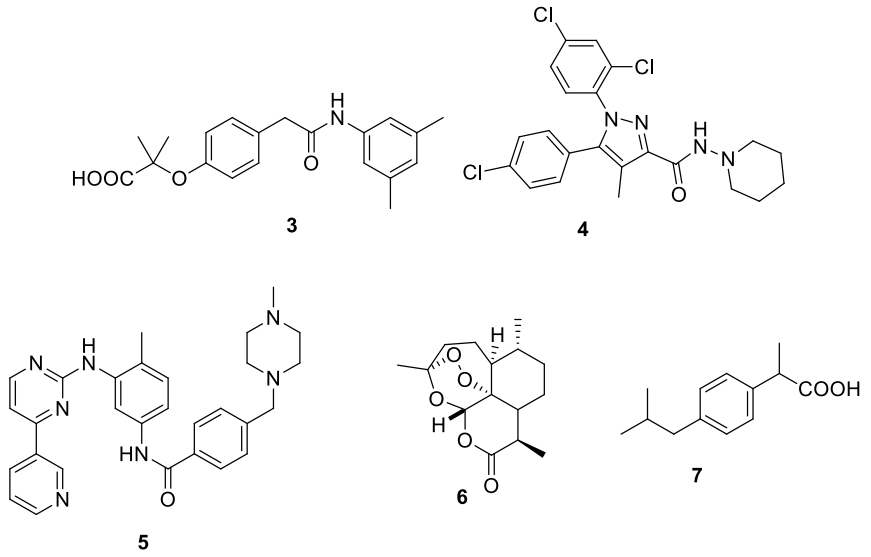

Figure 2: API's synthesised in flow.

1.2.1 Batch v/s Flow

The use of standardised glassware in synthetic chemistry has remained fundamentally unchanged since the 1800's. A picture of a reactor in 1900 is largely similar to that carried out in 2018, with the exception of an internal magnetic follower for mixing. Chemists have been using consistent techniques to carry out crucial reaction steps and post reaction work-up protocols for centuries. The practice of using round bottom flasks, condensors, pear shaped flasks, measuring cylinders, filter funnels, etc. remain the essential toolkit of a traditional chemist. Pharmaceutical and special purpose industries still use these very same techniques due to their robustness and versatility. However, the switch in the fundamental thought process with regards to the technical requirements of a flow system when compared to batch synthesis is what merges both chemistry and engineering. This ability to continuously 'manufacture' a desired module by designing its individual reaction steps into the flow protocol not only minimises waste, but also reduces costs. The low level of handling owing to the use of fully automated equipment makes the overall process far more streamlined.

The diagram below shows the flow path suitability of a reaction to be carried out in flow. It illustrates the key factors to consider when deciding to switch to a continuous method.

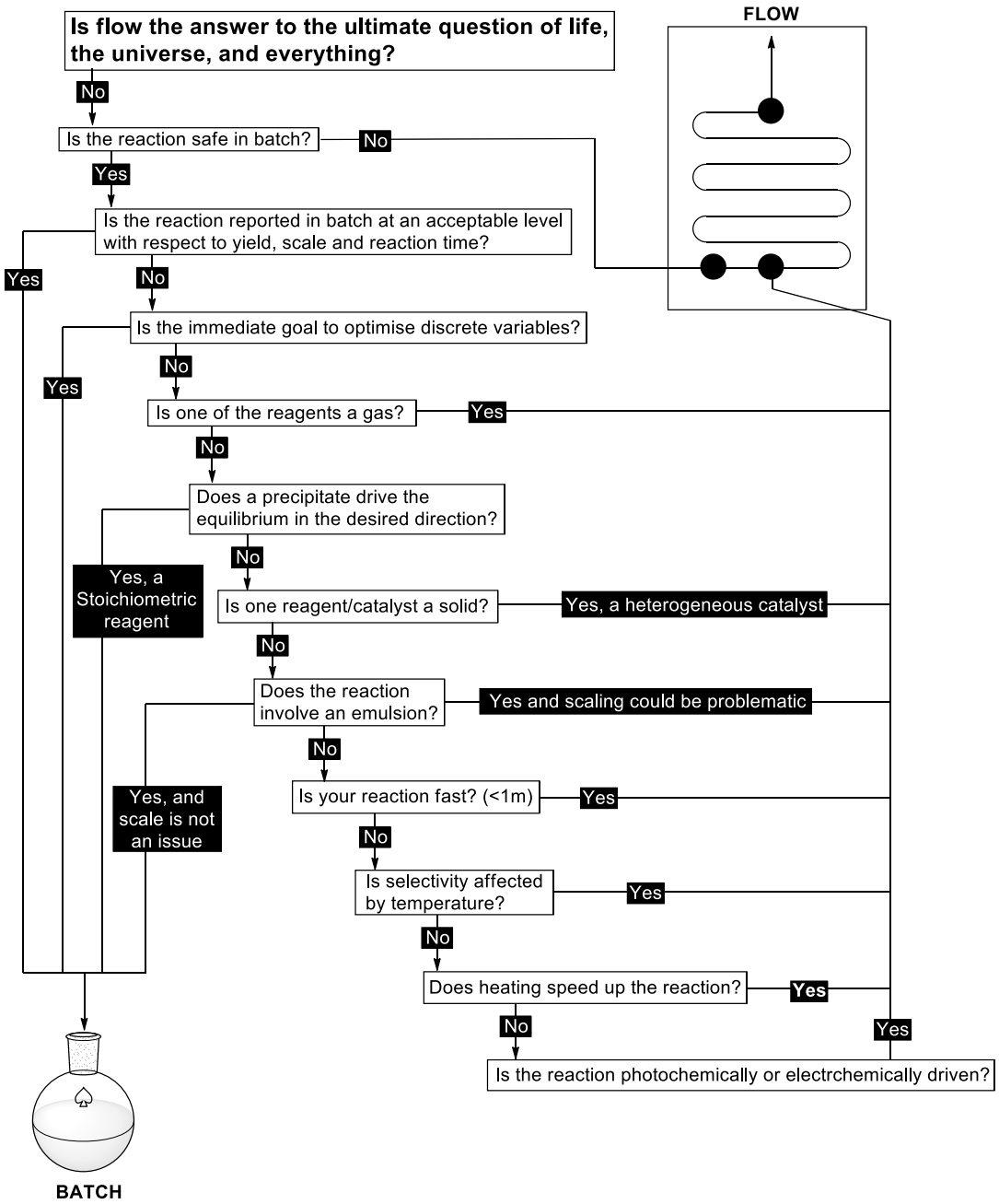

Figure 3: Adapted from decision diagram for flow chemistry [20].

1.2.2 Why run a reaction in flow?

- **Multiphasic Systems**

If a reaction uses a multiphasic system (gas-liquid, solid-liquid or liquid-liquid) then, switching to flow could prove beneficial [20]. Effective phase mixing is essential in such reactions and this is better achieved in flow when compared to batch. Microfluidic systems offer higher surface area to volume ratios which give rise to different types of flow patterns i.e. bubble flow, slug flow and annular flow in gas-liquid biphasic systems as shown below (**Figure 4**).

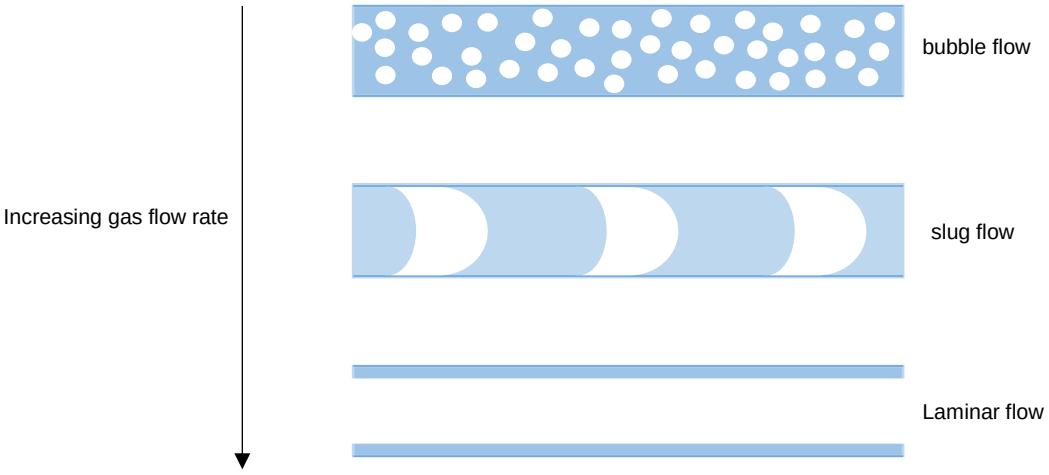

Figure 4: Change in flow patterns for gasses when the liquid flow rate is constant in gas-liquid biphasic systems.

In solid-liquid systems packed bed reactors restrict particle movement and the flow of liquid is termed as plug flow. However, this can be made turbulent when the particles are free flowing as in a fluidized bed reactor. These systems are however not used largely as they are still not entirely understood [21]. Mixed bed systems offer properties of both packed and fluidized beds. When dealing with liquid-liquid systems, flow patterns such as laminar flow and slug flow are observed (**Figure 5**).

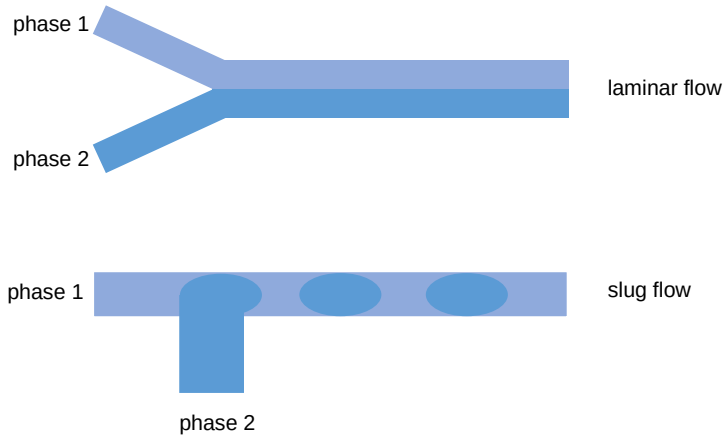

Figure 5: Change in flow patterns seen in liquid-liquid immiscible biphasic systems.

- **Mixing**

Mixing plays an important role in the transformations of molecules in reactions as well as in selectivity. Reynolds number (*Re*) can be used to predict flow patterns and can divide mixing into three categories: laminar, transitional and turbulent. Laminar flow is a consequence of parallel streams of liquids not interrupting each other's longitudinal flow. When flow rates are low, the two immiscible liquids are viscous and the channel size is large, the Reynolds number is usually low (<2300) and this results in laminar flow. High flow rates and high *Re* (>4000) usually results in turbulent flow. Transitional flow is a combination of the two with an *Re* between 2300 and 4000 and usually consists of more turbulent mixing towards the centre of the flow path while mixing towards the edges remains slow. While considering mixing in batch reactors, flow is usually laminar or transitional [22]. Another concept to consider while discussing mixing is the Damköhler number (*Da*). This is a dimensionless number, which is the ratio of the rate of the reaction to the rate of mass transfer by diffusion. This becomes important when there are competitive side reactions alongside product formation. In other words, when *Da*<1, mixing is complete before product formation, giving a cleaner reaction. When *Da*>1 less homogeneity in the reaction solutions is observed, and the overall reaction tends to be less clean due to concentration gradients that build up in parts of the reactor.

- **Temperature control**

Efficient heat transfer is a key characteristic that has to be considered while designing a procedure to be adapted in flow reactors. “Runway” reactions are those where the heat generated from the reaction increases the overall temperature medium further increasing the rate of the reaction. Such exothermic reactions can be dangerous when performed in batch, with hazards such as increased side product formation, rapid boiling of solvents and even explosions when the energy in the system cannot be contained appropriately. Performing such reactions in flow permits a more efficient heat transfer due to the narrow size of the channels in which the reaction takes place. There is also a crucial dependence between temperature and pressure in flow reactions. According to Arrhenius’ rate law the reaction rate exponentially increases as the absolute temperature is increased. The ability to change these conditions quite easily by adjusting the flowrates and the back pressure regulators means that reactions can be heated to greater than the boiling points of their respective solvents and this leads to an increase in the rate of the reaction. This also reduces the time that the reaction requires. A classic example of this is seen below in the one pot hydrolysis of 6-aminocapronitrile **8** to give ε-caprolactam **9** where the reaction was heated at 400 °C in super critical water, clearly illustrating the potential of continuous flow in the synthesis of **9** (**Scheme 3**) [23].

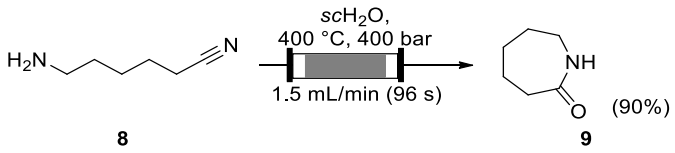

Scheme 3: Flow synthesis of ε-caprolactam **9** under supercritical conditions.

The use of microwave irradiation (MW) in combination with flow is another excellent combination of the two reaction enabling technologies. It proves highly beneficial to overcome the problems associated with dual phase systems as the microwave irradiation can penetrate the centre of the reactor and heat the entirety of the reaction. This is greatly important when dealing with large scale processes as the possibility to conduct microwave synthesis in batch on such scales is very unsafe and is rarely adopted. Specially made

coils are used in microwave setups to carry out flow reactions covering a range of chemistries (S_NAr, esterification's and Suzuki-couplings) [24]. Another example showcasing the technique comes from the work carried out by Shieh wherein they have shown a less toxic way to methylate phenols using such irradiation (**Scheme 4**) [25]. By using a combination of dimethyl carbonate (DMC) and 1,8-diazabicyclo[5.4.0]undec-7-ene (DBU) in an ETHOS continuous-flow microwave reactor, they were able to significantly reduce the time taken to synthesize 1,3,5-trichloro-2-methoxybenzene **11** from 192 hours (thermal conditions) to 54 minutes.

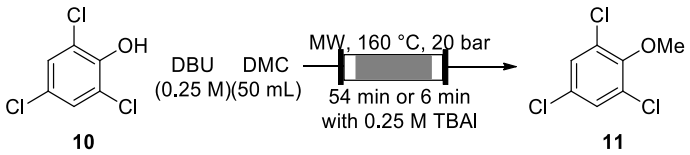

Scheme 4: *O*-Methylation of 2,4,6-trichlorophenol **10** with DMC and DBU using a continuous-flow microwave reactor.

- **Photochemistry**

Photochemistry offers a great advantage over heated reactions due to the ability to control the exact energy input in the reaction medium. While irradiating a reaction mixture in flow, only a small volume at any given time is being exposed to the light source, keeping the bulk of the material away from it. The light exposure can be easily controlled by the flow rate. This is very beneficial when dealing with flammable solvents, as their potential to reach the ignition point is drastically reduced. Immersion well reactors fitted with high-pressure mercury lamps, xenon lamps or halogen lamps are usually employed to carry out such reactions in batch. Due to the large amount of heat produced in using such systems, cooling jackets are additionally fitted to dissipate any extra heat generated within the system. Again, with regards to scale up this process becomes more unsafe as larger lamps would be required to be immersed into even larger vessels containing reaction solutions further complicating the safe handling of such equipment. By wrapping tubing directly over lamps or placing multiple microreactors directly in front of the light source, these problems are automatically eliminated. This has been elegantly displayed by Fukuyama *et al.* in their work on [2+2] cycloaddition reactions

between cyclohex-2-enone **12** and vinyl acetate **13** in a glass microreactor and a 300 W Hg lamp (**Scheme 5**) [26].

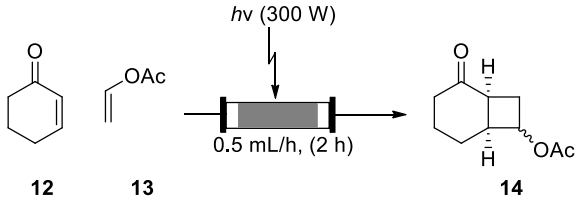

Scheme 5: Photochemical [2+2] cycloaddition under flow conditions to synthesize (1*S*,6*S*)-2-oxobicyclo[4.2.0]octan-7-yl acetate **14**.

Large volumes of very low concentration solutions can be continuously handled in flow. This is advantageous when competitive side reactions are a factor to consider in the chemistry. A single continuous flow device can process substrates from a few milligrams up to nearly kilogram quantities daily. When using microreactors with very narrow path diameters (>0.5 i.d.), high concentration solutions can be very effectively irradiated. Continuous evaporation techniques can be incorporated and solvents can be recycled. This altogether reduces costs and waste [27] . The biggest problem with photochemistry reaction setup is that the solution has to be very dilute in order for the light to penetrate throughout the entire reaction. This is where flow chemistry offers an obvious advantage.

1.2.3 Green Chemistry and Flow Reactors

With a view to develop cleaner and 'greener' techniques in the chemical industry in order to reduce waste, the chemical sector has been changing its approaches over the past decades to address the view by wider society of it being 'dirty' in its processes [28]. Anastas has clearly outlined many important principles of green chemistry that can be applied to flow techniques demonstrating their value [29].

- **Prevention of waste:** Quite obviously, this concept is relevant in our understanding, in that it is better to prevent waste than to clean up or treat systems after its formation. This can be achieved by using solvent-free systems although it hasn't been observed to a great extent in production scale batch synthesis due to poor thermal management and low safety profiles owing to uncontrolled reaction exotherms that can arise in such methods [30]. The potential to apply such systems to continuous flow chemistry has been shown by Schwalbe in their use of steel micro-reactors giving the authors the advantage of precise thermal control in the Paal-Knorr reaction between 2,5-hexanedione **15** and ethanolamine **16** under solvent free conditions [31]. They identified that the formation of the substituted pyrrole **17** required optimized reactor conditions of a 5.1 minute reaction time at 65 °C affording 91% yield of the product (**Scheme 6**).

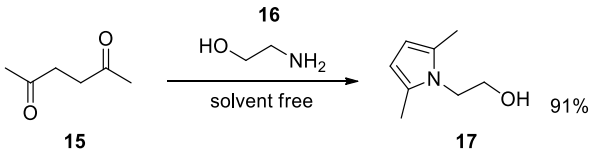

Scheme 6: Solvent free Paal-Knorr reaction between 2,5-hexanedione **15** and ethanolamine **16** using steel micro-reactors.

The ability to conduct hundreds of reactions in flow quite easily by rapidly changing reaction conditions when compared to batch during reaction optimisation processes results in reduced reagent consumption and waste production. It also increases the chemist's understanding of the process as reactions can be investigated in a more detailed manner and under more controlled conditions thereby allowing the user to consider their scale-up management [32].

- **Atom economy:** This concept measures waste production by assessing the percentage of the mass of reactants incorporated into the product. By precisely controlling the reaction conditions, flow chemistry offers the potential to reduce or even eliminate purification steps thereby increasing the purity of the reaction product. Atom economic reactions such as intramolecular re-arrangements have been performed as demonstrated by Kappe in their use of high temperature and pressure stainless steel tube reactors in flow to conduct the Claisen re-arrangement for the synthesis of 2-allylphenol **18** (**Scheme 7A**) [33]. Addition reactions also offer the potential to provide atom economy as seen in the Diels-Alder cycloaddition reaction between isoprene **19** and maleic anhydride **20** using a microflow disc reactor heated to 60 °C yielding the benzofuran dione derivative **21** in 98% (**Scheme 7B**) [34]. Asymmetric synthesis offers another means to increase the efficiency of a synthetic protocol by increasing the enantiomeric excess (*ee*) of the product and reducing the amount of the consumed substrate in forming the undesirable product [32]. This has been shown in a synthetic strategy towards (±)-fluoxetine adopted by Sanderson in the enantioselective reduction step on a ketone **22** to give the corresponding (*S*)-alcohol **23** using borane-*N*,*N*-diethylaniline and a chiral oxazaborolidine catalyst (**Scheme 7C**). The reaction was optimised when performed in a coil reactor at an increased concentration of 0.70 M and resulted in a 88% yield and 92% *ee* with a residence time of 10 minutes [35].

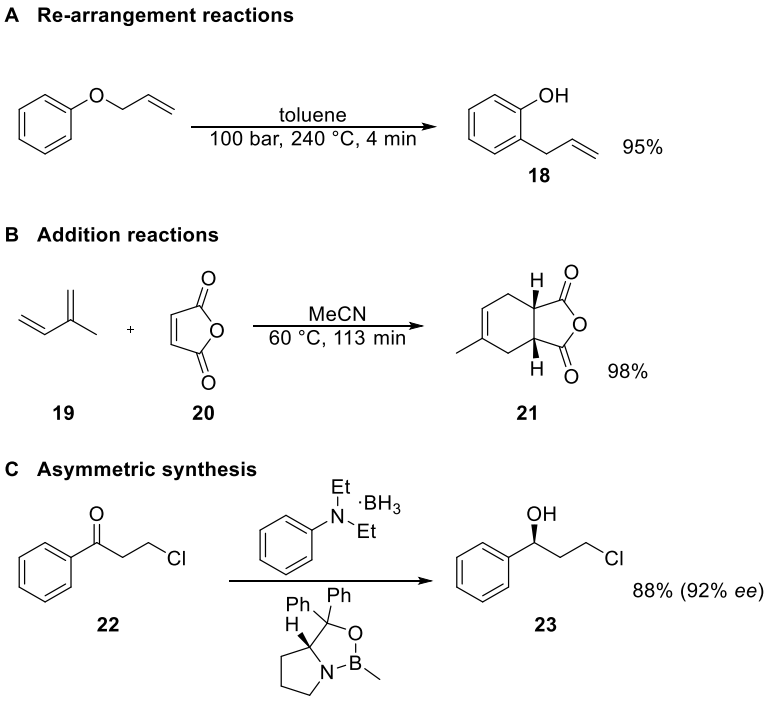

Scheme 7: A) Reactions showing good atom economy: Claisen re-arrangement for the synthesis of 2-allylphenol **18**; **B)**Diels-Alder cycloadditions for the synthesis of benzofuran dione derivative **21**; **C)** Enantioselective reduction of a ketone **22** using a oxazaborolidine catalyst.

- **Less hazardous syntheses and safer design:** Flow reaction technology has been attributed to higher yields and greater selectivity for the desired products. When this is used on a production level scale, the toxicity associated with the production of the final product is often minimised as the number of by-products and side reactions in previous steps have the potential to be lowered giving an overall less hazardous chemical route [32]. This can even be applied to the synthesis of chemicals, wherein the specific function of that chemical should be considered whilst designing its synthetic route. The toxicity profile must also be considered and efforts to minimise it wherever possible must be made.
- **Safer solvents and auxiliaries:** In large scale chemical processes, choosing the right solvent plays a huge part in the costs and safety of the procedure and can have a profound impact on the environment. The use of “green” solvents has therefore gained a lot of attention in the pharmaceutical industry to address these issues [36]. As seen in the earlier section of this thesis,

flow chemistry offers the potential to improve biphasic reactions by substantially increasing the interfacial surface area between the two phases in the reactor system which can have a direct effect on the rate of the reaction. It also give the user the potential to recycle material in those phases. Mikami and co-workers have demonstrated this in their use of a Lewis-acid catalyst scandium *bis*(perfluorooctanesulfonyl)amide in a perfluoromethylcyclohexane biphasic solvent along with toluene for an aldol reaction between an aldehyde and a silyl enol ether. After the reaction, the Lewis-acid catalyst remained in the perfluorinated phase and the product was extracted from the toluene phase allowing the catalyst solution to be reused without the need for any post reaction purification [37]. The ability to perform reactions under extreme conditions of heat and pressure in flow systems allow chemists to assess reactions that would otherwise be deemed too extreme or unsafe under batch conditions.

- **Design for energy efficiency:** Flow reactors have the potential to intensify reaction conditions thereby reducing the energy impact on a production scale by providing precise control over the reaction conditions tailoring it for the transformation at hand. This can have a significant impact with relation to both costs and energy consumption. It also mimics the microwave conditions which are rarely adopted in batch production scale-up synthesis due to the high energy and low safety profiles offered by such systems. Although there exists a potential to carry out such microwave reactions in flow on an industrial scale, the saving in energy is attributed to the time spent performing such reactions [38]. The potential to perform radiofrequency heating where the reactor is filled with superparamagnetic nanoparticles or steel beads and placed in an electromagnetic field, allowing reactions to be heated more efficiently to temperatures reaching 350 °C, is a great advantage [39]. Photochemistry in flow by using micro-reactors also offers the potential to perform reactions very efficiently due to the small reaction volumes (and channel size) and homogeneous light penetration of an exact frequency optimised for the reaction. The same goes for active cooling and the ability to efficiently carry out the transformation reactions at reasonable temperatures. This has been investigated using micro-reactors in flow and was compared to batch processes in Yoshida's synthesis of disubstituted pyridines

via the generation of a pyridyllithium intermediate, which is then further reacted with electrophiles, giving the substituted products. In this case flow conditions do not require the need for cryogenic conditions where reactions with 2,3-dibromopyridine **24** can be completed at 0 °C (**Scheme 8**). When the same reaction was repeated in batch, higher temperatures did not produce any product. This was attributed to the dependence of the flow reactions on residence time and the batch reactions on temperature [40]

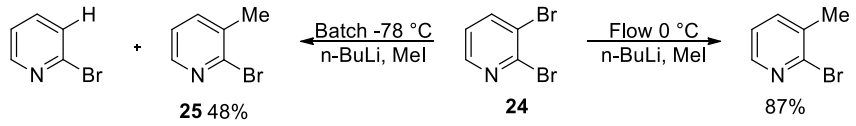

Scheme 8: Comparison of flow and batch conditions for the synthesis of 2-bromo-3-methylpyridine **25** from 2,3-dibromopyridine **24**.

- **Reduce derivatives and use renewable feedstocks:** Unnecessary derivatization is one approach to reduce the environmental influences such reactions tend to bring. The use of protecting groups should be minimised wherever possible as the approach itself has a low atom economy and is inherently wasteful. Wild has developed a novel flow-based reusable non-covalent nitrogen protection group strategy by employing solid supported crown ethers coupled with a base as releasing agent, to *N*-protect bifunctional compounds in column reactors [41]. By using micro-reactor systems, subtle changes in reaction conditions can be precisely controlled causing a difference in reaction rates, which can afford the desired product over the competing one. Such an advantage can potentially eliminate the need for protection group strategies [32]. This, combined with the potential to carry out feedback processes renewing raw materials wherever possible makes synthetic research more economically practical.
- **Catalysis:** This tool offers an increased selectivity and efficiency in reactions. The problem concerning such methods arises in optimisation processes. By employing micro-flow technology, reactions can be screened with a range of substrates and can utilise minimal material. Flow chemistry offers the ability to incorporate both homogeneous and heterogeneous catalysts into its systems through packed-beds, monoliths, coated films, etc. by exploiting its high surface to volume ratio. Even biocatalysts used in

steroselective reactions can be incorporated into such systems and reused whenever feasible [42].

- **Design for degradation:** While designing chemicals and chemical products for use, it should be taken into consideration that their breakdown products are not detrimental to the environment or persist in bio-systems.
- **Real-time analysis for pollution prevention:** Process analytics offer the ability to monitor flow experiments in real time giving a live representation of the reaction taking place. Deviations from accepted specifications can be identified more quickly thus lowering the amount of waste generated if the whole batch were to be disposed of. The ability to incorporate spectroscopic techniques (Raman, IR, mass-spectrometry) demonstrates the synthetic utility of such systems.
- **Inherently safer chemistry for accident prevention:** The ability to carry out hydrogenation reactions in flow systems is something that has been of significant interest in the field. The hazards associated with handling H_2 gas render such techniques unsafe and require stringent precautions due to its potential flammability. Hydrogenations are still one of the most relevant synthetic strategies adopted in chemistry. This concept has been utilised and discussed in detail in the later sections of this thesis (Page 91). Another example of such chemistry is shown by Tarleton and McCluskey in the hydrogenations performed using an H-Cube under different conditions for the synthesis of 2-phenyl-3-(1-*H*-pyrrol-2-yl)propan-1-amine **28** and analogues [43]. It can be seen from **Scheme 9** that a change in the solid supported catalyst can change the outcome of the reaction from **27** to **28**. A more detailed discussion of the progress in these types of reactions on various structural scaffolds of synthetic relevance have been shown by Kappe [44].

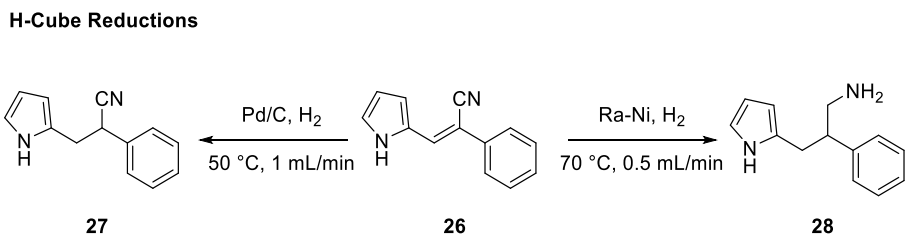

Scheme 9: Key hydrogenation steps employed under flow conditions for the synthesis of structurally interesting pyrroles.

Oxidations, ozonolysis and fluorination reactions find themselves very applicable to use in flow chemistry because flow reactor systems have the potential to safely incorporate gases into reaction mixtures. This, coupled with the use of micro-reactors where the reaction volumes of potentially dangerous or hazardous intermediates or reagents are so small, means such reactions can easily be assessed and handled [10].

1.2.4 Reactor Unit

This is the principal unit in every flow system. It is the site where the reaction takes place. Based on the nature of the chemical transformation, an appropriate reactor is chosen by the user as to their specific requirements. There are three basic types- chip reactors, coil reactors and packed bed reactors (**Figure 6**). When dealing with slurries, effective mixing units sometimes also act as reactors themselves to reduce the number of side products [45]. Tube-in-tube reactors are also used when rapid liquid-gas reactions take place [46]. Here, a gas permeable membrane that spatially separates the liquid and gas provides the interface for such reactions to take place.

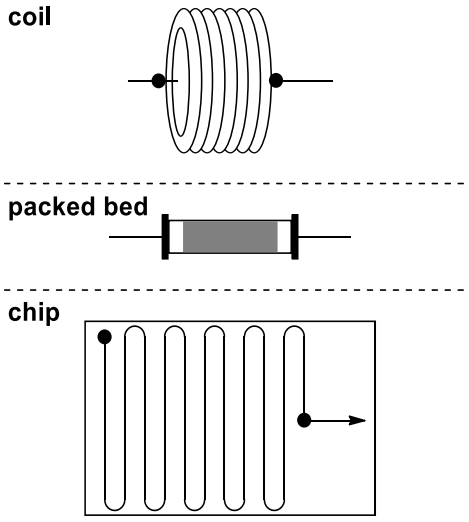

Figure 6: Types of flow reactors.

- **Chip Reactors**

Of all the reactor types, chip reactors offer the greatest heat transfer properties due to the small channels these reactors contain and the high surface area-to-volume ratios [47]. Usually these are made of glass, silicon-glass, ceramic, stainless steel or by microfabrication techniques [48]. These reactors can often be expensive and can block quite easily. Recent advances in 3D-printing have allowed for the rapid prototyping of such devices and their quick and easy use in chemical syntheses [49]. The ability to functionalize channels in chip reactors by immobilising heterogeneous catalysts is helpful and an example of this has been shown below. Boyle has shown how a glass microfluidic device's internal

channels can be functionalized with photoactive porphyrins (**Scheme 10B**). These generate singlet oxygen *in situ* and can be used to carry out the photochemical oxidation of α-terpinene **29** to give ascaridole **30** and side product p-cymene **31** *via* a Diels-Alder [4+2] reaction (**Scheme 10A**) [50].

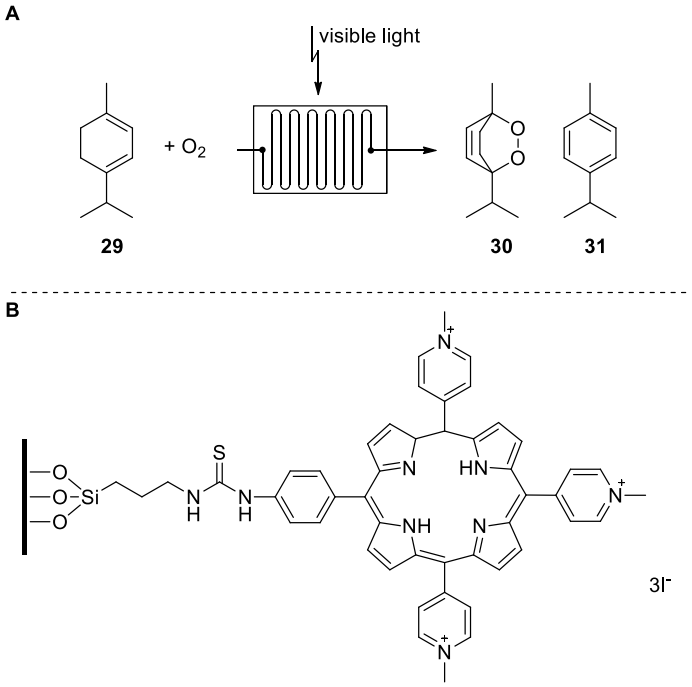

Scheme 10: A) Photochemical oxidation of α-terpinene **29** using porphyrin functionalized channels in glass microfluidic device; **B)** Structure of immobilized photoactive porphyrin.

- **Coil Reactors**

Coil reactors have a relatively low cost when compared to chip reactors as the tubing used in these reactors is made from commercially available standard fluoropolymers (PTFE, PFA, FEP) or stainless steel (SST). It is therefore used extensively in synthetic flow chemistry. The table below (**Table 1**) explains the use of different coil materials in systems with increasing temperature and pressure conditions. The wall thickness of the tubing is related to its stability under high temperature and pressure conditions.

Table 1: Application range of coil materials [20].

Application	PTFE	PFA	FEP	SST
low T/p (<50 °C, < 5 bar)	*	*	*	*
high T/p (<150 °C, < 20 bar)	o	o	o	*
very high T/p (>150 °C, < 20 bar)	×	×	×	*
UV-vis	o	o	*	×
corrosive reagents	*	*	*	o

***** = ok to use; o = some concerns, check datasheet; × = not feasible.

The use of FEP was found to be ideal in UV-vis irradiation photochemistry [51]. Stainless steel is best suited for reactions with very high temperatures and pressures however it is not as inert to corrosive agents as the fluoropolymers. An example of the usage of such reactors in flow chemistry has been demonstrated by Ley, where fluorination reactions on alcohols **32** were carried out using DAST (diethylaminosulfur trifluoride) in inductive heated FEP coil reactors to give the corresponding fluoro-derivative **33** (**Scheme 11**) [52]. This reagent, being volatile and highly reactive with water made it perfectly suited for these reactors. In addition the chemical undergoes dis-mutation to SF_4 and $(Et_2N)_2SF_2$ when heated above 90 °C and these by-products are extremely corrosive [53].

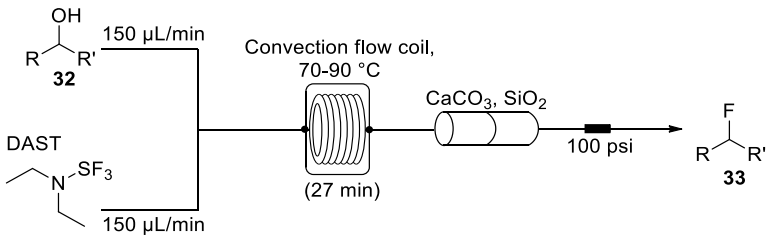

Scheme 11: Fluorination of alcohols using DAST in a convection heated FEP coil reactor.

- **Packed Bed Reactors**

Such reactors are usually used when heterogeneous catalysts or reagents need to be incorporated into the flow based synthetic protocol. They are typically made of glass, polymeric materials or stainless steel and the catalytic or reactive component is immobilized between two frits on a prepacked

cartridge. The advantages of using such systems is that the loading of material can be much higher than batch protocols giving faster reaction times. The use of frits containing the catalyst/reagent in the cartridge can eliminate post reaction work-up steps. However, this is not always the case with immobilized-transition metal catalysis, where leaching is typically observed [54]. Particle size determines surface-to-volume ratios and in turn relates to reaction times. An example of using packed bed reactors is shown below (**Scheme 12**) where Kappe has demonstrated the use of Mizoroki-Heck couplings with immobilized palladium on carbon columns. However due to significant amounts of leaching, they eventually switched to a homogeneous palladium pre-catalyst to carry out the optimized reaction in flow [55].

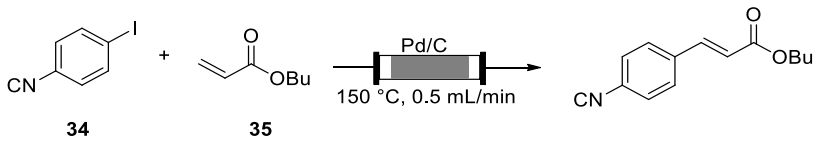

Scheme 12: Mizoroki-Heck coupling in flow between aryl iodide **34** and butyl acrylate **35**.

Another example in which flow chemistry and the use of such columns shows a significant benefit is in asymmetric chemistry. Pericàs and his group have shown a highly stereoselective Mannich reaction using polystyrene functionalized (2*S*-4*R*)-hydroxyproline **38** in a packed bed reactor (**Scheme 13**) [56]. This reaction between propanal **36** and *N*-(*p*-methoxyphenyl) (N-PMP) ethyl glyoxylate imine **37** in a continuous flow, single-pass system proceeds in only six minutes and the diastereomerically pure adducts are obtained in 72% yield at up to 7.8 mmol scale.

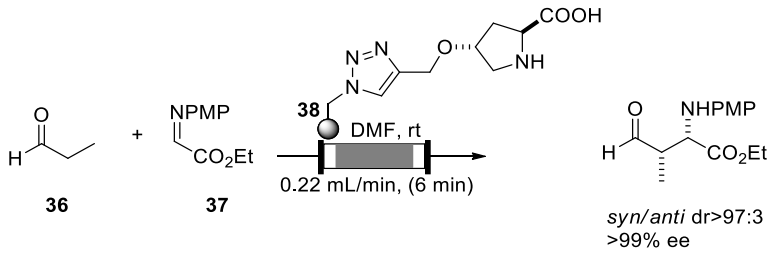

Scheme 13: Asymmetric organocatalytic reaction between propanal **36** and imine **37** using polymer bound (2*S*-4*R*)-hydroxyproline **38**.

1.3 3D-Printing

3D-Printing or additive manufacturing (AM) has received a lot of attention in academia in recent years. The ability to manufacture a three-dimensional product from a digital model using a CAD (computer-aided design) program which splits the digital file into layers thus allowing the printer to form the various shapes because of such layering has led it to being applied in many fields including education [57] [58] [59], biotechnology [60], biomedical [61], flow chemistry [62], microfluidics [63] and even the food industry [64].

The 3D-printing process involves a series of steps, the first of which is the production of a 3D file. This can be designed using CAD software or even reverse engineered from digital models such as MRI scans or scanning the object in question using a 3D-scanner. The second step involves converting the file into a readable format for the 3D-printer. This is usually an STL (Standard Tessellation Language) file which uses polygons to describe the surface of the designed object thereby simplifying the complex object into a code decipherable to the printer. OBJ and 3DP are less commonly used files but are also acceptable for use in 3D-printing. Once the correct file has been imported to the printer, an inbuilt program (usually proprietary to each brand of printer) called a slicer program slices the design into layers that will be used by the printer to build the object. Such programs allow the operator to define print settings such as support additions, heights and exposure settings (if applicable) of the individual layers, orientation of the object, etc. which are all important descriptors to include to generate a printed object. The printer then reads this information and prints the object as described. Post processing is another important step involves removing the part from the build platform either simply or by precise extraction if it is still encased in the build material. Depending on the type of technology used for the 3D-printing process, such a step could involve washing the object with appropriate solvent and/or curing under UV irradiation before handling. The removal of supports is also done at this stage [65].

1.3.1 Material Extrusion

Fused filament fabrication (FFF) or fused deposition modelling (FDM) technology is relatively old as the process was first patented in the 1980's by S. Scott Crump [66]. It involves the use of a thermoplastic filament which is unreeled and fed into a heated nozzle causing it to partially liquefy. This makes the now viscous plastic flow through an extruder that can be moved along the surface of a build plate in the X and Y directions forming the first layer. The build plate is then lowered or the print head is raised and this process repeats itself methodically. In such a manner liquified material is sequentially deposited upon the previous layers and allowed to cool and harden, thus forming the object. Nowadays, commercial printers are available that have fine-tuned this process and companies such as MakerBot and Ultimaker are being used in academic environments for the purposes of research, including our laboratories [67]. Materials that can withstand high temperatures are usually synthetic polymers such as acrylonitrile/butadiene/styrene (ABS), polylactic acid (PLA), high impact polystyrene (HIPS) and polyvinyl alcohol (PVA). Resolutions of such printers are as low as 250 µm (XY axis) and 50 µm (Z axis) [68]. Recent studies have shown that it is even possible to incorporate drugs such as paracetamol and caffeine with PLA polymer [69]. The dual head print design allowed layering of the two drugs thus affecting its release profile [69]. Relatively low-cost machines and materials give FDM printing an advantage for the users to produce low-cost custom parts. The anisotropic nature of such parts however, cause them to be weaker depending on the direction of print. Infill (low density structures printed within the object) percentages need to be very high (average setting in FDM printers is 20%) in order to produce a strong and dense object however, this can increase the time to print and also the cost [65].

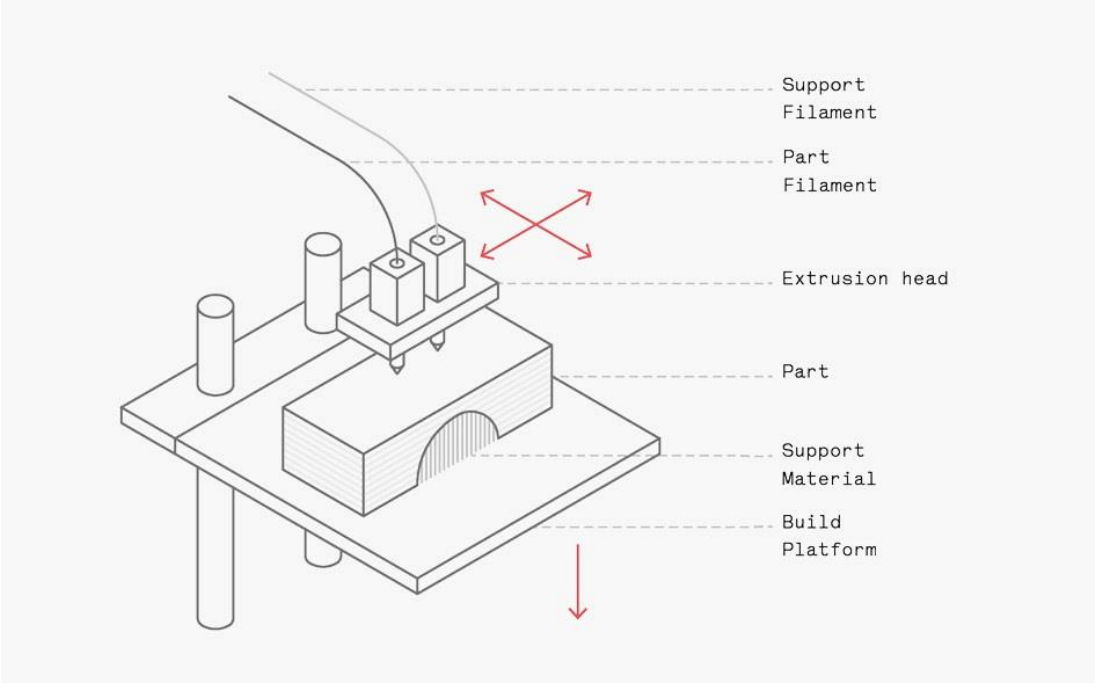

Figure 7: Schematic diagram of a FFF (FDM) printer [65].

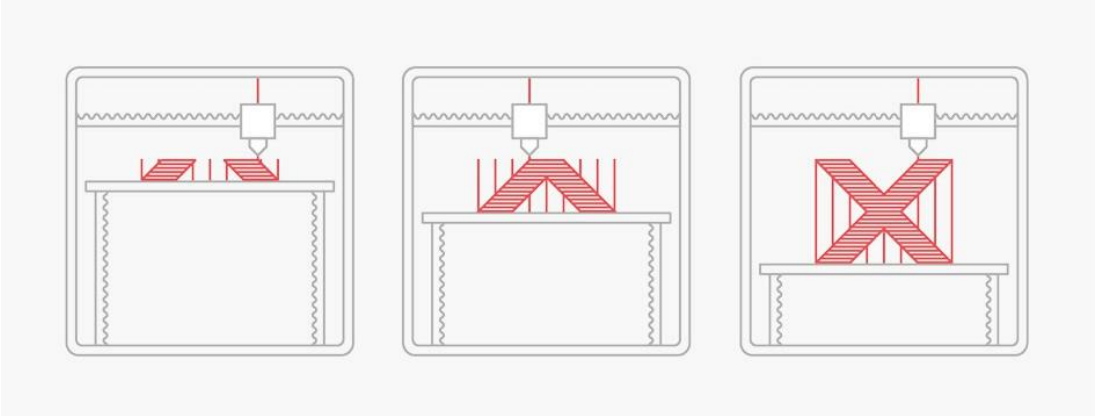

Figure 8: The FFF printing process [65].

1.3.2 Vat Polymerization

Stereolithography (SLA) and digital light processing (DLP) fall under this category of 3D-printing. Both use a photo-polymer resin in a vat that is cured by light. The photosensitive resin is exposed to the light and this causes it to undergo a polymerisation reaction thereby instantaneously solidifying it. The main difference between the two processes is the light source. SLA was invented in 1984 by Charles Hull [70]. SLA systems use UV lasers as a light source thus giving high resolutions as low as 25 µm layers [60]. These lasers aim at mirrors called galvanometers each on the X and Y axis that point the laser beam across the vat curing the resin layer by layer. The time required to scan a single layer will depend on the speed at which the laser beam travels across the surface of the vat. The slice information is determined by the coordinates set by tilting these mirrors thereby directing the laser beam along the plane. The accuracy will however, depend on the laser spot size and resin. DLP was invented by Larry Hornback in 1987 [71] [72]. DLP systems on the other hand use a digital light projector (LED screen) to flash a single image on to the vat, curing an entire layer at a time making this a comparatively faster process. Because the screen is made up of pixels, the cured layer consists of rectangular bricks called voxels [65]. A digital micromirror device (DMD), which consists of a series of mirrors, directs the light from the screen on to the vat. These tiny mirrors can be tilted to an “on” or “off” position thus generating a bright or dark voxel. The resolution achieved in such systems is 50 µm in all axes [73]. Continuous liquid interface production (CLIP) is another technique that falls under this category. It uses an oxygen permeable membrane right above the UV source which inhibits polymerization at the surface and eliminates the slow peeling and re-coating step for each layer. This reduces the time it takes to produce an object, giving it advantages over DLP and SLA systems [74]. Benefits of such processes include the smooth surfaces that such prints can attain. The accuracy in printing makes such systems perfect for printing very detailed structures. The disadvantage in using such systems is governed by the restriction to use only photopolymers, which tend to be brittle and can degrade over time in the presence of sunlight. Coatings are available to prolong the life of parts produced in such systems however, material

properties such as low impact strength do not allow the widespread use of such systems for functional applications.

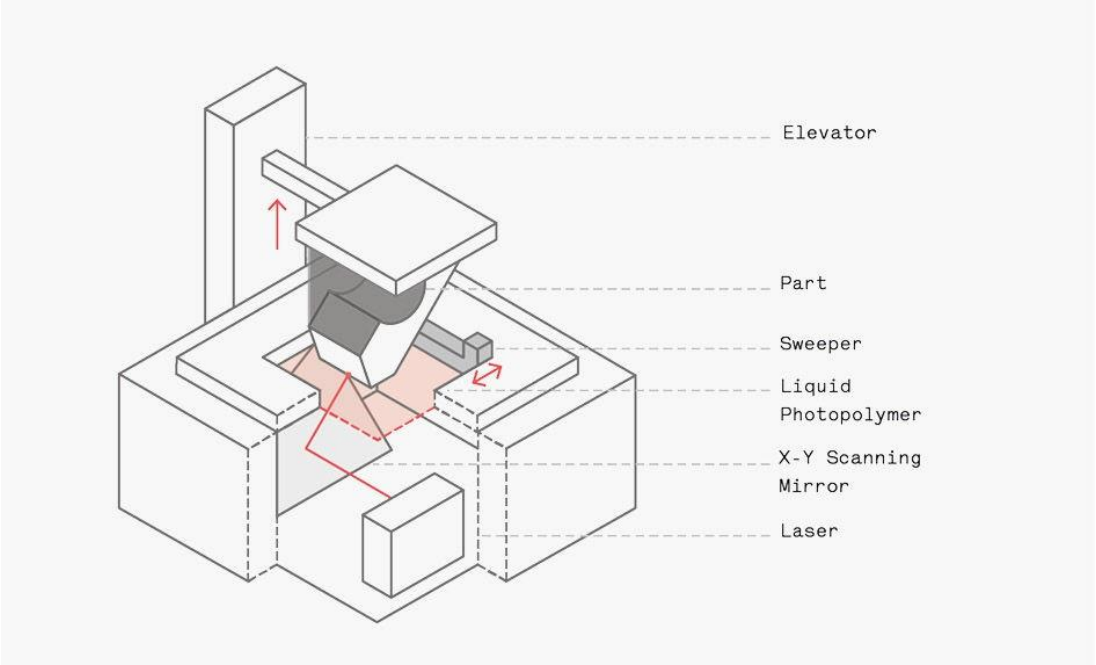

Figure 9: Schematic diagram of an SLA printer [65].

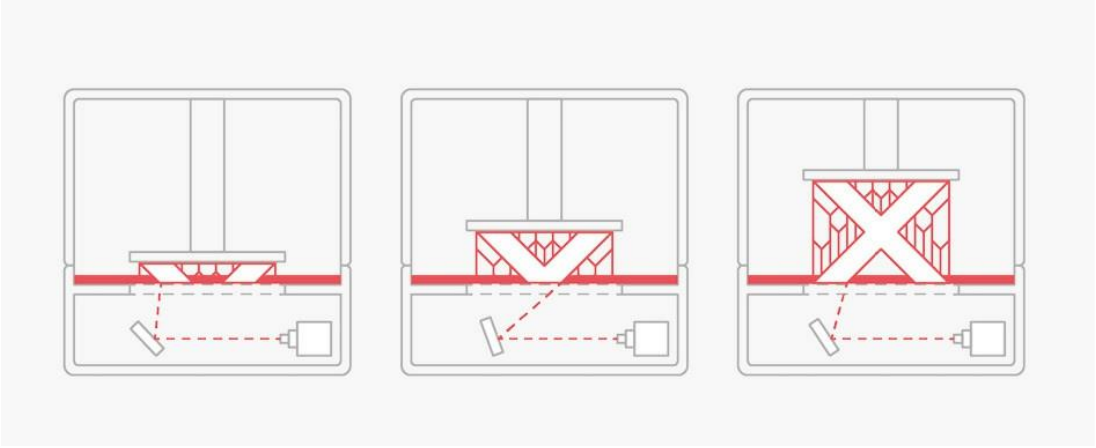

Figure 10: The vat polymerisation (SLA) printing process [65].

1.3.3 Powder Bed Fusion

Selective laser sintering (SLS) was developed by Carl Deckard and Joe Beaman in the late 1980's [75] [76]. This process is quite similar to SLA in that it uses a high power laser however, the polymeric material is in a powdered form as opposed to a photo-resin. The laser sinters a cross-section of this powdered material bed causing it to bind together and solidify. The bed is then lowered by the thickness corresponding to a single layer and the material is deposited over the top. Upon repetition of such steps the object is built within the powdered material which also supports the structure internally. Therefore, the need for additional support structures is eliminated and this is highly advantageous in the manufacture of parts where mechanical stress properties play an important role in their function. Materials commonly used in such processes include ABS, polycarbonates, PVC (polyvinyl chloride) and even ceramics and nylon [77] [78]. The limiting factor in SLS printing is the high cost of machinery (up to $250,000) along with the need for specialized operators to handle equipment and post processing of the products due to the hazardous dust associated with such a technique [65].

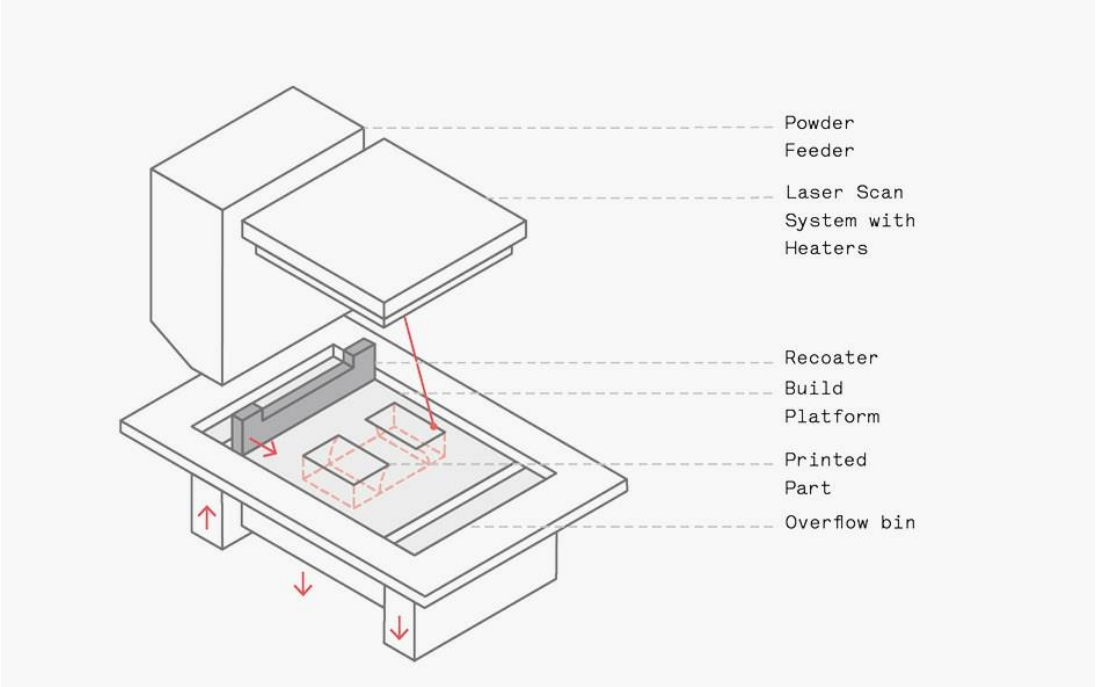

Figure 11: Schematic diagram of an SLS printer [65].

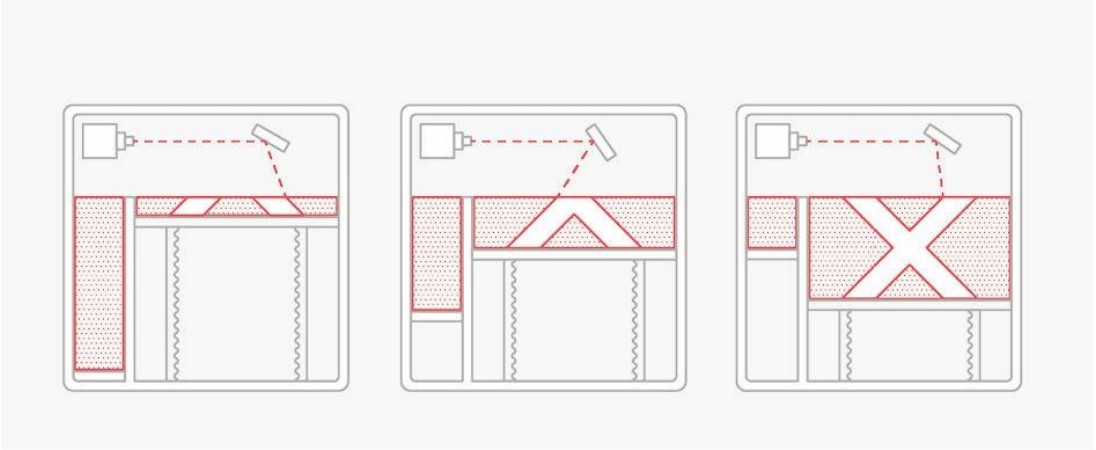

Figure 12: The SLS printing process [65].

1.3.4 Material Jetting and Binder Jetting

Material jetting is a form of printing where the print head deposits droplets of photo-curable polymer layer by layer whilst curing it simultaneously. Drop on demand (DOD) printers use the same principle with the addition of a second print head: one to deposit a wax-like material and the second to deposit a soluble support material which can be washed off during post processing steps. The use of thermoset photopolymer resins in such systems limits their utility in operations where mechanical strength is vital owing to the brittle nature of such parts. The finish on these parts is exceptionally good compared to other forms of 3D-printing and even injection moulding procedures. This is due to the continuous curing of the layers giving an almost homogeneous finish to the product.

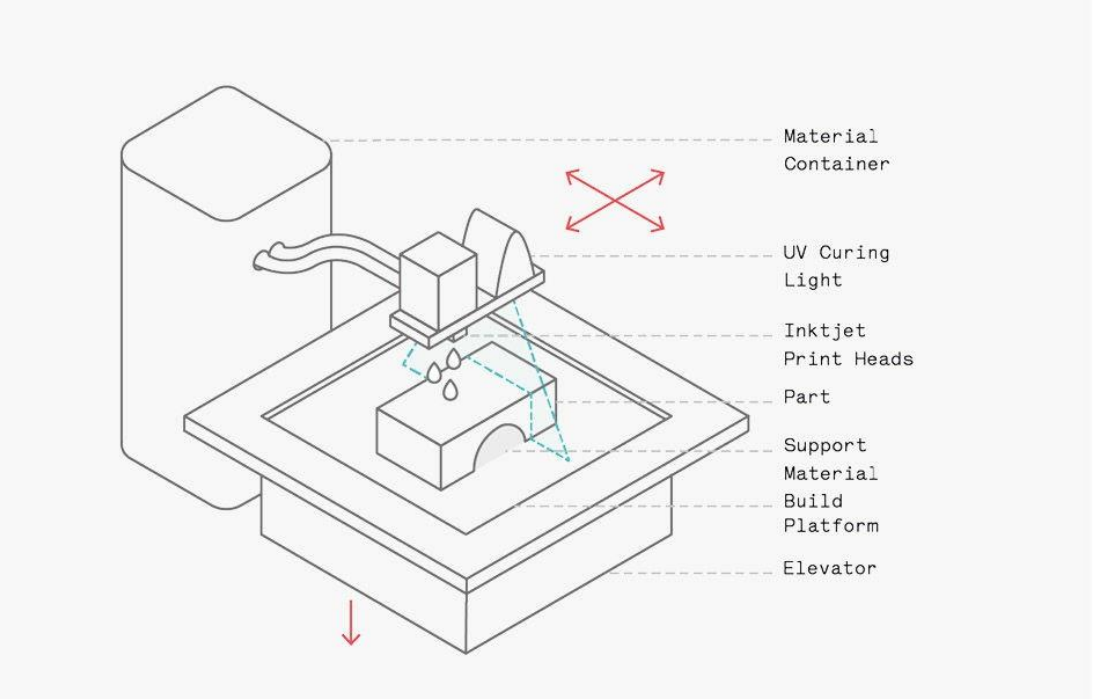

Figure 13: Schematic diagram of material jetting printer [65].

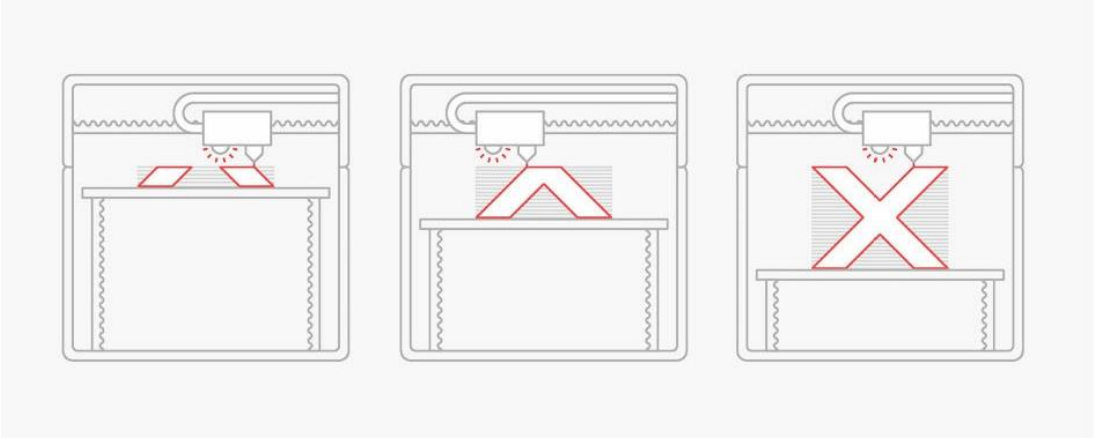

Figure 14: Material jetting printing process [65].

Binder jetting, also known as “powder bed printing” or “drop-on-powder printing”, is similar to SLS except the printing material consists of two states: a solid powder and a water-base binder. The laser for sintering is replaced by an inkjet print head depositing the binding agent across the surface of the layer. This glues the powders together and just like SLS, the bed is lowered and a new film of powder is deposited over the previously printed layer [79]. This technology can be applied to several materials such as starch and plaster bound together with aqueous inks or metal printing where a polymer binding agent is used to produce the part [74] [65].

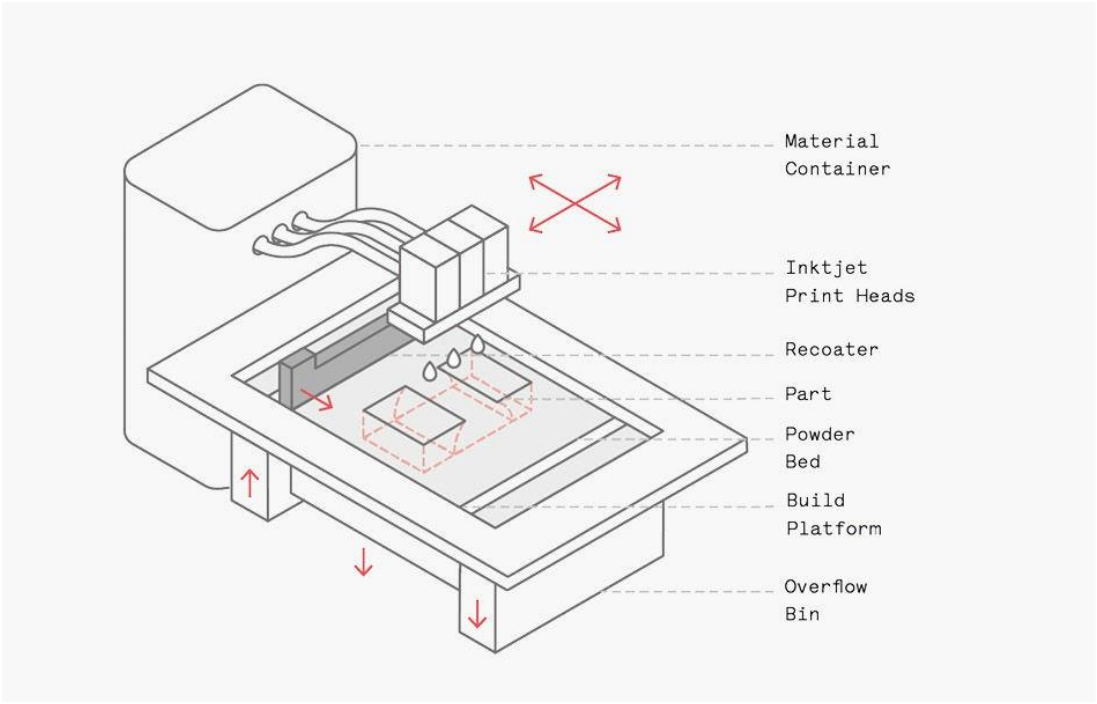

Figure 15: Schematic diagram of a binder jetting printer [65].

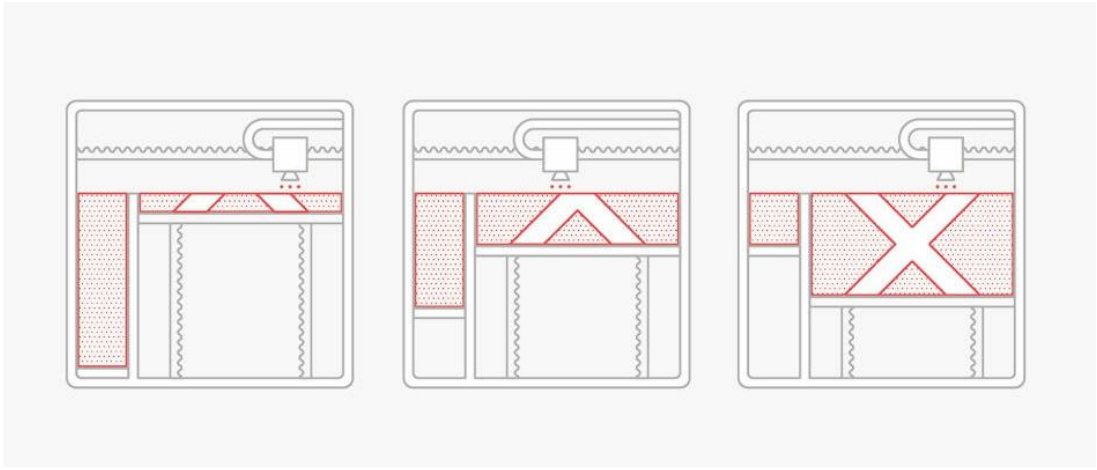

Figure 16: Binder jetting printing process [65].

1.3.5 Powder Bed Fusion (Metals)

Direct metal laser sintering (DMLS) and selective laser melting (SLM) use procedures similar to SLS except they specifically produce metal parts or objects [65]. DMLS does not melt the powdered metal but heats it to a point using a high powered laser where it fuses it on a molecular level. SLM on the other hand uses a laser to melt the powdered metal thereby forming a homogeneous part. Such systems usually require additional support structures due to the high stresses caused while operating at elevated temperatures, which can lead to distorted prints. EBM (electron beam melting) utilises a high energy electron beam to fuse the metal powders across the surface of the powdered bed. Due to the high power of the electron beam, this is a faster process as compared to DMLS and SLM but the disadvantage is that such a process is carried out in a vacuum environment and can only be used with conductive materials. The advantage with using such systems is the ability to generate a high level of intricacy and customisation in parts where traditional methods of manufacturing are unable to produce. The mechanical strength is also comparable to that of the metal in question as all parts produced are fused or melted together giving a solid object. High costs and low build size/build volume make such processes difficult to integrate into standard manufacturing lines and are currently only seen in bespoke part production like dental, aviation and aerospace, racing and medical engineering despite the high energy demands for such techniques [80].

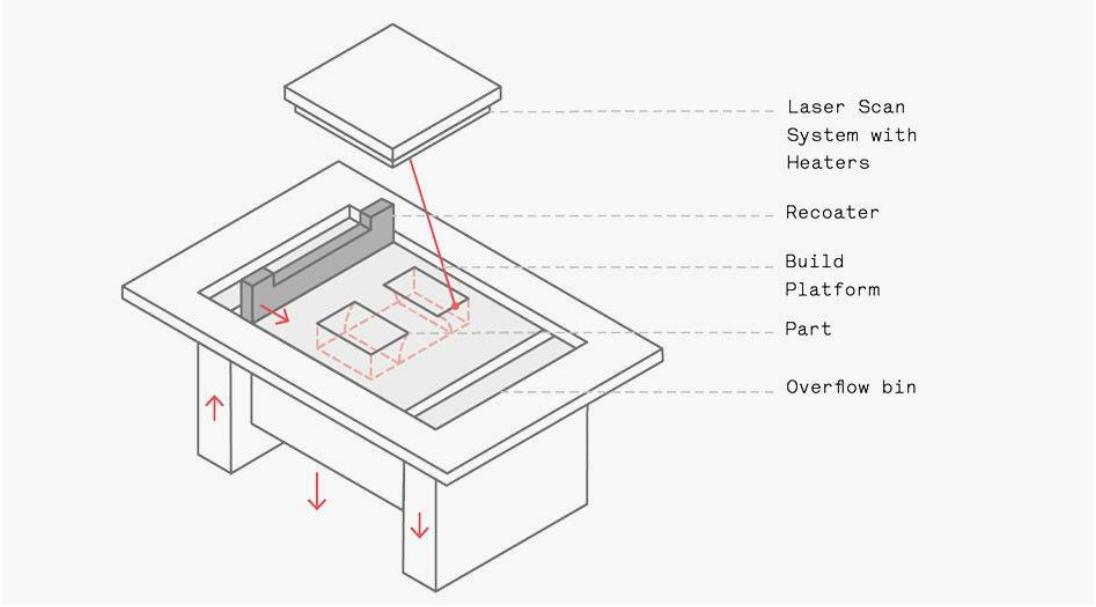

Figure 17: Schematic diagram of DMLS/SLM printer [65].

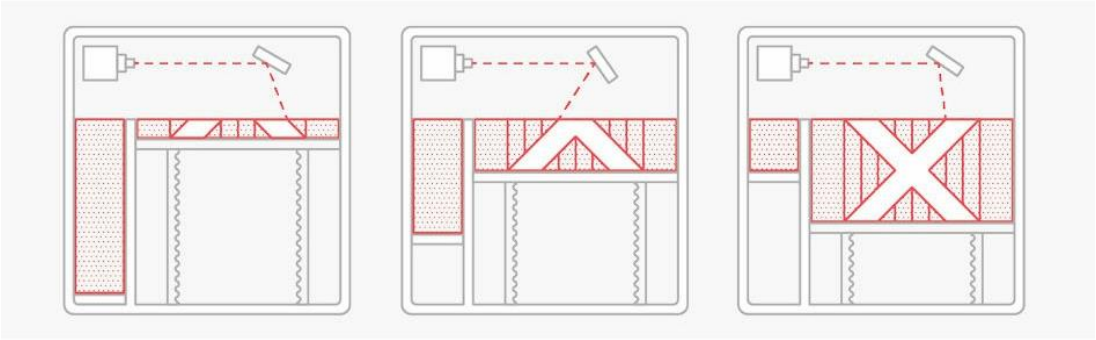

Figure 18: The DMLS/SLM printing process [65].

1.4 3D-Printing and Organic Synthesis

This relatively new field combines rapid prototyping and explores its scope in the synthesis of organic molecules. Given the vast array of 3D-printing techniques to choose from, the selection process for use in organic chemistry depends on the nature of the reaction to be performed and on the polymeric material used. As seen in the previous chapter, each of the 3D-printing techniques use different materials and their products have mechanical properties depending on the material chosen. This plays a very important role in chemistry processes as inertness to solvents and reagent interaction, the ability to withstand high temperatures and pressures will determine the practicality of its use.

1.4.1 3D-Printing and Catalysis

This concept is not only interesting from the point of view of organic chemistry but also plays an important role in the development of protocols that have a significantly lower impact on the environment. The need to assess the environmental impact (E-Factor) in both research and industry has challenged the chemical community and the development of low waste catalytic systems helps address this problem [81]. 3D-Printing allows the integration of different materials into polymeric systems and the immobilisation of catalysts in such systems not only gives higher catalytic performance but also allows for the recovery of the catalytic material thereby significantly reducing waste.

The first reported use of a reusable 3D-printed copper/alumina heterogeneous system was by Sotelo and Gil wherein a gel based ink was prepared with Al_2O_3 ceramic powder, polymer binders and $Cu(NO_3)_2$ (5% w/w). It was then extruded through a robotic assisted syringe to generate woodpile structures and finally sintered at 1400 °C to give a high strength catalytic device. To test the device, the Ullmann reaction was selected and the synthesis of imidazoles, benzimidazoles and *N*-aryl amides was carried out (**Scheme 14**) [82].

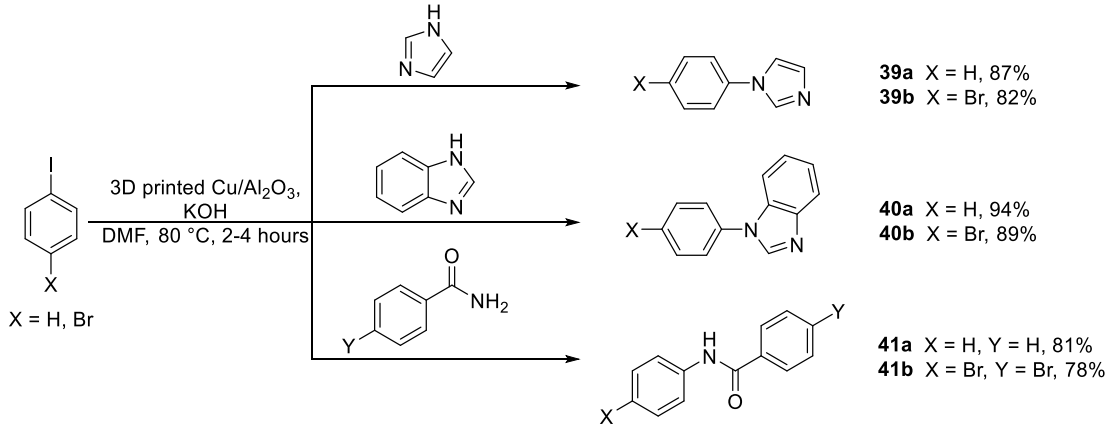

Scheme 14: Ullmann reaction for the synthesis of imidazoles **39a**, **39b**, benzimidazoles **40a**, **40b** and N-aryl amides **41a**, **41b** using 3D-printed Cu/Al_2O_3 structure.

The same 3D-printed catalyst was used to synthesize 3,4-dihydropyrimidin-2(1H)-ones **42** and 1,4-dihydropyridines **43** in multicomponent Biginelli and Hantzsch reactions [83]. These reactions were conducted under solvent-free conditions and using microwave irradiation with the printed catalytic structure (**Scheme 15**).

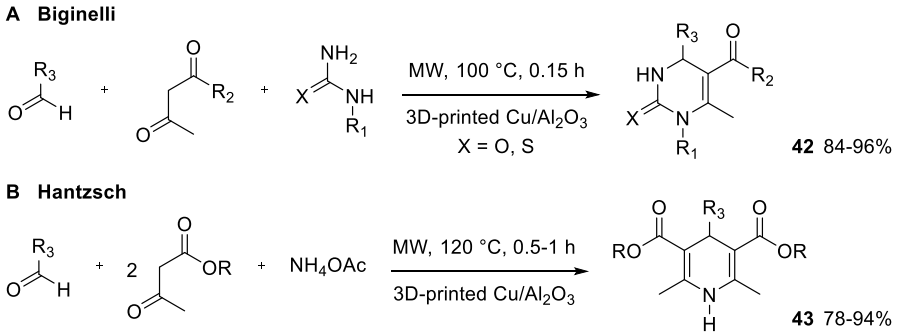

Scheme 15: A) Biginelli reaction using 3D-printed Cu/Al_2O_3 structure to give 3,4-dihydropyrimidin-2(1H)-ones **42**; **B)** Hantzsch reaction using 3D-printed Cu/Al_2O_3 structure to give 1,4-dihydropyridines **43**.

1.4.2 3D-Printed Reactors (Batch Chemistry)

The ability to design bespoke labware and research equipment using 3D-printing and a free and open-source software (FOSS) can be very advantageous as raw materials for such products tend to be cheap and the user interface relatively simple [84]. Ananikov described the manufacture of labware such as Erlenmeyer flasks, roundbottom flasks, etc. using PLA, ABS, PP and PETG (polyethylene terephthalate glycol) and established their resistance to solvents under normal and pressurized conditions [85]. The group also went on to conduct Suzuki-Miyaura cross-couplings and hydrothiolation reactions in capped test tubes printed from these materials (**Scheme 16**). Although conversions were high (>90%), reactions were low yielding in the Suzuki cross-couplings owing to the sorption of *p*-bromotoluene **44** in the plastic structure. For the hydrothiolation reactions, ABS could not be utilized as it was dissolved in the reaction solvent. The group were also able to demonstrate the functionality of such materials and showed that PP>PLA>ABS>PETG.

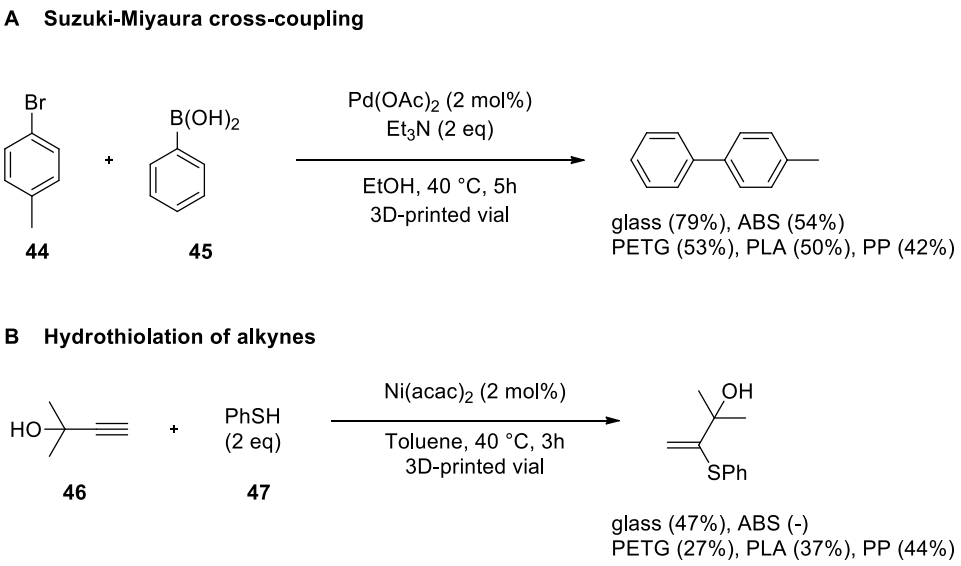

Scheme 16: A) Suzuki-Miyaura cross couplings between *p*-bromotoluene **44** and phenyl boronic acid **45** in 3D-printed vials; **B)** Hydrothiolation of alkyne **46** with thiophenol **47** in 3D-printed vials.

Bearing this concept in mind, Cronin developed the first reaction vessel by 3D-printing acetoxysilicone using a syringe printer (Fab@Home version 0.24 RC6

freeform printer). This research aimed to assess the effect of reactor geometry on the outcome of the reaction. The team reported two reaction vessel designs (Reactor design A and Reactor design B), each containing two solution-holding chambers and a reaction chamber. The two designs varied in the size of the reaction chamber (9.5 mL and 2 mL). By loading a solution of 5-(2-bromoethyl)phenanthridinium bromide **48** (3 equiv., 3 mL) in one holding chamber and a solution of trimethylamine and 4-methoxyaniline **49** (1 equiv., 1 mL) in the second holding chamber and connecting a vacuum linked needle to the reaction chamber, the solutions were drawn into the respective reaction chambers. Through this experiment the group was able to evaluate the importance of reactor volume size in the formation of the desired product [49] [86]. **Scheme 17** shows the selectivity for **50** when all reagents are allowed to mix in the reaction chamber and a change in selectivity to **51** when there is a forced 1:1 ratio of **49** to **48** as seen in reactor design B. The yield obtained after 21 hours is >90% for reactor design A and an 80:20 ratio of **51** and **50** after 21 hours for design B.

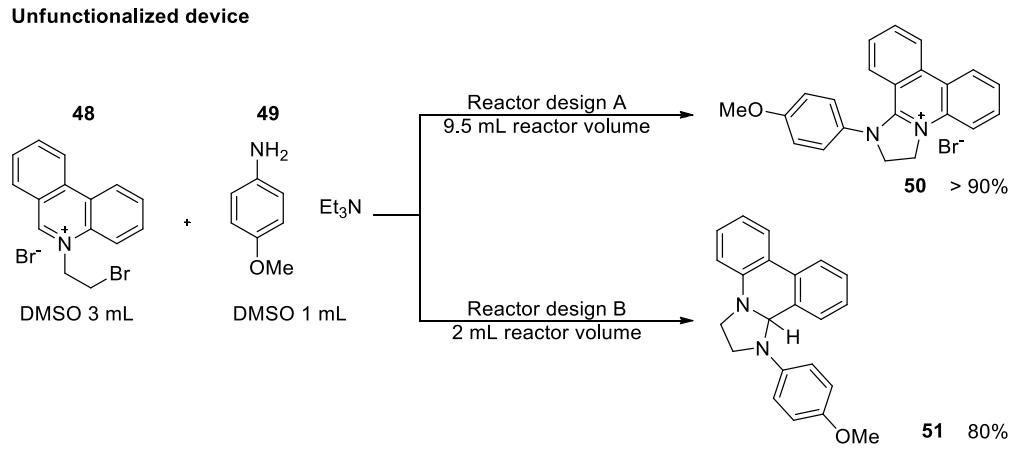

Scheme 17: Synthesis of phenanthridine based heterocycles (**50** and **51**) in 3D-printed reactionware with different reaction volumes.

The group also investigated the use of a catalytic version of the reaction vessel by printing with a mixture of acetoxysilicone and Pd/C. The acetoxysilicone was thinned by the addition of toluene after which Pd/C was added until a paste was formed and it was ready for syringe printing. In this case the two solution chambers were loaded with a solution of styrene **52** (1 equiv.) and triethylsilane **53** (TES) (15 equiv.) in methanol to carry out a supported

hydrogenation of styrene to ethylbenzene **54**. Yields were quantitative and **54** was obtained in 30 minutes as compared to inert reactors where no product was obtained even after 2 hours (**Scheme 18**).

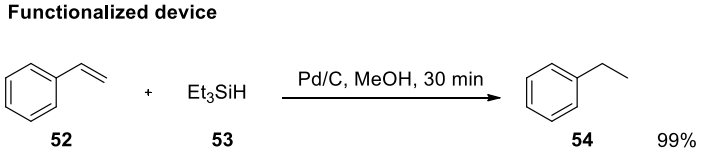

Scheme 18: Synthesis of ethylbenzene **34** using a catalytic 3D-printed reactor.

In 2013, the same group developed a 3D-printed three-reaction-chamber device consisting of four 20 mm cubes integrated with catalytic components and purification section to carry out a three step reaction sequence in each of the chambers. The device was fabricated using two printers: Bits from Bytes 3DTouch^{TM} FDM printer to build the polypropylene (PP) body of the device and a Fab@Home version 0.24 RC6 freeform syringe printer to introduce the catalytic components into the various chambers. The catalytic components comprised of a mixture of acetoxysilicone and Lewis acid Montmorillonite K10 in the first chamber and the same with Pd/C in the third chamber. A purification housing space was also 3D-printed with the rest of the device where cotton wool separated a packed bed of silica and Celite®. **Scheme 19** shows a Lewis acid catalyzed Diels-Alder cyclisation reaction that occured between a substituted cyclopentadiene **55** and acrolein **56** which took place in the first chamber. On the completion of the reaction, a bicyclic bridged structure with a pendant aldehyde group **57** was formed and the device was simply rotated by 90° pouring it's contents into the second chamber which was prefilled with aniline thus forming the corresponding imine **58**. The device was rotated by 90° again, transferring its contents into the final chamber containing the immobilized Pd/C and prefilled TES (reducing agent), thus carrying out the hydrogenation of the C=N bond and giving the secondary amine **59** final product. This solution was passed through the integrated silica column and into a flask by rotating by 90° yet again [87]. This elegant multistep protocol with minimal operator handling demonstrated the ease in integrating a robust

synthetic sequence with 3D-printing thus exhibiting its value in organic chemistry [88].

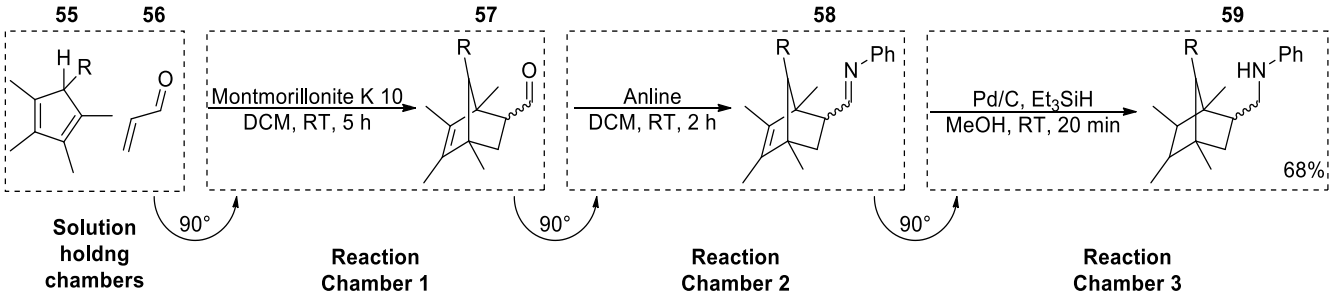

Scheme 19: Multistep synthetic sequence for the synthesis of secondary amine **59** using a four chamber 3D-printed reaction vessel.

In 2014 Cronin demonstrated the use of FDM printed sealed PP reactor vessels containing solutions of aluminum nitrate and trimesic acid in an aqueous-DMF solution heated above its boiling point to synthesize metal organic frameworks (MOFs) MIL-96, a porous aluminum trimesate complex [89]. The reactor vessel printing was halted after 80% of the print completed. This was followed by the introduction of reagents into the vessel and the printing process was continued thereby sealing it shut. These vessels were heated in an oven at 130 °C for 18 hours to synthesize MIL-96. In a similar manner, the synthesis of HKUST-1 [90] was reported by heating solutions of the respective starting materials above their boiling points in sealed reactor systems [91] [92].

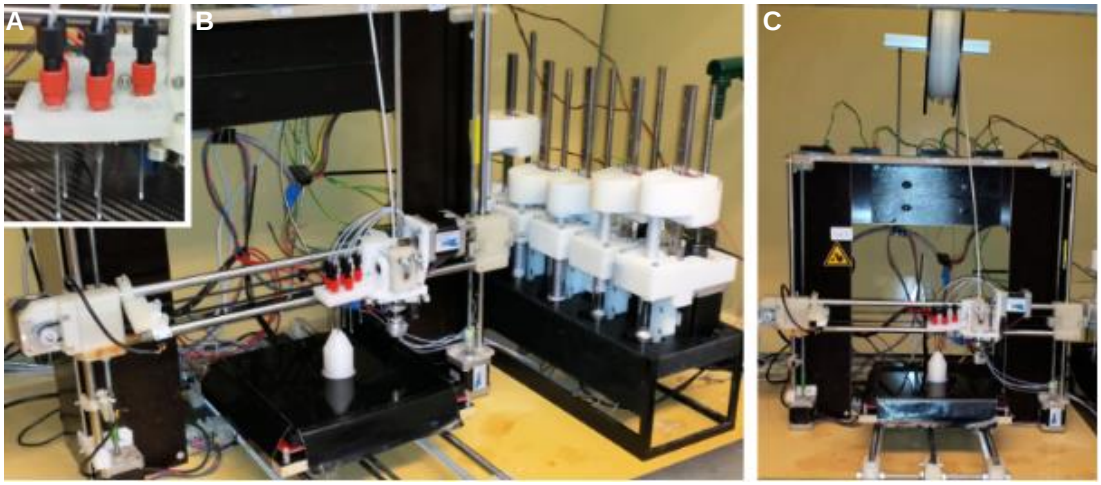

Figure 19: A) Modified 3D-printer used for the automated synthesis of Ibuprofen; **B)** dispensing needle for reagent deposition; **C)** Front view of the apparatus showing the PP vessel on platform an feedstock reel [93].

The group also reported a fully automated synthesis of anti-inflammatory drug ibuprofen using a modified Prusa i3 RepRap FDM printer. The printer was able to produce an inert PP reaction vessel as well as carry out the reaction sequence within it by an Arduino-controlled liquid handling unit dispensing the required solutions of starting materials and reagents (**Figure 19**). The modified print head was able to extrude the reaction vessel as well as deliver all reagents necessary to carry out the three step reaction over a period of 24 hours affording a 34% overall yield of the product (**Scheme 20**) [93]. Isobutyl benzene **60** and propanoic acid (1.05 M in $CHCl_3$) were added to the PP reaction vessel followed by the slow dropwise addition of neat triflic acid in order to reduce the exotherm produced as a result of this reaction. The reaction was agitated for 18 hours to form **61**. In the next step a solution of $PhI(OAc)_2$ (1.4 M solution in MeOH:TMOF 1:0.8 v/v) was added over a course of 10 minutes and the reaction was agitated for another 3 hours. The final solution of KOH (5 M in MeOH:H_2O 4:1 v/v) added by the automated synthesis robot was delivered to the reaction vessel containing **62** and agitated for 2 hours after which an acidic workup was carried out followed by simple column chromatography giving the final product **7**.

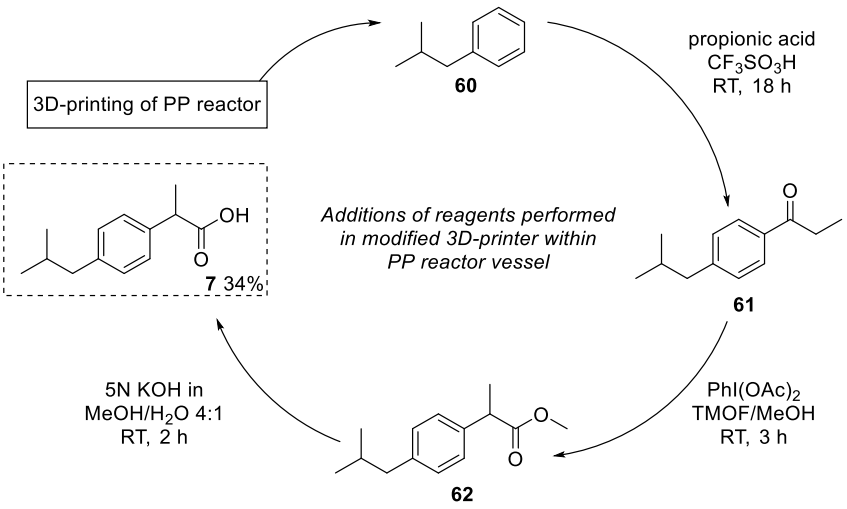

Scheme 20: Synthesis of Ibuprofen **7** using modified 3D-printer with automated liquid handling unit.

The use of additive manufacturing (AM) technology in organic chemistry is not limited to only reactionware but it has been demonstrated by Ananikov on using the technology to customize a housing for an LED light in their exploration of photoredox chemistry. They designed a modified case for a 530 nm LED light source with a twist-lock mechanism making it easy to change the light if required and that can be fitted on a standard glass vial (**Figure 20**).

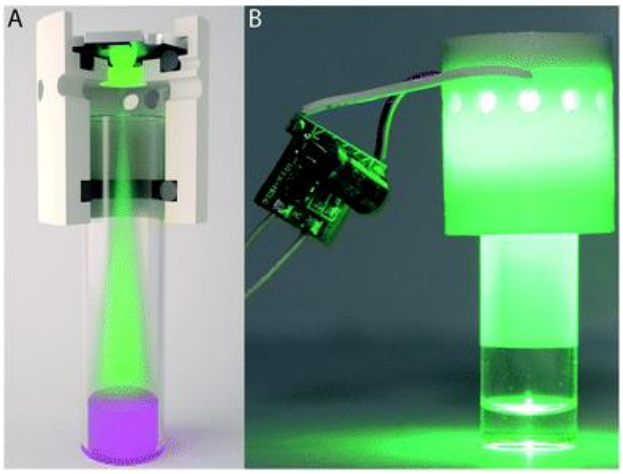

Figure 20: A) Computer designed model of photoreactor; **B)** Image showing the printed housing with glass vial and light source.

This photoreactor device was then printed with ABS using a Picaso Designer 250 FDM printer in under 30 minutes and used in the reaction between thiols **64** and alkynes **63** in the presence of Eosyn Y at 530 nm (**Scheme 21**). A

range of S-functionalized products **65** were obtained in good yields and remarkable atom-economy efficiency (the only by-product being water). Reaction showed higher selectivity for the *E*-isomer (*E*:*Z* from 96:4 to 98:2) [94].

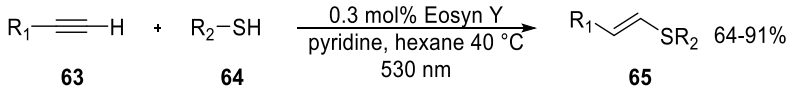

Scheme 21: Photocredox thiol-yne click reaction with Eosyn Y carried out in a 3D-printed photoreactor.

A bespoke NMR tube/spinner combination apparatus has also been printed as seen in the work carried out by Hübner in 2017 [95]. They reported using an UP Plus 2 FDM 3D-printer from TierTime Technology Co. Ltd. (PP3DP) to print polyamide (Taulman 910) as the material is invisible to NMR spectroscopy. The NMR tube/spinner combination was designed using CAD by obtaining precise measurements from the manufacturer of the original part. The printer was placed in an inert environment (glove box) and the device as seen in **Figure 21** printed upside down on the build platform.

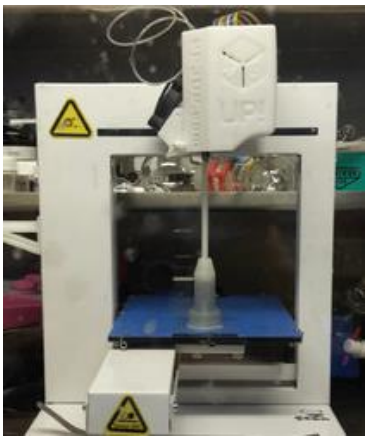

Figure 21: 3D-print of hollow NMR tube/spinner combinations using polyamide showing dark solution of reagents for Sonogashira coupling reaction.

Reagents were introduced into the cavity of the device by temporarily pausing the print and the device was eventually sealed shut. The palladium catalyzed Sonogashira decarboxylative cross-coupling reaction between aryl halides **67** and acetylenic acids **66** was investigated and a set of arylnaphthylalkynes **68**

was synthesised by monitoring their reaction in the custom NMR tube/spinner gear (**Scheme 22**).

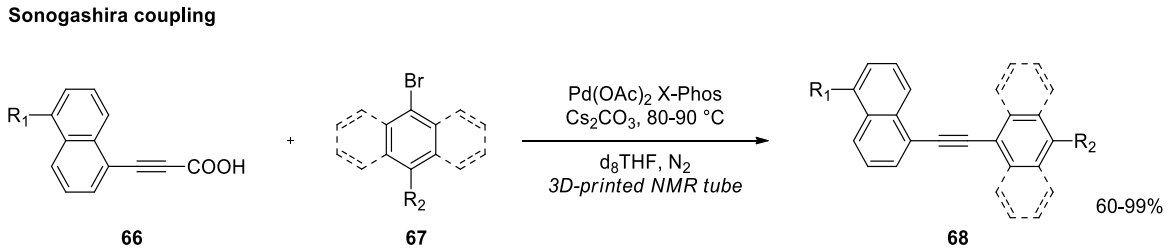

Scheme 22: Sonogashira decarboxylative cross-coupling reaction for the synthesis of arylnaphthylalkynes **68** using 3D-printed NMR tube/spinner combination device.

The potential of 3D-printing has been realized with the emerging development of bespoke reactors for flow chemistry applications. This section details the various devices produced for flow-based synthetic approaches. There have been several investigations of using 3D-printing in microfluidic systems, especially for the development of devices utilized in analytical applications. Devices for use in electrophoresis (micro free-flow electrophoresis device or *μ*FFE device) have been FDM printed in ABS in an efficient manner and compared to their glass counterparts in fluorescent dye separation experiments between myoglobin and cytochrome c, giving comparable results [96]. In 2017 Kotiaho reported printing a PP reactor using FDM adapted with a stainless steel nano-ESI capillary and a 10 mm polytetrafluoroethylene-coated magnetic stir bar giving an internal reactor volume of 250 µL. This reactor was held in a 3D-printed jig with built-in connectors for the introduction of solutions into the reactor and interface with a mass-spectrometer. Diels-Alder and retro Diels-Alder reactions were studied using this system [97]. Another analytical application of such microfluidic devices was shown by Rusling where a PET microfluidic device was fabricated using FDM printing and used to synthesize Prussian blue nanoparticles (PBNs). These nanoparticles were sequentially attached to PEEK tubing with insulated gold electrodes fitted to the same device using an ABS printed screw thread and used in hydrogen peroxide sensing experiments [98].

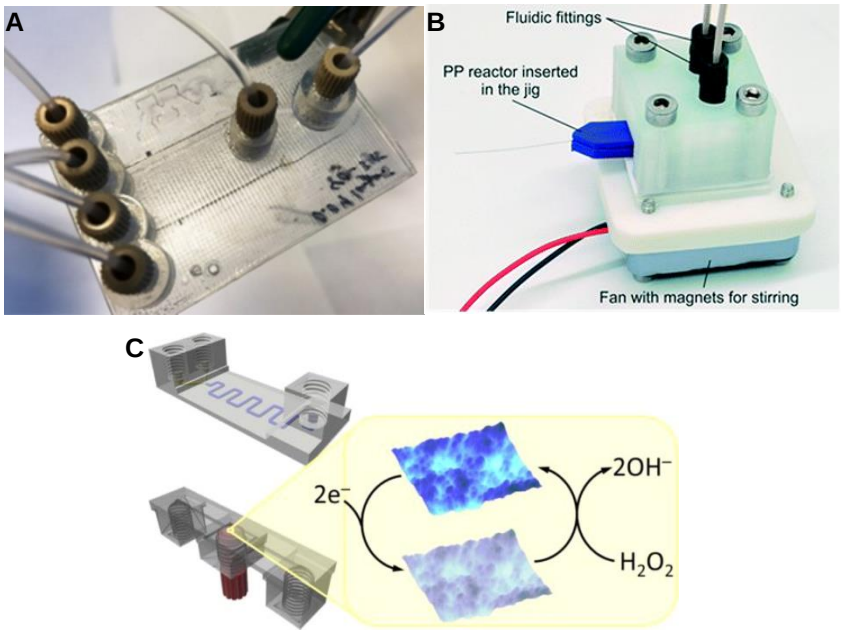

Figure 22: A) 3D-printed *μ*FFE device used for the separation of Myoglobin and cytochrome C; **B)** PP reactor fitted with nanospray ionization capillary held in the jig to be used in mass spectrometry measurements; **C)** PET microfluidic reactor for hydrogen peroxide sensing using PNBs.

Cronin also reported a milli-fluidic device 3D-printed in PP which was directly linked to an electrospray ionisation mass spectrometer (ESI-MS) for carrying out supramolecular chemistry in order to demonstrate its versatility. The device featured three inlets adapted with standard PEEK screw fittings allowing easy connection to syringe pumps. A 0.57 mL flow path with a 1.5 mm internal diameter was fabricated and the outlet connected to a T-piece so that an appropriate dilution step could be carried out to suit the ESI-MS conditions. In addition, a PEEK microsplitter valve was attached splitting the flow to a collection point whilst the remaining led to the MS. In this manner they have been able to show that changing the flow rates of the reactants changes the product stoichiometry ratio from 1:1 to 2:1 as determined by in-line ESI-MS [99] (**Figure 23**).

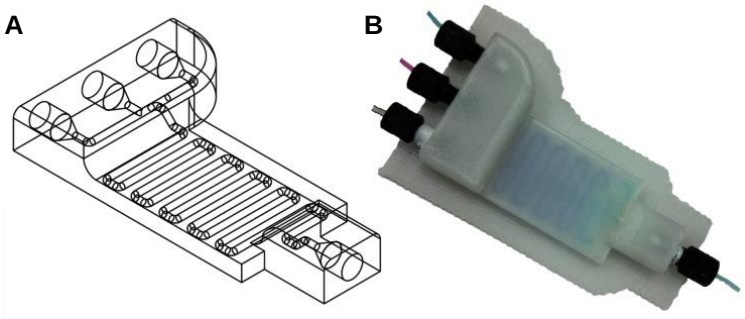

Figure 23: A) STL file showing inlet/exit ports and internal channels of reactor; **B)** PP printed reactor with fitted PEEK screw threads.

Three milli-fluidic reactors were also fabricated in the same group using PP and FDM printed using a 3DTouch^{TM} printer and used in several reactions [100]. These devices were also designed using CAD software (Autodesk123D) and printed in approximately 4 hours. The first reactor design featured two inlets and a reactor volume of 60 µL. The second design incorporated a third inlet after the two initial inlets completed a reaction volume of approximately 270 µL. The third and final reactor design featured 'silos' in which solid reactants (sodium molybdate and hydrazine dihydrochloride) were previously incorporated into the device during the printing process.

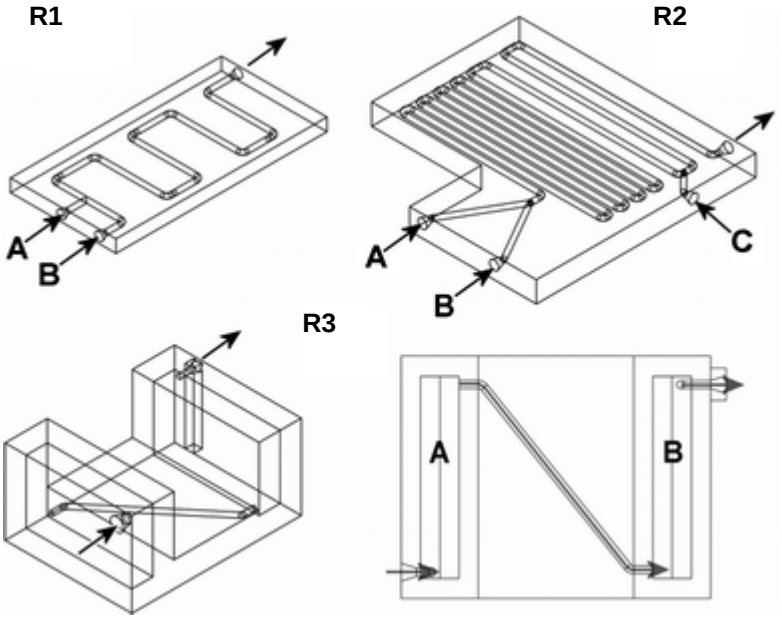

Figure 24: STL drawings of three PP reactor designs R1 showing two inlets and a single outlet (V_R=60 µL), R2 showing three inlets and a single outlet

(V_R=270 µL) and R3 showing a single inlet and outlet and integrated silos for solid reagents [100].

On passing solvent through such a device, the reactants would dissolve and carry out the necessary transformation. **Scheme 23** shows initial experiments using the three inlet reactor R2 for synthesizing dibenzylamine **71**. PTFE tubing was attached to inlets and outlets of the device and sealed with epoxy adhesive. The two inlets of the reactor were fed using syringe pumps with a 1 molar methanolic solution of benzylamine **69a** and benzaldehyde **70a** at a low flow rate of 5 µL/min and residence time of 42 minutes to ensure imine formation. A 1 molar methanolic solution of sodium cyanoborohydride was introduced through the third inlet at 2.5 µL/min thereby reducing the imine to the subsequent secondary amine.

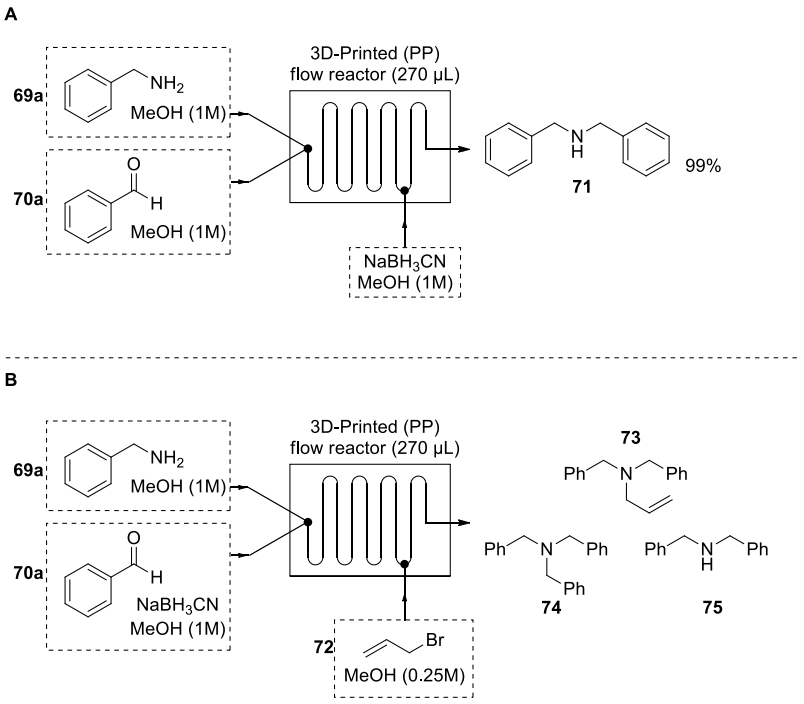

Scheme 23: A) Flow synthesis of dibenzylamine **71** in 3D-printed PP reactor R2; **B)** Alkylation reactions performed using 3D-printed PP R2.

The reactor R2 was also used for alkylation reactions. In this case a 1 molar methanolic solution containing sodium cyanoborohydride along with the aldehyde **70a** (1:1 ratio) was introduced into the first inlet at 5 µL/min and a 1 molar methanolic solution of the benzylamine **69a** was introduced into the second inlet at 2.5 µL/min respectively. A 0.25 M methanolic solution of allyl

bromide **72** was introduced into the third inlet at 7.5 µL/min in order to carry out the necessary alkylating reactions but a mixture of products **73**, **74** and **75** was obtained using this protocol. All reactions were analyzed using ATR-IR and MS to ensure product formation.

In the third experiment using R3, hydrochloric acid (aqueous, pH 1) was introduced though the single inlet into the first chamber containing the solid sodium molybdate ($Na_2MoO_4 \cdot 2H_2O$, 300 mg, 1.24 mmol) dissolving it and passing into the second chamber. This solution dissolved the reducing agent hydrazine dihydrochloride ($NH_2NH_2 \cdot 2HCl$, 20 mg, 0.19 mmol) and the reaction mixture exited through the outlet and into a UV-Vis spectrometer which was followed by DLS-analysis to detect the presence of $\{Mo_{154}\}$ in the product stream.

To continue this work, the group reported a two-step process using two linked PP 3D-printed reactors for the synthesis of aromatic secondary amines [101]. In initial experiments, 2 molar methanolic solutions of aldehydes **70, 76, 77** and amines **78a-d** were fed using syringe pumps into the two inlets of the first reactor (V_R 0.4 mL) at 0.25 mL/min. The reactor was attached to an ART-IR flow cell with a PTFE tubing with an internal volume of 0.1 mL. The total volume of this reactor hence added up to 0.5 mL or 500 µL.

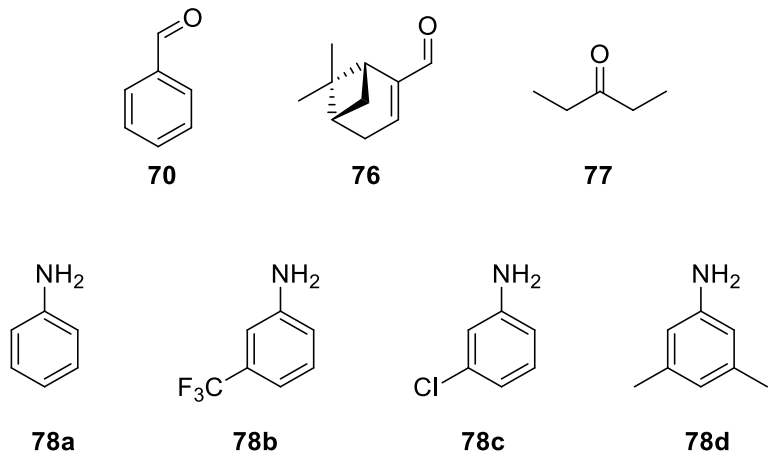

70 **76** **77**

78a **78b** **78c** **78d**

Figure 25: Carbonyl compounds and amines used in the synthesis of aromatic secondary amines.

On optimizing the conditions for imine formation with a range of substrates, the two reactors were connected and 2 molar methanolic solutions of benzaldehyde **70** and aniline **78a** derivatives were introduced into the two inlets at a much lower flow rate (0.0125 mL/min) to ensure complete formation of imine **79a** (**Scheme 24**). The ratio of aldehyde to amine was maintained at 1:1 (v/v). This gave a residence time of 14 minutes in the first reactor and its outlet was connected into one of the inlets of the second 3D-printed PP reactor. A 1 molar methanolic solution of reducing agent sodium cyanoborohydride was pumped into the second inlet of this reactor at the same flow rate (0.0125 mL/min) to produce the corresponding secondary amine **80a** product. The residence time of solutions in this reactor was 7 minutes. Solutions leaving this were passed into an ART-IR flow cell to monitor product formation. Additionally, HPLC and MS and ^{1}H NMR analysis was also conducted to gather complete data on all products generated in this manner.

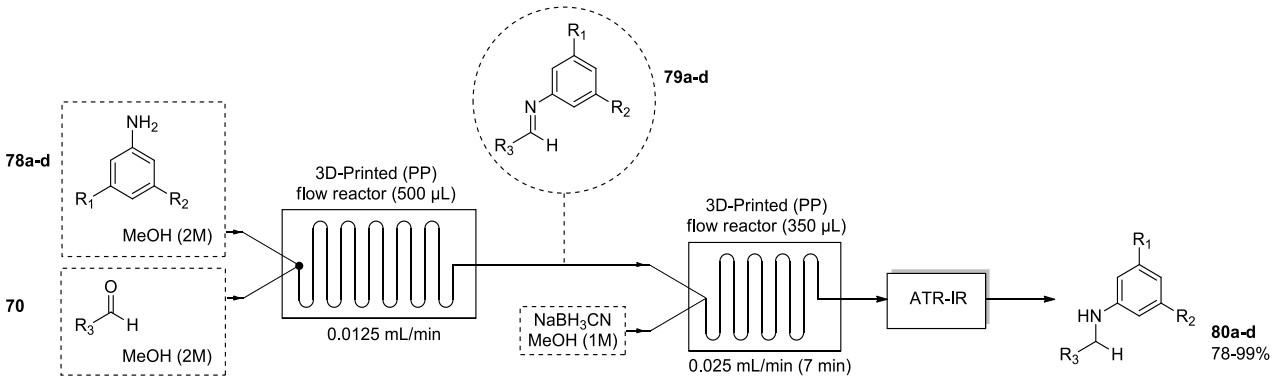

Scheme 24: Two step reaction for the synthesis of secondary amines using two 3D-printed PP flow reactors with different reactor volumes (V_R).

The reactor design can be varied depending on its use in chemical synthesis. In the work shown by Rudolf von Rohr, SLS or selective laser sintering technology has been employed in the fabrication of designed porous structure reactors (DSPR) static mixers [102]. The inner core of such reactors consist of a negative imprint of overlapping spheres fitted within a stainless steel tube (**Figure 26A**). Such complex intricacies in design render it best suited for fabrication using SLS 3D-printing. The internal structure is 200 mm long, ID of 7 mm and an overall porosity of 84%. The reactor was first coated with an aluminium oxide–zinc oxide base layer and subsequently impregnated with a

solution containing palladium nanoparticles for its use in hydrogenation reactions of 2-methyl-3-butyn-2-ol (MBY) to 2-methyl-3-buten-2-ol (MBE) under solvent-free conditions.

Similarly, catalytic static mixers (CSMs) have been fabricated using EBM as seen in the work presented by Hornung and co-workers [103]. An Arcam A1electron beam 3D-printer was used to fuse metal powders of either TiAl64V at 730 °C or cobalt-chrome at 850 °C in a layer-by-layer manner building the three dimensional object. This was followed by catalyst deposition by either electroplating or cold spraying with platinum(0) and nickel(0) to carry out the hydrogenation reaction of methanolic solutions of alkenes and carbonyl compounds with conversions ranging from 90-100% in 4.5-6.5 minutes.

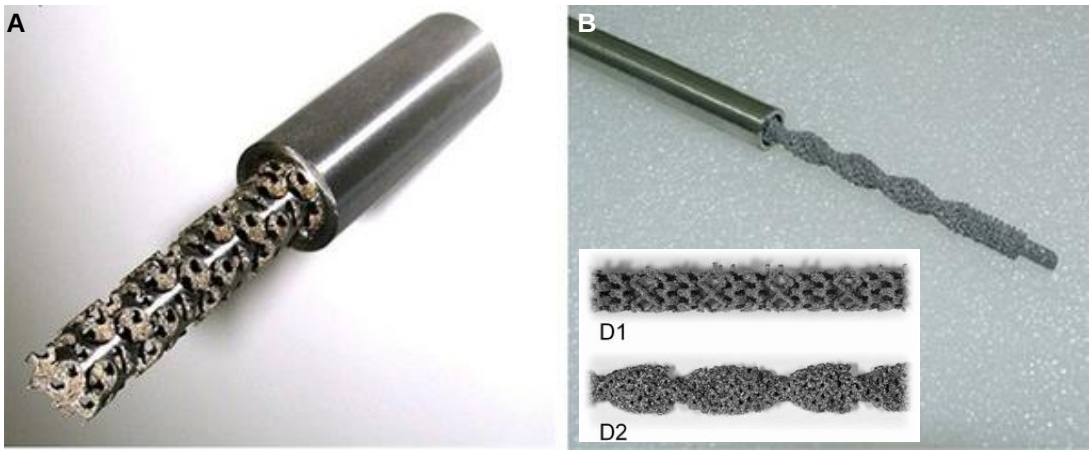

Figure 26: A) Uncoated DSPR showing internal structure used in hydrogenation reactions; **B)** CSM fitted inside tube with internal structure optimised for laminar mixing; (**B** insert) Zoomed images of D1 and D2 internal structure.

Such reactors have been used in the hydrogenation of many functional groups such as alkenes, alkynes, carbonyls, nitro- and diazo-compounds, nitriles, imines and halides, demonstrating their versatility. The selectivity can also be predefined as pressure changes within the system can influence alkene or alkane formation [104].

Christie reported using SLA printing to fabricate a reactor (RD1) or flow cell (**Figure 27A**) that could be housed in the DAD (diode array detector) compartment of an Agilent 1100 series HPLC system for in-line spectroscopic

measurements [105]. It was made from a polycarbonate based photoresin and included a 1.5 mm cylindrical channel and a reaction volume of 2.8 mL. Its external geometries mimicked the internal dimensions of the DAD compartment. It was connected to a 5 mL stainless steel coil in one thermostatted column compartment module of the HPLC and used to analyse the conversion of (*R*)-(−)-carvone **81** to its corresponding semicarbazone **82** using semicarbazide and sodium acetate (**Scheme 25**). In order to determine the optimum conditions for reaction residence time and temperature, a macros software was developed that allowed automated control over the pumping, temperature controlled column and detector modules by accessing the graphical user interface Chemstation software. Using this program, the optimum conditions for the reaction were found to be 69 °C and 0.27 mL/min.

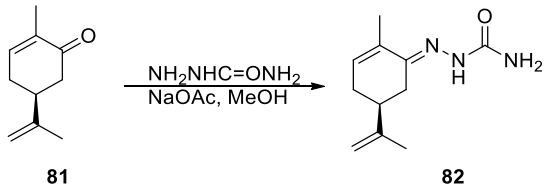

Scheme 25: Synthesis of semicarbazone **82** from (*R*)-(−)-carvone **81**.

Another reactor (RD2) was designed to sit in one of the two column compartment modules, leaving the potential for in-line separation if required. This reactor aimed to mimic the coil and required a material capable of handling the high temperature and pressure conditions observed in the system. The 100 mm long rectangular reactor was SLS printed using Ti6Al4V alloy powder and featured circular channels with an ID of 2 mm and a total reaction volume of 10 mL (**Figure 27B**). This newly printed reactor replaced the stainless steel coil and was positioned in the thermostatic control unit of the HPLC system. The reaction took place in this heated device by pumping solutions of the starting materials at optimal conditions of 0.24 mL/min when heated to 79.6 °C as determined by the software. Again, the analysis took place in the SLA printed flow cell in the DAD compartment of the HPLC machine. The third reactor design (RD3) aimed to replace the SLA printed flow cell with an SLS printed one thus allowing a larger range of reagents and solvents to be used in the system. Again, Ti6Al4V alloy powder was used to

fabricate the flow cell featuring in built windows, a 2 mm internal cylindrical channel and a total reaction volume of 0.6 mL (**Figure 27C**). The device was connected to the system as previously done and semicarbazone formation was investigated. In this manner, the group showcased very elegantly a reaction using a 3D-printed device, its optimization using a software developed in house and its analysis using a 3D-printed flow cell, all in a single HPLC system.

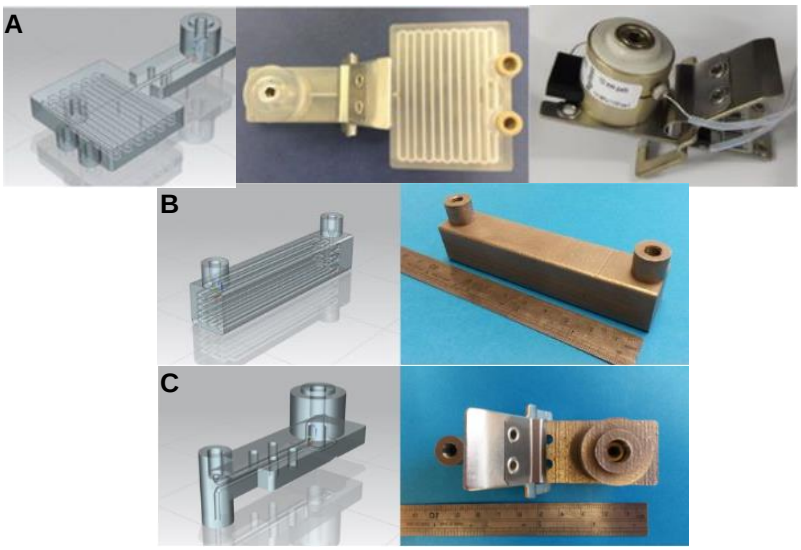

Figure 27: A) (Left) CAD drawing of RD1, (centre) SLA printed RD1 and (right) commercially available Agilent flow cell; **B)** (left) CAD drawing of RD2 and (right) SLM printed RD2; **C)** (left) CAD drawing of RD3 and (right) SML printed RD3.

In 2017 Puglisi and Benaglia demonstrated the use of 3D-printing in the synthesis of (1*R*,2*S*)-metaraminol, (1*R*,2*S*)-norephedrine and (1*R*,2*S*)-methoxamine by combining a catalytic and stereoselective Henry reaction with a hydrogenation, all performed under flow conditions [106]. Initially reactors were fabricated using FDM printing technology in HIPS, PLA and nylon all differing in their internal geometries. The Henry reaction between the aromatic aldehyde **70** and nitroethane **83** in the presence of a copper catalyst composed of $Cu(OAc)_2 \cdot H_2O$ and an aminopyridine camphor derivative was investigated first in batch then in the PLA reactor in flow where it was optimized. The optimum conditions for the nitroalcohol formation from this 1.41 × 1.41 mm PLA reactor with a total volume of 1 mL was found to be -20 °C

when the residence time was 30 minutes in the presence of 5% catalyst. Such conditions gave high yields and enantioselectivity with good diastereoselectivity. In the next step the nitroalcohol **84** was reduced to the corresponding aminoalcohol **86** by using an H-Cube apparatus with a 10% Pd/C cartridge at 30 °C for 2-2.5 hours. Stereochemical integrity was retained in all cases. In a complete two step flow-based setup towards the synthesis of norephedrine, previously optimized Henry reaction conditions were utilized in the 3D-printed PLA reactor and the solution was passed through a pad of silica followed by a washing step with ethanol to remove the catalyst complex. 30 equivalents of acetic acid was added to this solution prior to the second hydrogenation step affording the product in the acetic salt form **85**. On treatment with ammonium hydroxide, 1,2-aminoalcohol **86** was isolated in a 90% yield 70:30 *anti*:*syn* ratio and a 78% ee for the major isomer (*anti*). A device incorporating the silica pad and reaction channels was also fabricated and the reaction was repeated giving the nitroalcohol in 96% yield, 65:35 *anti*:*syn* dr and 83% ee (*anti*).

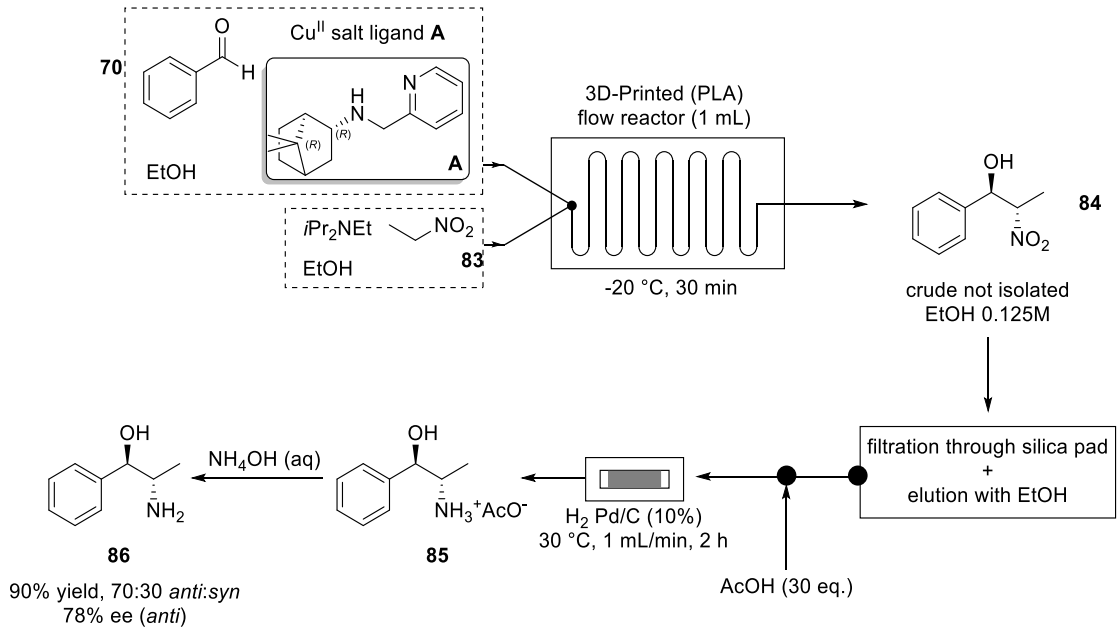

Scheme 26: Multistep reaction sequence for the synthesis of 1,2-amino alcohols **86** using 3D-printed PLA reactor.

1.5 Heterocyclic Synthetic Targets

There are a plethora of worthwhile synthetic targets available to any research programme, but this present thesis focuses on compounds that are related to biologically active natural products whose structures are synthetically challenging and whose core structures can be found in a number of therapeutically active heterocycles - either used commercially as medicines or whose effects have been investigated in a number of therapeutic areas. Compounds and structures of interest are shown below (**Figure 28**), with an emphasis on the natural products based on the lycorane, erythrina and artemisinin families and the bicyclic core structures of panadiplon **94** and praziquantel **95**. A short number of previous synthetic routes of each class will be discussed in the following sections.

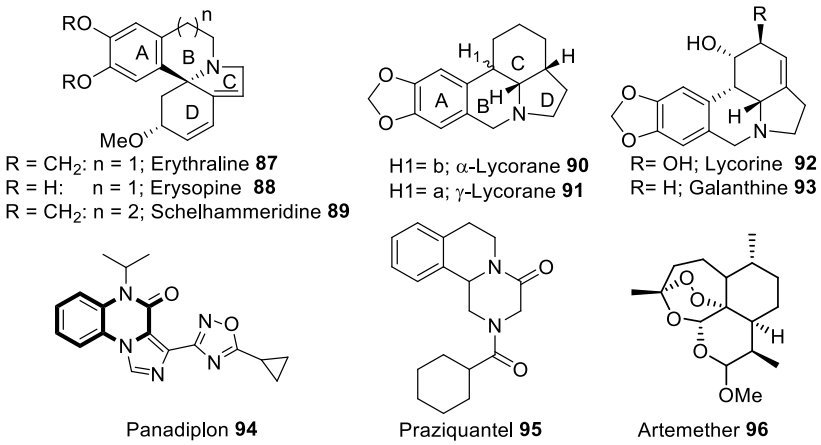

Figure 28: Heterocyclic Synthetic Targets.

1.5.1 Bicyclic Heterocycle Ring Formation Relating to Lycorane and Erythratin

Heterocycles based on indole and substituted hydroindole derivatives are found in an array of natural products and have been heavily exploited in medicinal chemistry due to their potent and wide-ranging biological activities [107] [108] [109]. Examples of natural product alkaloids incorporating this bicyclic motif include the erythrina and lycorane alkaloid families (**Figure 28**) which display potent and wide ranging biological activities[107-113]. Erythrina derived compounds display anxiolytic, anticonvulsant, sedative, antidepressive and antiepileptic effects[114-118], whilst lycorane derivatives display central nervous system effects, acethylcolinesterase inhibition and antimalarial, analgesic and anti-inflammatory activity[119-122]. These alkaloids have also been shown to display significant antiproliferative activity in various cancer cell types including melanoma, multiple melanoma, leukaemia, carcinoma, lymphoma, glioblastoma and non-small cell lung cancer[123-128].

Due to their potent and wide ranging activities and their associated structrual complexity, they have accordingly attracted significant efforts towards their syntheses[112][129-178], including radical cyclisation, aminocyclisation, intramolecular addition reactions and several metal-catalysed amidations amongst others[179-184]. Despite the structural diversity of both classes of compound and the wide array of synthetic methods used in their syntheses, many have focused on the synthesis of the dihydroindolone core **97**, due to its ready elaboration to either of the CD ring core structures of erythratin or lycorane (**Figure 29**)[135-143][179-186]**.**

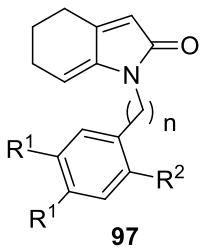

97

Figure 29: The dihydroindolenone **97** intermediate used in the synthesis of both lycorane and erythratin.

Some of the previous routes to the bicyclic dihydroindole CD cores of these compounds have focused on nickel-promoted radical cyclisation of vinylic and allylic trichloroacetamides using $Cu(OAc)_2$ as an oxidant as shown below (**Scheme 27**). Cyclisation of the trichloroacetamide **98** in the presence of nickel and acetic acid in refluxing *t*-butanol resulted in dichloro-cyclised compound **99**. This was subjected to $Cu(OAc)_2$ forming intermediate **100**, which in the presence of Cu (I) in AcOH formed hydroindolone **101** as a major component along with oxindole **102** as a by-product. Generally, most approaches use a sequential oxidation-reduction method to obtain the pyrrolidine ring, however this unique method uses an oxidant and reductant in the same reaction [110].

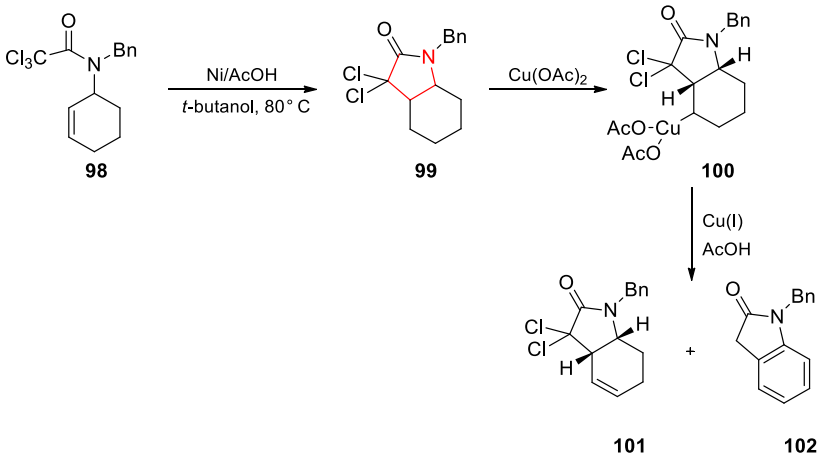

Scheme 27: Radical cyclisation of compound **98** resulting in the pyrrolidine **99**.

Wai Kean Goh provided an example of using synthetic natural products as building blocks in more complex molecules. Using this simple method a large number of analogues were produced. Reaction of benzofuranone **103** with benzylamine resulted in hydroxyl-dihydroindolone **104**. An acid mediated elimination followed by bromination formed 7-bromoindolone **105**. Bromide **105** was then subjected to Suzuki-Miyaura coupling to form a series of related compounds [111] which could then be applied to molecular investigation (**Scheme 28**).

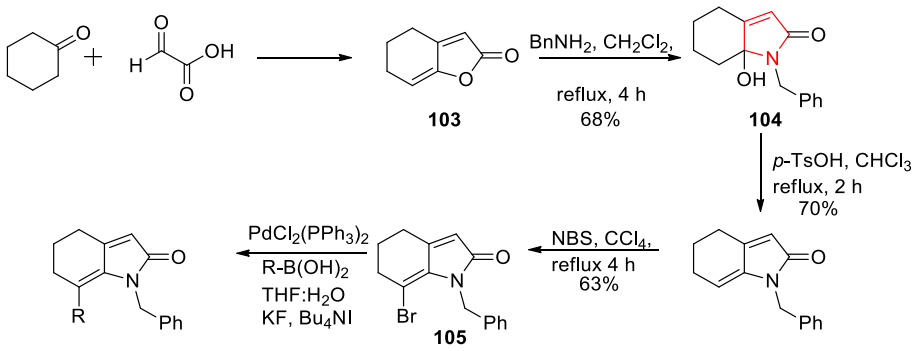

Scheme 28: Synthesis of dihydroindolone **104** from benzofuranone **103**.

1.5.2 Quinoxalinones

Quinoxalines and quinoxalinones belong to a class of benxodiazines with two nitrogen heteroatoms in the 1 and 4 positions respectively. They represent a class of biologically active molecules showing antimicrobial activity against bacteria like *Staphylococcus aureus, Proteus vulgaris, Escherichia coli*, etc; antitubercular activity against *Mycobacterium tuberculosis*; antiviral activity against HSV-1 (herpes simplex virus type 1) and even inhibition of HIV-1 RT or human immunodeficiency virus 1 reverse transcriptase; antifungal activity against *Candida albicans* and antiprotozoan activity against *Entamoeba histolytica* and the malarian parasite *Plasmodium falciparum* [112]. The quinoxalinone core **107** is also found in compounds such as Panadiplon **94**, a $GABA_A$ partial agonist, neuroprotective agent YM827 **106**, AMPA antagonists, and various anti-HIV-1 RT inhibitors [113] (**Figure 30**). 2-Fluoro-1-nitrobenzene **108** has frequently been used as a starting point to synthesize quinoxalinones due to its low cost and ease of use. A few strategies in which such molecules and derivatives have been synthesised in the literature are described below.

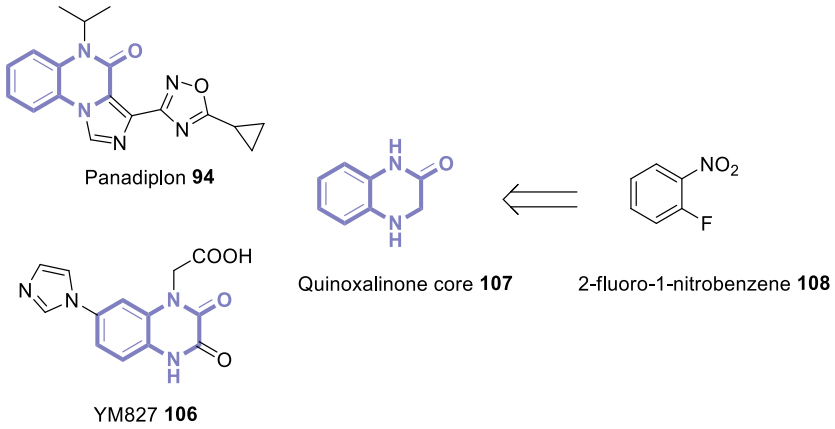

Figure 30: Panadiplon showing quinoxalinone core; 2-fluoro-1-nitrobenzene **108** used as a starting material for synthesis of such structures.

1.5.2.1 Synthesis of Quinoxalinones from solid support

The synthesis of quinoxalinones from 2-fluoro-1-nitrobenzenes involve two basic steps: (i) substitution of the halide with a nucleophile and (ii) reductive cyclisation. The use of solid phase supports (MBHA or *p*-methylbenzhydrylamine resin) to synthesize dihydroimidazolyl dihydroquinoxalin-2(1*H*)-ones **110** has been described by Acharya and colleagues (**Scheme 29a**) [114]. They describe the selective acylation of the primary amine in the diamine formed by the reduction of a resin bound amino acid amide with 4-fluoro-3-nitrobenzoic acid. Treatment with $POCl_3$ resulted in the formation of the dihydroimidazole derivative through an intramolecular dehydrative cyclisation and formation of an *in situ* imidoyl chloride intermediate. The displacement of the aryl fluoride with an amino acid methyl ester followed by the alkylation on the dihydroimidazoyl moiety afforded compound **109**. A reduction of the aromatic nitro group with tin (II) chloride dihydrate followed by the intramolecular cyclisation and cleavage from the resin using anhydrous HF yielded the dihydroimidazoyl dihydroquinoxalin-2(1*H*)-one **110** in moderate yields over the several steps.

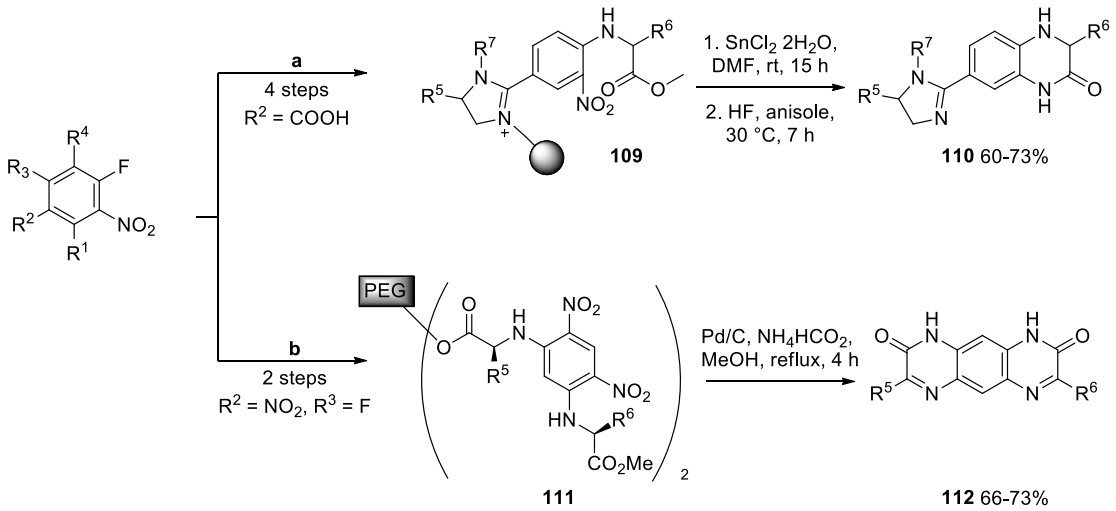

Scheme 29a,b: Synthesis of quinoxalinones from solid supports.

Poly(ethylene glycol) 6000 (OH-PEG_{6000}-OH or PEG) supported amines have been used in substitution and tandem reductive cyclisation reactions in an attempt to synthesize bioactive quinoxalinones **112** (**Scheme 29b**) [115]. The Fmoc-L-amino acids were attached to the soluble polymer support using *N*,*N'*-

dicyclohexylcarbodiimide (DCC) as coupling agent and 4-dimethylaminopyridine (DMAP) as catalyst using microwave irradiation. An incubation with a 10% solution of piperidine produced the free PEG-tagged L-amino acids to which an S_NAr reaction with 1,5-difluoro-2,4-dinitrobenzene and a second with amino acid methyl ester hydrochloride salts yielded compound **111**. The next steps were a reduction of the aromatic nitro group, cyclisation and the cleavage off the PEG support. This was done using a catalytic amount of Pd/C along with ammonium formate in refluxing methanol to produce the pyrazino[2,3-g]quinoxalindiones **112** in good yields.

1.5.2.2 Synthesis of Quinoxalinones in solution

The room temperature substitution reaction of the nitrofluorobenzene derivatives with α-amino acids and diisopropylethylamine (DIEA) have been used to generate the respective S_NAr products **116** as shown below (**Scheme 30b**) [116]. The reaction of ammonium hydroxide in water with this product was used to carry out the substitution of the second fluorine followed by a catalytic reduction of the nitro group and cyclisation using wet Pd/C to produced the qionoxalinone derivative 6,7-diamino-2-quinoxalinols **117**. In the same manner 7-aminoquinoxalin-1(2*H*)-one-3-carboxalate **115** was obtained by the substitution of the nitrofluorobenzene derivative with **113** giving the S_NAr product **114**, followed by an intramolecular reductive cyclisation (**Scheme 30a**) [117].

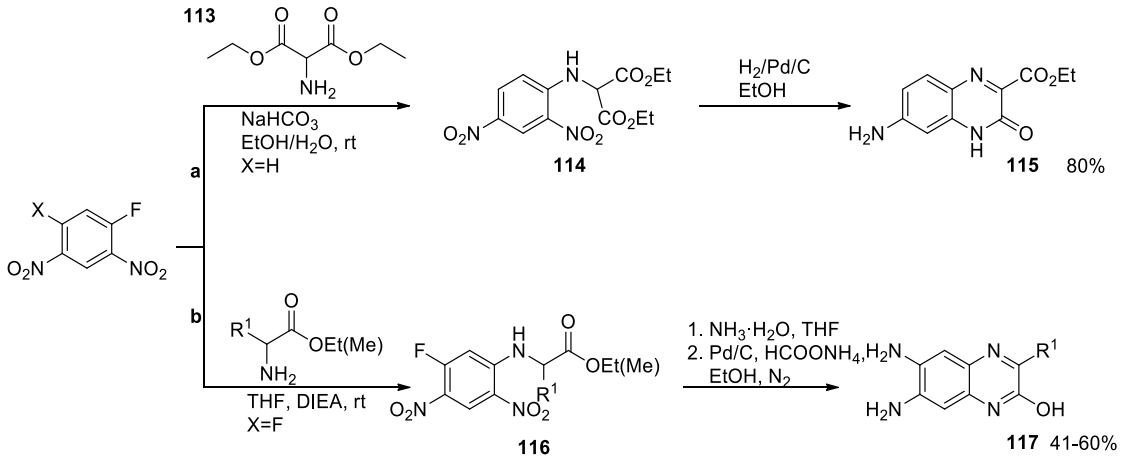

Scheme 30: Synthesis of quinoxalinones in solution.

Pyrrolo[1,2-*a*]quinoxalines **119** were generated in a one-pot process by reacting pyrrole-2-carboxamide **118** with 1-chloro- and 1-fluoronitrobenzenes in excellent yields [118]. This transition metal-free process of regioselective synthesis is another useful approach used to access to the quinoxalinone core (**Scheme 31**).

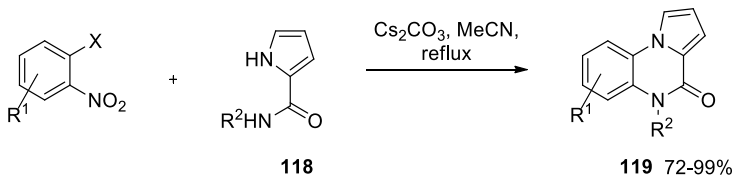

Scheme 31: One-pot synthesis of pyrrolo[1,2-*a*]quinoxalines **119**.

2.0. Project Objectives

As outlined in the introductory chapter, continuous flow chemistry and 3D-printing are two separate emerging and exciting technologies which have huge potential to influence the way in which we carry out chemical reactions and will change our approaches towards these in the future. As such, this thesis aims to combine these two separate areas and demonstrate that they can be successfully harnessed and combined in a chemical laboratory to access a number of challenging chemical targets in an efficient manner. The targets selected and outlined in the introduction were chosen due to their structural complexities and synthetic challenges, as any published combined use of these technologies would need to demonstrate that this methodology is robust and applicable to complex targets. This present thesis therefore aims to demonstrate that they can be successfully combined and used to access these. The following sections therefore detail the necessary steps that we envisaged to achieve this.

The first part of our planned research program was designed to explore the 3D-printing of inert chemical plastics and to develop small reactors that would be suitable for continuous flow chemistry to replace glass column reactors (**Figure 31**).

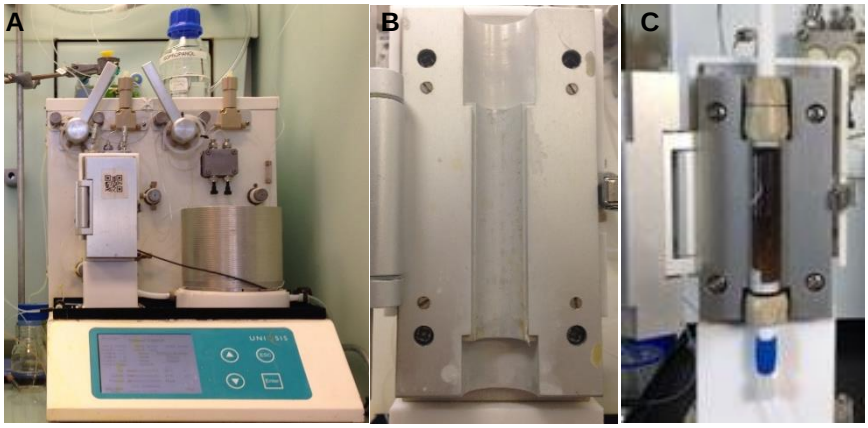

Figure 31: A) Uniqsis flow chemistry apparatus setup; **B)** Housing for glass reactor; **C)** Glass reactor fitted inside existing setup.

The first phase of the research program would therefore focus on examination of the flow reactors available in the Hilton laboratory and investigate the design and incorporation of a 3D-printed reactor into the flow chemistry setup.

The second aim of the research program was designed to select appropriate challenging chemical reactions to understand the scope of the designed reactor and to see where its limits lay. In this manner, we envisaged that we would ultimately use polypropylene (PP) as the base material of our printed reactor and as such want to explore the solvents and reagent scope tolerances of our device.

This section of the thesis would therefore focus on chemically challenging S_NAr reactions. In this manner we wanted to explore challenging temperatures and solvents such as DMF which have not previously been used with printed reactors. The planned reactions focus on reaction of an amine with an unreactive *o*-fluoronitrobenzene with DMF as solvent as shown below (**Scheme 32**).

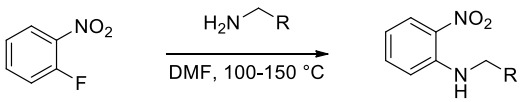

1-fluoro-2-nitrobenzene **108**

Scheme 32: Proposed S_NAr reaction to explore reactor utility.

Once complete, the next phase of the research program will investigate the potential of the reactor with a focus on more complex chemistries involving corrosive reagents and challenging synthetic targets. In this manner we will focus on chemistries developed in the Hilton group looking at developing chemical routes towards the core structures of the natural products erythratin and lycorane and the planned synthetic route is outlined below (**Scheme 33**).

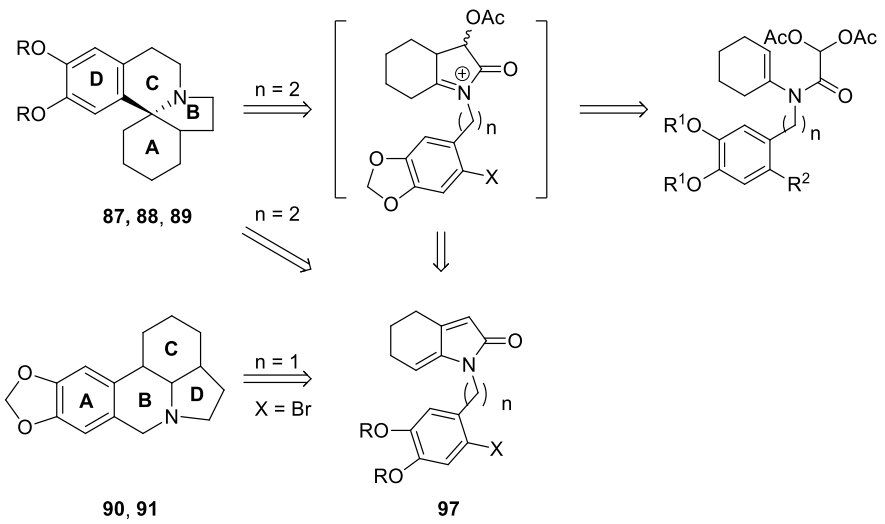

Scheme 33: Proposed synthetic route to the lycorane **90**, **91** and erythratin **87**, **88**, **89** cores.

In each case, the reaction involves ready access to the bicyclic dihydroindolenone core **97**. Previous synthetic endeavours in the group have focused on batch methodology to access this core and this thesis will therefore focus on expanding this chemistry and translate it to a flow based approach with an emphasis on the synthesis of a range of analogues relating to this key structure.

We also intend to investigate a new route towards the synthesis of quinoxalinones using a flow chemistry based setup. In this manner we intend to develop a novel route to compounds related to panadiplon **94** and our proposed route is outlined below (**Scheme 34**).

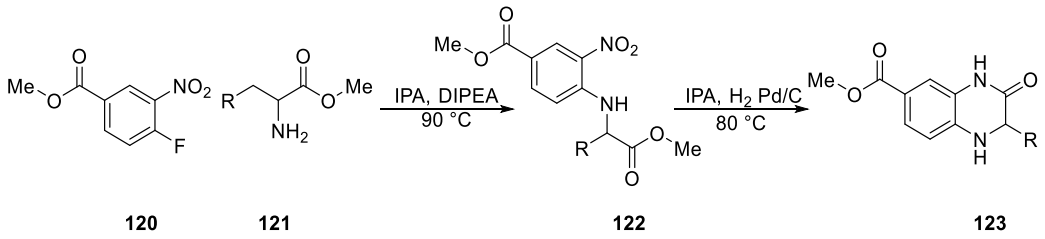

Scheme 34: Proposed synthetic route to quinoxalinones.

In this manner, the quinoxalinone core can readily be accessed *via* reaction of an amine **121** with the fluoronitro compound **120** as shown to give the S_NAr addition product **122**. The next step of the reaction will rely on a reductive

cyclisation where upon hydrogenation, the nitro group is reduced to an amine and can cyclize onto the intramolecular ester to give the six-membered ring **123**. Using this methodology, there exists the possibility that we will be able to link two separate flow reactions into one, whereby the intermediate ester can be passed through the H-cube hydrogenation reactor to provide a facile process route to biologically active heterocycles.

The next phase of our research involved the development of a 3D-printable formulation that would utilize SLA printing and develop that into a catalytic device that could be used to assist batch chemistry experiments. This device would be adapted to fit a magnetic flea and can be printed from photopolymers and a small concentration of photoinitiator (**Figure 32**). In the first generation formulation, Hantzsch dihydropyridines would be synthesised by the incorporation of tosic acid in the stirrer bead device.

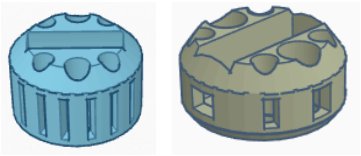

Figure 32: STL drawings of first (left) and second (right) generation stirrer bead devices.

The formulation would be further optimized and two other catalytic stirrer bead devices will be shown. One would incorporate palladium(0) tetrakis(triphenylphosphine) into its formulation and Suzuki coupling reactions in both RBF experiments and microwave experiments will be shown. The second device would introduce Lewis-acid yttrium triflate into its polymer matrix and the protection of carbonyl groups using dithiols will be demonstrated (**Figure 33**).

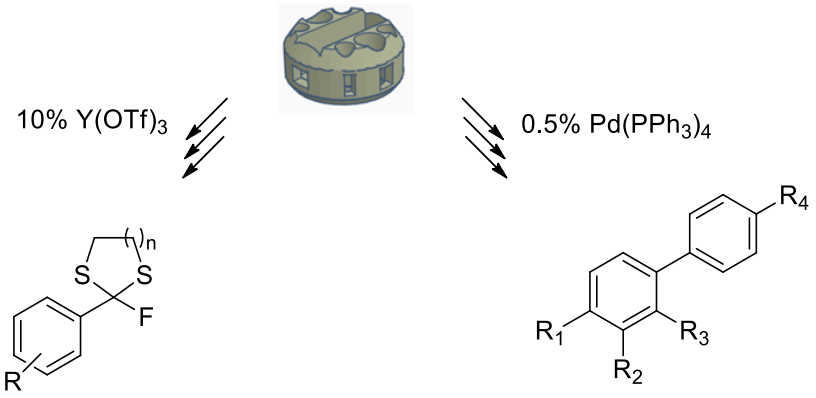

Figure 33: Catalytic stirrer bead with yttrium triflate producing dithianes and with palladium(0) tetrakis(triphenylphosphine) producing biphenyls.

The optimized blank formulation would also be used to print a circular hotplate-adapted reactor that could be used with the existing flow reactor by the incorporation of screw threads that fit standard ferrules (**Figure 34**). Using this device, a flow based photochemical C-H functionalization of indoles will be investigated to demonstrate the utility of the device and also its limitations.

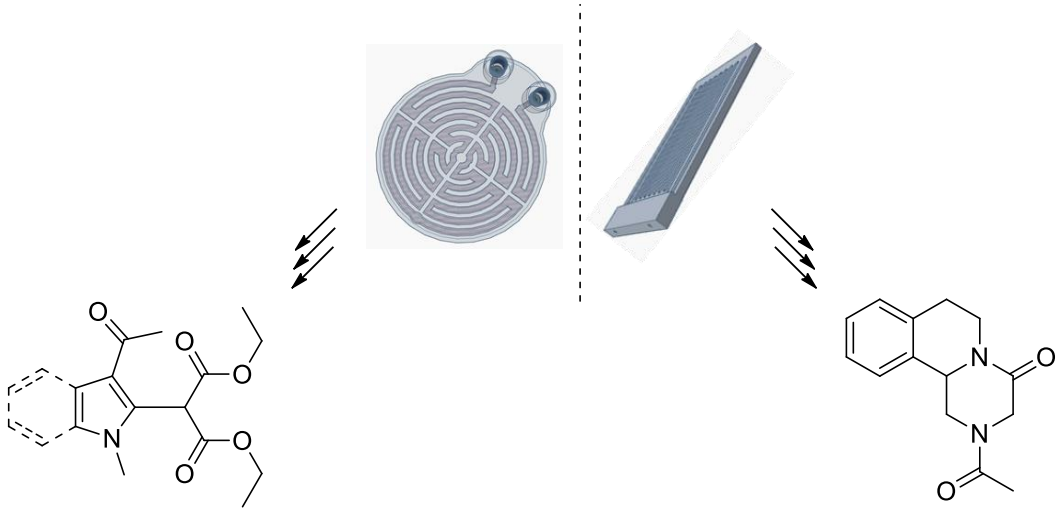

Figure 34: (Left) STL drawing of circular disc reactor used in C-H functionalization photochemistry; (Right) Chip reactor tested in photo-decarboxylation reaction in Praziquantel synthesis.

The last part of our research would involve using all the concepts developed and combine them into a synthetic route for an API. We intend to choose praziquantel as a target due to its moderate complexity and will devised a

synthetic route that could be adapted to flow and could potentially use our devices.

3.0. Results and Discussion

3.1 Design of the column reactor and printing

As outlined in the previous section, the initial aim of this research program was to design and 3D-print an inert column reactor which could be combined into an existing continuous flow-chemistry setup. Given that we wished to integrate our reactor with the existing commercial flow chemistry system available in the Hilton laboratory, we first examined the heating unit of the Uniqsis FlowSyn® reactor. There are two reactor modules built in the system: a coil module and a mixed block module. The block module can be fitted with glass tube (packed bed) or chip reactor.

By using a freeware web-based application- Tinkercad® (Autodesk) software [119], and by measuring the cavity of this heating block module, an approximate 3D structure was generated (**Figure 35**). This was designed by combining cylinder shapes and an internal spiral which was later made into a 'hole' when the individual shapes were combined. Columns were designed to be 125.64 mm high and 23.71 mm at their widest point to fit within the reactor column compartment.

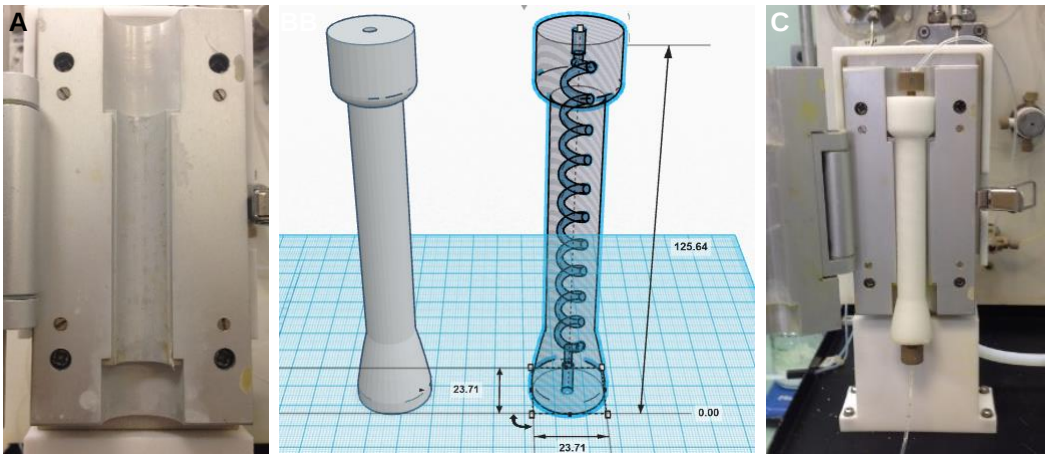

Figure 35: A) Housing for glass reactor; **B)** Design of the reactor showing internal coil in CAD software; **B)** 3D-Printed PP reactor fitted in the reactor space on the Uniqsis FlowSyn.

The structure was modified slightly by adding a slope in the lower section of the reactor and small curves in its upper section in order to allow for easy printing and avoid any need to print support structures. An internal coil close to the edge of the surface was designed such that the maximum possible path length could be generated in the existing structure. This would allow for facile heat transfer to take place into the cavity where the reaction mixture would flow. If the coil was too close to the outer edge, solvent would potentially leak through the plastic under high temperatures. In order to solve this problem, the infill percentage in the print settings was changed to 100% and the number of shells increased to ensure adequate enclosure of the reactor coil.

Once designed, the file was exported in the STL (standard tessellation language) format to Cura software (**Figure 36**). This program was used to manipulate the print settings for the Ultimaker printer, which was used to print the reactor.

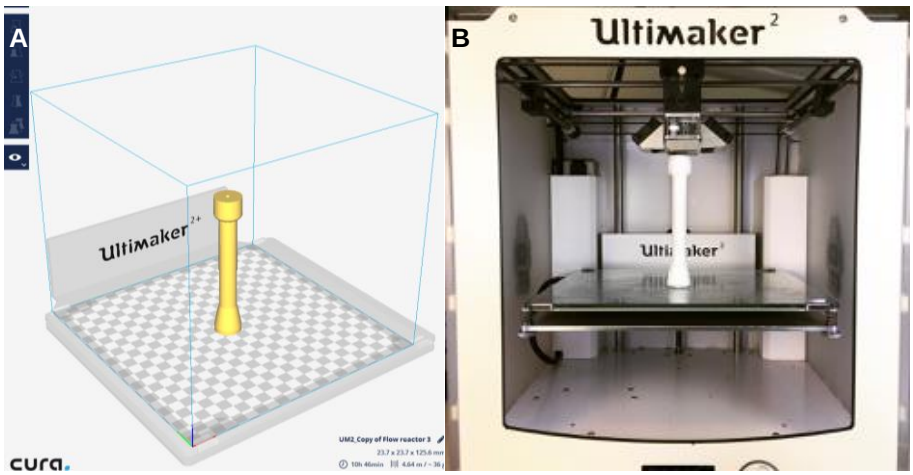

Figure 36: A) STL file of column reactor to Cura software; **B)** Image showing 3D-printed column reactor in Ultimaker printer.

Table 2: Print parameters for PP reactor on Ultimaker printer using Cura software.

Quality	Value	Speed	Value
Layer height (mm)	0.1	Travel speed (mm/s)	60
Shell thickness (mm)	0.8	Bottom layer speed (mm/s)	20
Enable retraction	Yes	Infill speed (mm/s)	20
Initial layer thickness (mm)	0.3	Outer shell speed (mm/s)	0
Cut off object bottom (mm)	0.0	Inner shell speed (mm/s)	20
Dual extrusion overlap (mm)	0.15		
Fill	**Value**	**Cooling**	**Value**
Bottom/Top thickness (mm)	0.6	Minimal layer time (s)	5
Fill density (%)	100	Enable cooling fan	No
Material flow (%)	110		

The column reactor was printed in polypropylene (PP) with an Ultimaker 3D-printer. To allow for easy printing, an LDPE (low density polypropylene) board was attached to the build plate and the nozzle height was adjusted accordingly so that it was just above (0.1 mm) the board (**Figure 37A**). Shell thickness was increased to 0.8 mm to ensure no seeping of the reaction mixture through the coil into the body of the reactor. A density of 100% was used in the settings to ensure the reactor maintains a higher heat capacity. The material flow rate was also increased to 110% to ensure that there were no gaps in between layers and that the seal was maintained throughout the print. This also ensures the reactor is solvent resistant and not prone to leakage. The speed at which the extrusion took place to print the layers and shells was lowered to 20 mm/s. The speed was increased however, to 60 mm/s to travel in between layers. Cooling fans are usually employed for prints where distortion is an issue. This occurs when the layers do not have enough time to cool and set. In our case this was not an issue and the fan was turned off. The final and most crucial parameter in the print settings was the temperature at which the PP was extruded. This was set to 215 °C, a much higher temperature than the melting point PP (180 °C). This because the commercially available PP filament used

was 3 mm wide and extrusion with a thicker filament requires an increased temperature to accommodate for an increase in mass at the extruder head.

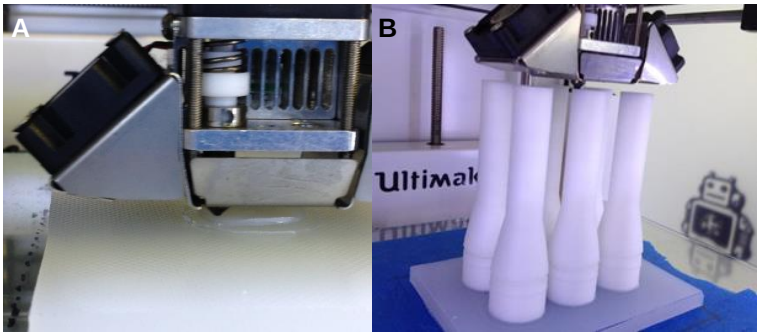

Figure 37: A) Printing of the reactor onto LDPE board; **B**) Printing process of the reactors.

The reactors were printed in groups of 6 in 6 hours (**Figure 37B**). Each reactor has an average polypropylene mass of 21 g with an internal diameter of 2 mm and a theoretical internal volume of 1.6 mL and costs £0.50 to produce making this a cheap alternative to traditional glass reactors. It has a simple design which was chosen depending on the available Uniqsis FlowSyn system. Screw threads suitable for PEEK fittings were tapped into the two ends of the column reactor (**Figure 38**).

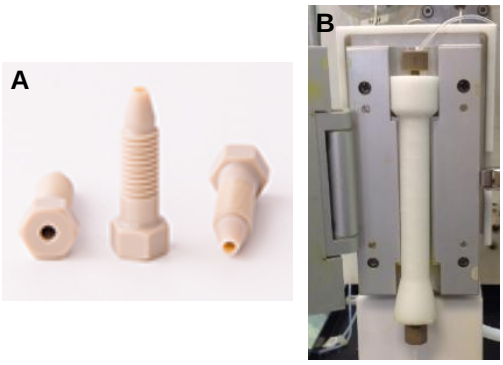

Figure 38: A) PEEK fittings used with reactor showing its screw thread and tubing insert [120]; **B**) PP reactor connected to PEEK fittings through its inlet and outlet.

The reactor was next integrated with the flow system; the inlet was connected to a syringe pump to check that solvent was able to pass through the system. While this was demonstrated to work effectively with no leakage of solvent, the

next phase of the program focussed on the use of the reactor with chemical reactions.

3.2 S_NAr Reactions using the 3D-Printed Coil Reactor

The starting point of our chemistry was to develop a method to perform S_NAr reactions with simple amines in flow using our bespoke 3D-printed reactors. The conditions employed in such reactions were harsh, using polar solvents and high temperatures. With such experiments as a starting point, the limits of our 3D-printed reactors could be sufficiently explored. The unactivated 1-fluoro-2-nitrobenzene **108** and phenylethylamine **124** were used initially for exploration of the chemistry (**Scheme 35**).

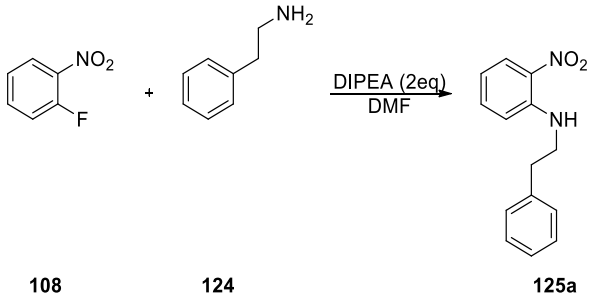

Scheme 35: S_NAr reaction of phenylethylamine **124** with 2-fluoro-1-nitrobenzene **108**.

The mechanism of this reaction (**Scheme 36**) involved nucleophillic addition of the amine *ipso* to the fluoride **126**, resonance stabilization forming the intermediate **127**, rearomatization and displacement of fluoride **128** to give the substituted product **125a**.

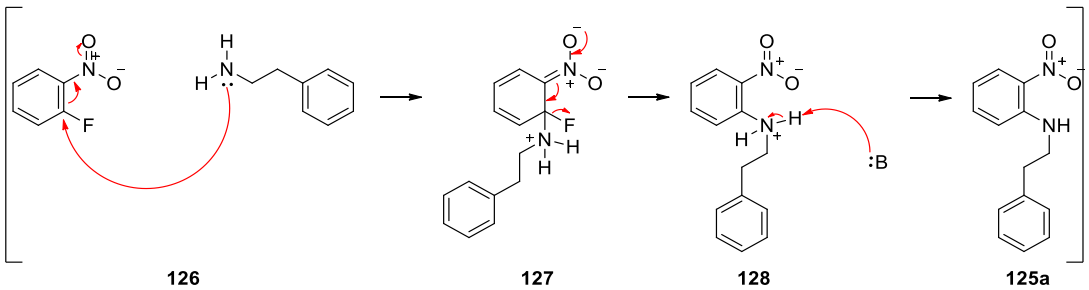

Scheme 36: Mechanism showing S_NAr reaction.

The flow rate of the individual pumps (A and B) in the flow reactor was calibrated at the beginning of each experiment. The volume of solvent in each

solution and the flow rate was set such that the solutions flowing through each pump completed at the same time. This ensured efficient mixing in the flow system and no loss of either starting material. Upon complete consumption of the starting materials in each flask, small amounts of solvent were re-introduced into the flask to ensure no material was lost at the end of each run (**Scheme 37**).

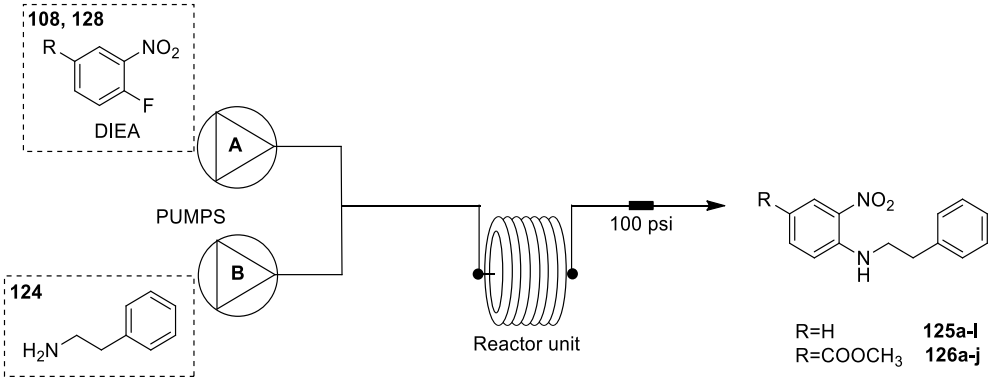

Scheme 37: Schematic representation of S_NAr reaction in flow.

The solution from the flow reactor was collected and concentrated under reduced pressure. The percentage conversion was calculated based on the ^1H NMR spectrum of the crude material. The table below (**Table 3**) shows the optimal flow rates and temperatures for this reaction (**Table 3**, Entry 3) with a residence time of 5 minutes in the printed reactor. They were able to withstand the harsh conditions and maintain the seal with the PEEK fittings as no leakage was observed from the 3D-printed columns.

Table 3: [a] Ratio of peaks of starting material *vs* product compared using ^1H-NMR.Conditions showing optimal flow rates at different temperatures and use of pumps.

Entry	Temperature (°C)	Pump A flow rate (mL/min)	Pump B flow rate (mL/min)	Conv. (isol.) (%)[a]
1	100	1	0.65	21
2	100	0.5	0.32	36
3	150	0.25	0.16	66 (63)
4	150	0.125	0.08	55
5	150	0.16	-	58

Once the conditions had been optimized, a range of amines were used in subsequent reactions and their percent conversions calculated (**Table 4**). When benzylamine was used in place of phenylethylamine, a reasonable reaction conversion (47%, Entry 1) was observed. However, use of electron withdrawing and donating groups on the aromatic ring did not improve the conversion rate and yields remained low (33% and 34%, Entries 2 and 3 respectively). Increasing the number of electron donating groups on the aromatic ring also led to reduced conversion (18%, Entry 6); linear saturated primary amines increased conversion (65%, Entry 8), increasing the unsaturation of linear amines reduced the conversion (57% and 20%, Entries 9 and 10 respectively); electron donating groups on linear saturated amines also showed a reasonable conversion (42%, Entry 5), whilst aniline proved unreactive under the reaction conditions; reaction with cyclohexylamine worked slightly better (34%, Entry 3) indicating that saturation is favoured in this case; secondary amines showed lower conversion (26%, Entry 8). The number of equivalents of amine was also shown to have an effect on the conversion rate, where reactions had higher conversions with 2 equivalents of amine versus 1 equivalent.

Table 4: [a] Reactions carried out at 150 °C with flow rates of 0.25 mL/min (Pump A) and 0.16 mL/min (Pump B). % Conversions with amines showing reaction conditions for the products **125a-l**.

Entry	Product	Amine	Equiv.	Conv. (%)[a]
1	**125b**	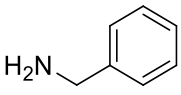	2	47
2	**125c**	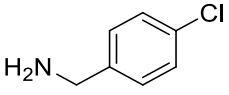	2	33

Entry	Product	Amine	Equiv.	Conv. (%)[a]
3	**125d**	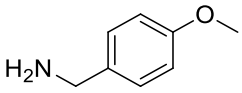	2	34
4	**125e**	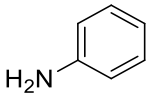	2	0
5	**125f**	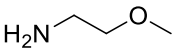	2	42
6	**125g**	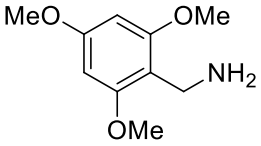	2	18
7	**125h**	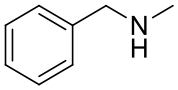	1 2	6 26
8	**125i**	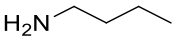	1 2	48 65
9	**125j**	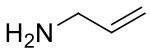	1 2	18 57
10	**125k**	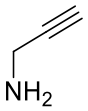	1 2	7 20
11	**125l**	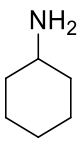	1 2	22 34

In the next series of experiments, the presence of an electron withdrawing group or an activating group on the electrophile was investigated. Methylation of acid **126** with iodomethane **127** afforded the ester **128** in excellent yield (95%). With the ester **128** in hand, the S_NAr reaction was again carried out using a range of amines and the results obtained are shown in **Table 5** (**Scheme 38**).

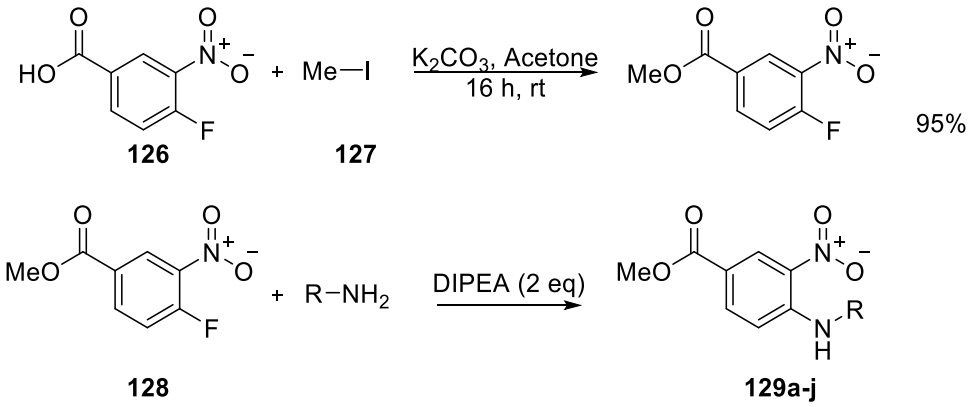

Scheme 38: Synthesis of methyl-4-fluoro-3-nitrobenzoate **128** and its S_NAr reaction with amines to synthesize **129a-j**.

Excellent conversions were seen in reactions with phenethylamine, benzylamine, *p*-chlorobenzylamine and *p*-methoxybenzylamine (100%, 100%, 100% and 97% respectively, Entries 1, 2, 3 and 4). The conversion with aniline was low (24%, Entry 5) but vastly improved over the non-ester containing congener, whilst reaction with *p*-fluoroaniline showed increased conversion (40%, Entry 6) but when *p*-chloroaniline was used, conversion decreased (18%, Entry 7). Linear saturated and partially saturated amines also showed excellent conversion (95% and 100%, Entries 8 and 9); whilst cyclohexylamine again showed low conversion (22%, Entry 10).

Table 5: [a] Reactions carried out with 2 equivalents of amine at 150 °C with flow rates of 0.25 mL/min (Pump A) and 0.16 mL/min (Pump B). % Conversions with amines showing reaction conditions for the products **129a-j**.

Entry	Product	Amine	Conv. (%)[a]
1	**129a**	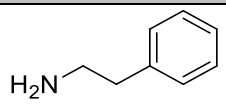	100
2	**129b**	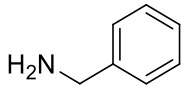	100
3	**129c**	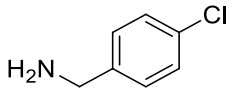	100
4	**129d**	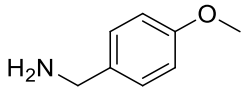	97
5	**129e**	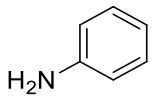	24
6	**129f**	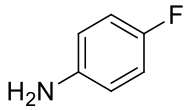	40
7	**129g**	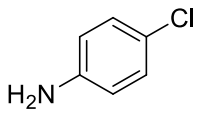	18

Entry	Product	Amine	Conv. (%)[a]
8	**129h**	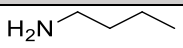	95
9	**129i**	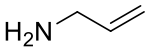	100
10	**129j**	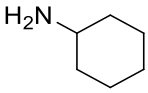	22

3.3 Intramolecular Acylal Cyclisations (IAC's)

After demonstrating the utility of the 3D-printed reactors in the S_NAr chemistry, we decided to explore their scope in the synthesis of the erythrina (**87**, **88**, **89**) and lycorane (**90**, **91**) family of natural products. To contribute to the ongoing research in the area of medicinally active fused bicyclic and heterocyclic compounds, the chemistry involving intramolecular acylal cyclisations (IAC) in flow was investigated. Previous research in the Hilton group described a microwave based synthetic route towards these structures from acylal precursors using 1,2-dichloroethane (1,2-DCE) as a solvent and BF_3 as the Lewis acid which was focused around the development of the hydroindolenone core (**Figure 39**) [121]. We therefore elected to employ these precursors in our testing of the 3D-printed column reactors as we reasoned that the elevated temperatures and corrosive reactants would provide a suitable challenge to explore their utility.

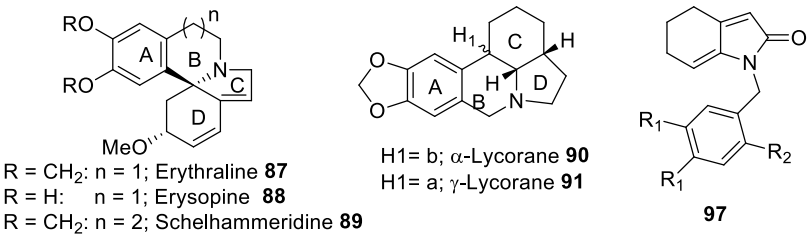

Figure 39: Hydroindolenone intermediate and related structures.

This route described the addition of BF_3 to a solution of the IAC precursors in 1,2-DCE and their reaction in a microwave at 65 °C for 15 minutes. The precursors were synthesised by the addition of benzylamine **69** to the corresponding ketone under Dean and Stark water-removal conditions. The intermediate **131** obtained was subsequently reacted with diacetoxyacetyl chloride **130** and pyridine to give the IAC precursors (**Scheme 39**) as per previously published methodologies [122] [123] [124] [125].

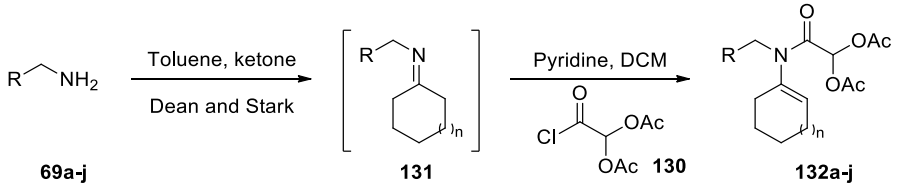

Scheme 39: Synthesis of IAC precursors **132a-j**.

A proposed mechanism of the formation of the bicyclic heterocycles *via* the intramolecular acylal cyclisation shows the co-ordination of the Lewis acid followed by the reaction of the nucleophilic enamine with the oxonium ion giving the bicyclic acetate **134** (**Scheme 40**). This was originally anticipated to be the predominant product obtained from the reaction. However, owing to its unstable nature it underwent loss of a proton to give **135**. Further co-ordination by Lewis acid BF_3 **136** followed by the loss of acetate group **137** and tautomerization generated the dihydroindolone core **133b**.

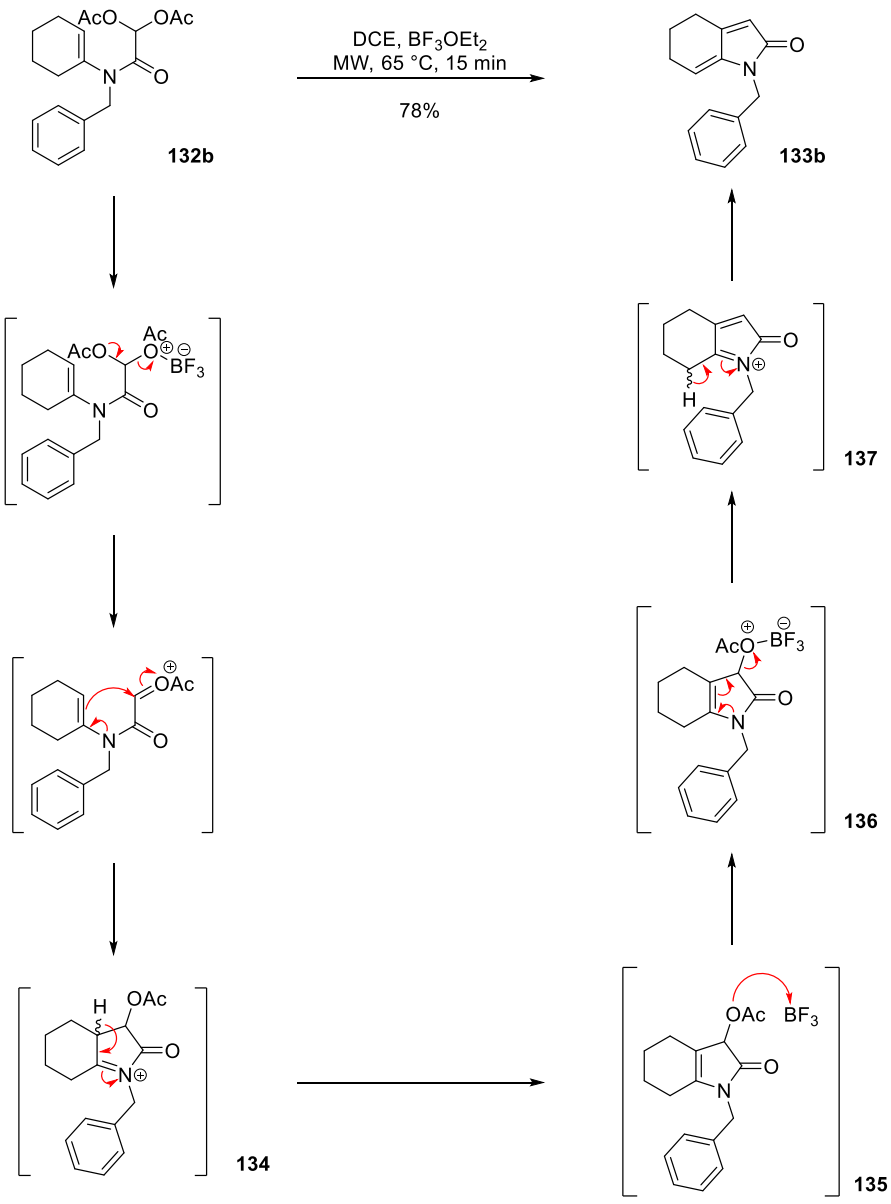

Scheme 40: Proposed mechanism for the formation of **133b**.

We then translated the synthetic route to a flow based protocol using our 3D-printed reactors by slightly elevating the temperature to 80 °C and maintaining a flow rate of 0.1 mL/min [126]. This gave us a residence time of 16 minutes in the flow reactor which had an internal volume of 1.6 mL (**Scheme 41**). This was analogous to the microwave based reactions at 15 minutes reaction time and the slightly elevated temperatures ensured that the reaction was as close as possible to the microwave based conditions.

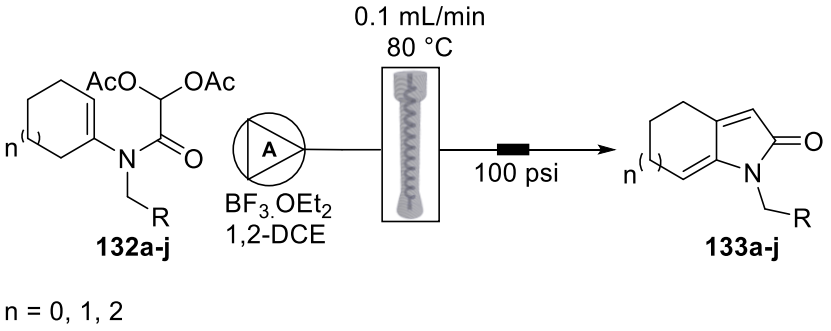

Scheme 41: IAC reaction using 3D-printed flow reactor.

Cyclisation precursors **132a-i** were dissolved in anhydrous 1,2-DCE and $BF_3 \cdot OEt_2$ (5 equiv.) was added. This solution was then passed through a single pump of the flow reactor into a pre-warmed (80 °C) polypropylene reactor at 0.1 mL/min. The tubing exiting the reactor was connected to a 100 psi BPR before collecting in a flask. The scope of this reaction was explored with the synthesis of analogues with a varying ring size in the fused bicyclic product and the incorporation of substitution in the aryl ring.

Table 6: [a] Reactions were carried out at 80 °C with a flow rate of 0.1 mL/min (Pump A). % Conversions with amines showing reaction conditions for the products **133a-j**.

Entry	Cyclisation precursor	Product	Isolated yield (%)[a]
1	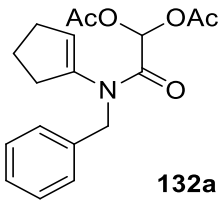 **132a**	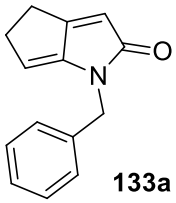 **133a**	34
2	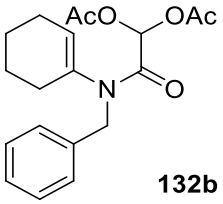 **132b**	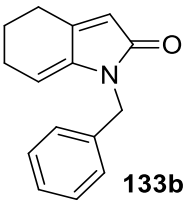 **133b**	51
3	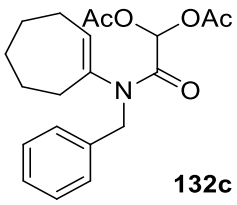 **132c**	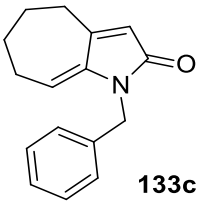 **133c**	70
4	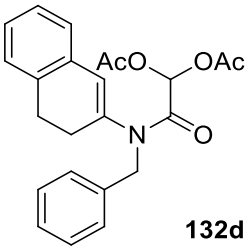 **132d**	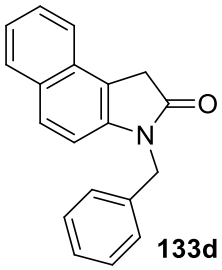 **133d**	43
5	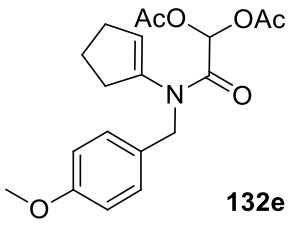 **132e**	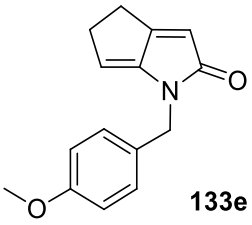 **133e**	13

Entry	Cyclisation precursor	Product	Isolated yield (%)[a]
6	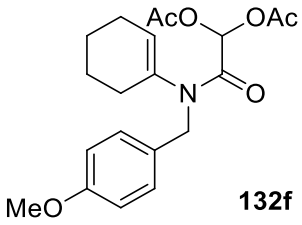 **132f**	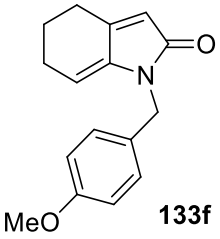 **133f**	61
7	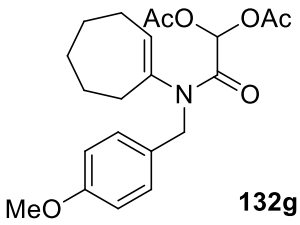 **132g**	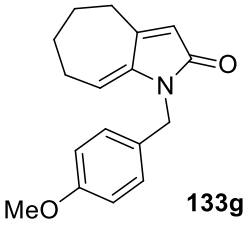 **133g**	47
8	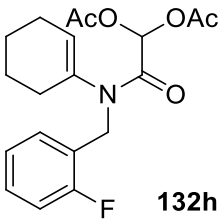 **132h**	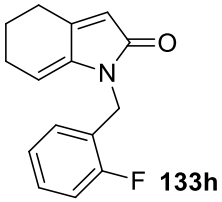 **133h**	40
9	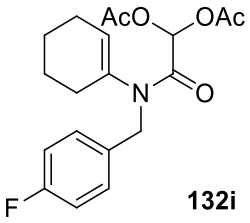 **132i**	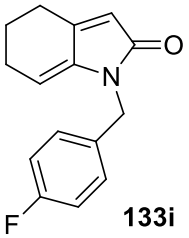 **133i**	77
10	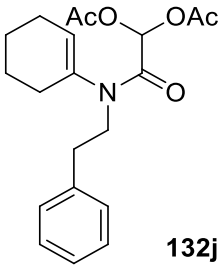 **132j**	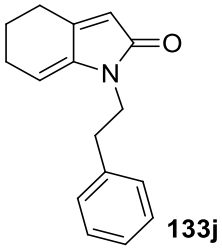 **133j**	39
11	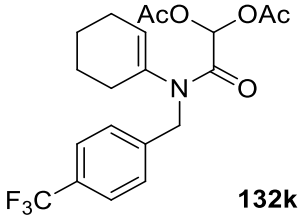 **132k**	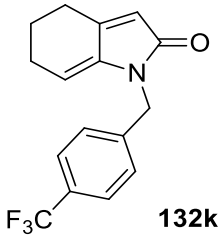 **132k**	37

Entry	Cyclisation precursor	Product	Isolated yield (%)[a]
12	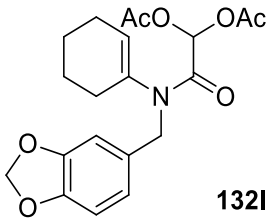 **132l**	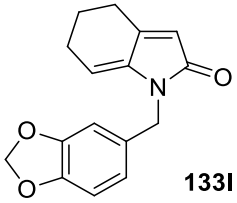 **133l**	85

All cyclisation precursors gave yields ranging from 13-77%. The bicyclic fused and highly strained [3.3.0] ring systems **133a** and **133e** were low yielding (34% and 13%). Compound **133e** with electron donating methoxy group in the *para*-benzyl position was the lowest yielding in the series (13%). This was followed by the *N*-benzyl fused [4.3.0] ring system with the electron withdrawing CF_3 group in *para*- position **113k** yielding 37%. The *N*-phenethyl fused [4.3.0] ring **133j** was also obtained in a low yield (39%). For all other [4.3.0] fused bicyclic ring systems **133i**, **133b**, **133h** and **133f**, the presence of electron withdrawing groups in the *para*-position on the *N*-benzyl ring gave the highest yield (77%) compared to no products where there was no substitution (51%). The presence of the same electron withdrawing group in the *ortho*-position showed a reduction in yield (40%). The presence of electron donating groups on the *N*-benzyl ring in the *para*- position showed a slightly increased yield (61%) for the same heterocycle system. For the [5.3.0] fused bicyclic ring systems **133g** and **133c**, the presence of an electron donating group on the *N*-benzyl ring showed a reduced yield (47%) compared to the product obtained without substitution, which was relatively high yielding (70%). For the cyclisation of **132d**, the original hypothesis was to obtain **133x** (**Figure 40**). However, on detailed analysis of ^1H spectral data, it became obvious that the tricyclic compound with extended conjugation was obtained and in a moderate yield (43%).

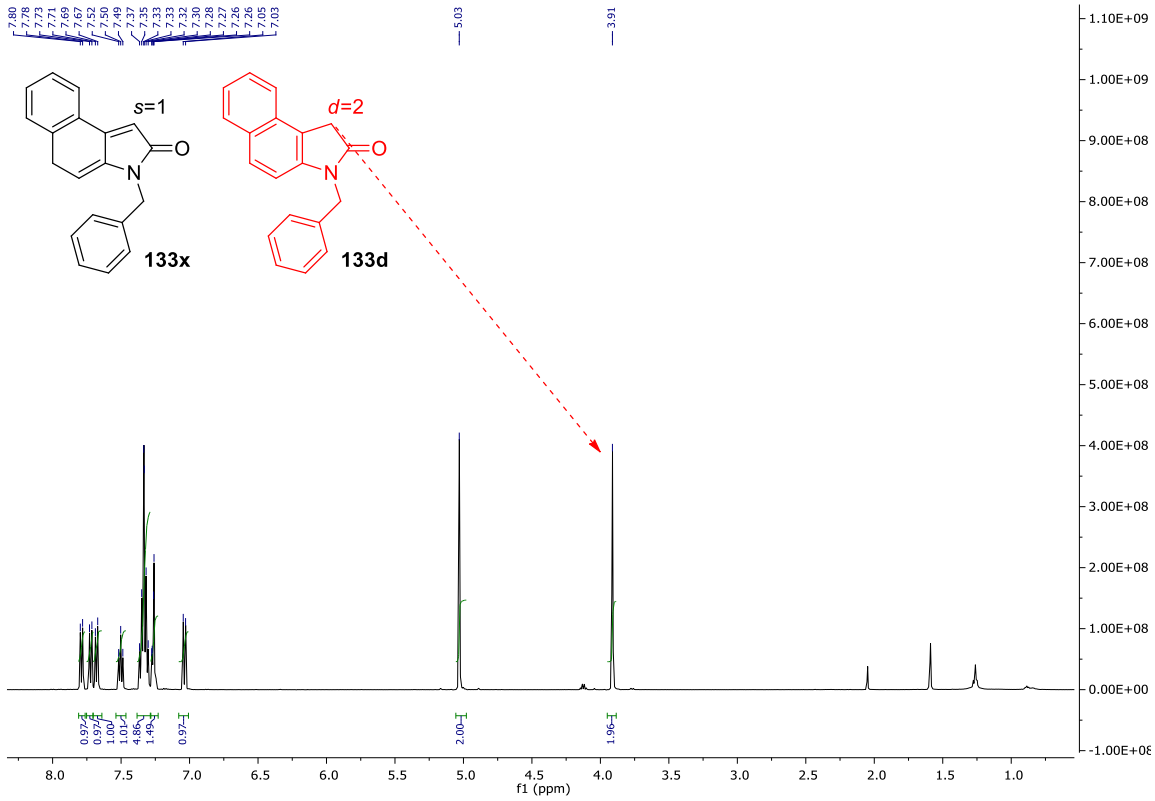

Figure 40: Fused tricyclic compound with extended conjugation.

These results were comparable to the previously reported microwave results [121]. The best yield observed however, was in the cyclisation of compound **132l** to **133l** (85%). This molecule represents an important intermediate in the synthesis of the lycorane family of compounds.

The second part of our research focused on achieving a more complex four ring heterocycle by translating a previously described domino cyclisation process [122] to flow facilitating the formation of the B and C ring of the erythrina core (**Figure 38**, page 75). In a similar manner, the precursors were synthesised *via* the condensation reaction of the substituted amine **138** and the ketone under Dean and Stark conditions. The imine **139** intermediate was immediately reacted with **130** in the presence of pyridine affording the cyclisation precursors **140a-d** (**Scheme 42**) [122].

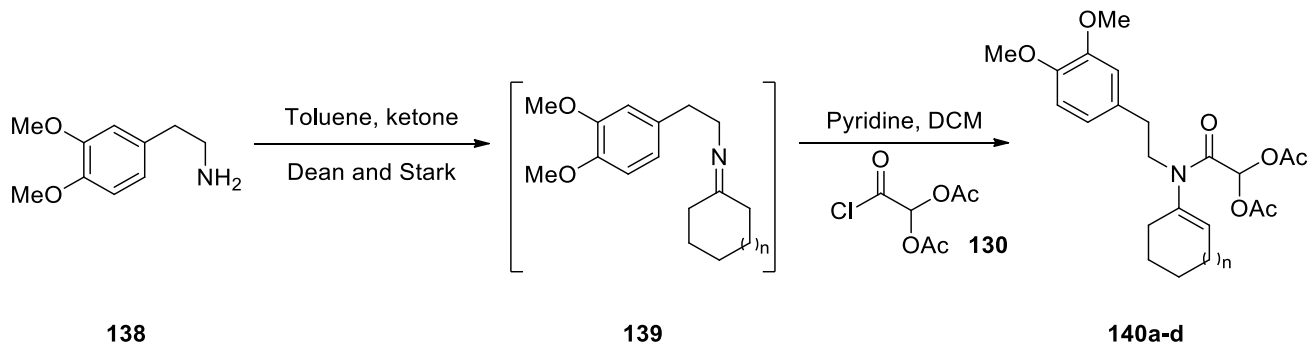

Scheme 42: Formation of the tetracyclic precursors **140a-d**.

Using the same approach as the bicyclic compounds, the IAC tetracyclic precursors were dissolved in anhydrous 1,2-DCE and $BF_3 \cdot OEt_2$ (5 equiv.) was added. The reaction mixture was again passed through the 3D-printed flow reactor heated to 80 °C and connected to a 100 psi BPR. The flow rate was maintained at 0.1 mL/min and a single pump was used to carry out the reaction (**Scheme 43**).

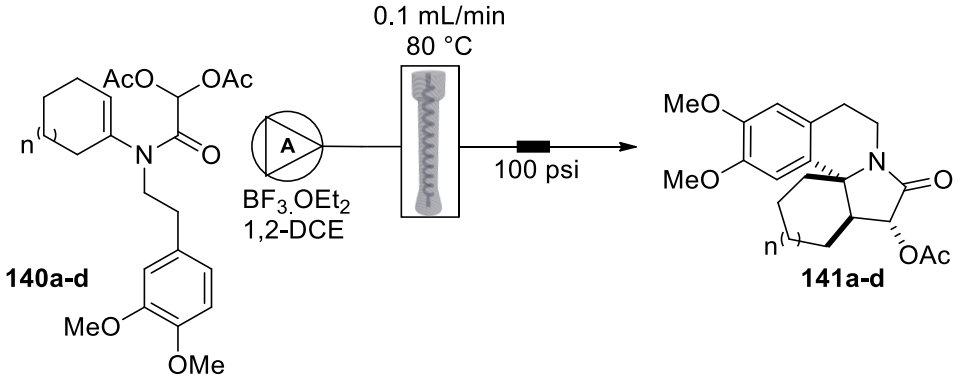

Scheme 43: IAC reaction to access the tetracyclic core of the erythrina alkaloid family.

As seen in **Table 7** the tetracyclic products **141b** and **141c** with 6- and 7-membered A rings were synthesised in good yields (45% and 54% respectively) and stereoselectivity. They were isolated as a single diastereoisomer when compared to the mixtures obtained from batch experiments [122]. A highly reduced yield was observed in compound **141a** when the A ring was more strained (9%). This is probably due to degradation of the product in the purification step. When a heteroatom was introduced in the A ring as in product **141d**, yields were still seen to be low (20%). The

stereochemistry of compounds **141a** and **141d** have been assigned based on the coupling constant values on adjacent hydrogen atoms as seen in the ^{1}H NMR analysis of the purified material.

Table 7: [a] Reactions were carried out at 80 °C with a flow rate of 0.1 mL/min (Pump A). % Conversions with amines showing reaction conditions for the products **141a-d**.

Entry	Cyclisation precursor	Product	Isolated yield (%)
1	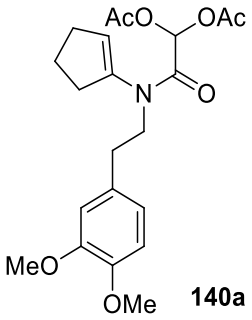 **140a**	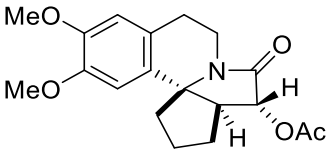 **141a**	9
2	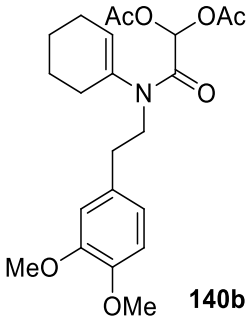 **140b**	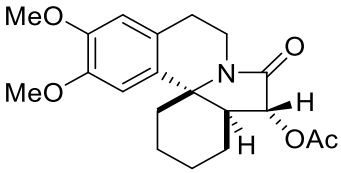 **141b**	45
3	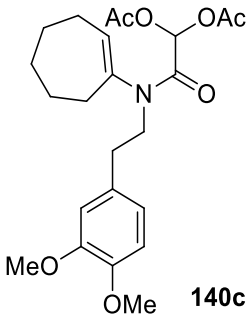 **140c**	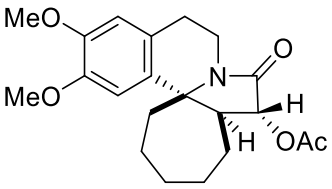 **141c**	54

Entry	Cyclisation precursor	Product	Isolated yield (%)
4	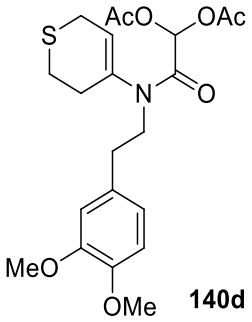 **140d**	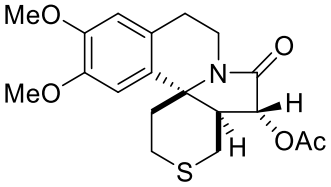 **141d**	20

3.4 Quinoxalinones

3.4.1 Initial Experiments

In this series of experiments the viability of a two-step flow based protocol towards the synthesis of quinoxalinones was investigated. The combination of two flow instruments was used in this sequence namely, the Uniqsis FlowSyn® and the ThalesNano H-Cube Pro. The Uniqsis FlowSyn as described earlier has two heating modules. In these experiments the coil module was used as longer reaction times were required. The ThalesNano H-Cube Pro is specifically used for hydrogenation chemistry. It works on the principle of passing hydrogen through a pre-packed cartridge containing supported heterogeneous catalysts. With the help of an external HPLC pump, the reaction mixture is then made to flow over this cartridge where the interaction of the three components (catalyst, H_2, and reactive group in the molecule) take place. The cartridge is also placed within a heating block to accelerate this process if required. The solution then flows past a pressure sensor and BPR after which it can be collected in a flask.

Initially the substrate for the S_NAr chemistry **128** was made to react with phenylalanine methylester (2 equiv.) **142** in the presence of Hüing's base or DIPEA (4 equiv.) in IPA. This reaction mixture was passed through pump A of the flow reactor into a 20 mL Teflon coil pre-heated to 90 °C at 0.45 mL/min. IPA was passed through pump B which was set to 0.05 mL/min. Although all reagents were passed through a single pump (pump A), the reason for using pump B with only solvent was to create a slight positive pressure in the line and to stop diffusion of the reaction mixture through the T-piece into the tubing connected to pump B. The reaction mixture was passed through the coil for 40 minutes at a combined flow rate of 0.5 mL/min. This solution was then passed through a 100 psi BPR after which the S_NAr product **143** was collected. This solution was subsequently made to pass through the next instrument- the H-Cube Pro. A 10% Pd/C cartridge was used and the flow rate was set to 0.5 mL/min. The cartridge was heated to 70 °C in this step.

The hypothesis for this second step was to reduce the nitro group on the S_NAr adduct to the amine. With the elevated temperature (70 °C) of the system, the

loss of methanol would promote an intramolecular cyclisation driving the reaction to completion. In this manner, a two step, single process flow approach towards the synthesis of quinoxalinones was developed (**Scheme 44**).

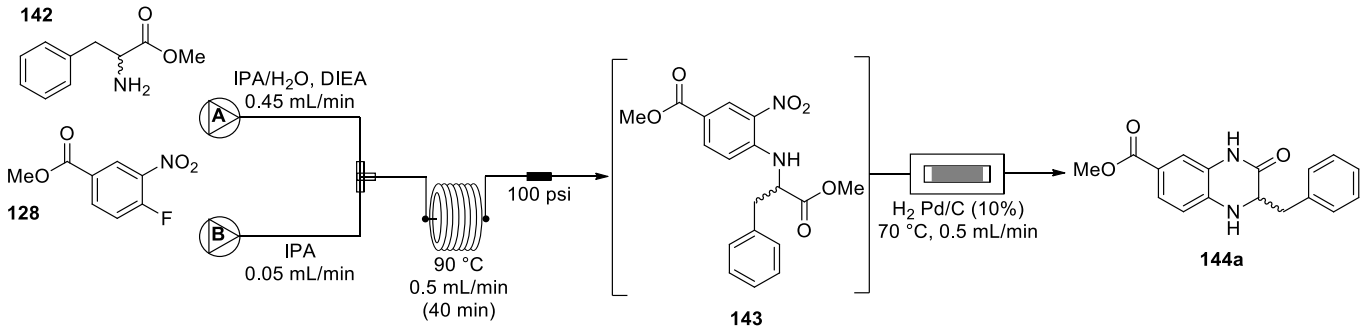

Scheme 44: Synthesis of **144a** from methyl-4-fluoro-3-nitrobenzoate **128** and phenylalanine methyl ester **142**.

3.4.2 Use of Amino Acids

Having an established a working protocol to carry out S_NAr reactions and their subsequent reductive cyclisations in flow we decided to switch our attention to using readily available starting materials. By switching to amino acids, we could not only expand the scope of our work but also test the robustness of our method.

Initial reactions were carried out with racemic alanine **145x** in order to optimise flow conditions on both stages of the process. We envisaged the S_NAr reaction would proceed as normal under flow conditions. The next step however, would require more forcing conditions as the driving force for the cyclisation of such reactions is no longer the loss of methanol, but the loss of water. Hence we decided to elevate the temperature in the reductive step of the flow cyclisation to 80 °C and leaving all other conditions unchanged. Another issue in this process was solubility; we found the esters of amino acids to be more soluble in IPA than their corresponding carboxylic acids. It was therefore required to add a small amount of water along with the IPA in order to keep all starting materials in solution for the S_NAr step. Keeping these points in mind, we

developed a two step protocol for the synthesis of quinoxalinones from amino acids (**Scheme 45**).

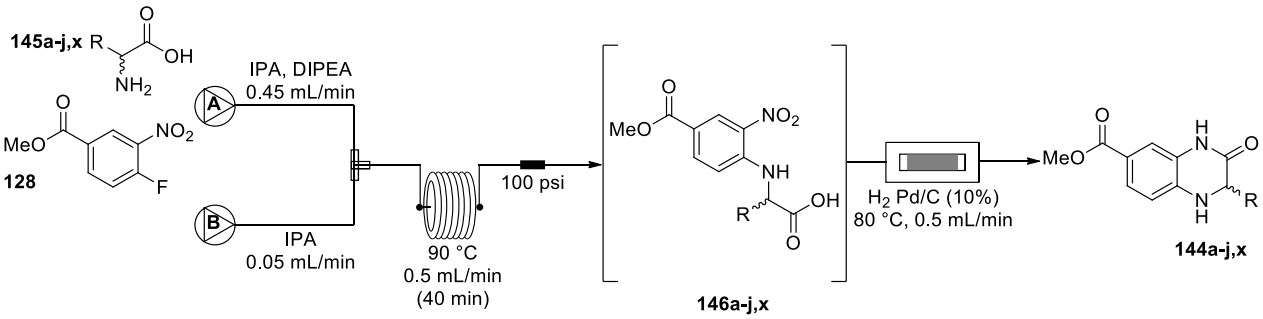

Scheme 45: Synthesis of **144a-j,x** from 4-fluoro-3-nitrobenzoate **128** and *D*/*L*-alanine **145x**.

3.4.3 Use of Microwave reactions

This technique was found to be very beneficial in establishing the exact conditions required to perform the initial S_NAr reaction in batch between the substrate and the amino acids. Research has shown that using a microwave reactor can be a viable tool to translate reactions from batch to flow [127] [128]. It mimics the temperature and pressure conditions seen in the flow reaction and is able to give the user a rough idea on how the reaction will proceed in flow. If the product of a reaction carried out in the microwave is insoluble in the reaction mixture then such reactions would not be suitable in a flow system using the same conditions. Either the solvent system would need to be changed completely or altered with regards to concentration of reactants. This would in turn affect the reaction molarity and therefore the rate of the reaction. When a product starts to crash out within the tubing of a flow system, high pressures are built up, hot spots could be created and sensors would eventually trigger the pumps to stop, thereby halting the reaction until the blockage is located and removed. This too, is not as straightforward as it seems. Due to the complexity in a flow reactor and the intricacy of its various parts, clearing a blockage is usually very tedious and time consuming.

The S_NAr substrate, amino acid and Hünig's base were mixed in a solution of water and IPA. This was subjected to microwave irradiation for 30 minutes at 90 °C to see complete conversion of the starting materials to the desired

products. In comparison to previous experiments, these carboxylic acids required a reduced reaction time under such conditions compared to the esters in flow. Reactions were carried out on a range of *L*- amino acids using these conditions and their S_NAr adducts were concentrated under reduced pressure and washed with a saturated solution of potassium carbonate to remove the persisting diisopropyl ethylammonium salt. The crude mixture from this step was taken forward to the next stage. Upon carrying out ^1H NMR analysis of the crude material in the early experiments, we were able to confirm that the post reaction work-up was effective and we proceeded to build a small library of compounds (**Figure 41**).

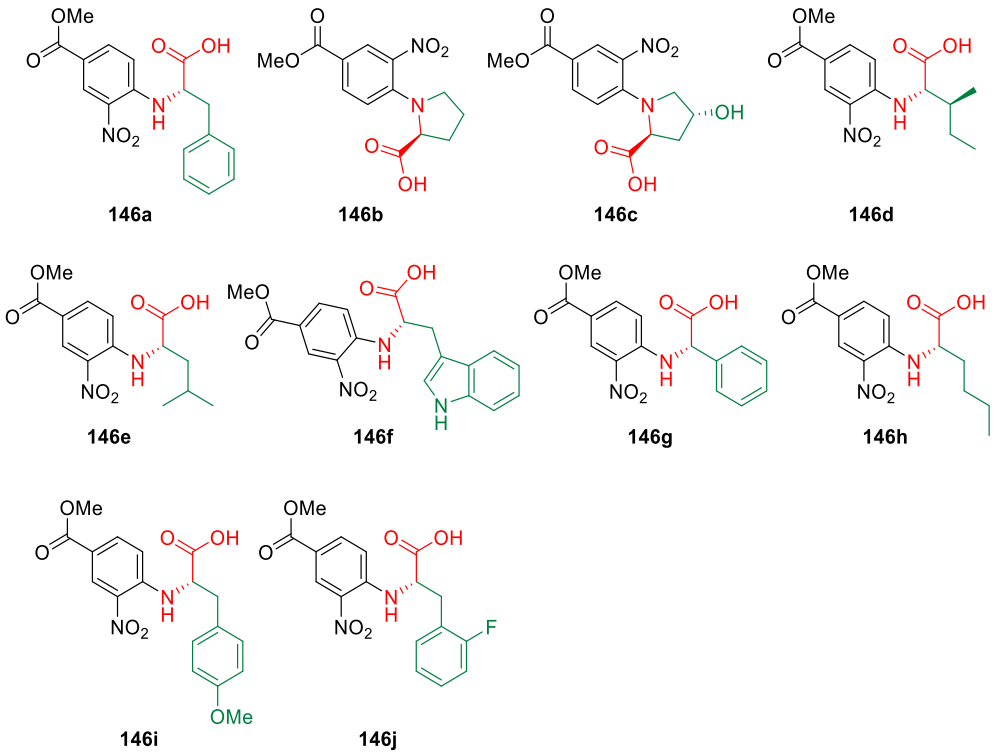

Figure 41: S_NAr products with amino acids.

3.4.4 Reduction using H-Cube and Telescoped Approach

The crude substitution products from the previous step were taken up in IPA and passed through the H-Cube at 0.5 mL/min with a 10% Pd/C cartridge heated to 80 °C. We investigated the use of a lower loading Pd/C cartridge (5%) however, it was found to not be as efficient in carrying out the reduction. The completion of the reaction was monitored by TLC and ^1H NMR. We were also able to visually judge the completion of the reaction by a distinct colour

change (yellow to colourless). The quinoxalinones were precipitated by the addition of water and filtered to afford the clean product without further purification.

After performing all reactions in the microwave, they were repeated in the flow coil and directly taken through to the next step. In this final sequence a solution of the S_NAr substrate, amino acid and Hünig's base (1.1 equiv.) in a 2:1 ratio of IPA and water was made. A 1 mL injection of this solution was passed through the sample loop of pump A at a flow rate of 0.45 mL/min and into the flow reactor. After injecting the sample into the system, the line was switched to solvent containing IPA alone. The flow rate of pump B was set to 0.05 mL/min and IPA was passed through it. Again, this was done to give the line a slight positive pressure at the T-piece and to stop diffusion of the reaction mixture at that section. Both solutions were made to pass through a 20 mL Teflon coil pre-heated to 90 °C giving the reaction a residence time of 40 minutes. This was slightly above that which was required in the microwave but ensured the completion of the reaction with all amino acids. The solution exiting the coil was passed through a 100 psi BPR and collected in a flask.

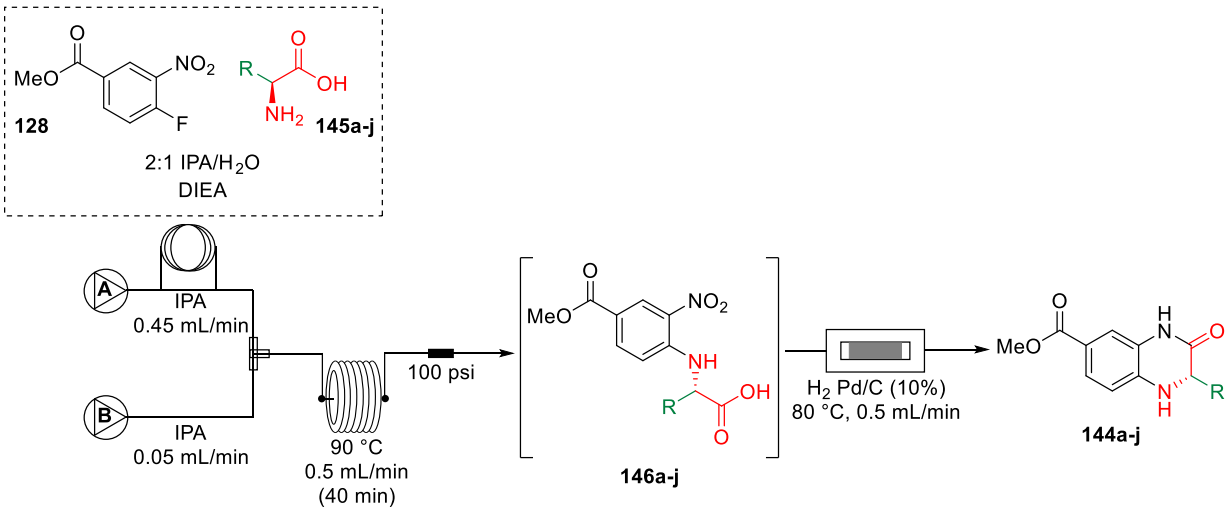

Scheme 46: Synthesis of **144a-j** from 4-fluoro-3-nitrobenzoate **128** and amino acids **145a-j**.

We opted to use injection loops to demonstrate the robustness of this method even with small quantities of starting materials. The high BPR ensured very little diffusion in the coil. The small amount seen was due to the low flow rate.

After injecting 1 mL of solution containing the starting materials, a total volume of 10 mL of product solution was collected. This solution contained mainly IPA as solvent which proved beneficial as we required the water only to solubilize the amino acid. The water also caused the product in the next reduction step to precipitate out of solution and this could be problematic as it would cause blockages in the tubing of the H-Cube.

As such, the 10 mL of solution from the Uniqsis FlowSyn reactor unit containing S_NAr products were passed directly into the H-Cube pre-fitted with a 10% Pd/C cartridge heated to 80 °C. The flow rate was set to 0.5 mL/min and a series of quinoxalinones were synthesised in this manner (**Table 8**).

Yields obtained over the two steps were found to be good to excellent for most of the quinoxalinones studied (49-99%). The amino acids chosen in these reactions had varying alkyl chains, aromatic functionalities and substitutions on those moieties. We hoped to display a range of functionality while selecting these reagents. The general trend in yields were seen to be quantitative, however a drop in yields were observed when the alkyl chain on the amino acid was saturated (**Table 8**, Entries 4, 5, 6 and 8). The use of proline and hydroxyproline in this synthetic sequence was interesting as reactions are high yielding and it offers the possibility to form fused ring quinoxalinones (**Table 8**, Entries 2 and 3). The S_NAr products **146a-j** were taken through to the hydrogenation step without further purification. However, data for compounds **146a**, **146b**, **146d** and **146e** were collected from microwave experiments and this has been discussed in this experimental section of rthe thesis.

Table 8: [a] Reactions were carried out at 80 °C with a flow rate of 0.5 mL/min. % Conversions with amines showing reaction conditions for the products **144a-j**.

Entry	Cyclisation precursor	Product	Isolated yield (%)[a]
1	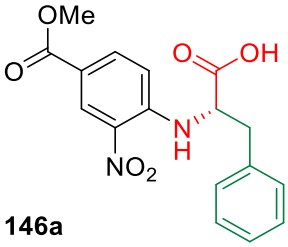 **146a**	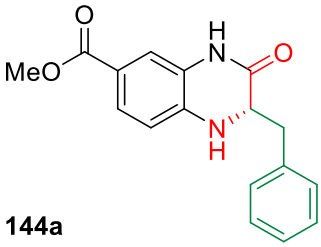 **144a**	71
2	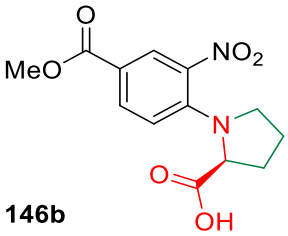 **146b**	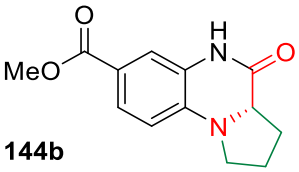 **144b**	99
3	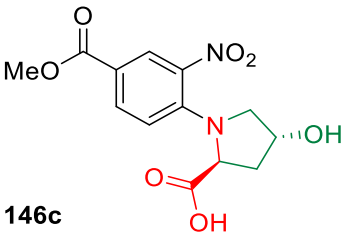 **146c**	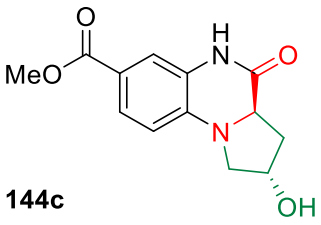 **144c**	99
4	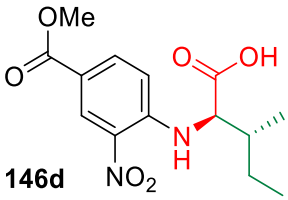 **146d**	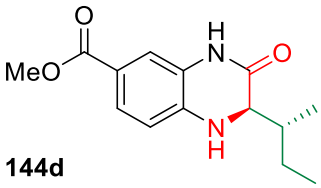 **144d**	71
5	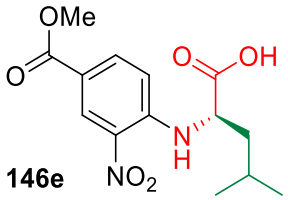 **146e**	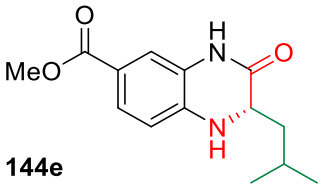 **144e**	63

Entry	Cyclisation precursor	Product	Isolated yield (%)[a]
6	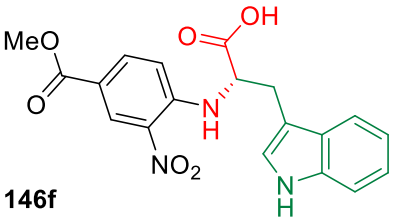 **146f**	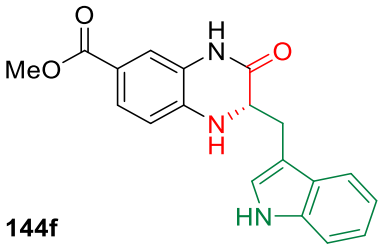 **144f**	77
7	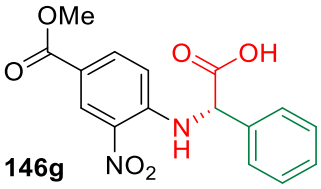 **146g**	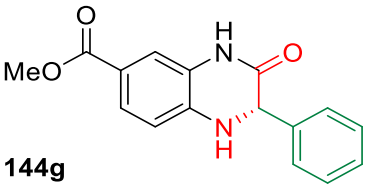 **144g**	99
8	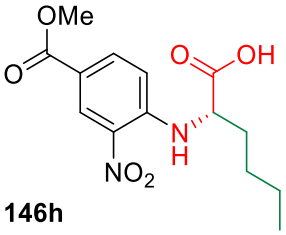 **146h**	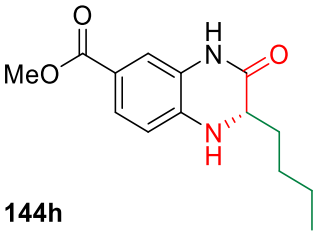 **144h**	70
9	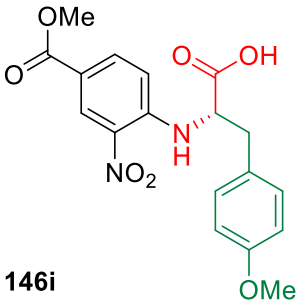 **146i**	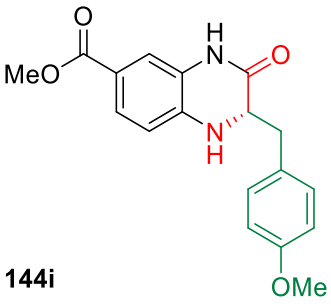 **144i**	77
10	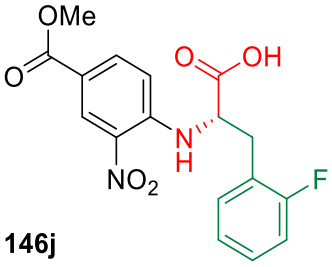 **146j**	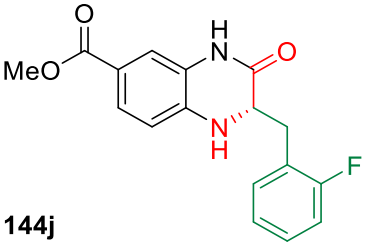 **144j**	49

3.5 Stirrer Beads and Catalysis

Having established a working protocol for integrating 3D-printed reactors in flow systems, as well as demonstrating the robustness of a flow based route towards the synthesis of relatively complex heterocyclic systems, we next proceeded to demonstrate the use of 3D-printing in batch chemistry.

As flow chemistry is still infrequently used in most laboratories, we wanted to develop an approach for batch chemists to use 3D-printing in their synthetic steps. For this particular part of the research programme, we decided to focus on SLA printing and the development of a device using this technique. Stereolithography printing (SLA) was chosen as a technique as it can offer more detail and intricacy in the print. We also wanted to explore the scope of resins used for such prints and develop a formulation [62], which would be chemically inert and resistant to reagents, solvents, and mechanical stresses that develop within a reaction mixture.

The primary objective or starting point for the conception of such a device was looking at how reactions were performed in batch. In our own laboratory we used round bottom flasks to contain reaction mixtures, glass manifolds delivering the required vacuum and inert gasses as well as magnetic hotplates with stirrer beads to control the heat and stirring required in reactions in order to homogenise them. Previous work in the group had introduced the idea of a stirrer bead assisted device that would improve the stirring i.e. increasing the level of mixing by introducing more turbulence in the reaction mixture. A rough 3D model of such a device was created to fit a standard 20 mm magnetic flea. It showcased ridges along its outer edge to increase the overall surface area as well as holes on its upper and lower face to draw solvent through it, thereby increasing its interaction with the device. The magnetic flea would simply sit in a pocket created in the centre of the device and placed in the reaction mixture as normal (**Figure 42**) [129].

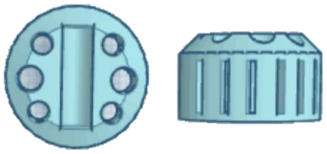

Figure 42: Original CAD stirrer bead design showing the upper and peripheral face.

Initially, the device was printed using commercially available FormLabs clear resin on the FormLabs Form 1+ SLA printer. However, due to the nature of the formulation it was found to be compatible with very few solvents. It was also in our interest to develop a formulation that would be suitable to print and be chemically unreactive.

3.5.1 Photopolymers for SLA Processes

In SLA printing processes, since light is used as a source of energy to cross-link a photoresin in a layer by layer fashion; the chemistry behind such cross-linking induced by light needs to be investigated as there are a range of chemical systems that achieve this [130].

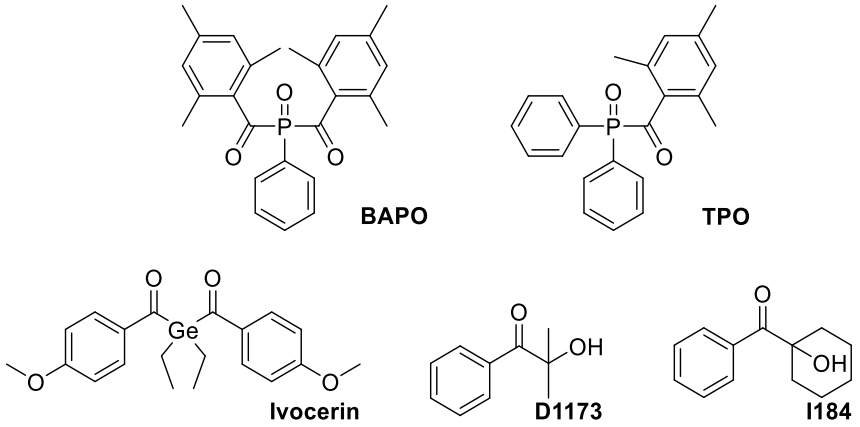

Figure 43: Commonly used photoinitiators in SLA printing processes.

The first are radical based systems wherein certain molecules (photoinitiators) absorb the photolytic energy, carry out the rapid radical generation, initiation and propagation reactions thereby generating reactive species and inducing the necessary polymerization of the monomers within the system. There are two types of initiators; Norrish Type I or Type II [130]. The first type consist of single molecules that cleave into radical fragments upon light exposure.

Scheme 47 shows the mechanism of radical formation of a common benzyl ketal Type I initiator Darocur 1173.

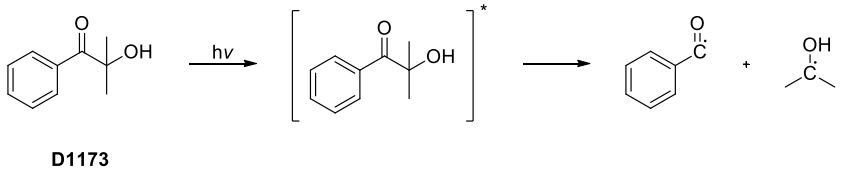

D1173

Scheme 47: Radical formation of **D1173** upon excitation from light source.

Other benzyl ketal initiators belong to the Irgacure series (I184, I1651, I369). Acyl phosphine oxides (TPO and BAPO) belong to the same class and absorb at higher wavelengths [131]. The second type of initiator (Norrish Type II) systems consist of two molecules which assist each other to cause the photoinitiation reactions: an absorbing molecule or a sensitizer; and a co-initiator or a synergist. **Scheme 48** below shows the mechanism of how benzophenone **147** (sensitizer) upon reaching an excited state, accepts a hydrogen atom from a tertiary amine (synergist) thereby generating the initial radicals.

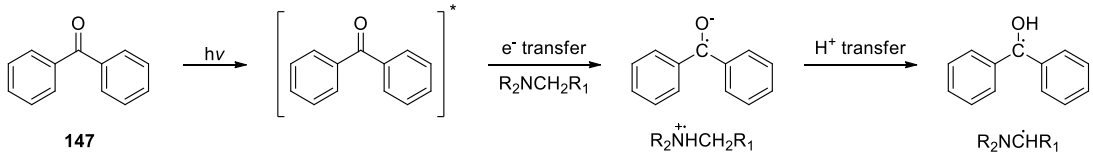

147

Scheme 48: Radical formation of benzophenone **147** through electron and hydrogen transfer.

For such radical based systems, the monomers most commonly used belong to three classes, the first of which are acrylates and methacrylates. Typically, a combination of the two are used owing to the low cure of methacrylate systems. Some patents describe using urethane based acrylate and DGEBA (bisphenol A diglycidyl ether) formulations [132]. These monomers show high mechanical strength but due to their increased viscosity, reactive diluents which enable rapid cross-linking are often added to resin mixtures. These include DPDGA (dipropylene glycol diacrylate) and PETA (pentaerythriol tetraacrylate), amongst others. Although such systems show advantages with regards to their mechanical properties, there is an issue of shrinkage. Aromatic

acrylates are known to shrink less than diluents (bisphenol dimethacrylate *bis*-GMA shrinks 5%, triethyleneglycol dimethacrylate shrinks 12%) [133].

The next class of monomers is comprised of the thiol-ene systems. Compared to acrylate based formulations, thiol-ene systems alone exhibit reduced shrinkage [134] and also in combination with acrylate/methacrylate systems during the photopolymerization process, they result in reduced mechanical stress and sharper formed objects [135]. This is attributed to the shifting in gel point owing to the step-growth mechanisms displayed in thiol-ene systems. Additionally, ***β***-allyl sulfones can be added as addition-fragmentation chain transfer (AFCT) reagents to control the polymer architecture. This gives an added advantage over thiols by overcoming issues associated with them such as benchtop stability, bad odour, etc. AFCT reagents narrow polydispersity of linear polymers and copolymerize in a statistical manner [136] (**Figure 44**).

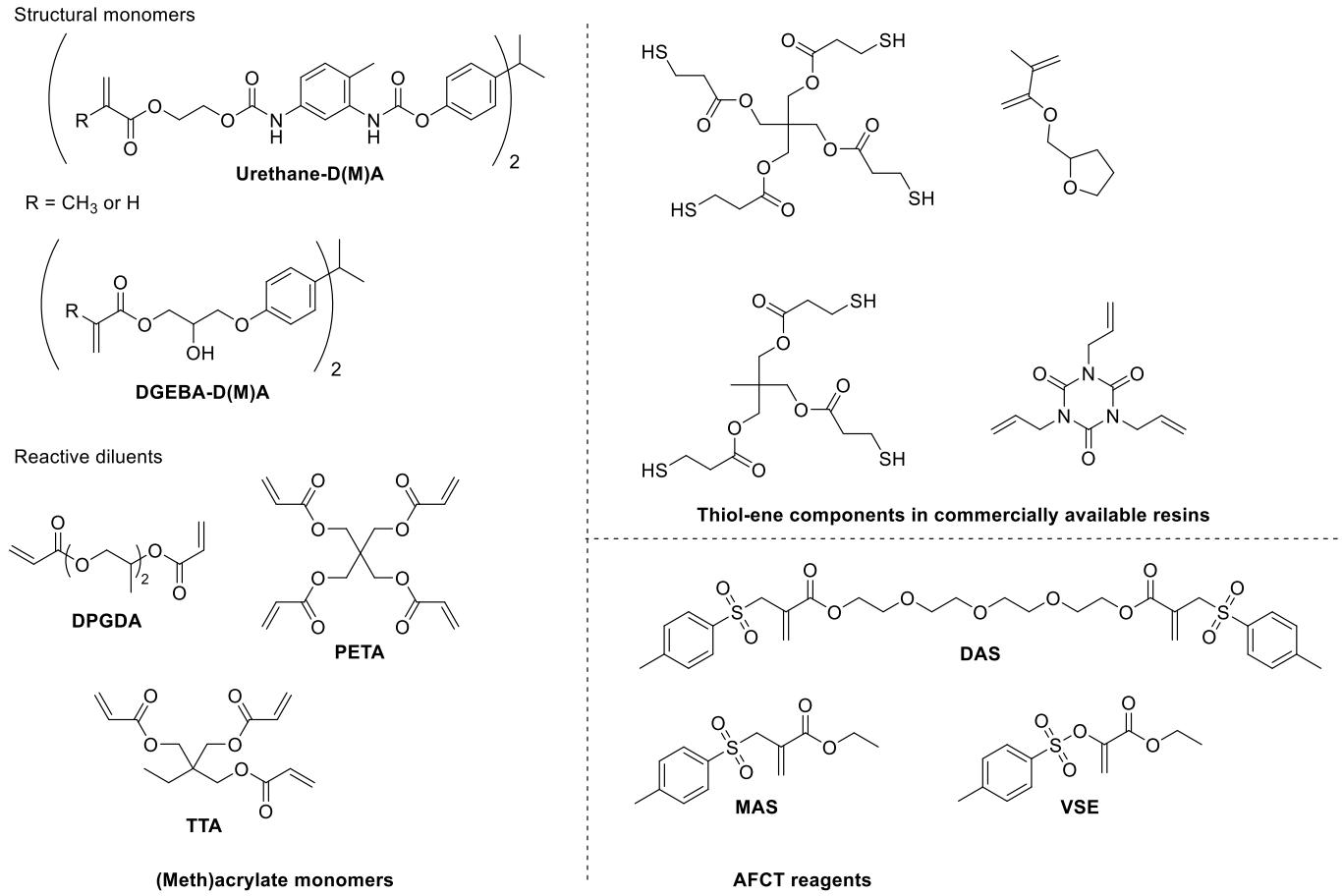

Figure 44: Common examples of monomers belonging to each of the acrylate/methacrylate, thiol-ene and AFCT classes in radical systems of photoinitiation.

Cationic systems consist of photoacid generators (PAG's) which are usually aryl iodonium salts ($Ar_2I^+X^-$) with non-nucleophillic counterions (BF_4^-, PF_6^-, AsF_6^- and SbF_6^-). Their UV instability however, causes them to decompose into reactive intermediates, radicals and radical cations. On interaction of such species with solvent or monomers, the formation of a super acid occurs which acts as the primary initiator for polymerization to take place [137]. Epoxides are one of the most commonly used classes of monomers in such systems. This is attributed to the low shrinkage (2-3% volumetric) due to the ring opening reaction seen in the epoxide group as compared to acrylate and methacrylate based systems [138]. Some commonly seen monomers in this category are DGEBA (diglycidyl ether derivatives of Bisphenol A) and ECC (3,4-epoxycyclohexylmethyl-3,4-epoxycyclohexanecarboxylate). Due to their low

cure speeds, epoxides are usually used in combination with vinyl ethers, which are more reactive and also cationically polymerizable [138]. CDVE (1,4-cyclohexane dimethanol divinyl ether), TTVE (trimethyloyl propane trivinyl ether) are examples of such monomers. Disubstituted oxetanes are more reactive than epoxides and can also be used along with vinyl ethers as they too, offer low shrinkage properties [139].

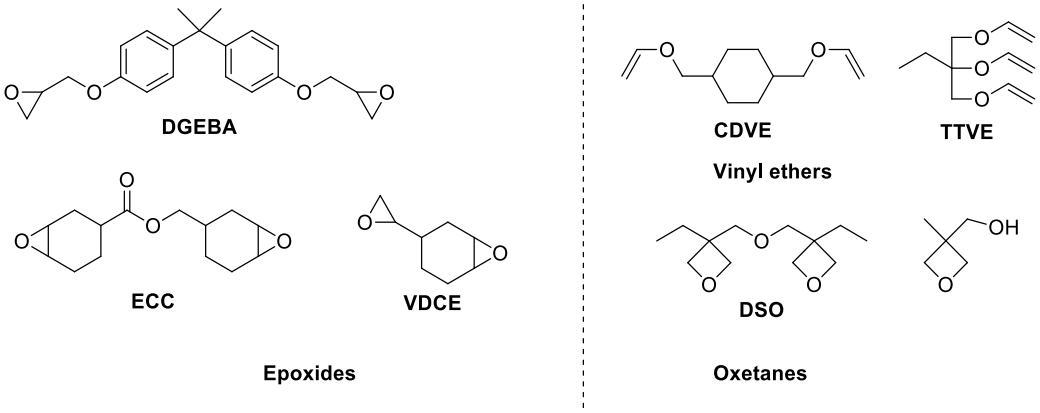

Figure 45: Commonly used monomers in cationic systems of photoinititation.

Additives such as stabilizers and light absorbers are also seen to be used in photoresins. Radical based stabilizers (inhibitors) BHT (butylated hydroxyl toluene) and MEHQ (methoxy hydroquinone) are commonly used and at very low concentrations (50-200 ppm) [140]. Benzyl *N*,*N'* dimethyl amine (BDMA) is a mild base (used at concentrations between 5-250 ppm) that stabilizes photopolymerization reactions through neutralization of radical cations [141]. Light absorbers like EDMA (2-ethyl-9,10-dimethoxy anthracene) or stilbene derivatives like BMSB (1,4-*bis*(2-dimethylstyryl)benzene) lower the depth penetration of the light, resulting in thinner layers and a better z-resolution [142].

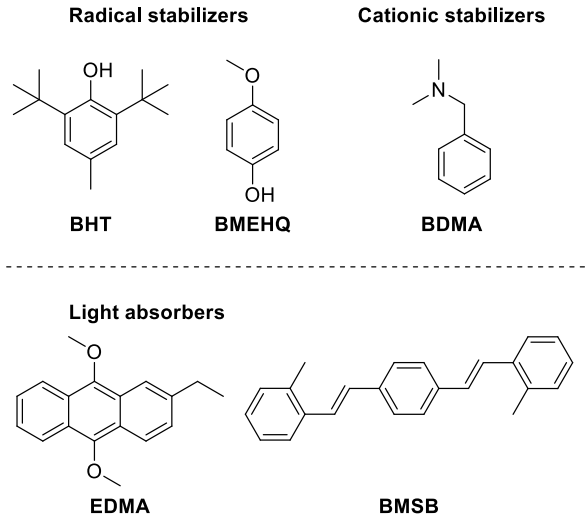

Figure 46: Commonly used additives in photoresins.

3.5.2 Hantzsch Dihydropyridines (DHP)

In the first efforts to develop a formulation for a device and its use in chemical reactions, acrylate based systems were investigated owing to their common applications in patents describing work in similar areas. Having carried out initial experiments with ratios of monomers and the percentage of initiator used, the following formulation was found to print well and show a certain degree of solvent resistance.

1st Generation Formulation: Isobornyl acetate 33%, bisphenol A ethoxylate diacrylate 50%, trimethylolpropane triacrylate 15% and diphenyl(2,4,6-trimethylbenzoyl) phosphine oxide (TPO) 2%.

For the catalyst incorporation, *p*-TsOH (*p*-toluene sulfonic acid or tosic acid) was chosen due to its widespread use in organic chemistry. It has been widely used for the formation and cleavage of acetals. In the protection of ketones, under reflux conditions tosic acid promoted reactions have been high yielding [143] [144]. For the cleavage of carbonyls in acetals, it has been used in aqueous systems [145]. It has been used in the esterification of carboxylic acids [146] and hydroxy acids to form lactones [147]. It has been shown to catalyse dehydrations of ketols to α,β-unsaturated compounds [148], as well as Wagner-Meerwein rearrangements of tricyclic undecanones [149]. Tosic acid was found to be very useful in the enolization of ketones to enol acetates [150] and for the cleavage of amine protecting groups [151]. Given this widespread use of tosic acid, we decided to use it as a starting point for our research in catalysis and 3D-printing.

Hence, 5% w/w tosic acid was incorporated into the resin formulation and this was stirred until fully dissolved. All mixtures were stirred in amber bottles or duran covered with aluminium foil to minimize the light penetration into the formulation prior to prints.

The design as shown below (**Figure 47**) featured a 15 × 15 mm cylindrical housing with a height of 9 mm. It had a pocket to fit a standard 12 mm magnetic flea in the centre on the upper face. Six vertical channels/holes and a cage like structure around the outer edge of the device would encourage solvent to

be drawn through the device thereby increasing its interaction with the reaction medium.

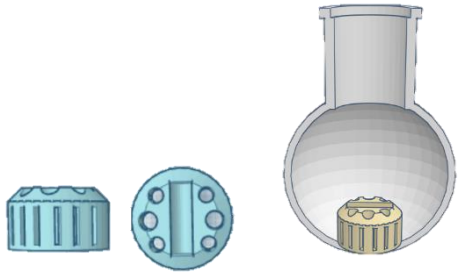

Figure 47: CAD drawing of first generation stirrer and its fit in a standard round bottom flask.

The resin was then transferred to a FormLabs Form 1 printer and the device was printed using Clear 02 setting. Layer height was adjusted to 0.1 mm. Supports were added to the structure to ensure overhangs on object were printed accurately. The volume of the object was found to be 1.5 mL. The time taken to print a single device was 15 minutes. After the print, the device was removed from the build platform and rinsed with IPA. It was then left to cure in normal light (alongside a window) for an additional 24 hours. The supports were removed and the 12 mm magnetic flea was fitted into the cavity.

We decided to explore the scope of this catalytically active stirrer bead in a reaction that was well known and understood, yet showed a certain degree of complexity. The Hantzsch three component reaction describes the addition of an aldehyde, *β*-keto ester and a dimedone catalytically driven by tosic acid to form the dihydropyridine core structure [152].To an equimolar mixture of ammonium acetate, dimedone, and *β*-keto ester in ethanol, a 5% w/w *p*-TsOH stirrer bead was added and the reaction was stirred at room temperature for 6 hours. Progression of the reaction was checked *via* TLC and after completion, the stirrer bead was simply removed from the reaction thereby stopping it (**Scheme 49**). The solution was then concentrated under reduced pressure and purified *via* column chromatography affording the clean product in good yield.

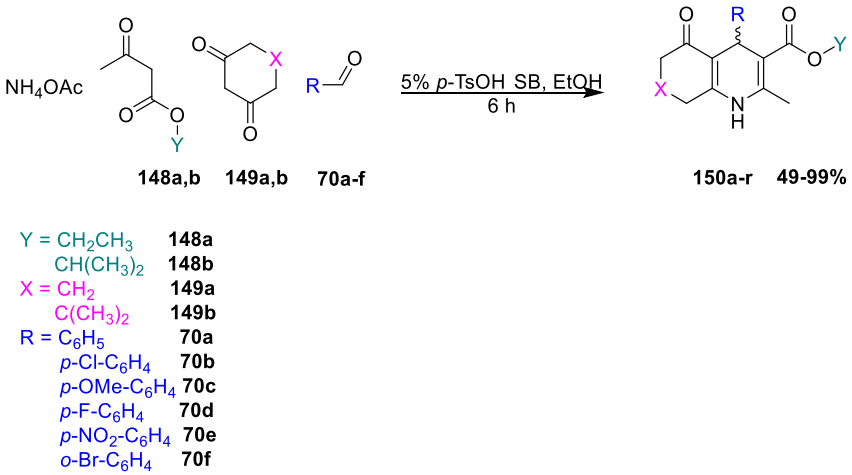

Scheme 49: Three component reaction for the synthesis of Hantzsch dihydropyridines.

The tentative mechanism suggested by the authors proceeded *via* steps 1-3 or 4-6 as seen in **Scheme 50** to form the polyhydroquinoline. The *p*-TsOH is thought to catalyze the Knoevenagel condensation of the aldehydes with methylene compounds in steps 1 and 4. It is also thought to catalyze the Michael type addition reaction of intermediates 1 and 2 obtained as a result from steps 1, 2, 4 and 5.

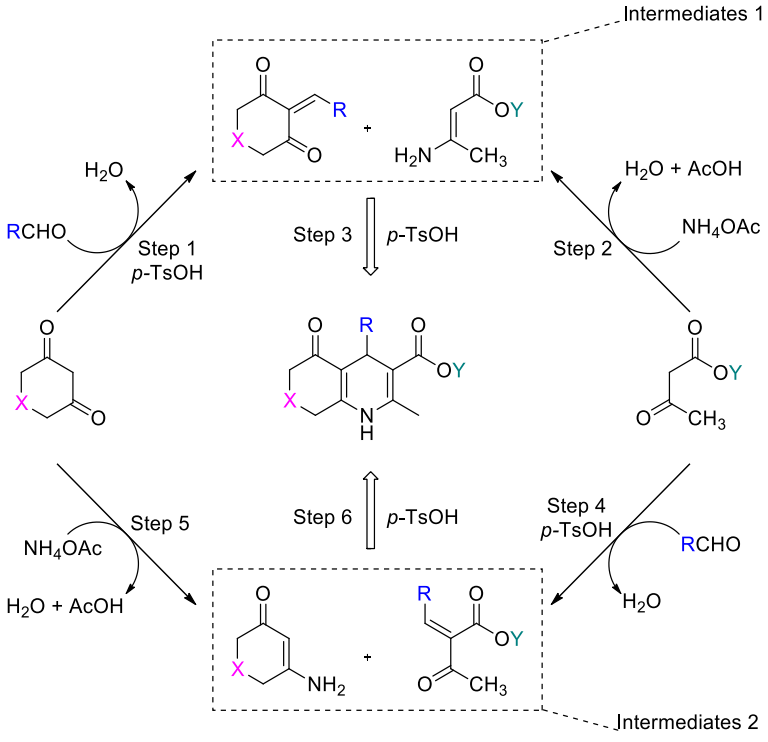

Scheme 50: Mechanism for the synthesis of polyhydroquinolines.

Bearing this mechanism in mind, we hoped to derivatize this scaffold by varying the substitution in the different components that make up the reaction. We were successfully able to vary the aldehyde group, the keto-ester as well as introduce a slight change in the diketone and produce a small library of compounds in good yields as seen below.

A drop in yields was seen in compounds **150o**, **150h** and **150f** in reactions where the diketone had no substitution (55%, 50% and 51%) compared to compounds **150l**, **150d** and **150b** where 5,5-dimethylcyclohexane-1,3-dione was used instead (73%, 65% and 73%). This was however, not found to be the case for the reaction where 4-chlorobenzaldehyde was used in compound **150i**. The presence of substitution on the diketone led to a reduced yield (49%) compared to the unsubstituted diketone (66%) in compound **150p**. The general trend in yields for the other reactions too, depended on the diketone. The presence of electron withdrawing and donating groups on the aldehyde did not show much difference in yield. A variation in the keto-ester (ethyl and isopropyl) did not seem to have an impact on the yield of the reaction.

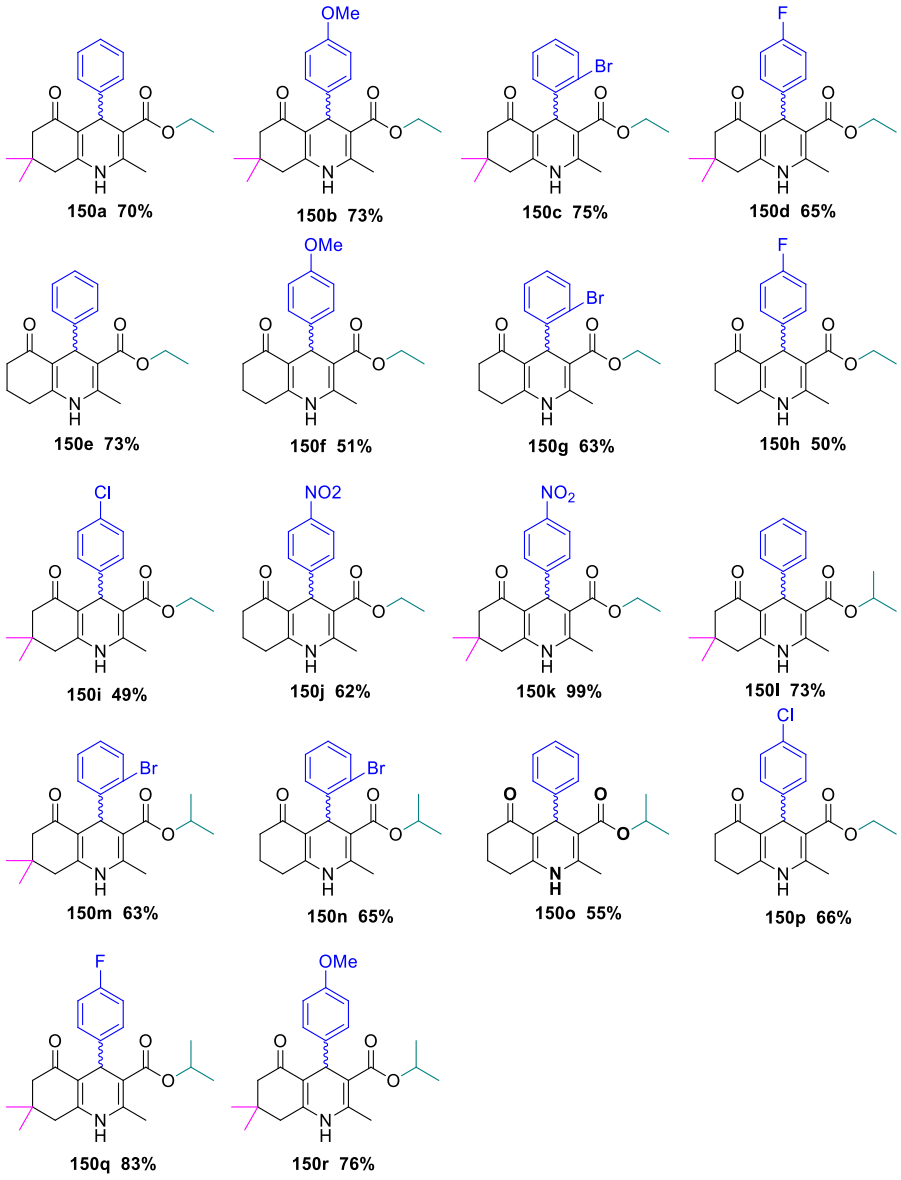

Figure 48: Examples of 1,4-dihydropyridines **150a-r** synthesised using 3D-printed *p*-TsOH stirrer bead.

When attempts for further substitution on the amine were made by replacing the ammonium acetate with benzylamine, no product was observed even after 6 hours. The same reaction was repeated by swapping the benzylamine with a slightly deactivating 4-fluorobenzylamine and 3-fluorobenzylamine to understand whether substitution at such positions had an effect on product formation. No product was observed from these reactions. An inductively activating 4-methoxybenzylamine was also tested in this series, but this reaction too did not result in product formation. It became clear that such substitutions on the amine had an effect on its nucleophilicity thereby making

its introduction into the skeleton of the molecule difficult. As observed in the mechanism, the first reaction taking place is that between the keto-ester and the aldehyde. This step is quite important as the ammonium acetate or ammonia would prefer to attack the more electrophillic aldehyde rather than the ketone. The fact that no product is observed when there is substitution on the amine could possibly correlate to this very step.

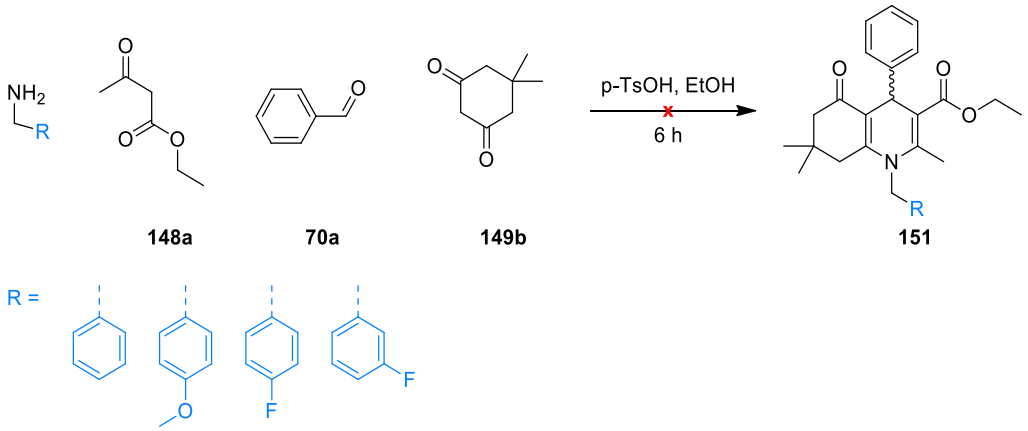

Scheme 51: Substitution of ammonium acetate with tertiary amines in Hantzsch DHP synthesis using 3D-printed *p*-TsOH stirrer beads.

We decided to move on from this chemistry after synthesizing these molecules and investigate other catalytic systems, as well as optimize the formulation used so as to create more robust protocols in the following sections of this thesis due to the constraints in the project.

3.5.3 Suzuki Couplings

Having demonstrated the effectiveness of a catalytically active stirrer bead though the DHP synthesis, the aim was to look into formulating a more robust resin that could be used with a wider range of solvents. A serendipitous discovery within the group led to a formulation containing simply poly(ethylene glycol) diacrylate Mn 250 and the radical based photoinitiator diphenyl(2,4,6-trimethylbenzoyl) phosphine oxide. The optimisation of the exact formulation that has been used in this part of the project was carried out during the development of the circular flow reactors. Higher amounts of the initiator were required to avoid over-polymerization of the fine channels within them. This is discussed in more detail in the later sections of the thesis. However, it is important to note that palladium tetrakis(triphenylphosphine) $Pd(PPh_3)_4$ (0.5% w/w) was used as a catalyst with this formulation to carry out the coupling reactions.

Palladium has been used extensively in organic synthesis. Its first application was post World War II when acetaldehyde was synthesised from ethylene in a process called the Wacker Process [153]. Arylpalladium chemistry was made known by the work of Richard Heck who published a great deal of work on the reaction between organomercurial compounds with alkenes in the presence of catalytic lithium tetrachloropalladate ($Li[PdCl_4]$) [154] [155] [156]. Shortly after the work of Mizoroki [157] [158] and Heck [154] [159] [160] on the reactions using aryl, styryl, benzyl halides with alkenes and a palladium(II) catalyst paved the way for what is now known as the Mizoroki-Heck reaction.

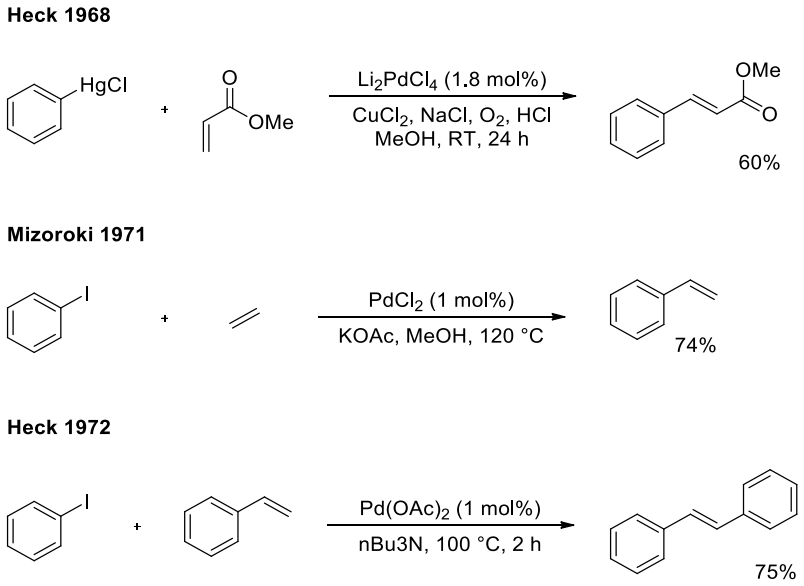

Scheme 52: The first palladium(II) catalyzed coupling reactions.

In the light of these early examples a wave of palladium chemistry was developed such as the Sonogashira Reaction (1975), palladium-catalysed Corriu-Kumada Reaction (1975), the Negishi Reaction (1976), the Stille Reaction (1976-1978), the Suzuki-Miyaura Reaction (1979), the Hiyama Reaction (1988-1994) and others, changing the outlook of the palladium-catalysed cross-coupling chemistries [161].

The reaction of $Pd(PPh_3)_4$ in the Suzuki coupling reactions involves a transition between the Pd(0) and Pd(II) oxidation state (**Scheme 53**). Sometimes a Pd(II) pre-catalyst is reduced to Pd(0) *in situ* allowing the oxidative addition of the aryl halide reforming the Pd(II)-intermediate. This then binds to the aryl boronic acid inserting it into the C-Pd bond, thus creating a new C-C bond. Reductive elimination allows the product to form leaving behind the Pd(0) species. [162].

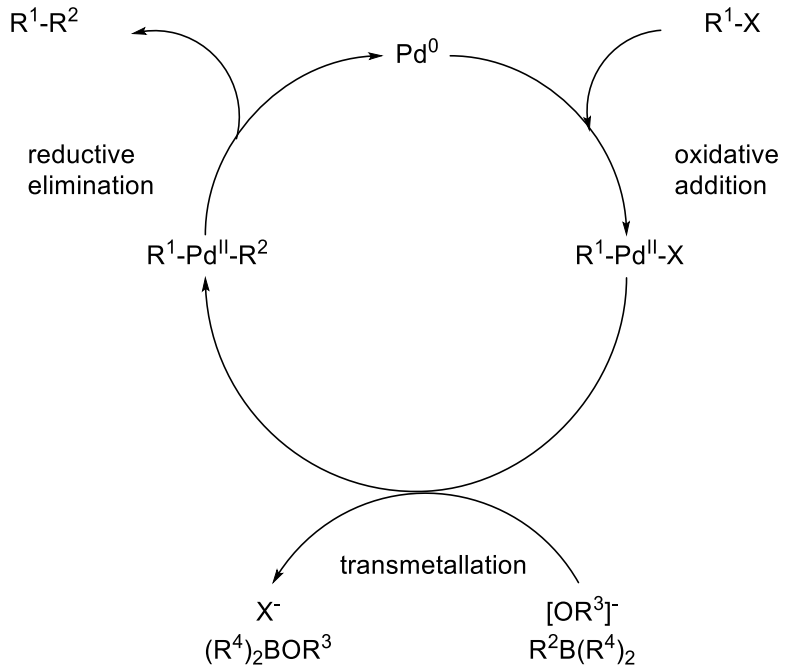

Scheme 53: Catalytic cycle for the Suzuki coupling of aryl halides and aryl boronic acids.

The Suzuki Reaction was chosen to be investigated using our newly developed formulation for the catalytically active palladium tetrakis(triphenylphosphine) ($Pd(PPh_3)_4$ 0.5% w/w) stirrer beads. The palladium tetrakis(triphenylphosphine) was mixed into the formulation and stirred in an amber bottle or glass duran bottle covered with aluminum foil to avoid any light penetration. Once dissolved in the resin mixture, it was poured into a tray fitted to the FormLabs Form 1 printer and printed using the Black 01 setting. The second generation design with a lowered height was used in this series (**Figure 49**).

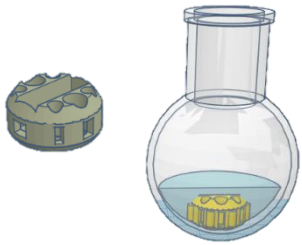

Figure 49: CAD drawing of second generation stirrer and its fit in a standard round bottom flask.

After the print was completed the device was removed from the build platform and washed with IPA to remove excess unpolymerized resin. It was then left to cure under UV irradiation using a UV curing oven for 20 minutes after which the supports were removed and the 12 mm magnetic flea was fitted into the cavity.

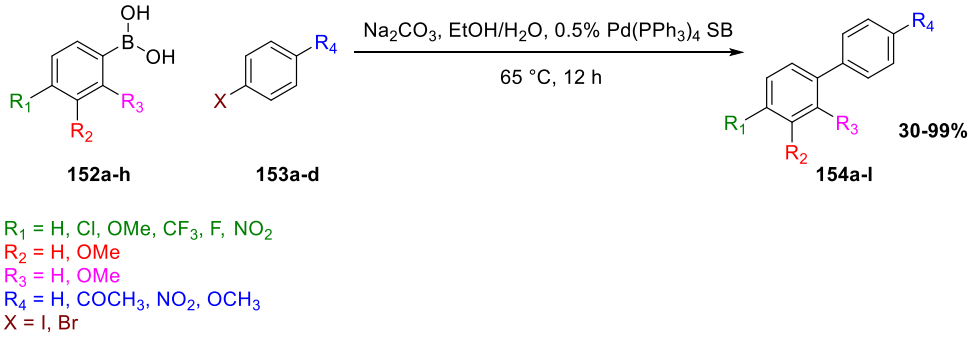

Scheme 54: Suzuki coupling between aryl halide and aryl boronic acid using 3D-printed palladium stirrer bead.

This catalytic stirrer bead was added to a flask containing the aryl iodide, boronic acid (1.1 equiv.) and sodium carbonate (2 equiv.) in a water-ethanol mixture. The reaction mixture was heated to 65 °C and monitored *via* TLC. The reaction was found to be complete after 12 hours. The reaction was stopped by simple removal of the stirrer bead. The bead was then washed with dichloromethane to remove any product that might have adhered to it. In contrast to the work performed in the previous DHP synthesis series, these catalytically active stirrer beards showed a higher solvent resistance and could tolerate the DCM washing step without breaking down. As a work-up procedure, the crude product was partitioned between water and DCM and

extracted into the organic phase. The product obtained from such a method was found to be clean by ^{1}H NMR analysis and also gave good to excellent yields of product (up to 99%).

Table 9: [a] Reactions were carried out at 65 °C for 12 hours. Examples of biphenyls **154a-o** synthesised using 3D-printed $Pd(PPh_3)_4$ stirrer bead.

Entry	Boronic Acid	Aryl Halide	Product	Thermal (%)[a]
1	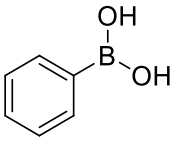 **152a**	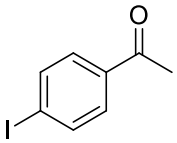 **153a**	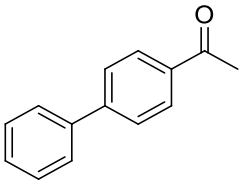 **154a**	97
2	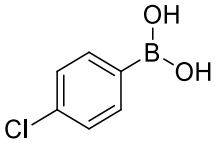 **152b**	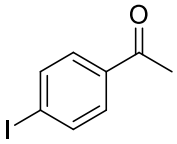 **153a**	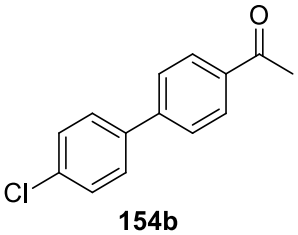 **154b**	85
3	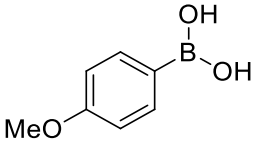 **152c**	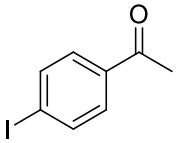 **153a**	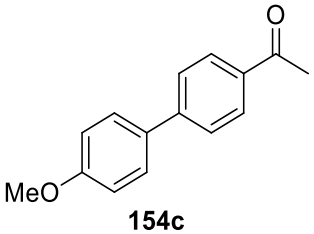 **154c**	98
4	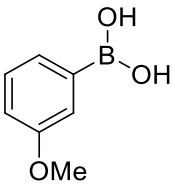 **152d**	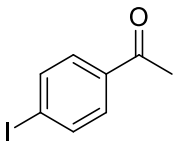 **153a**	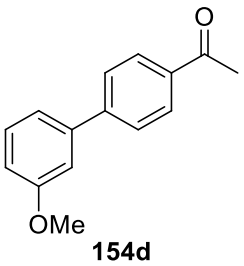 **154d**	93

Entry	Boronic Acid	Aryl Halide	Product	Thermal (%)
5	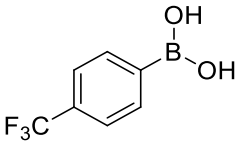 **152e**	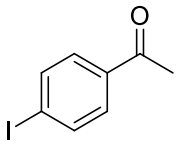 **153a**	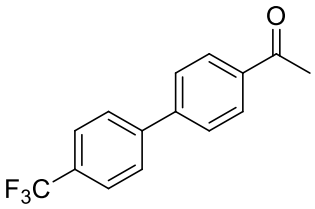 **154e**	96
6	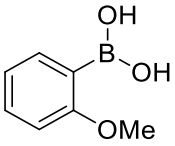 **152f**	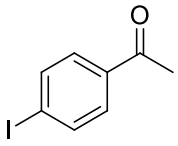 **153a**	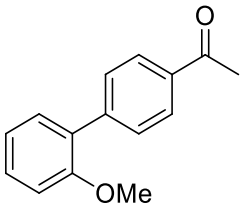 **154f**	60
7	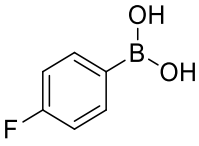 **152g**	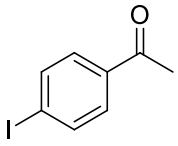 **153a**	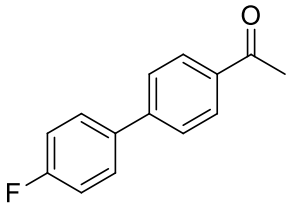 **154g**	100
8	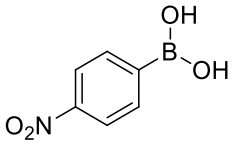 **152h**	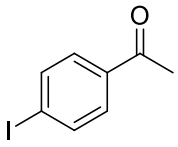 **153a**	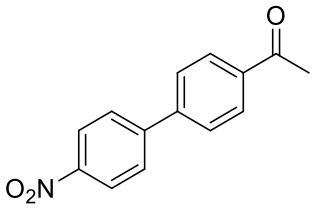 **154h**	94
9	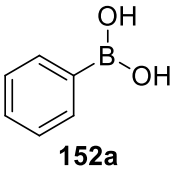 **152a**	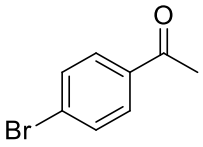 **153b**	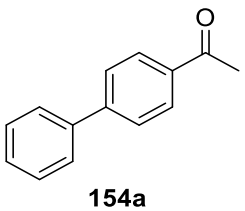 **154a**	76

Entry	Boronic Acid	Aryl Halide	Product	Thermal (%)
10	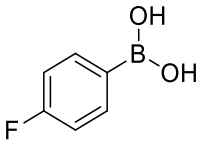 **152g**	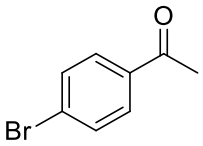 **153b**	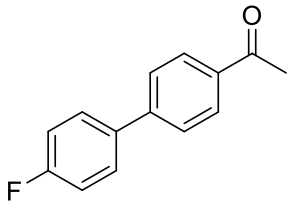 **154g**	56
11	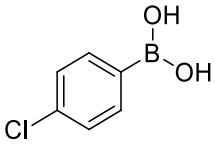 **152b**	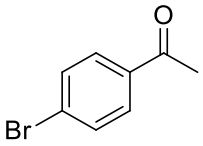 **153b**	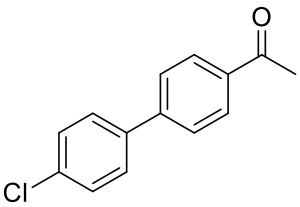 **154b**	47
12	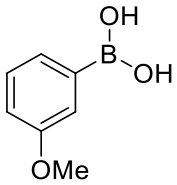 **152d**	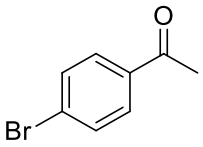 **153b**	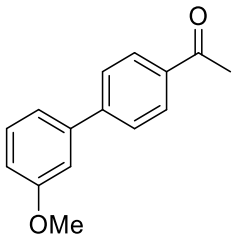 **154d**	69
13	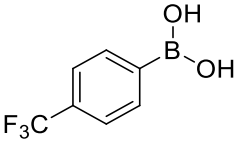 **152e**	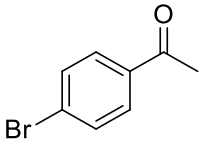 **153b**	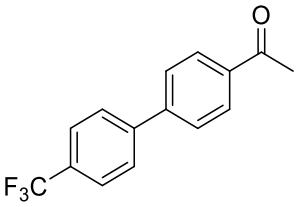 **154e**	58
14	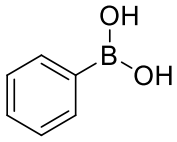 **152a**	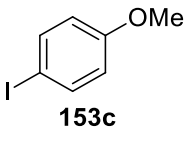 **153c**	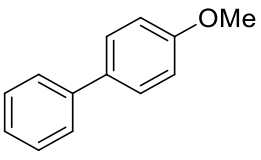 **154i**	99
15	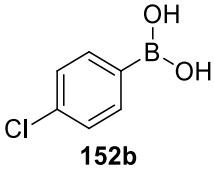 **152b**	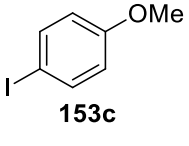 **153c**	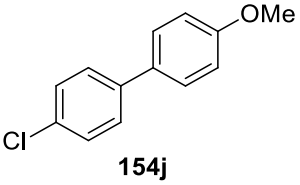 **154j**	94

Entry	Boronic Acid	Aryl Halide	Product	Thermal (%)
16	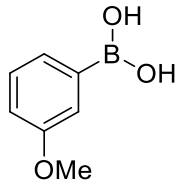 **152d**	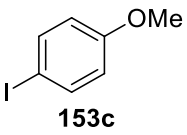 **153c**	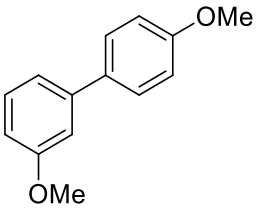 **154k**	87
17	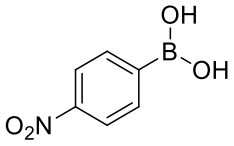 **152h**	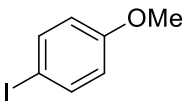 **153c**	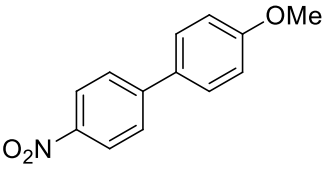 **154l**	30
18	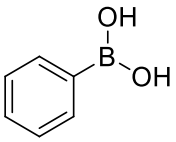 **152a**	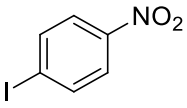 **154d**	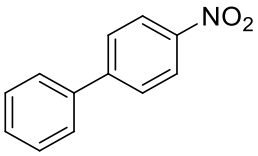 **154m**	73
19	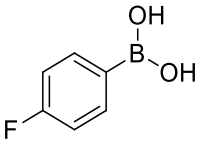 **152g**	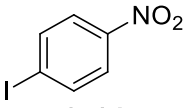 **154d**	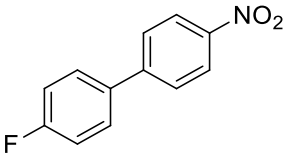 **154n**	81
20	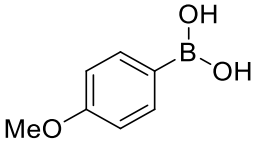 **152c**	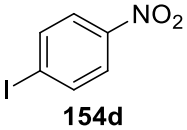 **154d**	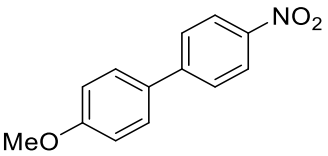 **154l**	97

The general trend in reactions for this thermally driven series of cross-couplings was that the iodoacetophenones (**Table 9**, Entries 1-8) expectedly gave higher yielding products compared to the bromoacetophenones (**Table 9**, Entries 9-13). These iodoacetophenones were reacted with a range of boronic acids with different substitutions at the *ortho*-, *meta*- and *para*-positions. Reaction with the unsubstituted phenyl boronic acid (**Table 9**, Entry 1) was quantitative (99%). Reactions with *para*-substituted electron

withdrawing groups on the boronic acid were high yielding (**Table 9**, Entries 2, 5, 7 and 8). This too was expected. The presence of electron donating groups in the *ortho*-, *meta*- and *para*- position of the boronic acid was investigated (**Table 9**, Entries 6, 4 and 3). Such a substitution on the *ortho*- position was found to be lowest yielding (60%). The yield dramatically increased for *meta*-substituted products (93%) and *para*-substituted products (98%).

Amongst the bromoacetophenone-coupled products, the lowest yielding was found in cases where electron withdrawing groups were used (**Table 9**, Entries 10, 11 and 13). No substitution on the aryl boronic acid significantly improved the yield (**Table 9**, Entry 9) (76%). When *meta*- substituted methoxy group on the boronic acid were used in the same reaction, the yield was slightly increased to 69% (**Table 9**, Entry 12).

Experiments with *para*-methoxy phenyl iodide were also carried out as increased yields for this series were expected. Its reaction with *para*-substituted nitrophenyl boronic acid gave the lowest yield of 30% (**Table 9**, Entry 18). Electron withdrawing *p*-chlorophenylboronic acid however, showed an increased yield of 94% (**Table 9**, Entry 15). When there was no substitution on the aryl boronic acid, quantitative yields were observed (**Table 9** Entry 14). The next highest in yield was the *meta*- substituted methoxy product (87%) (**Table 9**, Entry 16).

In the last three experiments for these series, the limiting reagent was changed to 4-nitrophenyl iodide. In its reaction with *para*-methoxyphenyl boronic acid, the highest yield (97%) was observed (**Table 9**, Entry 20). The reaction with electron withdrawing *p*-fluorophenyl boronic acid gave a product in a slightly reduced yield (87%) (**Table 9**, Entry 19). The absence of substitution on the aryl boronic acid, in this case, gave the lowest yield of 73% (**Table 9**, Entry 18).

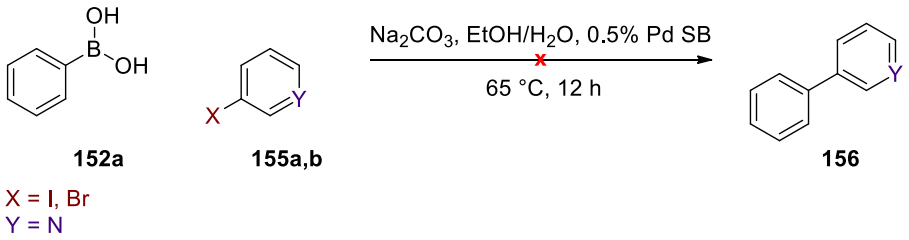

Scheme 55: Suzuki coupling between pyridyl halides **155a**,**b** and aryl boronic acid **152a** using 3D-printed palladium stirrer bead.

Several attempts were made to incorporate a pyridyl ring system into the coupling chemistry (**Scheme 55**), however it was quite unsuccessful under thermal conditions. Hence we looked at a microwave approach to not only optimize the existing reactions but also see if such iodo or bromopyridines could be incorporated into the biphenyl ring systems. We also wanted to test the effectiveness of the formulation under these harsher conditions. Hence a series of analogues was synthesised and their reactions can be summarized in **Table 10**. The .stl file corresponding to the round bottom flask adapted stirrer bead as used in the Hantzsch chemistry was slightly modified in Tinkercad to fit the 8 mm microwave adapted magnetic flea for this purpose. In the same manner as described earlier, the newly designed microwave stirrer beads were printed using this file. The stoichiometry of the reaction was maintained as in the previous experiments but the temperature was increased to 120 °C/130 °C. The reaction was checked by TLC every 10 minutes to determine consumption of starting material and it was found that reactions required between 30-120 minutes for all of the aryl halide to be used up depending on the type of cross-coupling. The other important point to note is that the stirrer bead was able to maintain its catalytic activity even at high temperatures and pressures without degradation.

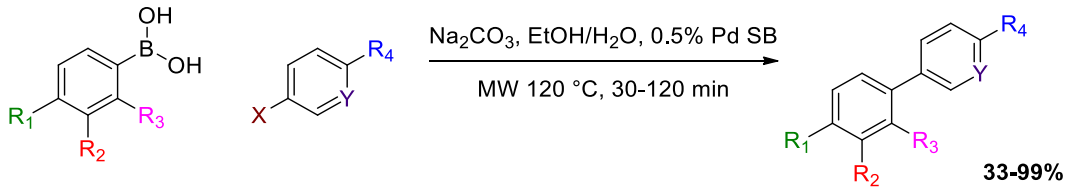

152a-d,g,h **153a-c, 155a,b** **154a,d,g,l, 156a-d**

R_1 = H, Cl, OMe, CF_3, F, NO_2
R_2 = H, OMe
R_3 = H, OMe
R_4 = H, $COCH_3$, NO_2, OCH_3
X = I, Br
Y = N, CH

Scheme 56: Suzuki coupling between aryl or pyridyl halides and aryl boronic acid using 3D-printed palladium stirrer bead under microwave conditions.

Table 10: [a] Reactions were carried out in the microwave at 120 °C; [b] = 130 °C. Examples **154a**,**d**,**g**,**l**, **155a-d** and **156a-d** synthesised using 3D-printed $Pd(PPh_3)_4$ microwave stirrer bead.

Entry	Boronic Acid	Aryl Halide	Product	Time (min)	Yield (%)[a]
1	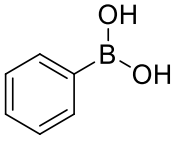 **152a**	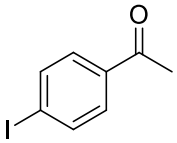 **153a**	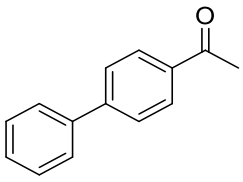 **154a**	30	99%
2	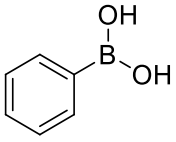 **152a**	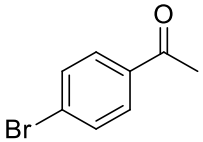 **153b**	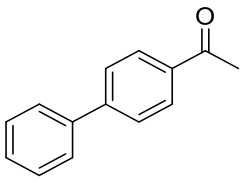 **154a**	40	99%
3	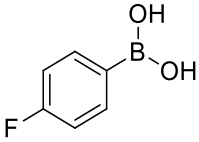 **152g**	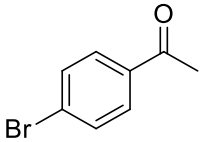 **153b**	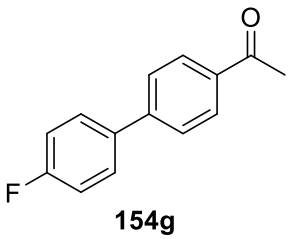 **154g**	60	93

Entry	Boronic Acid	Aryl Halide	Product	Time (min)	Yield (%)
4	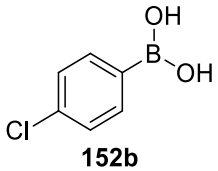 **152b**	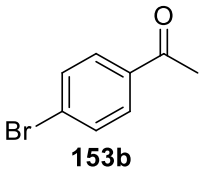 **153b**	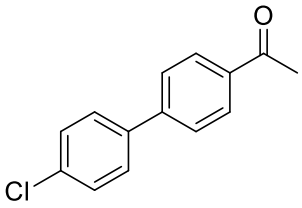 **154b**	60	97
5	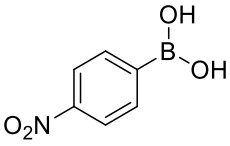 **152h**	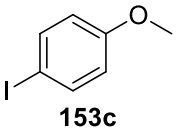 **153c**	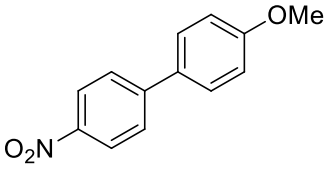 **154l**	40	83
6	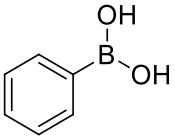 **152a**	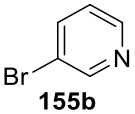 **155b**	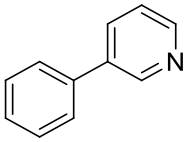 **156a**	120[b]	33
7	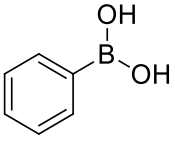 **152a**	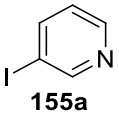 **155a**	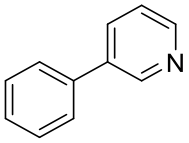 **156a**	20[b]	69
8	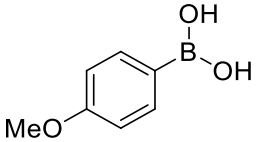 **152c**	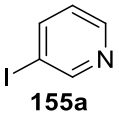 **155a**	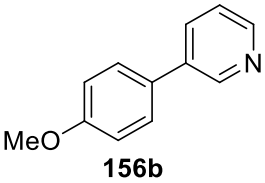 **156b**	20[b]	69
9	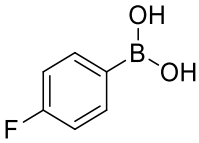 **152g**	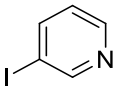 **155a**	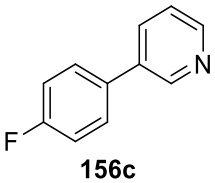 **156c**	20[b]	73

Entry	Boronic Acid	Aryl Halide	Product	Time (min)	Yield (%)
10	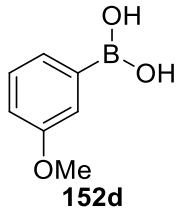 **152d**	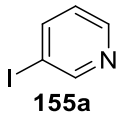 **155a**	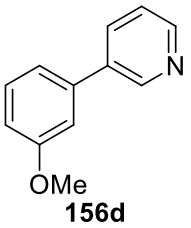 **156d**	20[b]	77

For the unsubstituted boronic acid, yields with bromo or iodoacetophenones were seen to be quantitative and the time drastically reduced to 30 minutes (**Table 10**, Entries 1 and 2). When electron withdrawing groups in the *para*-position on the boronic acid were reacted with bromo acetophenone (**Table 10**, Entries 3, 4 and 5) high yields were observed (93%, 97% and 83% respectively) and the reaction required 60 minutes for the halo boronic acids and 40 minutes for the nitro boronic acid.

When pyridyl systems were introduced as part of the aryl halide component, a higher temperature was required (130 °C). In reactions with unsubstituted phenyl boronic acid, the 3-iodopyridine gave a higher yield (69%) compared to 3-bromopyridine (33%) and required 120 minutes under microwave conditions (**Table 10**, Entries 6 and 7 respectively). A similar yield (69%) was observed when there was *para*-substitution on the boronic acid with an electron donating group, but proceeded in 20 minutes (**Table 10**, Entry 8). The yield was increased to 73% when there was *para*-fluoro substitution on the boronic acid and the reaction required 20 minutes under microwave conditions (**Table 10**, Entry 9). The highest yield in this series of cross-coupled aryl-pyridyl systems was observed when *m*-methoxyphenyl boronic acid was coupled to 3-iodopyridine giving a 77% yield in 20 minutes under microwave conditions.

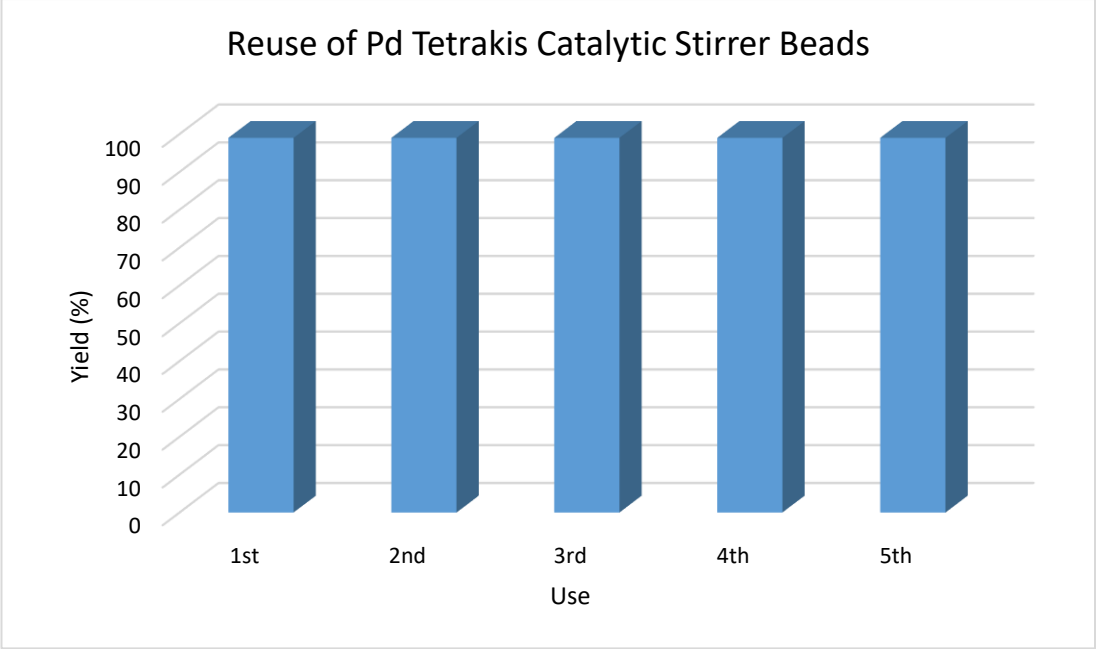

Graph 1: Reusability study of the reaction between phenyl boronic acid **152a** and iodoacetophenone **153a** to the corresponding biphenyl compound **154a** as determined by ^{1}H NMR in reactions with 3D-printed 0.5% Pd stirrer beads, inert stirrer beads with powdered catalyst and 8 mm magnetic flea with powdered catalyst.

A reusability study was also conducted to observe the efficacy of the catalyst after its first use. The reaction between **152a** and **153a** was carried out using microwave irradiation at 120 °C. Upon completion, the product **154a** was isolated and the stirrer bead reused in the next reaction. Its clear from the graph that the bead was stable and effective up to five uses.

Upon reviewing the chemistry, we have been able to achieve thus far using our 3D-printed catalytic beads stirrer beads (for thermal and microwave reactions), we decided to look at developing a flow based approach for the same reaction. As briefly mentioned in the introductory chapters of this thesis, glass rectors that house solid supported reagents are often used in conjunction with flow systems. Unlike the PP reactors which were developed and used in the S_NAr and intramolecular cyclisation chemistry, we decided to use SLA printing to develop a high surface area monolith device that would fit into already existing glass reactors.

Monoliths: This work was carried out towards the very end of the research programme. As mentioned above, we decided to look at systems wherein the glass reactor housing of the Uniqsis flow reactor could be harnessed and a monolithic design could be printed and placed directly inside it. As the length of the glass reactor was 100 mm with a diameter of 10 mm, we decided to design a cylindrical device with a repeating 3D mesh pattern inside it. The device was 35 mm long and had a diameter corresponding to the internal dimensions of the glass housing of the flow reactor. The idea was that multiple 35 mm sections could be combined into the glass reactor. The idea for the mesh pattern inside the device was derived from the tetrahedral geometry pattern seen in a methane molecule or the sp^3 hybridization of carbon in such a molecule. A simple structure corresponding to this was designed and repeated creating a three-dimensional lattice work. This was then subtracted from a simple cylindrical design to create the monolith (**Figure 50**).

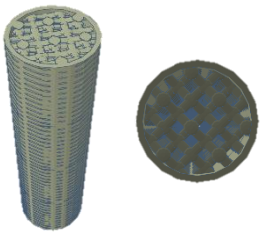

Figure 50: CAD design of monolithic device as seen from the front and top view.

In order to design and print such an object we envisaged that the original formulation would need to be altered slightly as the internal dimensions of the lattice work were far to small (< 0.1 mm) to print with photoinitiator alone. To think retrospectively, over-polymerization in such a case could be avoided by adding a photo-blocker or photo-absorber. Hence a new formulation was developed with a small amount of (BBT) as photo inhibitor.

In the initial phase of the formulation development, a small amount of the inhibitor (0.1%) was added to the existing 2nd generation formulation and the object was printed on the FormLabs Form 1+ SLA printer by using the Clear 01 laser setting and with a resolution of 0.025 mm. However, the structure

printed showed no internal definition and became very soft and jelly like. It was obvious that adding such amounts of inhibitor caused a drastic change in the physical nature of the polymerized object. Hence, we decided to drop the amount of TPO slightly and decrease the amount of the inhibitor by 10-fold to minimize this drastic change in the physical properties and observe if the object would be printable. Although, the details of this extensive process of formulation development have not been described in this thesis, the final formulation that was successfully printed is described below.

3rd Generation formulation: Poly(ethylene glycol) diacrylate Mn 250 98.53%, diphenyl(2,4,6-trimethylbenzoyl) phosphine oxide (TPO) 0.8%, 2,5-*bis*-(5-*tert*-butyl-benzoxazole-2-yl)thiophene (BBT) 0.01%.

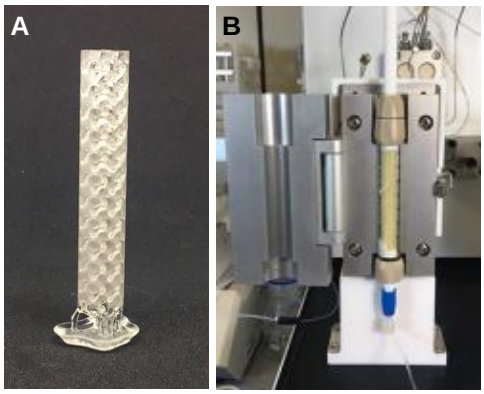

Figure 51: A) 3D-printed inert monolith with support structures; **B)** Monolithic device fitted inside the glass housing of the Uniqsis Flow reactor.

The next step was to incorporate the catalysts palladium (0) tetrakis(triphenylphosphine) and yttrium triflate into such a device and establish a printing protocol so as to perform the same chemistry (Suzuki couplings and carbonyl protections) under continuous flow conditions. Hence, in the same manner as with the stirrer beads, specific amounts of these catalysts were introduced into the blank resin mixtures and allowed to stir at room temperature before introducing into the printers.

Palladium Tetrakis(triphenylphosphine) monoliths: Poly(ethylene glycol) diacrylate Mn 250 99.09%, Pd tetrakis(triphenylphosphine) 0.5%, 2,5-b*is*-(5-

tert-butyl-benzoxazole-2-yl)thiophene (BBT) 0.01%, diphenyl(2,4,6-trimethylbenzoyl) phosphine oxide (TPO) 0.4%.

These devices were printed on the FormLabs Form1+ SLA printer using a higher power (Black 01) laser setting with a resolution of 0.025 mm. The volume of resin used in each monolith was 0.82 mL giving it a total catalyst loading of 0.0041 g. The devices were printed vertically and with supports on the upper face. The high resolution was required for the definition of the internal lattice work in the monolith. Black 01 setting was used in the print as the palladium in the formulation was behaving as a photo-blocker. Hence, a higher laser setting was required.

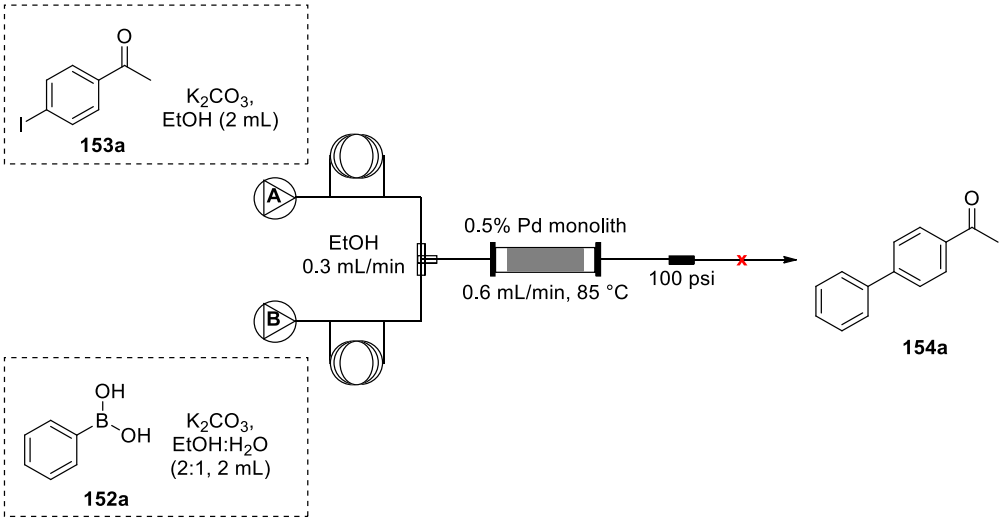

Scheme 57: Continuous flow route for the synthesis of **154a** using 3D-printed palladium monolith.

The scheme above demonstrates how we attempted to use the newly developed catalytic monoliths in the glass reactor fitted to an Uniqsis FlowSyn system. Firstly, the same catalyst was used as in the microwave and thermal reactions i.e. palladium tetrakis(triphenylphosphine). The catalyst loading was maintained at 0.5% w/w and the device was printed with the same setting, except with a higher resolution or layer height (0.025 mm) on the Form 1+ SLA printer. Once printed and appropriately cured post print, the monolith (2 × 35 mm) was placed inside an empty glass reactor and connected to the flow system with a 100 psi BPR. To begin our experiments, we prepared a solution of the iodoacetophenone with a single equivalent of potassium carbonate as

base in 2 mL of ethanol. A separate solution of a single equivalent of the phenylboronic acid and another equivalent of base was prepared, but this time we used 2 mL of a 2:1 ratio of ethanol and water in order to fully solubilize the mixture. The two solutions were injected into the individual 2 mL injection loops connected to pumps A and B. Ethanol was used as the solvent reservoir and the reactor fitted with the monoliths was first flushed with this solution and consequently heated to 85 °C. It was left to equilibrate for 10 minutes at this temperature while passing solvent through it at a combined flowrate of 0.6 mL/min or 0.3 mL/min at each pump. When the reaction was started the solutions from the individual loops were injected into the flow system at 0.3 mL/min each. They combined at a T-piece junction valve and passed through the reactor. The solution exiting the flow system was concentrated under reduced pressure and the crude product was analyzed by TLC. However, under these conditions no product was observed as the TLC showed spots corresponding to the individual starting materials.

The reaction was repeated under the same conditions using a fresh monolith (2 × 35 mm) and the amount of phenylboronic acid was increased to 1.5 equivalents. The solution was collected and concentrated under reduced pressure. A small workup by washing with water to remove any excess boronic acid and base was carried out and the crude material obtained from this step was investigated. The ^{1}H NMR spectrum showed that some amount of product was obtained however, there was still a considerable amount of iodoacetophenone. The ratio of the iodoacetophenone to product in the ^{1}H NMR sample was 1 : 1.41.

In the next series of experiments, the reaction molarities were kept the same and the temperature was gradually increased from 85 °C to 105 °C and the flow rate lowered from 0.6 mL/min to 0.2 mL/min. We were however, unable to drive the reaction to completion in all these reactions. The ratio of iodoacetophenone to product when the reaction was run at 105 °C and at a combined flow rate of 0.2 mL/min had decreased to 1 : 1.22. To check whether decreasing the flow rate was impeding the reaction, the temperature was further increased to 110 °C and flow rate lowered to 0.06 mL/min. This reaction too, showed a significant amount of starting material which led us to rethink

our protocol. We therefore swapped the base from potassium carbonate to triethylamine. This can be seen in **Scheme 58**.

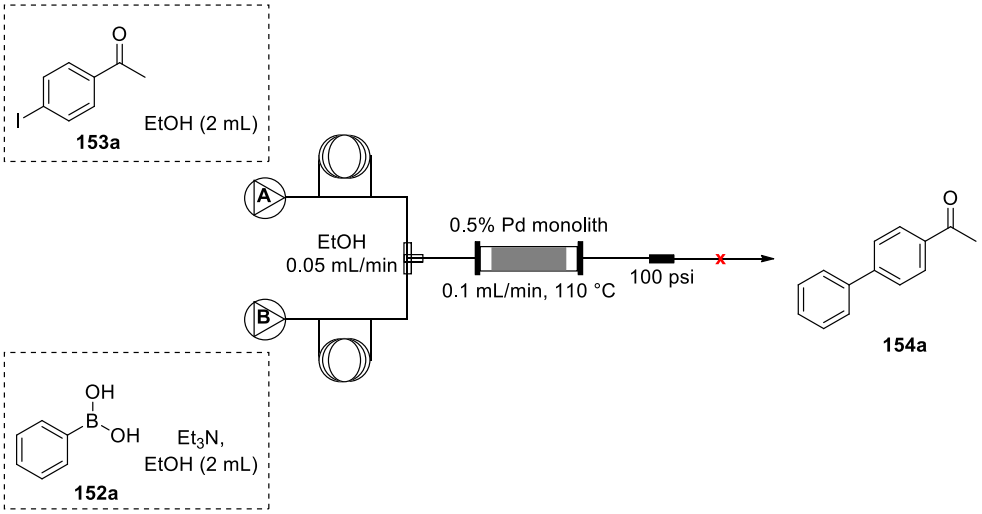

Scheme 58: Continuous flow route for the synthesis of **154a** using 3D-printed palladium monolith.

The iodoacetophenone was dissolved in 2 mL ethanol and injected into one loop of the flow system. Separately, a solution of the boronic acid with 1.5 equivalents of triethylamine in 2 mL ethanol was made and injected into the second loop. The reaction was run at 110 °C and a flow rate of 0.1 mL/min. However, no product was seen. Using the same base and reaction stoichiometry, the temperature was increased to 120 °C and flowrate decreased to 0.2 mL/min. This too, unfortunately did not yield any product. An even lower flowrate of 0.1 mL/min was tested at 120 °C under the same reaction conditions, however no product was obtained.

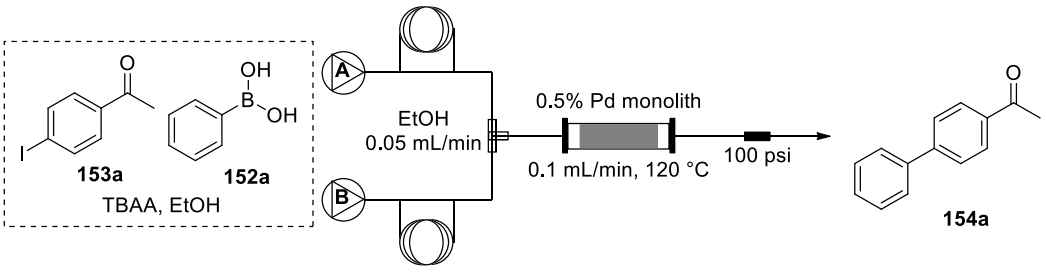

Scheme 59: Continuous flow route for the synthesis of **154a** using 3D-printed palladium monolith.

In a final attempt to make this reaction work better than our initial conditions, the base was swapped yet again from triethylamine to tetrabutylammonium acetate (TBAA). In this case, a solution of the iodoacetophenone, phenylboronic acid (1.5 equiv.) and TBAA (2 equiv.) in ethanol (4 mL) was made and 2 mL of the mixture was injected into each of the two sample loops. A fresh monolith with 0.5% w/w $Pd(PPh_3)_4$ was used and equilibrated at 120 °C with ethanol at a flowrate of 0.1 mL/min for 10 minutes. The reaction was run under these conditions after equilibration and the solution was concentrated under reduced pressure and purified by column chromatography. Interestingly, a ratio of the iodoacetophenone to product was 1 : 7. This can be seen in the ^{1}H NMR below (**Figure 52**).

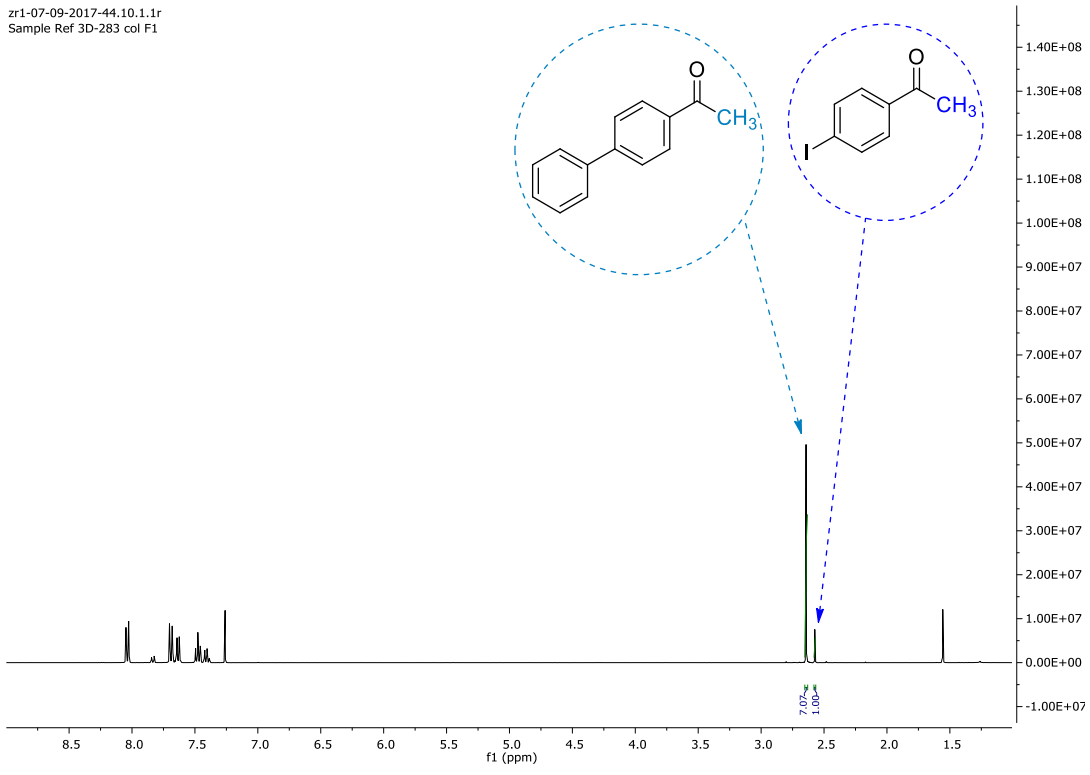

Figure 52: ^{1}H NMR showing iodoacetophenone **153a** and 1-([1,1'-biphenyl]-4-yl)ethanone **154a** in the ratio of 1 : 7.

Although this is the best result we had achieved thus far, it became quite obvious that the palladium monolith chemistry needed further development and hence we decided to move on with the project due to time constraints.

3.5.4 Yttrium Chemistry

Having demonstrated the relevance of an organic acid catalyst and a transition metal catalyst impregnated in a stirrer bead adapted device, we now wanted to explore the scope of Lewis acid catalysis using the same principle. For this section of the thesis we elected to explore the use of yttrium triflate ($Y(OTf)_3$) and its use in the protection of carbonyl groups in simple aldehydes. This principle was subsequently developed into a flow based protocol, which is discussed in the later sections of this thesis.

The versatility of this Lewis acid catalyst has been demonstrated below through its use in a variety of reactions namely aldol, Mannich, Michael, Freidel-Crafts, etc. making it an interesting compound to work with during our research. The cross-aldol reaction between ketone **157** and isobutyraldehyde **158** seen in **Scheme 60** Reaction A uses a stoichiometric amount of the catalyst and a tertiary amine to give the products **159** and **160** in good yields and *anti* disastereoselectivity (80:20) [163]. In the Mannich type reaction between the imine **161** and the ketene silyl enol ether **162** and 5 mol% $Y(OTf)_3$, the corresponding *β*-aminoester **163** was obtained in high yields (**Scheme 60** Reaction B) [164].

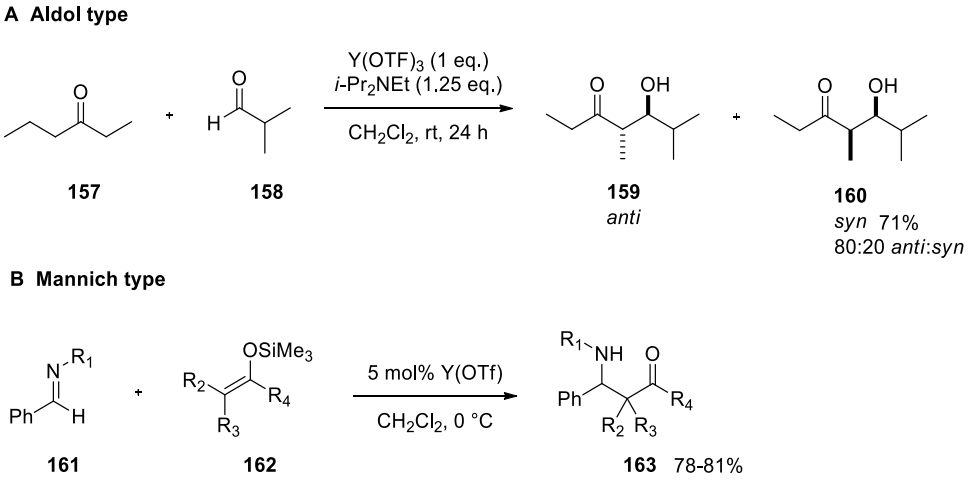

Scheme 60: A) Yttrium triflate catalyzed aldol reaction between ketone **157** and isobutryaldehyde **158**; **B)** Mannich-type reaction between imine **161** and ketene silyl enol ether **162** using yttrium triflate.

As seen in **Scheme 61**, the yttrium triflate catalyzed reaction between indole **164** and electron deficient olefins like *α*,*β*-unsaturated ketone **165** and *β*-nitrostyrene **167** give the corresponding 3-substituted Michael adducts **166** and **168** in good yields [165].

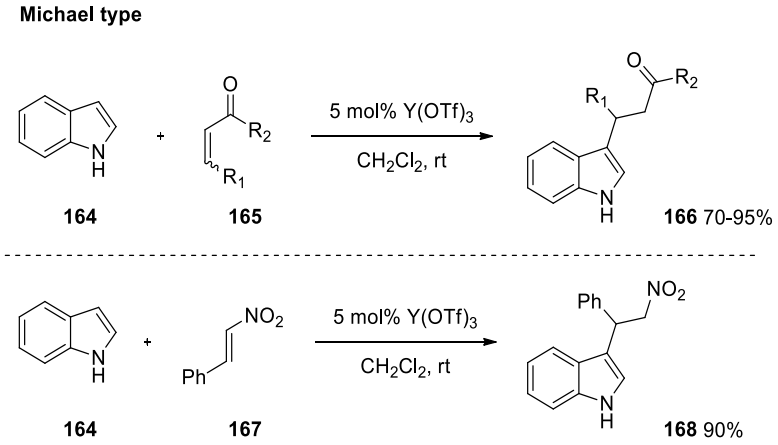

Scheme 61: Yttrium triflate-catalyzed reactions of indole **164** with electron-deficient olefins **165** and **167**.

In the acylation of 1-(phenylsulfonyl)pyrrole **169** using 10 mol% $Y(OTf)_3$ as reported by Kobayashi (**Scheme 62** Reaction A), it was found the 2-acylated adduct **170** was preferred over the 3-acylated adduct **171** and the reaction was high yielding as well as highly regioselective [166]. The imino-Diels-Alder reaction between *N*-aryl imine **172** and cyclopenta-1,3-diene **173** (**Scheme 62** Reaction B) was catalyzed by 20% $Y(OTf)_3$ and the tetrahydroquinoline derivative **174** was obtained in moderate yield [167].

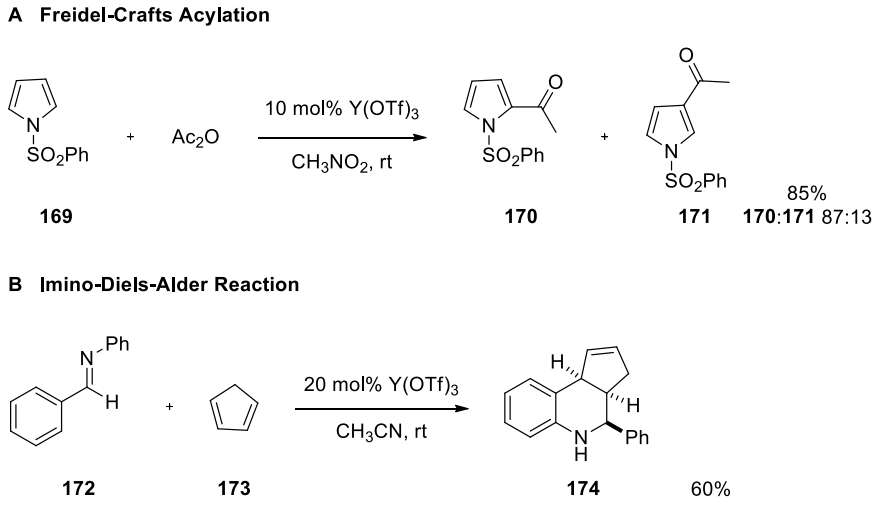

Scheme 62: A) Yttrium triflate catalyzed Freidel-Crafts acylation of 1-(phenylsulfonyl)pyrrole **169 X**; **B)** Yttrium triflate catalyzed imino-Diels-Alder reaction.

In the work described by De, catalytic amounts of yttrium triflate were used to protect carbonyl groups on aldehydes and ketones using 2-mercaptoethanol, 1,2-ethanedithiol, and 1,3-propanedithiol converting them to the corresponding dithianes [168]. We envisaged using this as a starting point to carry out similar reactions with impregnated $Y(OTf)_3$ stirrer bead devices adapted for microwave reactions. Using the same optimised formulation as in the palladium catalysed chemistry, a microwave route was developed for the protection of carbonyl groups in aldehydes using thiols to give the corresponding dithianes. The advantage of the 3D-printed $Y(OTf)_3$ stirrer bead over an inert 3D-printed stirrer bead and a normal stirrer bead was also investigated.

The first part of the Lewis acid catalysed protection of aldehydes using thiols involved the purification of the aldehydes in question. They were either distilled using a high-vacuum pump and distillation glassware or recrystallized and stored under nitrogen at 4 °C. The second part involved the preparation of the stirrer beads. A higher catalyst loading was used in comparison to the palladium chemistry seen earlier. We decided to start with creating a 2.5% w/w $Y(OTf)_3$ stirrer bead.

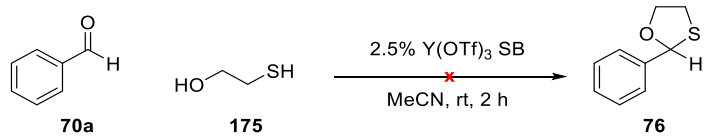

70a **175** **76**

Scheme 63: Synthesis of **176** using 3D-printed yttrium triflate stirrer beads.

In the initial reactions, we wanted to see if we could obtain the product under thermal conditions. As such, the aldehyde **70a** and 2-mercaptoethanol **175** (1.2 equiv.) were dissolved in acetonitrile and the 2.5% w/w $Y(OTf)_3$ stirrer bead was added to the reaction mixture (**Scheme 63**). The net weight of catalyst in each stirrer bead was calculated based on the average weight of each bead and was found to be 0.022 g. This reaction was stirred at room temperature for 2 hours and checked for product formation *via* TLC. No product was seen and upon working up the reaction, the ^{1}H NMR spectrum showed only starting material.

In the next experiment we examined the effect of adding the same amount of catalyst (0.022 g) directly into the reaction as a powder and stirring it with a normal stirrer bead. After stirring for 3 hours at room temperature and working up the reaction, the ^{1}H NMR spectrum of the crude material showed a 1 : 0.45 benzaldehyde to product ratio (**Figure 53**).

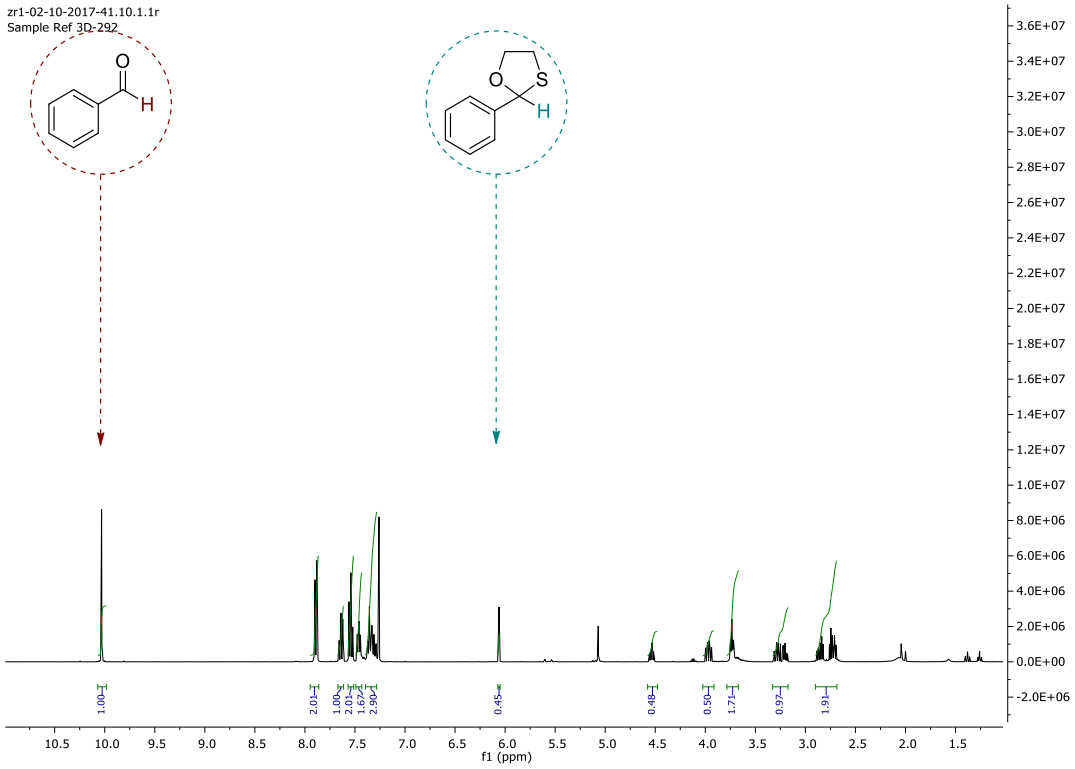

Figure 53: ^{1}H NMR showing benzaldehyde **70a** and 2-phenyl-1,3-oxathiolane **176** with 0.05 equiv. $Y(OTf)_3$ powder.

After observing such results, we decided to drive the reaction to completion by heating it in a microwave, increasing the loading on the stirrer beads from 2.5% to 10% and also increasing the reaction molarity to 1 molar by concentrating the mixture (**Scheme 64**).

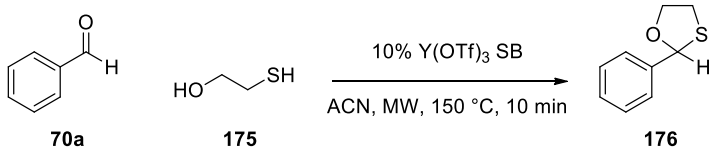

Scheme 64: Synthesis of **176** using 3D-printed yttrium triflate stirrer beads under microwave conditions.

As such, the appropriate microwave stirrer bead .stl file was printed with the increased catalyst formulation and the reaction was carried out by heating in the microwave at 150 °C for 10 minutes. As seen in the ^{1}H NMR spectrum below (**Figure 54**), the reaction was significantly improved giving a benzaldehyde to product ratio of 0.08 : 1. The reaction could therefore in

theory be pushed to completion by simply heating it for an additional 10 minutes.

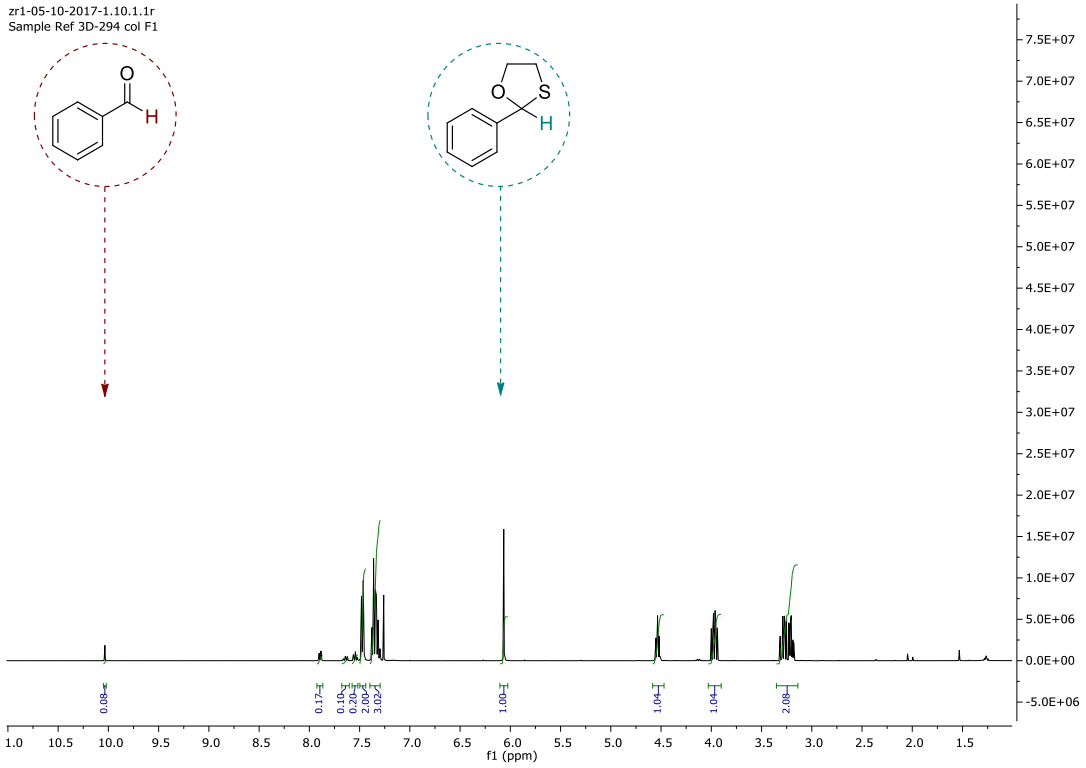

Figure 54: ^{1}H NMR showing benzaldehyde and 2-phenyl-1,3-oxathiolane product with 10% $Y(OTf)_3$ microwave stirrer bead.

With these results, we decided to check if the original formulation with the lower catalyst loading (2.5%) would be sufficient to carry out the reaction in a fitting timescale. Hence, a microwave adapted stirrer bead with the 2.5% w/w loading $Y(OTf)_3$ formulation was printed and used in the reaction by irradiating it at 150 °C. A very small amount of product was seen after 10 minutes (as observed by TLC) and the reaction was stopped after 40 minutes. Upon concentrating the reaction mixture, the ^{1}H NMR spectrum showed a ratio of benzaldehyde to product of 0.35 : 1. It became obvious that the increased loading had a direct impact on the rate of the reaction and thus we decided to use the 10% w/w $Y(OTf)_3$ loaded stirrer beads in our reactions.

As seen in the palladium chemistry in the previous section, we also developed monoliths using this higher loading (10% w/w $Y(OTf)_3$) and decided to investigate the chemistry further.

Yttrium Triflate monoliths: Poly(ethylene glycol) diacrylate Mn 250 89.19%, Yttrium triflate 10%, 2,5-b*is*-(5-*tert*-butylbenzoxazole-2-yl)thiophene (BBT) 0.01%, diphenyl(2,4,6-trimethylbenzoyl)phosphine oxide (TPO) 0.8%.

These devices were printed on the FormLabs Form 1+ SLA printer using a lower power (Clear 01) laser setting with a resolution of 0.025 mm. Similar to the palladium monoliths, these devices were printed vertically with supports on the upper face. The Clear 01 setting was sufficient to produce the detailed intricacies in the monolith lattice structure.

The monoliths were placed inside the glass reactor and the flow system was fitted with a 45 psi BPR. The aldehyde and 2-mercaptoethanol (1.2 equiv.) were dissolved in 4mL anhydrous acetonitrile and injected into each of the 2 mL sample loops of the Uniqsis FlowSyn flow system. As the aldehydes had been previously distilled and stored under nitrogen, the injection loops were flushed with anhydrous acetonitrile prior to these reaction mixture injections. The reactor was equilibrated at 150 °C with anhydrous acetonitrile at 0.30 mL/min for 30 minutes before starting the reaction. Once injected, the reagents were made to pass over the monolith until it exited the flow system. The solution was concentrated and a ^{1}H NMR of the crude mixture showed that most of the starting material had been consumed and the ratio of benzaldehyde to product was 0.17 : 1. The only drawback with this procedure is that the BPR did not produce enough pressure to keep the acetonitrile within the system. As the temperature had been elevated well above its boiling point a drop in system pressure (0.2 bar) was observed and the acetonitrile was bubbling out of the flow system.

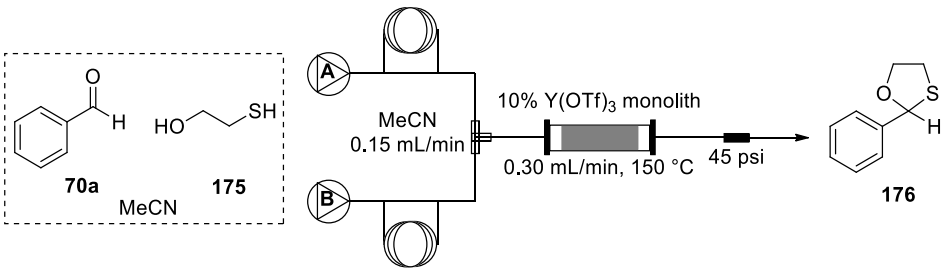

Scheme 65: Continuous flow route for the synthesis of **176** using 3D-printed yttrium triflate monolith.

Hence in the next experiment, a 75 psi BPR was used and the flow rate was decreased to 0.1 mL/min. Upon collecting and purifying the crude material the ^{1}H NMR revealed a lower conversion to product as the ratio of benzaldehyde to product was 0.23 : 1.

At this point, we decided to swap the 2-mercaptoethanol **175** with 1,3-propanedithiol **177a** as a protecting group and analyse the reaction using this new strategy. As such, a solution with benzaldehyde **70a**, thiol **177a** (1.2 equiv.) in 4 mL of anhydrous acetonitrile was made and injected into the two 2 mL injection loops of the Uniqsis FlowSyn. As per the previous experiments, these loops had been flushed with anhydrous acetonitrile and the solvent reservoir was also filled with a flask containing the same solvent. Fresh 10% $Y(OTf)_3$ w/w monoliths were placed inside the glass reactor and it was equilibrated at 120 °C in acetonitrile at 0.2 mL/min for 30 minutes. Once the reaction mixture solutions were injected into the system, the flowrate was maintained and the solution exiting the flow system was concentrated and checked by TLC. The presence of a new spot on the TLC plate proved exciting as it was the clean product as observed by ^{1}H NMR spectrum analysis in an excellent yield of 91%.

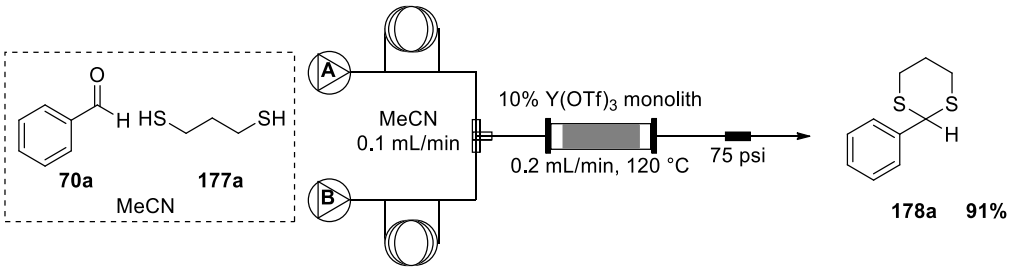

Scheme 66: Continuous flow route for the synthesis of **178a** using 3D-printed yttrium triflate monolith.

It became evident from these experiments that the dithiol proved to work better in reactions compared to mercaptoethanol **175**, under the reaction conditions using our 3D-printed monoliths. We hypothesized that the same outcome would be observed if we were to translate this chemistry back to microwave conditions.

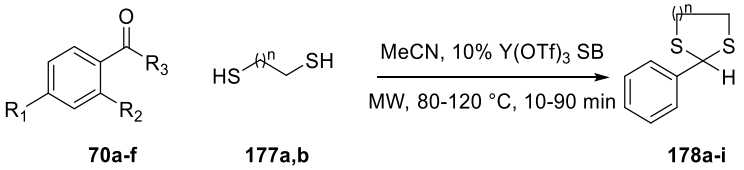

70a-f **177a,b** **178a-i**

R_1 = CH, Br, F, OMe, NO_2
R_2 = CH, Br
R_3 = H, CH_3
n = 1, 2

Scheme 67: Synthesis of compounds **178a-I** using microwave irradiation and 3D-printed $Y(OTf)_3$ stirrer beads.

In order to start building this dithiane protected library and experimenting with microwave conditions using the same 10% $Y(OTf)_3$ microwave adapted stirrer beads, a range of aldehydes **70a**-**f** were selected and reacted with 1,3-propanedithiol **177a** and 1,2-ethanedithiol **177b** to form the corresponding dithianes **178a**-**i**. Depending on the reactivity of the aldehyde, the optimum conditions for each reaction was found and demonstrated as seen in **Table 11**.

Table 11: Microwave assisted synthesis of compounds **178a**-**i** using 3D-printed $Y(OTf)_3$ stirrer beads.

Entry	Aldehyde	Product	µw Conditions	Yield (%)
1	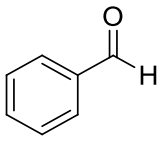 **70a**	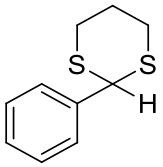 **178a**	120 °C, 10 min	91
2	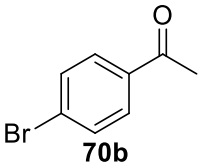 **70b**	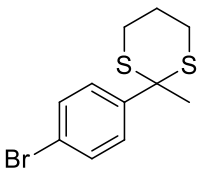 **178b**	120 °C, 90 min	36

Entry	Aldehyde	Product	µw Conditions	Yield (%)
3	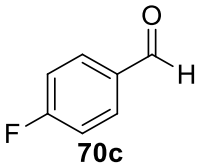 **70c**	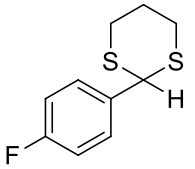 **178c**	100 °C, 10 min	99
4	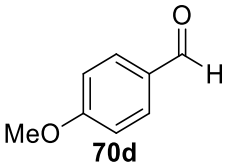 **70d**	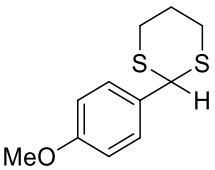 **178d**	80 °C, 30 min	99
5	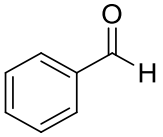 **70a**	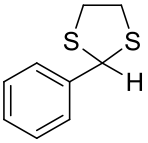 **178e**	120 °C, 40 min 120 °C, 60 min	90 93
6	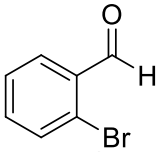 **70f**	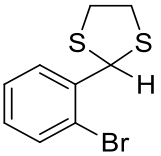 **178f**	120 °C, 20 min 80 °C, 10 min	99 76
7	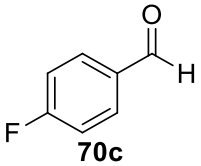 **70c**	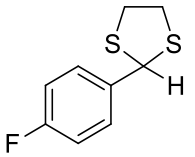 **178g**	100 °C, 50 min	94
8	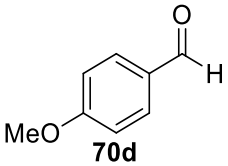 **70d**	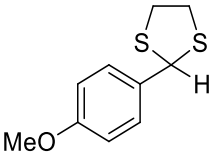 **178h**	100 °C, 50 min	99
9	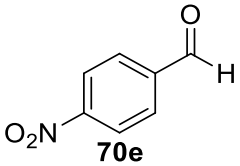 **70e**	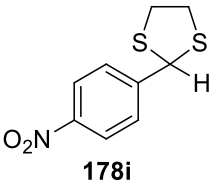 **178i**	100 °C, 50 min	74

Reactions with benzaldehyde **70a** and 1,3-propanedithiol **177a** catalysed by $Y(OTf)_3$ stirrer beads proceeded to completion in the microwave after 10 minutes, heating at 120 °C (Table X, Entry 1) giving a 91% yield. The 4-bromobenzadehyde **70b** required 90 minutes at this temperature and gave a low yield of 36% (**Table 11**, Entry 2). 4-Fluorobenzaldehyde **70c**, however required a lower temperature of 100 °C and proceeded to completion in 10 minutes (**Table 11**, Entry 3) in quantitative yield. With electron donating substituents on the aldehyde **70d**, an even lower temperature of 80 °C could be used and the reaction went to completion in 30 minutes (**Table 11**, Entry 4) also giving a quantitative yield.

Upon investigating the reaction of 1,2-ethanedithiol **177b** and aldehydes using the same $Y(OTf)_3$ stirrer beads, slightly different results were observed. Benzaldehyde **70a** required 120 °C for 60 minutes (**Table 11**, Entry 5) giving a 93% yield. The effect of 2-bromobenzaldehyde **70b** in the reaction was investigated owing to the low yields observed when 4-bromobenzaldehyde **70f** was used previously. This reaction (**Table 11**, Entry 6) required 120 °C for 20 minutes giving a quantitative yield. The 4-fluorobenzaldehyde **70c** as expected gave a high yield (94%) at 100 °C for 50 minutes under microwave irradiation (**Table 11**, Entry 7). The highly electron withdrawing 4-nitrobenzaldehyde **70e** also required similar conditions of 100 °C and 50 minutes giving a moderate 74% yield (**Table 11**, Entry 9). When anisaldehyde **70d** was used with the 1,2-ethanedithiol **177b**, the reaction proceeded to completion in quantitative yields with the same conditions (100 °C, 50 minutes) (**Table 11**, Entry 8).

Having generated a few examples using these catalytic beads in combination with aldehydes and the two thiol systems, we proceeded to investigate the effect of the 3D-printed stirrer bead against an inert 3D-printed stirrer bead with the same amount of powdered catalyst as well as a regular 8 mm stirrer bead with powdered catalyst. The average weight of a 3D-printed $Y(OTf)_3$ microwave stirrer bead was found to be 0.2 g. Given that the catalyst loading was 10%, the approximate weight in each bead was estimated to be 0.02 g. Using this information, a ^1H NMR experiment was carried out to investigate the effectiveness of the three systems.

The reaction between anisaldehyde **70d** and 1,3-propanedithiol **177a** was chosen owing to its moderate reaction time and low temperature requirement. In the first case, the 3D-printed $Y(OTf)_3$ (10% loading) stirrer bead was added to a solution of the two in deuterated acetonitrile and irradiated in the microwave at 80 °C. The reaction was paused every 10 minutes and a small aliquot of reaction mixture was removed and diluted with deuterated chloroform. A ^1H NMR spectrum (**Figure 55**) was observed on this sample immediately and this process was repeated every 10 minutes until the reaction was found to be complete. This reaction proceeded to completion in 50 minutes.

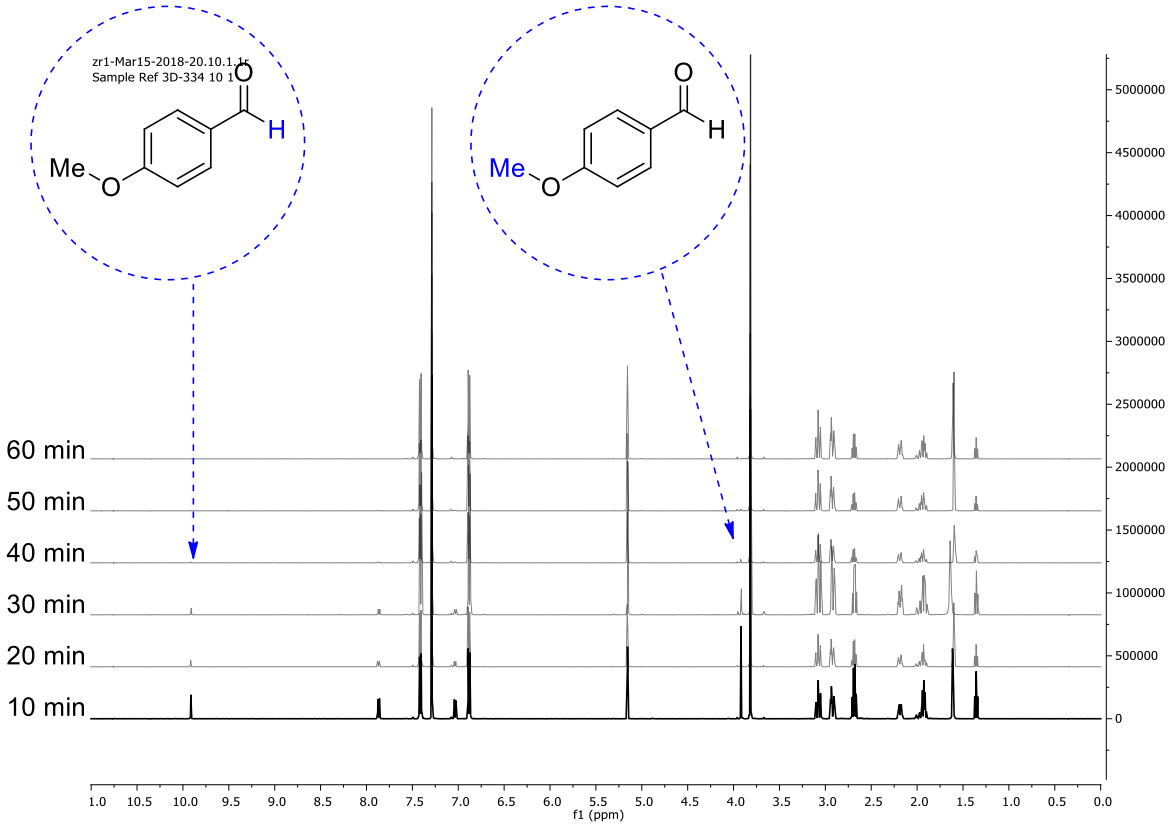

Figure 55: Aliquots taken out of the reaction between anisaldehyde **70d** and 1,3-propanedithiol **177a** every 10 minutes and a stacked ^1H NMR showing consumption of limiting reagent.

In the second case an inert 3D-printed stirrer bead was added to the same solution containing 0.02 g of $Y(OTf)_3$ in powdered form. The reaction was heated in the microwave under the same conditions (80 °C) and aliquots were

taken every 10 minutes. This reaction required a longer time in the microwave and only proceeded to completion in 170 minutes. This showed us that the catalyst impregnated in the stirrer directly affected the rate of the reaction.

The same reaction was carried out with a normal 8 mm microwave stirrer and 0.02 g $Y(OTf)_3$. The profile of this reaction was found to be similar to when the inert 3D-printed stirrer bead was used and only completed after 180 minutes.

The graph below clearly demonstrates the superior effect of our catalytic stirrer bead on the progression of the reaction.

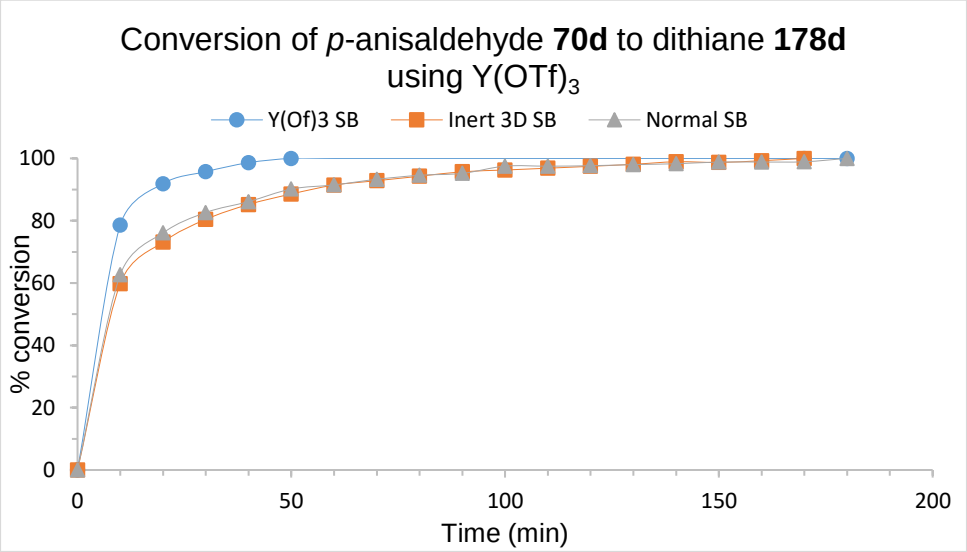

Graph 2: Conversion of *p*-anisaldehyde **70d** to dithiane **178d** as determined by ^1H NMR in reactions with 3D-printed $Y(OTf)_3$ stirrer beads, inert stirrer beads with powdered catalyst and 8 mm magnetic flea with powdered catalyst.

It can be observed that the stirrer bead impregnated with $Y(OTf)_3$ has the highest conversion (79%) in only 10 minutes as compared to the blank bead with powdered catalyst and magnetic flea with the same amount of powdered catalyst (60% and 63%). The trend seen in the graph shows that the reaction with inert bead and powdered catalyst performs slightly better than with the magnetic flea and powdered catalyst. It takes 170 minutes to reach completion versus 180 minutes when the magnetic flea alone was used. In contrast to this, the reaction with the $Y(OTf)_3$ impregnated stirrer bead proceeds to

completion in 50 minutes demonstrating the superiority of this system as compared to the other two.

3.6 Flow reactors

Having established a working protocol for catalysing reactions through stirrer bead devices, the search for an optimised formulation and printing of a reactor to carry out more robust chemistry in flow has been investigated herein. Such a process required a formulation that would not only be resistant to solvents and chemicals, but also able to withstand high temperatures and pressures. With regards to the design of a reactor, we wanted to incorporate channels as in the 3D-printed column reactors but also have the potential to carry out photochemistry through them.

When considering such a reactor, we wanted to incorporate the largest possible volume and surface area in a flow path within the device. Given that we were using SLA as a printing method, the formulation would be required to tolerate such intricacies within the structure in a single print and not overheat and over-polymerize. Coincidently, a group at the University of Washington published a report for printing microfluidic devices using poly(ethylene glycol) diacrylate (PEGDA) with Irgacure 819 and Irgacure 784 as dual photoinitiator systems [169]. Having a considerable amount of experience with the handling and printing of such acrylate based systems as seen in the work preceding this, it seemed to be a suitable starting point for the formulation development.

A rough channel design was first created on Tinkercad. This was comprised of a single 15 × 30 × 7 mm block with 0.1 mm straight channels passing through it as one would find in a chip reactor. A small section of this block was taken and used as a guide to optimise the formulation. As the report suggested, higher photoinitiator concentrations would be required to attain such a print. Hence keeping PEGDA as the monomeric unit, we investigated 4 different formulations with increasing amount of TPO (triphenylphosphine oxide). While the lowest concentration (0.5% w/w) showed over-polymerization in the fine channels, the highest (2.12% w/w) as suggested in the report caused severe hazing of the print tray and high heat emission from the resin mixture. The print however, showed well-defined channels. The

solution we found was to lower the photoinitiator just enough so as to reduce the wear on the trays and overheating of the resin mixture but still having the definition of channels in the test print. Hence the formulation was developed further.

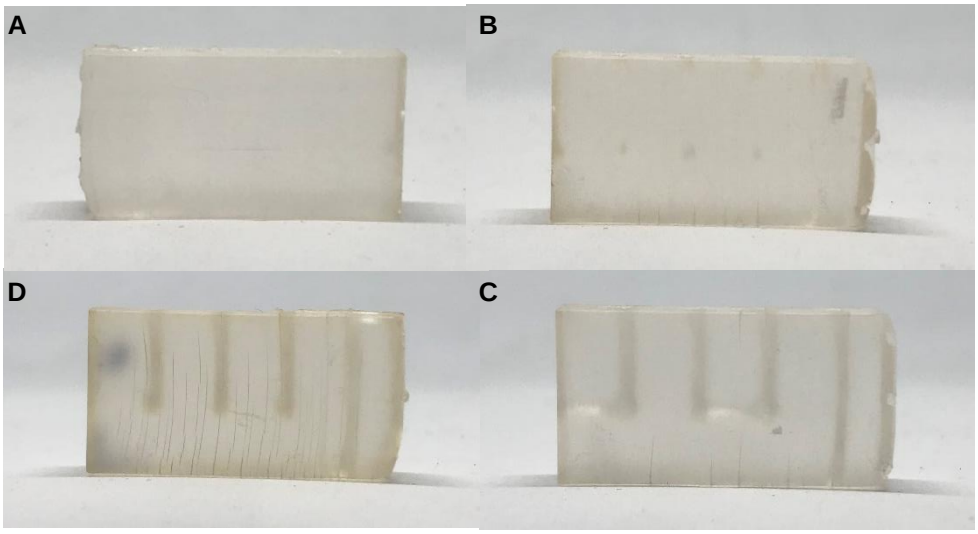

Figure 56: A) Test segment print with 0.67% photo-initiator; **B)** Test segment print with 1% photo-initiator; **C)** Test segment print with 1.5% photo-initiator; **D)** Test segment print with 2.12% photo-initiator.

3.6.1 TinkerCad Reactor Designs

Chip Reactor: While designing these reactors we wanted to incorporate channels occupying a maximum surface area in the reactor. The first design was a simple chip reactor. It consisted of a 55.5 × 102.5 × 4 mm block with 0.1 mm channels etched into the upper surface. A lip was created on one side that was 1.3 mm higher than the rest of the surface where the inlet and outlet ports would be present. Needle ports facilitated the inlet and exit of solutions in the reactor. The idea behind this was to have a glass top that would be sealed onto the surface bearing the channels. The glass was treated with silylacrylate in order to better bind to the surface of the reactor. It was left sitting in a hexane solution of 3-(trimethoxysilyl)propyl methacrylate overnight in order to functionalise it. The formulation used to print the reactor still utilised PEGDA, but the photoinitiator TPO was decreased to 0.5% w/w. The reactor was printed on the Form 1+ using Clear 01 setting and printed with a layer height of 0.1 mm. The object was printed vertically so as to allow for print definition in the channels and avoid over-polymerisation by allowing excess resin to drain off.

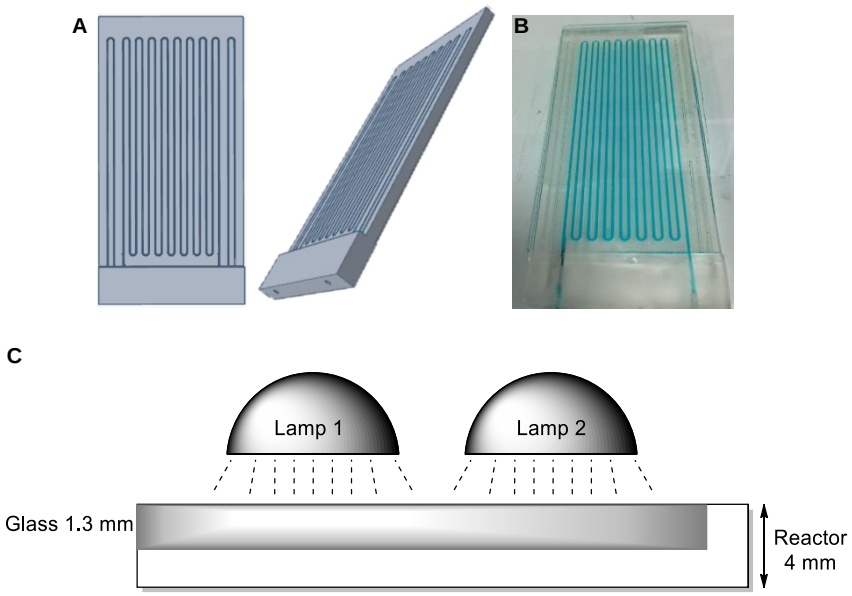

Figure 57: A) CAD design of chip reactor showing channels and needle inlet and exit ports; **B)** 3D-printed chip reactor with glass top and dye displaying channels; **C)** Schematic representation of the working chip reactor showing attached glass and lamps.

2nd Generation Formulation: Poly(ethylene glycol) diacrylate Mn 250 98.53%, diphenyl(2,4,6-trimethylbenzoyl) phosphine oxide (TPO) 1.47%.

We also wanted to allow such reactors to be heated using conventional hotplates used in the lab, so the design was made circular to allow them to fit into DrySyn equipment if needed. Hence, the name circular hotplate reactors or CHRs. All reactors were printed on the Form 1+ SLA printer and Clear 01 settings were used for laser exposure. After all prints were completed, the reactors were taken off the build plates and rinsed with IPA. This was followed by immediately connecting them to a compressed air tubing line to remove un-polymerized resin. IPA was reintroduced into the channels of the reactor and the reactor was connected to the compressed air tubing line again. This process was repeated three to four times or until the channels were found to be void of liquid resin after which the same compressed air tubing line was re-attached for the last time and air blown through the channels, thereby drying them.

The reactor was printed using 1.47% PI (TPO) and 98.53% PEGDA 250. It was printed vertically with the screw threads close to the base plate. Supports were added and the point density was increased to 0.82. After the print the reactor was first flushed with compressed air to remove any excess unpolymerised resin, then flushed repeatedly with IPA. This was repeated three to four times until the inter surfaces (channels) were clean.

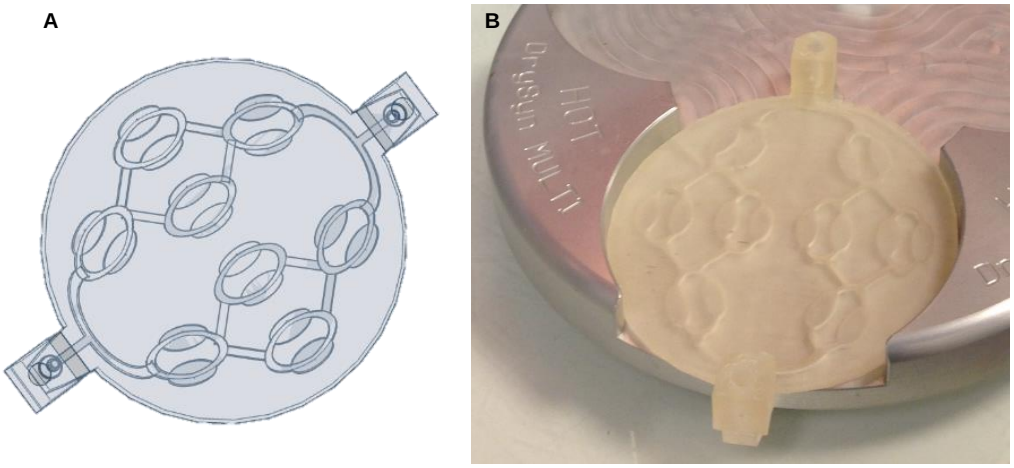

Figure 58: A) CAD drawing of circular hotplate reactor design 1; **B)** Printed circular hotplate reactor design 1 and placed in DrySyn.

CHR1: This reactor had a diameter of 75 mm and was 3 mm thick. It featured channels of the split and mix type. The inlet and outlet were positioned on opposite ends. This inlet or outlet composed of a 10 mm cube with a rough hole (4.44 mm ID) was created to allow the screw thread of the ferrule to be screwed into the device. The channels from the inlet were 2 mm wide and split in two separate paths upon entry into the device. They then divided again, opening out into wider oval shaped holes (5 mm) which would recombine into the smaller channel. This ‘unit’ repeated itself four times on each side of the reactor giving a total of eight split and mix type segments in total. The reactor was printed vertically with the inlet/outlet facing the build plate. Supports were added where required. Upon printing, the channels were found to be partially blocked.

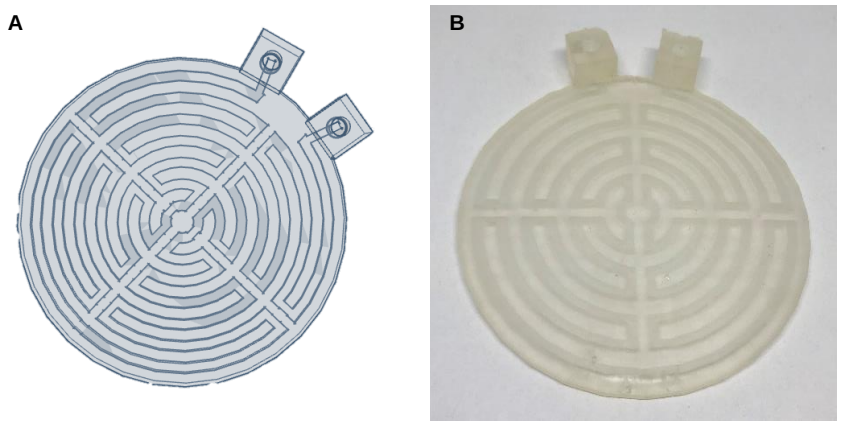

Figure 59: A) CAD drawing of circular hotplate reactor design 2; **B)** Printed circular hotplate reactor design 2.

CHR2: This reactor featured coil type channels. The dimensions of the reactor were left the same as CHR1 except the channels were 5 mm wide and square in cross-section. The design aimed to maximise the utilisation of surface area on the reactor with its intricate pattern splitting the channels into four distinct quadrants within the reactor. The inlet and outlet were placed on the same side in this case as it would be easier to fit in the desired hotplate without losing vital space.

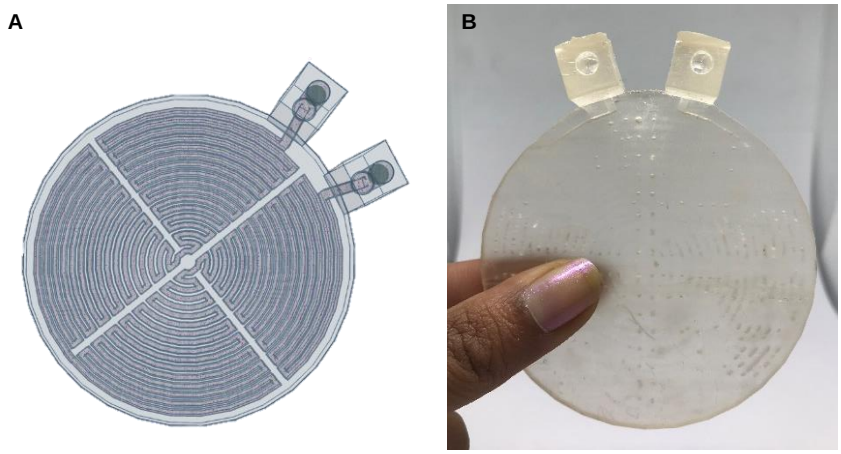

Figure 60: A) CAD drawing of circular hotplate reactor design 3; **B)** Printed circular hotplate reactor design 3 showing over-polymerization.

CHR3: The reactor was identical to CHR2 except the channel size was decreased to 2 mm in order to provide a higher residence time for reactions. Horizontal channels were 1 mm wide. The print appeared to be successful but

upon cleaning the reactor of un-polymerised resin it was found to be partially blocked along the horizontal channels due to the accumulation of resin and potential over-polymerisation.

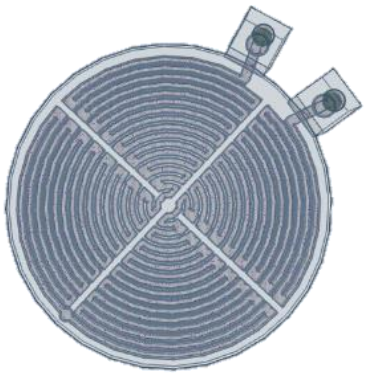

Figure 61: CAD drawing of circular hotplate reactor design 4.

CHR4: This design aimed to improve on the previous by increasing the thickness of the horizontal channels to 2 mm to allow for this potential over-polymerisation. A lip was added to the bottom-most channel connecting the two quadrants to also accommodate for this potential over-polymerisation. Heights of the inlet and outlet blocks were increased to 15 mm. Although the reactor printed successfully, the post-print processing required rapid removal of all excess resin before any over-polymerisation could occur. This often resulted in a partially blocked reactor due to the difficulty in removing the somewhat viscous resin from the fine channels.

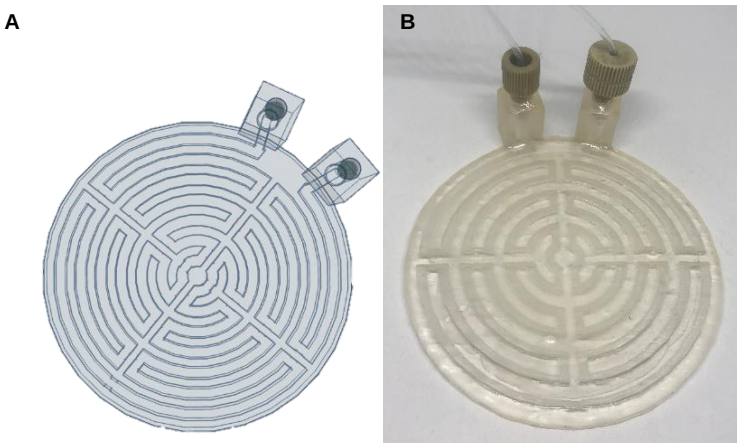

Figure 62: A) CAD drawing of circular hotplate reactor design 5; **B)** Printed circular hotplate reactor design 5 attched with PEEK ferrules.

CHR5: This design was a replica of CHR2 with the 5 mm circular channels. The only difference between the two designs was the height of the inlet and outlet blocks which were increased to 15 mm to give the ferrule enough room to secure itself in position in the device.

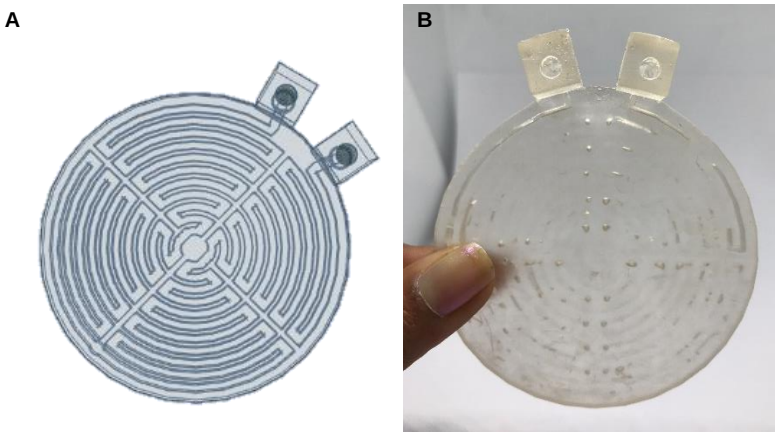

Figure 63: A) CAD drawing of circular hotplate reactor design 6; **B)** Printed circular hotplate reactor design 6 showing over-polymerization.

CHR6: This design aimed at improving slightly on the residence time the reactor could accommodate without potential issues of over-polymerisation. The coil type channels were therefore medium sized (3 mm). The height of screw blocks were maintained at 15 mm and the thickness of the horizontal channels increased to 2.20 mm. A lip in the bottom-most channel connecting the two quadrants of the reactor was added. Although the print was successful, the post-print processing issues led us to abandon efforts in decreasing channel size with the existing formulation and optimising reactor designs with 5 mm wide channels.

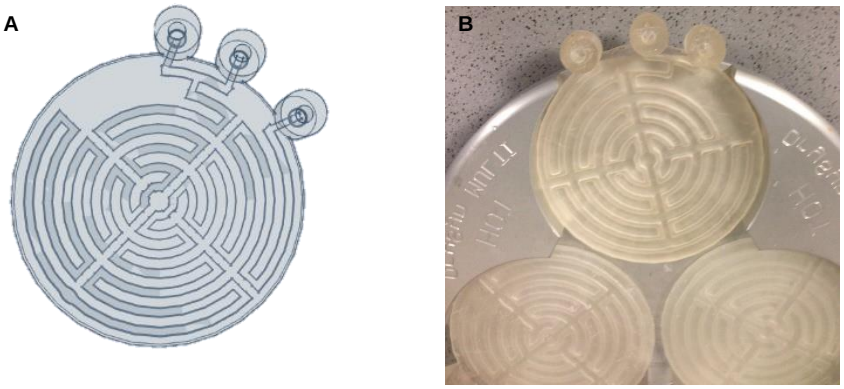

Figure 64: A) CAD file of circular hotplate reactor design 7; **B)** 3D-printed reactor fit in hotplate.

CHR7: This reactor featured a two inlet and single outlet design with 5 mm coil type channels. The inlet and outlet screw blocks were made cylindrical and its thickness slightly increased giving a width of 11 mm. The height of these cylindrical screw blocks was also increased to 15 mm as in the previous reactors. A lip was also added to the bottom-most channel connecting the two quadrants. The reactor was printed successfully, but a considerable amount of strain was observed at the points where the screw blocks met the reactor and over time, cracks at these junctions were observed.

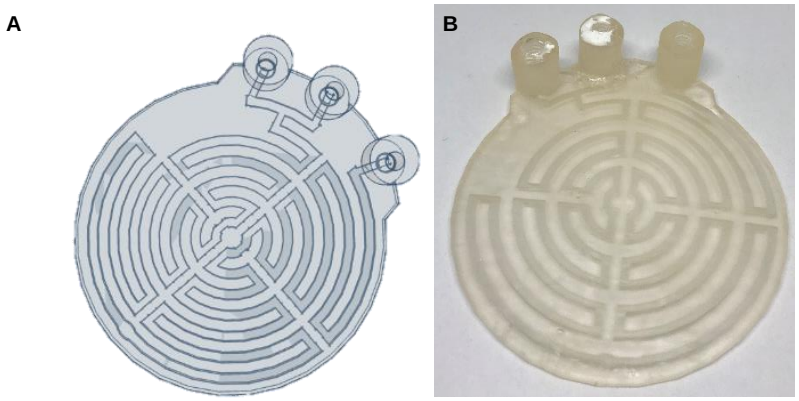

Figure 65: A) CAD drawing of circular hotplate reactor design 8; **B)** Printed circular hotplate reactor design 8.

CHR8: This design was identical to the previous except it included the addition of an extra lip or wedge that connected the screw blocks to the reactor surface to potentially ease the stress caused by the coil being so close to the edge of the reactor as in the previous design. Although the print was successful, small cracks were observed at the corners of this wedge.

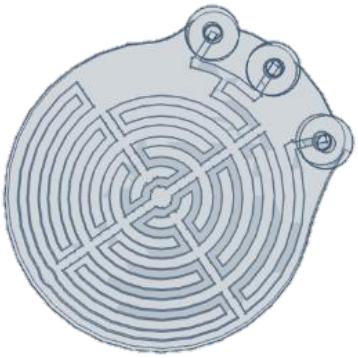

Figure 66: Circular hotplate reactor design 9.

CHR9: This reactor was identical to the previous except the wedge that connected the screw blocks to the reactor body was smoothened so that no corners or sharp edges were observed. This reactor was successfully printed and the formation of cracks along the stress points was alleviated.

Figure 67: Circular hotplate reactor design10.

CHR10: This reactor featured a scaled down version of CH7 to fit a 47 mm wide hotplate. The dimensions of the screw blocks, however, were maintained as previous. This reactor did not feature an additional wedge.

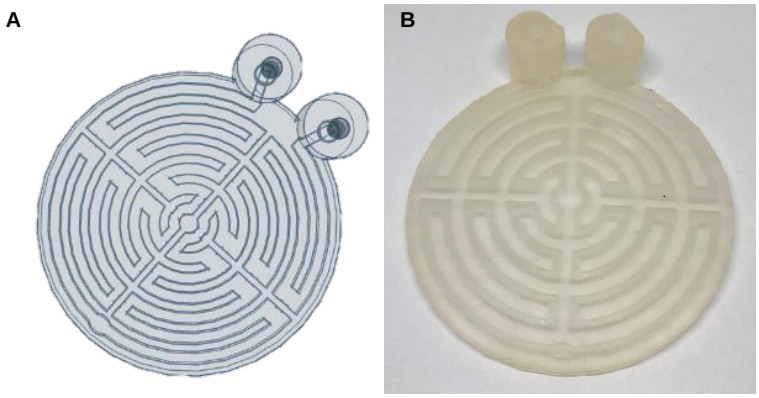

Figure 68: A) CAD drawing of circular hotplate reactor design 11; **B)** Printed circular hotplate reactor design 11.

CHR11: This reactor was an adapted version of CHR7 except it included a single inlet and outlet. The screw blocks maintained an increased height of 15 mm and the channel size 5 mm. The thickness of the reactor was increased to 5 mm and extra width along the horizontal channels (4 mm) was added. It also showcased a lip in the bottom-most channel connecting the two quadrants as in CHR7.

Screw thread optimisation:

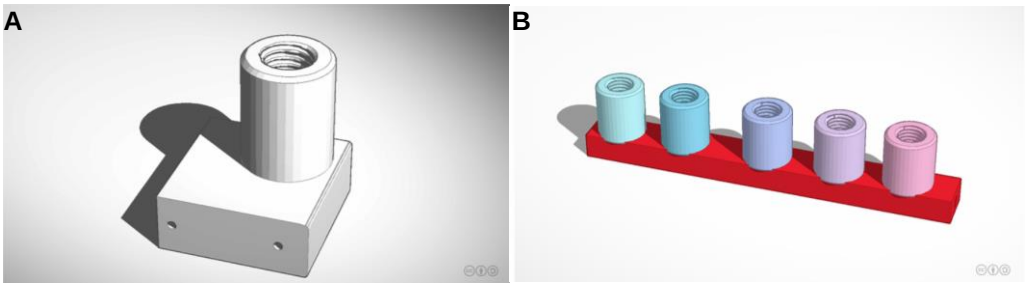

Figure 69: A) CAD file showing standard screw thread compliant with dimensions that match ferrules in flow systems; **B)** CAD file with screw thread designs showing 105-110% increase in dimensions.

A screw thread file was donated from Uniqsis' CAD designs for glass reactors and a section of this file was printed. A significant amount of shrinkage was observed with our formulation causing the screw block to be smaller than the ferrule size. Hence the design was modified and the screw block itself selected and placed on a rectangular plank with increasing dimensions. The scale was increased from 101%-111%. It was observed that the perfect fit with our formulation was the screw thread scaled to 110%.

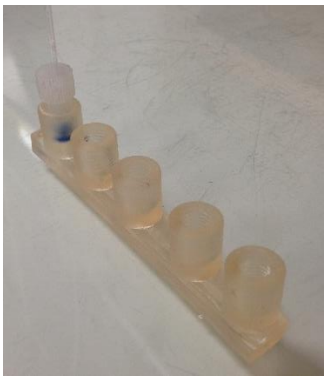

Figure 70: Image showing 3D-printed screw threads of varying sizes (106%-110%) with ferrule fit in correct size.

Unlike the PP reactors developed in the first portion of this thesis, this SLA formulated device seemed to be more brittle and harder and thus tapping out the screw threads would be disadvantageous. If the size of the thread was too small, inserting the ferrule would cause the entire block to crack. If the size was too big then the joint would be loose and would cause solvents to leak out

through this point. It was therefore essential to make sure the fit to the reactor was good and safe to work with.

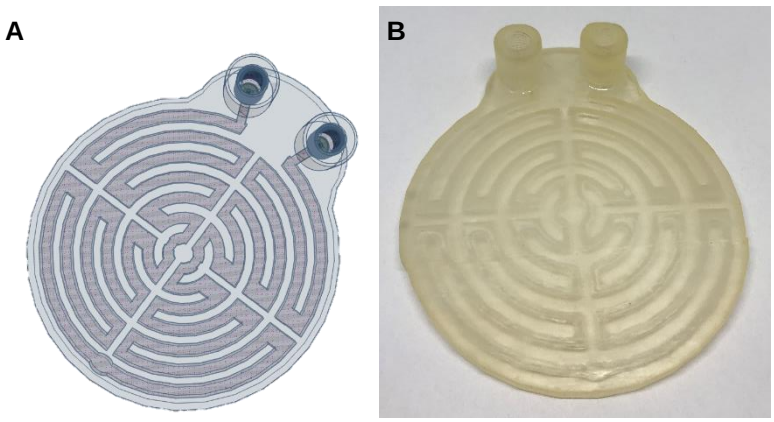

Figure 71: A) CAD drawing of circular hotplate reactor design 12; **B)** Printed circular hotplate reactor design 12.

CHR12: This was the final design in the series of circular hotplate disc reactors. It featured a screw thread designed by Uniqsis and optimised by us for the given formulation. The reactor consisted of 5 mm wide circular channels with an increased width of 4 mm along the horizontal edges. It also included a lip at the bottom-most channel connecting the two quadrants to avoid over-polymerisation in this area. A wedge joining the screw blocks to the reactor body was added and its edges were smoothened out to decrease stress points that could potentially cause cracks in the print after a given period of time. The thickness of the reactor was maintained at 5 mm to give sufficient space between the channels and outer body of the reactor.

In order to calculate the internal volume of the reactor, the CAD file of CHR12 was duplicated and channels made solid. This was loaded into Preform program and the volume was calculated. The difference in this volume and that of the original file was found to be 4.44 mL.

Figure 72: Circular disc reactors placed in hot plates showing channels by passing coloured dyes through them.

Reactor Testing:

These series of experiments aimed at establishing safe working conditions while using such reactors in flow. Considering the new formulation used, we wanted to establish pressure limits that the reactor could withstand as well as its behaviour towards changing temperatures. As the design of the reactor consisted of channels within its otherwise solid body, we expected certain stress points to evolve while subjecting it to such conditions and therefore wanted to know these thresholds as a starting point to our investigation.

We therefore connected the CHR12 to our Uniqsis FlowSyn using ferrules that would otherwise attach to a glass reactor unit or the coil unit in the system. Perlast O-rings made from PTFE were placed inside the screw blocks and the ferrules were screwed in. These O-rings provided the necessary seal required to maintain the high pressures that could develop in the system. The system configuration was set up as to allow a maximum pressure of 20 bar after which it would automatically shut down. Ethanol was used as a solvent and the flow rates at pumps A and B were set to 0.5 mL/min each respectively. The system pressure recorded while using such conditions was observed to be 15 bar. The reactor was stable under these conditions and showed no signs of leaks and or cracks developing on its body. The next part focussed on establishing the effects of adding heat to an already pressurised system. We therefore placed the reactor on a hotplate connected to a temperature probe and gradually

began to increase its temperature. We observed a sudden loss of system pressure due to a crack that developed in one of the channels causing it to leak. The crack developed when the system pressure reached a high of 18 bar and the temperature of the hotplate reached 67 °C. Given these results it became clear to us that such a reactor was more capable of handling high pressures as compared to high temperatures. We gathered that the brittle quality of the polymerized material was due to single monomer (PEGDA) used in the formulation and its potential randomised polymerisation that would occur in the printing process. The chain length being Mn 250, which is considered relatively short, would also be partially responsible for the hard and brittle nature of the polymerized product.

The next experiment consisted of testing the device's response to temperature alone, in the absence of solvents or in a flow system. We therefore placed a newly printed CHR12 on the hotplate and gradually began heating it. As there was no solvent in its channels, we expected a slightly different behaviour. In this case, several cracks started to develop along the edges of the reactor, as if it were expanding along its curved edge. The shape of the otherwise flat reactor also started to deform and warp slightly. All these changes happened as the hotplate reached 75 °C. It is possible that some of these results could have occurred due to the non-uniform heating pattern provided by the hotplate as it only heated the bottom face of the reactor. We concluded that due to the nature of the formulation and its moderate heat tolerance, all future experiments conducted should not include temperatures higher than 60 °C. We also hypothesized that in the event where heat is to be added to the system, the reactor could be immersed in an oil or water bath or if it were to be placed on a hotplate, appropriate measures would be taken to ensure that the heat is evenly dissipated throughout the reactor.

3.6.2. Flow photochemistry

3.6.2.1 C-H Functionalisations

Having established a working protocol for the printing of the circular hotplate reactor and considering its tolerances with regards to heat and pressure, we then set out to examine the scope of such a device in photochemical applications. Stephenson and co-workers previously reported a photoredox-mediated direct intermolecular C-H functionalisation of an indole or pyrrole with diethyl bromomalonate **179**. The use of visible light in this approach was investigated mainly due to its neutral conditions and activity at ambient temperatures, but also owing to the fact that such reactions showed low catalyst loading, functional group tolerance and the potential to be applied in flow [170]. The photoredox catalyst $Ru(bpy)_3Cl_2$ along with a suitable tertiary amine electron donor 4-methoxy-*N*,*N*-diphenylanaline, were used in the reaction and the authors proposed a mechanism wherein the catalyst in its $Ru(bpy)_3^{2+}$ form absorbs the visible light, exciting it to the $Ru(bpy)_3^{2+*}$ state. This is then supposed to be reductively quenched by the amine giving the $Ru(bpy)_3^{1+}$ state. This Ru^{1+} species then performs a single electron transfer between the C-Br bond of the bromomalonate regenerating the $Ru(bpy)_3^{2+}$ species and in turn generating the carbon radical on the malonate species. This electron deficient radical couples with the electron rich arene (indole or pyrrole) at the C2 position. This is followed by the oxidation and subsequent rearomatization affording the desired product (**Scheme 68**).

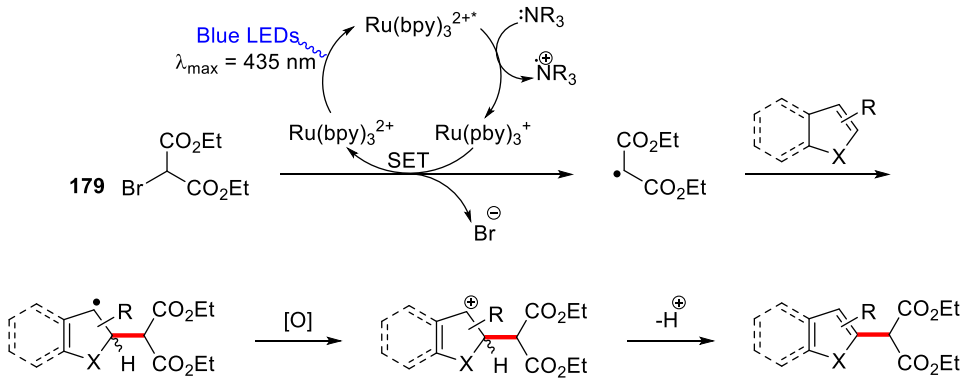

Scheme 68: Mechanism showing radical formation on bromomalonate **179** and C-H functionalization on indole.

The reaction with the *N*-methyl indole was first performed in batch to test the lights suggested by the authors of the publication and establish basic working conditions that we could then translate to flow. A solution of the indole **182** (1 equiv.), bromomalonate **179** (2 equiv.), amine **180** (2 equiv.) and tris(2,2′-bipyridyl)dichlororuthenium(II) hexahydrate **181** (0.01 equiv.) in anhydrous DMF (1.5 mL) was prepared in a oven dried round bottom flask. The solution was degassed by 3 freeze-pump-thaw cycles Blue LED's (400W A160 Actinic bulbs) were placed around the flask containing the reaction mixture at distance of no more than 2.5 cm. The bulbs were turned on and the reaction was monitored *via* TLC to observe consumption of the starting material and the formation of a new product spot. After 18 hours the reaction was stopped, although it was found that all the starting material had not been consumed. Upon working up the reaction and purifying it, a good yield (78%) was obtained and this gave us enough information about the reaction to try it in flow.

As with the batch experiment, a solution of indole **182**, bromomalonate **179**, $Ru(bpy)_3Cl_2$ **181** and amine **180** in anhydrous DMF was prepared in a flask and degassed sufficiently. This was then transferred into a single 2 mL injection loop of the Uniqsis FlowSyn flow reactor which had also been previously flushed with anhydrous DMF. This solution was made to pass through CHR12 disk reactor. The lights were placed directly in front of the reactor at a distance of 2.5 cm from the front face. A compressed air tubing line was also made to blow over the surface of the reactor so as to dissipate the heat produced by the intensity of the light source. The reaction was run at 0.03 mL/min using a single pump (Pump B) and the tubing exiting the reactor was connected to a 100 psi BPR. The solution exiting the tubing was partitioned between ethyl acetate and water and once the short work up was complete, it was purified by column chromatography yielding the product **183** in a good yield of 88%.

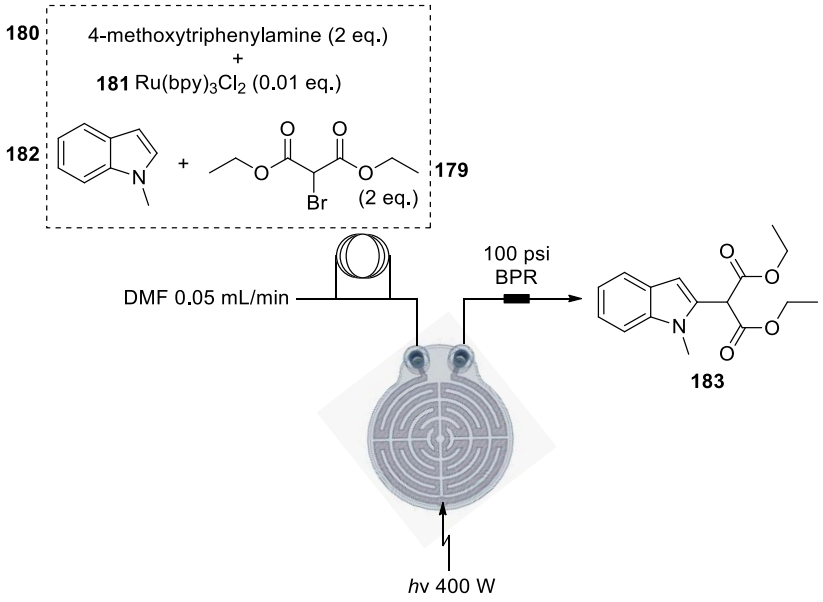

Scheme 69: Reaction of indole **182** and bromomalonate **179** using CHR12 and 400W lamp.

Using these conditions we attempted to replicate the procedure on a pyrrole **184** substrate. All conditions were kept the same and the solution containing the reaction mixture was injected into a single loop of the flow system and passed through the CHR12 disc reactor. In this example we saw a drop in yield (41%), possibly because the reaction required a longer time under these conditions. We hypothesized that the reaction could be improved if the reactor volume could be increased or if the channel size could be decreased as in a microfluidic system.

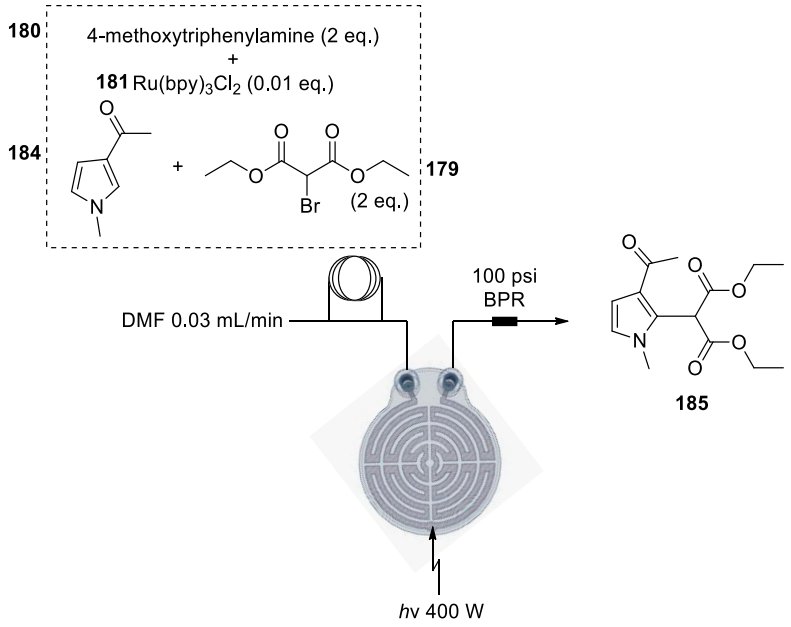

Scheme 70: Reaction of pyrrole **184** and bromomalonate **179** using CHR12 and 400W lamp.

Upon carrying out reactions such as these as well as test runs with no reacting material, we observed several improvements that could be made on these disc reactors. The most important point that needs to be considered, is the brittle nature of the fully polymerized formulation. Sharp cracks along weak points as seen in the initial development as well as cracks caused during experiments due to heat and pressure, all add up to us realizing the limits of the reactor printed with this given formulation. It is for this purpose that we decided to carry out the next phase of experiments in batch and optimize conditions for flow before their use in our reactors. All further optimization of the formulation and design will be discussed in the final section of this thesis.

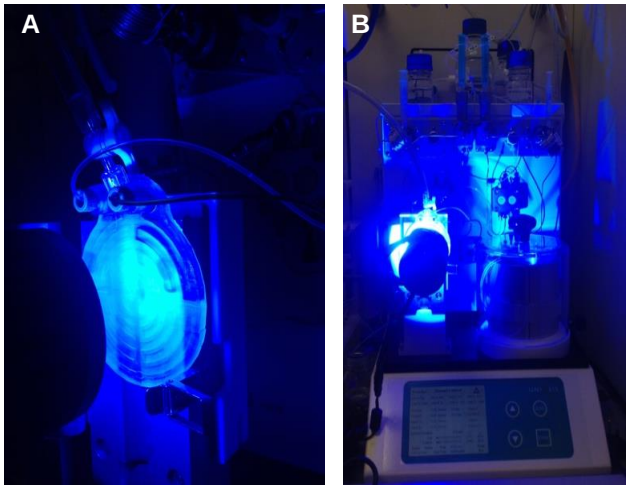

Figure 73: A) CHR12 under 400W lamp; **B)** CHR12 setup with Uniqsis flow reactor.

3.6.2.2 Flow Decarboxylation

The concluding work presented in this thesis involved the development of a synthetic route towards anti-helminthic drug praziquantel translatable to flow. This sequence featured a photodecarboxylation reaction amongst others, which was studied in detail (**Scheme 71**). We aimed initially to investigate the various steps and optimise them for a flow based protocol. The ultimate goal would be to combine our 3D-printing technologies developed over the past years and utilise them wherever possible in this sequence thus demonstrating effectively an endpoint to this research.

Seki and group reported a batch synthesis route to pyrazinoisoquinoline skeletons from *D*-phenylalanine methyl ester hydrochloride which we found interesting as it featured a stereocontrolled construction of the molecule [171]. In initial experiments *D*-phenylalanine methyl ester was used however, this was switched with the racemic compound for the purpose of examining the sequence and testing its robustness.

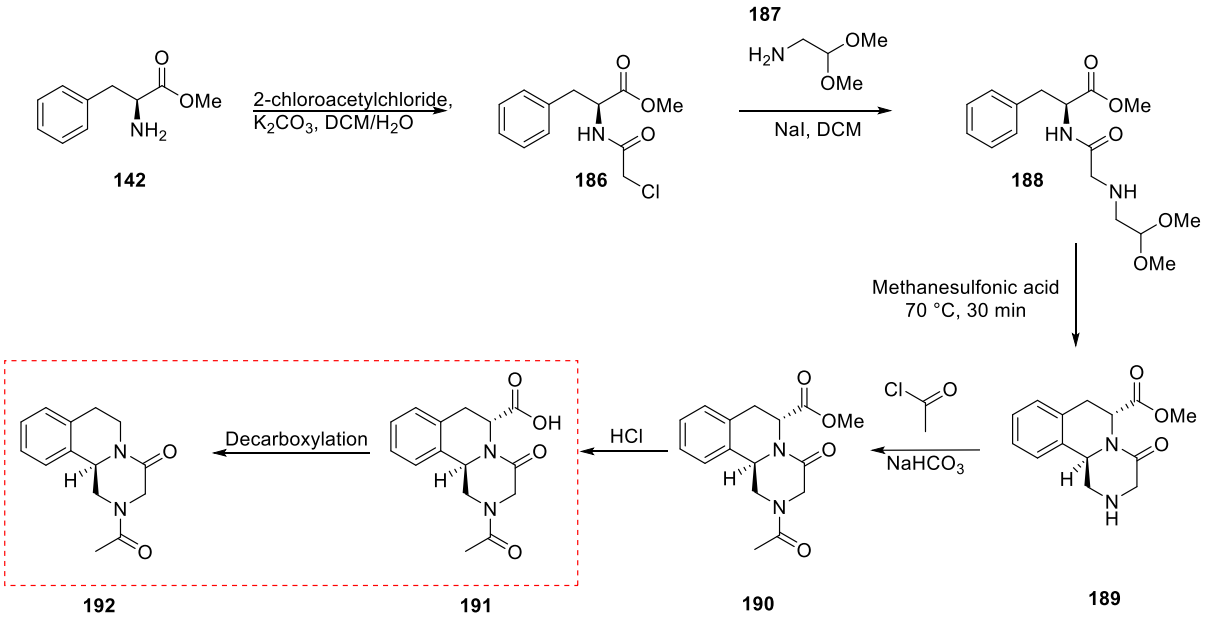

Scheme 71: Proposed synthetic route for Praziquantel analogue **192** with a focus on the decarboxylation reaction of such substrates.

The first step of this sequence featured a simple substitution type reaction where *D*-phenylalanine methyl ester **142** was treated with chloroacetyl chloride **193** in the presence of base (**Scheme 72**). The authors reported using

trimethylamine, however we switched to potassium carbonate due to its effectiveness in the reaction and the easy handling of the compound. The reaction was also performed in a separating funnel making the step far more simple. The crude product **186** obtained from this reaction was taken directly through to the next step.

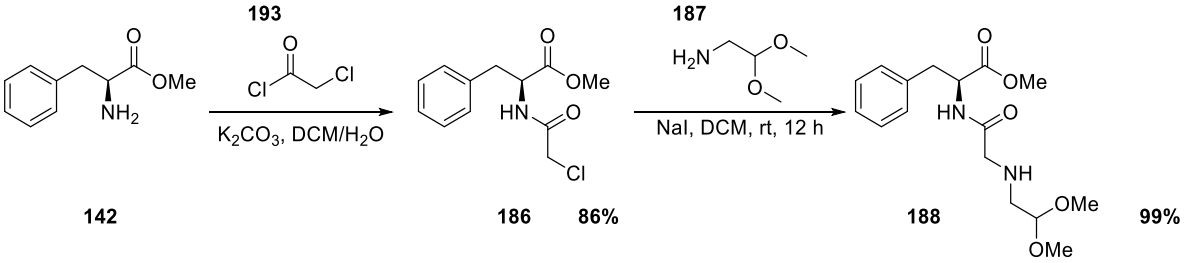

Scheme 72: Synthesis of **188** over two steps from phenylalanine methyl ester **142**.

This amination reaction between **186** and aminoacetaldehyde dimethyl acetal **187** was performed at room temperature and upon its completion as noted by TLC, a simple work up afforded the crude product in quantitative yield (**Scheme 72**).

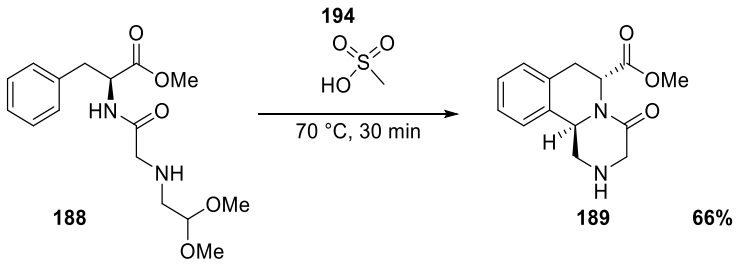

Scheme 73: Pictet-Spengler cyclisation of **188** to give **189**.

The third step featured a Pictet-Spengler cyclisation reaction using methanesulfonic acid as a solvent and proton source by heating it with **194** at 70 °C for 30 minutes (**Scheme 73**). In experiments where enantiopure *D*-phenylalanine methyl ester was used as starting material the *N*-acyliminium ion intermediate generated as a result underwent a diastereoselective cyclisation affording the cyclised product **189**. In our experiments we observed a dr of 92:8 for this reaction as seen in the ^{1}H NMR spectrum shown below (**Figure 74**). In order to obtain the clean product, the solution of the Brønsted

acid was simply neutralised by the addition of 1M NaOH and extracted with DCM. This crude material was taken through to the next step.

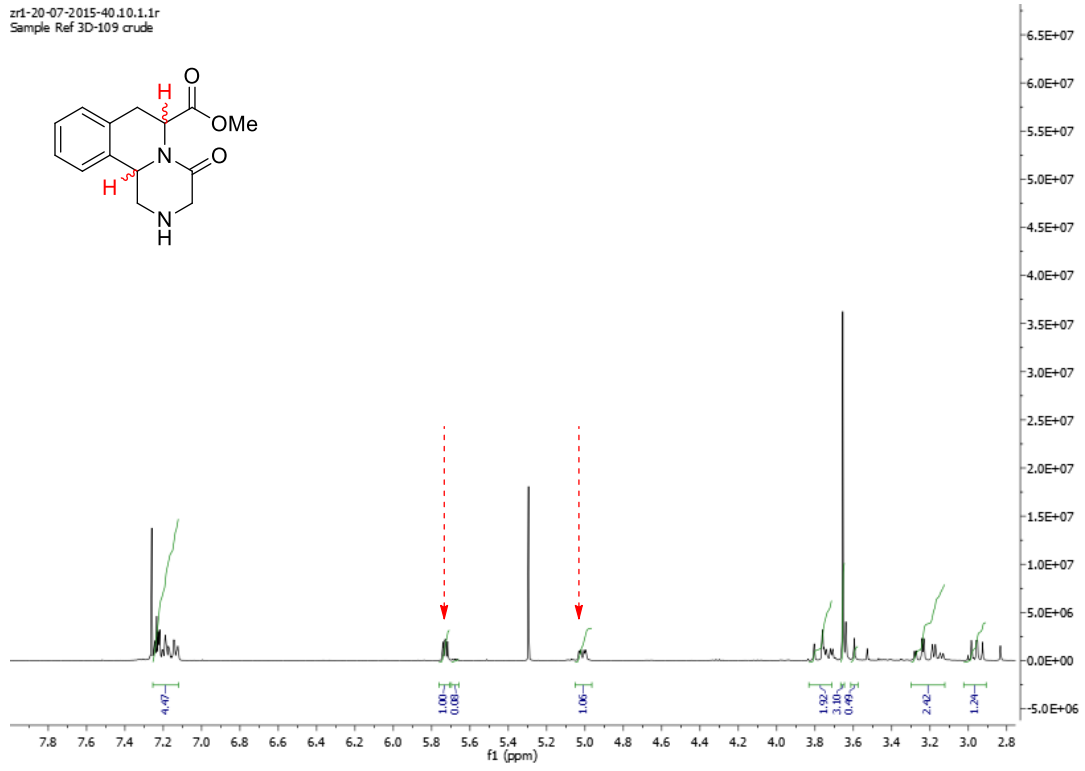

Figure 74: ^{1}H NMR spectrum showing the diastereomeric ratio of highlighted protons of cyclized product **189**.

The next three steps in the sequence were a hydrolysis, decarboxylation and acylation. The acid catalyzed hydrolysis of **189** (**Scheme 74**) was performed by heating under reflux with hydrochloric acid and the product from this reaction was obtained by trituration with a 10:1 solution of ethyl acetate and ethanol. The crude product from the reaction was used in the subsequent step without further purification.

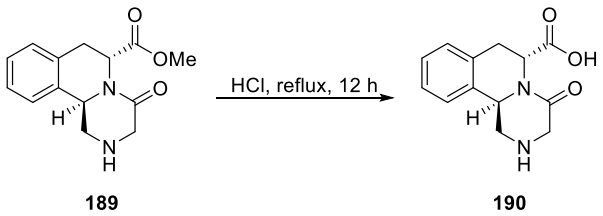

189 **190**

Scheme 74: Acid catalyzed hydrolysis of **189**.

The next step in the synthesis route featured a thermally promoted decarboxylation reaction. We hoped to explore the scope of such a reaction and its potential to be applied in a flow-based protocol. Almqvist reported a solvent-free microwave assisted decarboxylative procedure for carboxylic acid functionalized bicyclic 2-pyridones using *N*-methylpyrrolidinone (NMP) [172].

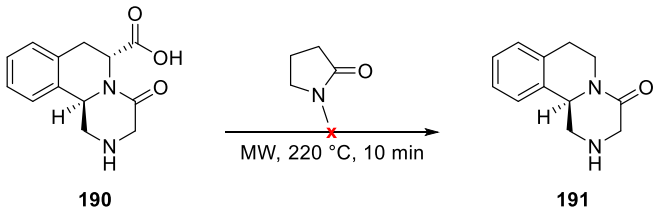

190 **191**

Scheme 75: Decarboxylation of **190** using NMP and microwave irradiation.

This article seemed particularly interesting as we hypothesized its applicability in a flow system with an added microwave insert. The reaction was repeated in a sealed microwave vial (**Scheme 75**) however, removing the NMP from the reaction mixture proved to be unsuccessful even after following the recommended workup procedure. An additional acidic wash was carried out on the organic residue in order to reintroduce the desired product into the aqueous phase. When separated, the aqueous phase was made alkaline again and re-extracted with DCM. This too, unfortunately did not yield the desired product and an observation of the ^{1}H NMR spectrum showed an absence of any aromatic protons and only traces of solvents and NMP.

The reaction was repeated a second time and no work up procedure was carried out. Instead, the solution was simply concentrated by using a high vacuum pump in order to better elucidate the effectiveness of the reaction. The ^{1}H NMR spectrum (**Figure 75**) showed only the starting material and a significant amount of NMP.

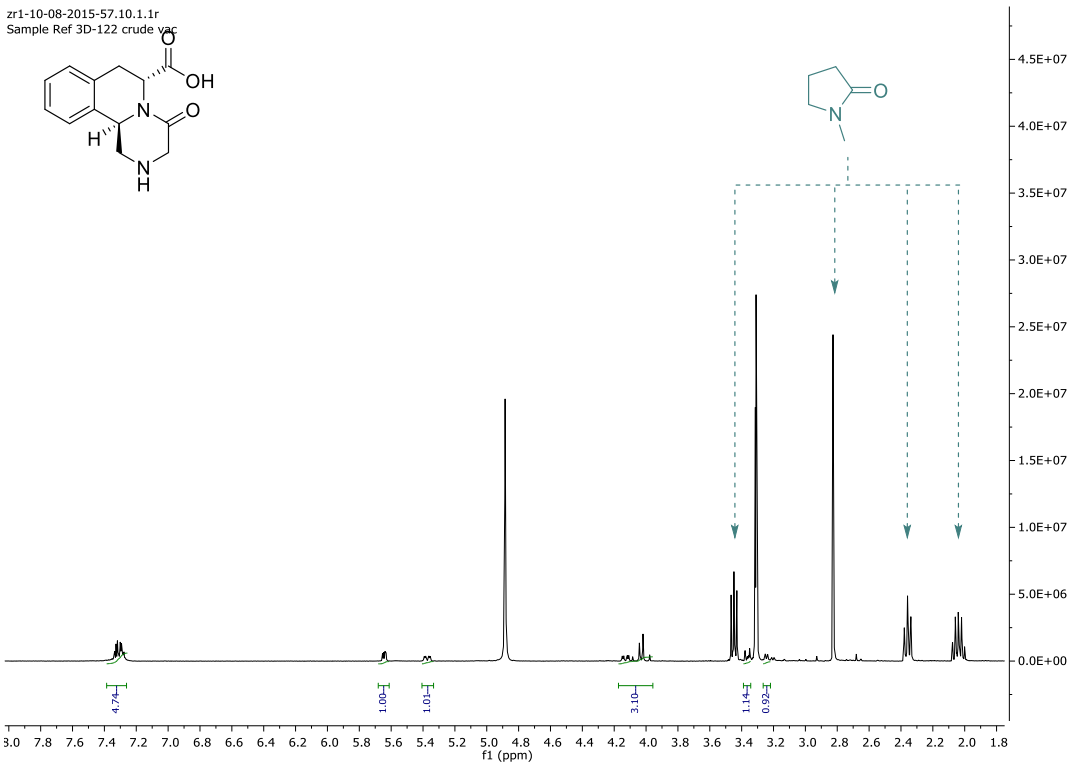

Figure 75: ^{1}H NMR spectrum showing trace amounts of strating material **190** and NMP.

The authors of the paper also reported another method using copper cyanide in NMP at 220 °C. Initially, it was decided to investigate whether copper acetate would be a suitable copper source for the decarboxylation reaction. The reaction was again carried out in a microwave and was heated to 220 °C for 10 minutes (**Scheme 76**) however no product was observed. Upon purifying the crude material by column chromatography, it was evident that the reaction did not work as the starting material appeared to have decomposed.

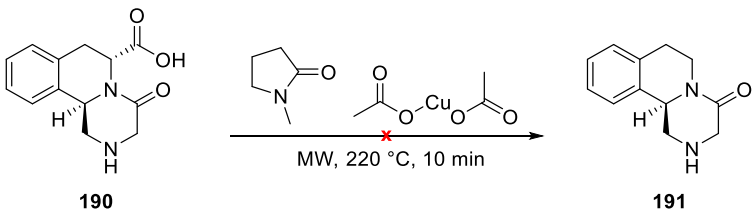

Scheme 76: Decarboxylation of **190** using NMP, copper acetate and microwave irradiation.

In the next approach to perform the decarboxylation reaction, we decided to swap the solvent from NMP to DMSO as we were having trouble separating it

from the crude material and we observed that it continued to persist even in purified fractions. In addition to this, we also decreased the temperature of the reaction to 120 °C to avoid decomposition of the product or starting material (**Scheme 77**). The reaction was again carried out in a sealed microwave vessel and checked for product formation in 10 minute intervals. After 30 minutes, the reaction was stopped and an aqueous workup afforded the crude material. The ^{1}H NMR spectrum confirmed that this reaction too, like the others did not work as no product was observed.

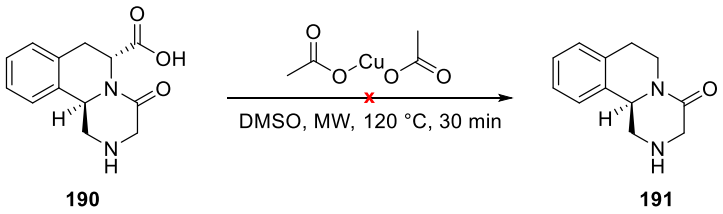

190 **191**

Scheme 77: Decarboxylation of **190** using DMSO, copper acetate and microwave irradiation.

After the failed reactions with copper acetate we decided to try the reaction with copper cyanide as literature suggested. A solution of the carboxylic acid and copper cyanide in NMP was irradiated in the microwave at 220 °C for 10 minutes (**Scheme 78**). However, it was quite evident from the TLC and crude ^{1}H NMR spectrum that no product was observed.

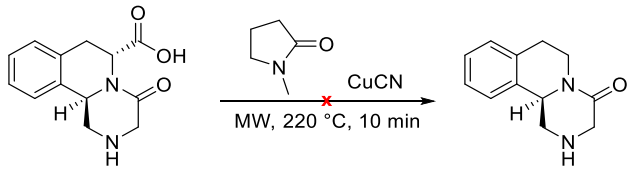

190 **191**

Scheme 78: Decarboxylation of **190** using NMP, copper cyanide and microwave irradiation.

While designing this sequence, we also investigated the effect of performing the second acylation step prior to the hydrolysis and decarboxylation steps and the reaction scheme is shown below (**Scheme 79**). In this series of reactions, racemic phenylalanine methyl ester was used as a starting material. The reaction between cyclized pyrazinoisoquinoline **189** and cyclohexanecarbonyl chloride **195** was performed in a biphasic solution of

DCM and water. The persistence of excess cyclohexanecarbonyl chloride in the crude material despite additional washes with a saturated solution of sodium bicarbonate led us to eventually remove it by column chromatography. Although we had hoped to avoid a purification step for this acylation reaction, it was important for us to get the product ready for the next step and continue to study the decarboxylation reaction. The yield obtained from this reaction was lower than expected (52%).

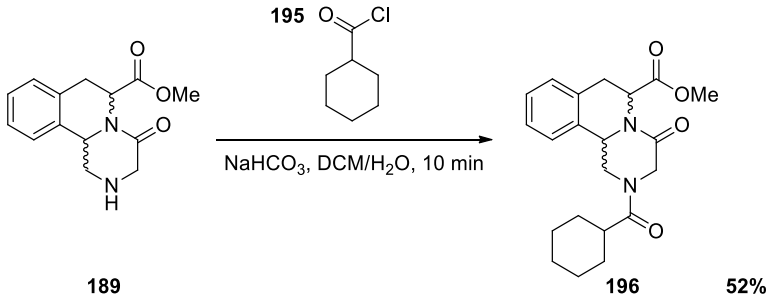

Scheme 79: Acylation of **189** using cyclohexanecarbonyl chloride **195**.

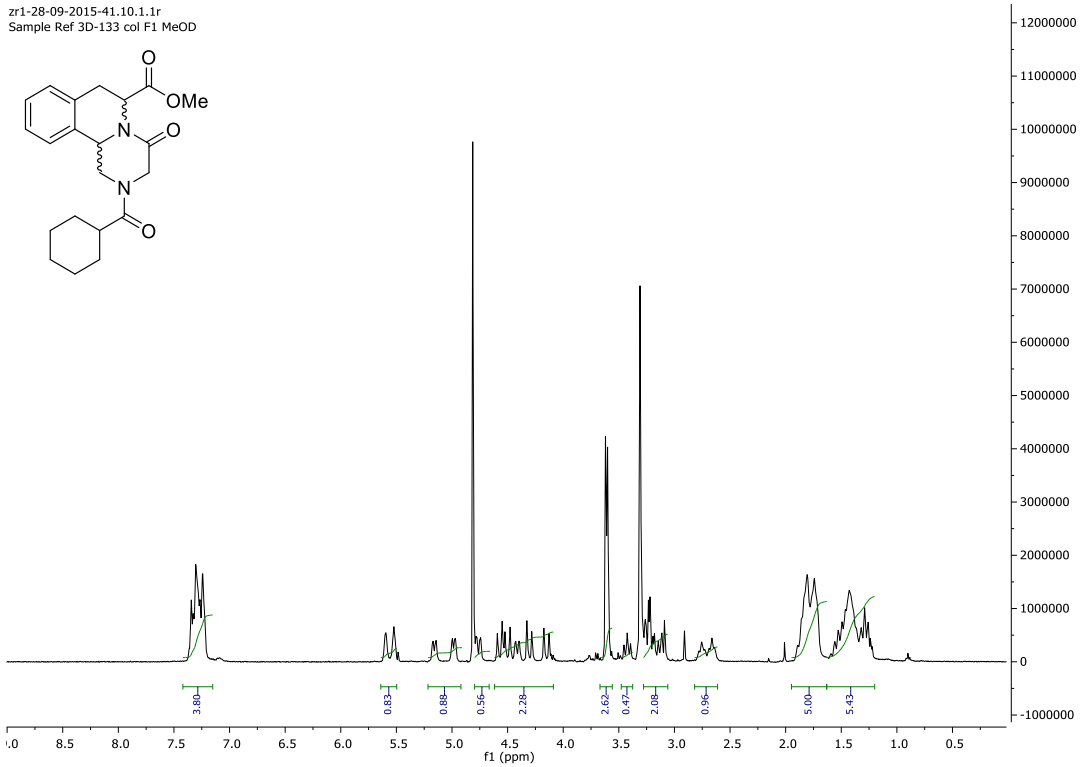

Figure 76: ^{1}H NMR spectrum showing acylated product **196**.

When the hydrolysis reaction was performed on the acylated product **196**, it had to be carried out in a solution of THF. In reactions where no THF was

added, loss of the cyclohexylcarbonyl group was observed. After the reaction was completed, the solution was made neutral by the addition of a saturated solution of sodium bicarbonate before extracting with DCM affording the crude material in good yield (65%).

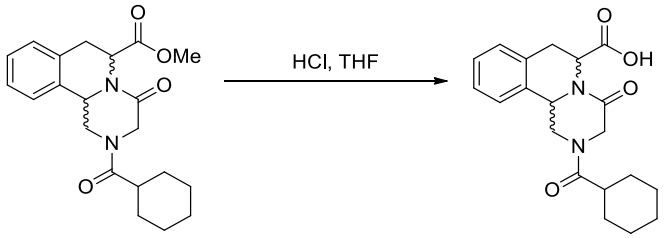

196 **197**

Scheme 80: Acid catalyzed hydrolysis of **196** in THF.

After failed attempts to perform the decarboxylation reaction using a thermally promoted route, we shifted our attention towards investigating a photogenerated radical route. The work published by Hatanaka and group describe a photogenerated cationic radical of phenanthrene (Phen) combined with 1,4-dicyanoebenzene (DCB) reacting with the carboxylic acid thus forming the initial radical fragment and eventually affording the reduced product in the presence of a thiol, which acts as an hydrogen donor [173]. This is a slightly different approach as compared to the classic Barton decarboxylation [174], wherein the decomposition of the thiohydroxamic ester into radical fragments is achieved by heat or light in the presence of a hydrogen donor such as a thiol or tributyltin hydride (**Scheme 81**).

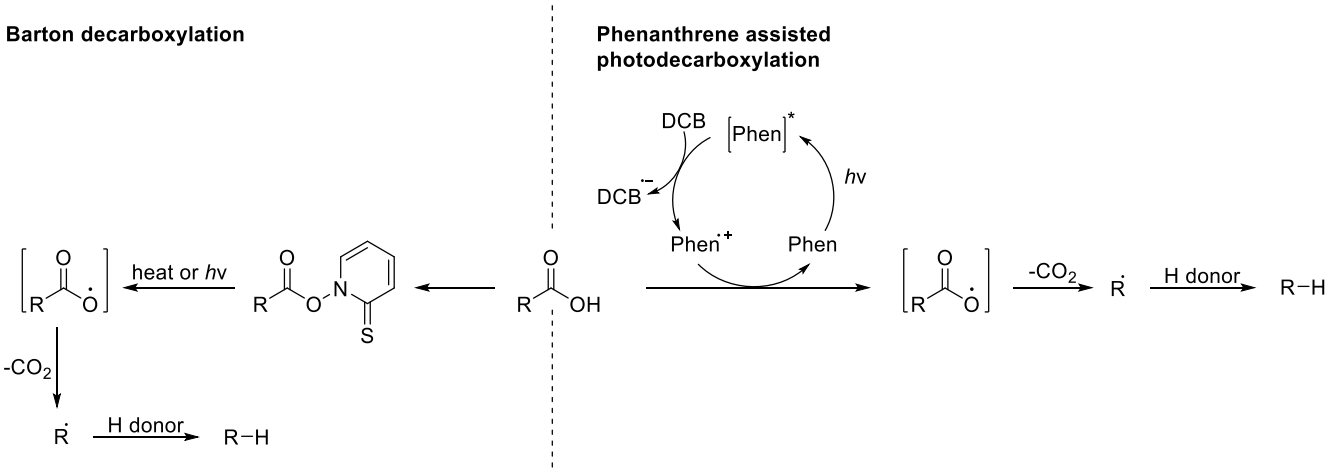

Scheme 81: Barton decarboxylation v/s decarboxylation using photogenerated cation radical of Phenanthrene.

This route seemed to be a relatively easy way to decarboxylate our analogue however it required the use of a 400 W high-pressure mercury lamp and a 6 hour reaction time (**Scheme 82**). The reaction time could potentially be lowered when optimizing in flow however, the need for a high energy light source such as the mercury lamp is what drove us to look back at the literature.

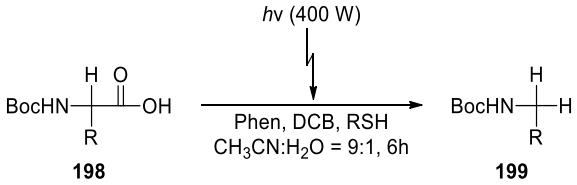

Scheme 82: Photo-decarboxylation of **198** using 400 W lamp as light source.

When phenanthrene was swapped with an acridinium photoredox catalyst, as in the work reported by Wallentin [175] it was found that the energy required in the system to generate the initial radical fragment was far lower. In this case, 8 W blue LEDs with a λ_{max} of 440 nm were sufficient to carry out the hydrodecarboxylation of protected amino acid derivative **198**. The authors selected this catalyst as it had a greater oxidation potential than that of the carboxylic acid. This was important as they hypothesized that the initial reaction seen in the system would be a photoinduced single electron transfer between the carboxylic acid and the excited state of the photocatalyst. This photoredox/thiol catalysis method is initiated by the photoexcitation of Mes-Acr to Mes-Acr* and the subsequent oxidation of the deprotonated carboxylic acid generating the alkyl radical. The thiyl radical formed from the excitation of the dithiol DDDS (*bis*(4-chlorophenyl)disulfide) reoxidizes the reduced catalyst and regenerates the hydrogen atom donor after protonation (**Scheme 83**).

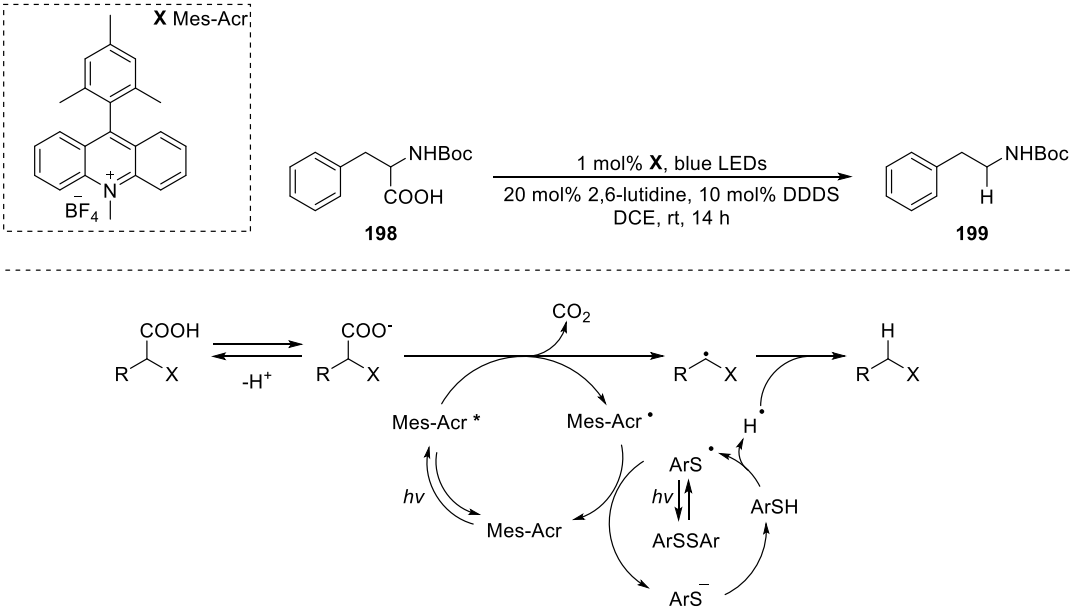

Scheme 83: Proposed mechanism for the photocatalytic decarboxylation of Boc-protected phenylalanine Boc-Phe-OH **198**.

In order to test the reaction, we used the same starting material as the paper reported. However, the disulfide used in this case was diphenyl disulfide **200**. All other conditions were kept the same, including the light source which according to the publication were 8 W blue LEDs. The reaction was carried out in batch however, even after 14 hours only a small amount of product was observed as the reaction did not seem to go to completion (**Scheme 84**).

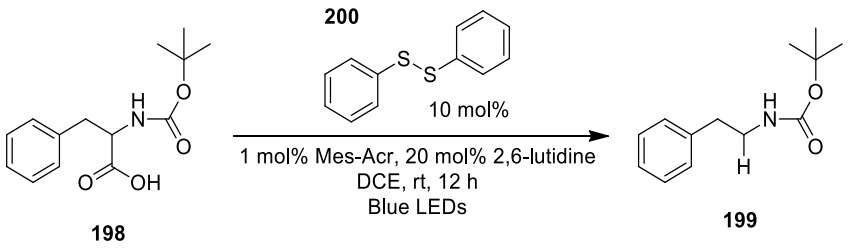

Scheme 84: Photocatalytic decarboxylation of **198** using 8W blue LEDs.

Under these conditions a conversion of 49% was observed. The reaction was repeated and an aliquot was taken out after 20 hours. Upon observation of a considerable amount of product the temperature was increased to 30 °C and the reaction was continued for an additional 25 hours. The reaction mixture was concentrated after this time and upon the observation of the ^{1}H NMR spectrum, it was evident that the conversion to product was still only 68% (**Figure 77**).

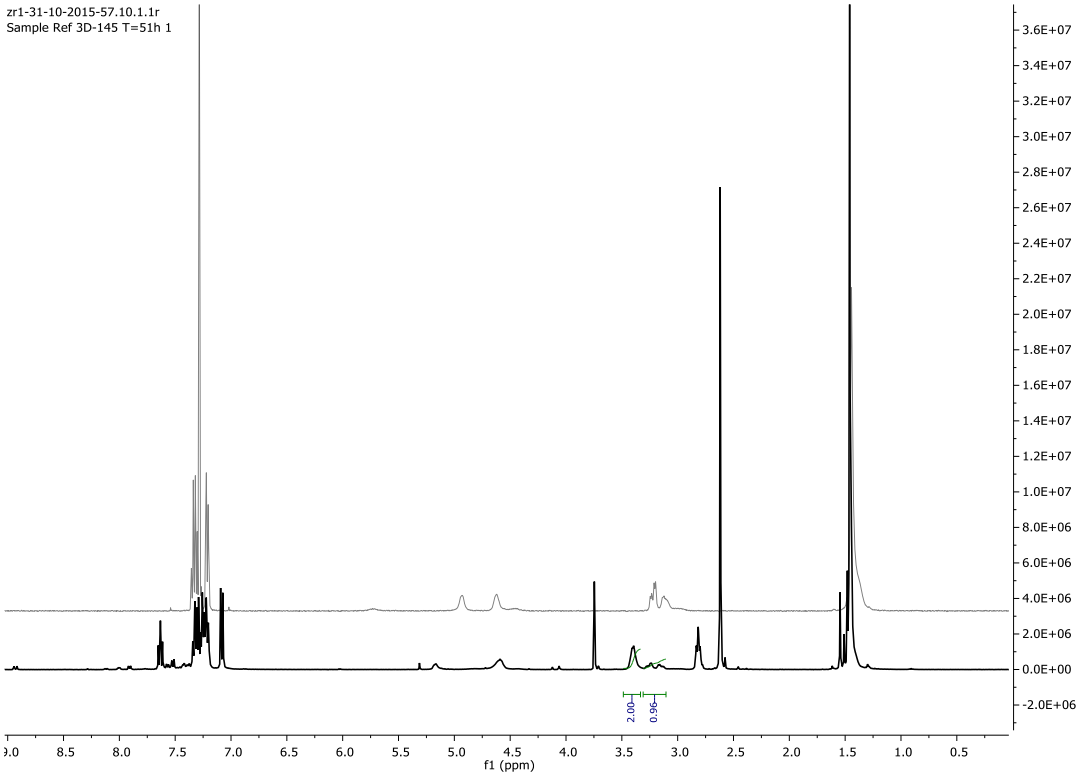

Figure 77: ^{1}H NMR spectrum showing Boc-PheOH **198** starting material stacked against reaction after 51 hours giving 68% conversion.

The reaction was repeated yet again and in order to reduce the time taken for it to proceed to completion, a second set of GU10 8 W blue LEDs were placed directly below the reaction vessel and it was left for 18 hours. Upon concentrating the reaction mixture and observing the ^{1}H NMR spectrum after this time we were able to significantly improve the reaction by getting a conversion of 82%. We hoped to improve the efficiency even further by exploring the scope of the same reaction using different thiols. When either 1,2-*bis*(4-nitrophenyl)disulfane or 1,2-*bis*(4-chlorophenyl)disulfane (DDDS) were used using the exact same conditions the reaction surprisingly did not proceed as expected. The reaction with DDDS only showed 38% product after 14 hours. The reaction with 1,2-*bis*(4-nitrophenyl)disulfane showed mainly starting material even after a duration of 14 hours.

Having established a basic protocol that could potentially be applied in to flow using our 3D-printed reactors, we decided to test the reaction on the original substrate (*D*-phenylalanine methyl ester). As seen in **Scheme 85**, the cyclized product **189** was reacted with acetyl chloride **193**. Given the fact that we wanted to eliminate any steps requiring purification at this stage, we switched

from cyclohexylcarbonyl chloride to acetyl chloride and reduced the number of equivalents used (1.1 equiv.). After a workup, the acylated crude product was concentrated under reduced pressure and used immediately in the hydrolysis step. We found through the course of such reactions that the acid hydrolysis step was efficient but risked the cleavage of the acetyl group and also required a long time under acidic conditions. We therefore performed a basic hydrolysis for this particular step. **202** was stirred in a solution of sodium hydroxide in THF at 0 °C for one hour. The solution was acidified to precipitate the product and further extracted with DCM. The crude product from this reaction was found to be clean enough to perform the final decarboxylation step.

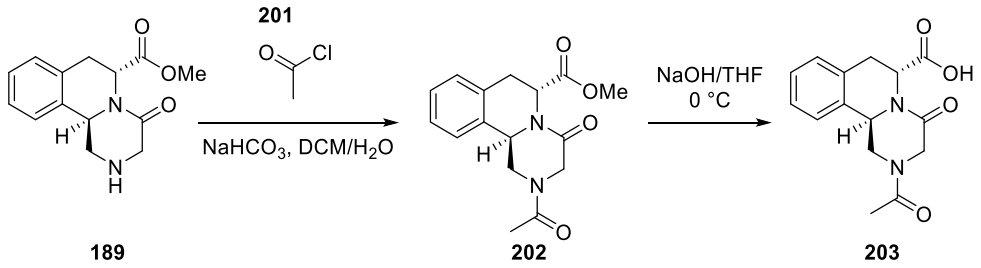

Scheme 85: Acylation of **189** followed by base hydrolysis to give the corresponding carboxylic acid **203**.

Upon observing the ^{1}H NMR spectrum of **202**, the dr had significantly changed to 70:30. This was an unexpected result for the reaction however we decided to proceed to the next step.

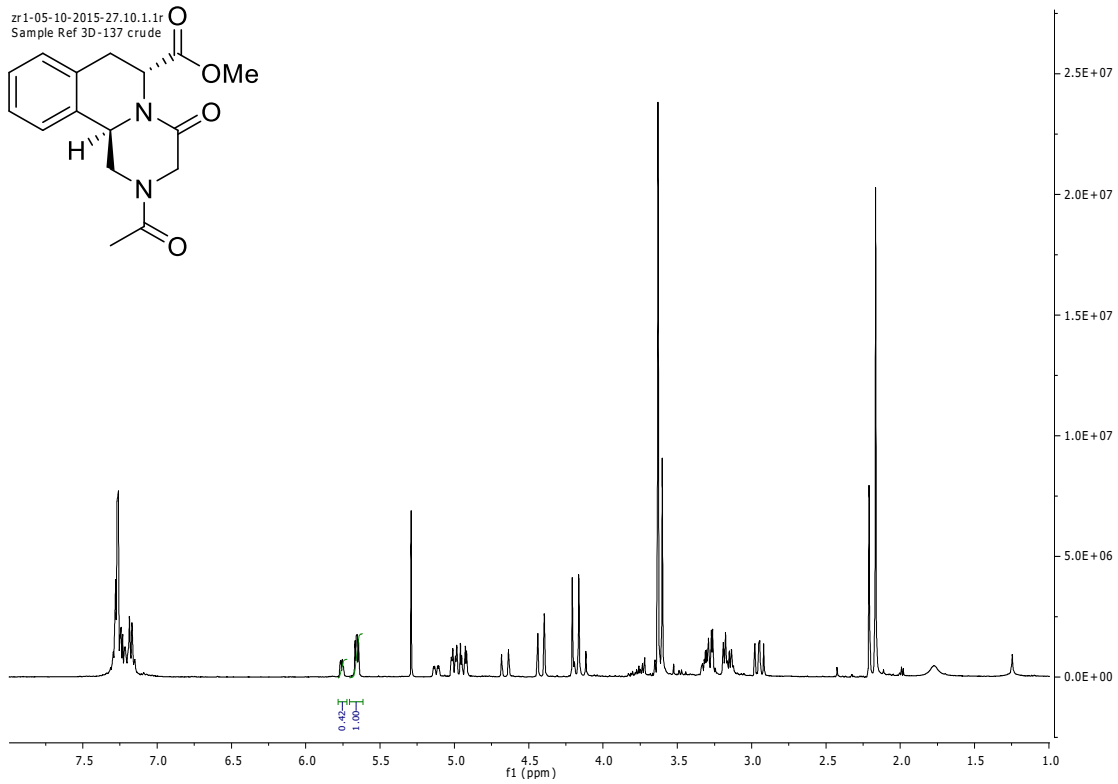

Figure 78: ^{1}H NMR spectrum of crude mixture of compound **202** showing change in dr to 70:30.

As seen in **Scheme 86**, the reaction of the carboxylic acid **203** to give the decarboxylated product **192** proceeded with the addition of two GU10 8 W LED lamps which were placed directly in front of the flask. After a period of 18 hours, a small workup followed by column chromatography afforded the product, albeit with a low yield of 26%.

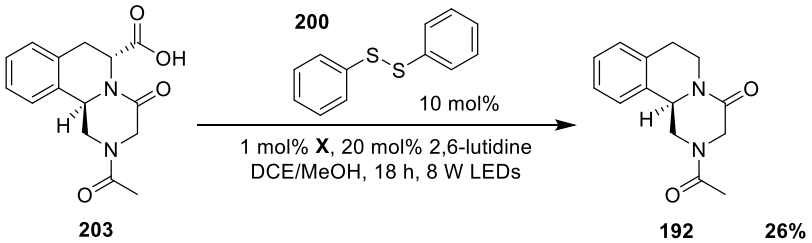

Scheme 86: Photocatalytic decarboxylation of **203** using 8W LEDs.

4.0 Conclusions and Future Work

The foregoing work presented in this thesis has shown the significance of 3D-printing not only as a manufacturing technique but also as a valid tool when implemented in organic synthesis. Its combination with flow chemistry has been effectively demonstrated through the development of polypropylene reactors and their use in the synthesis of fused bicyclic and heterocyclic compounds related to the Erythrina and Lycorane natural product families.

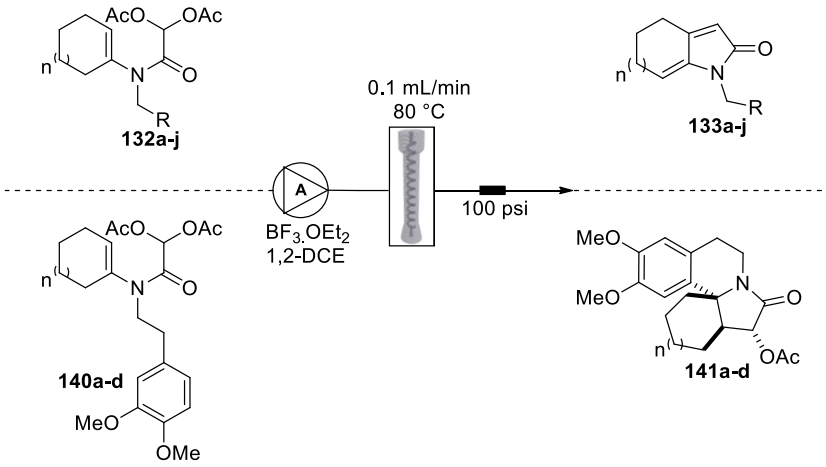

Scheme 87: Polypropylene reactor used in the synthesis of fused bicyclic and heterocyclic compounds **133a**-**j** and **141a**-**d**.

The importance of flow chemistry as a self-sufficient technique has been shown in the development of the quinoxalinone analogues. The combined use of thermal conditions provided by the flow chemistry apparatus along with packed-bed reactor technology in the hydrogenation assisted flow apparatus has shown to significantly improve on the synthesis of such molecules. This comprises of reduction in the number of steps as well as the use of green reagents and solvents and a drastic reduction in reaction time and lastly, a lowered side-product profile and reduction in purification steps.

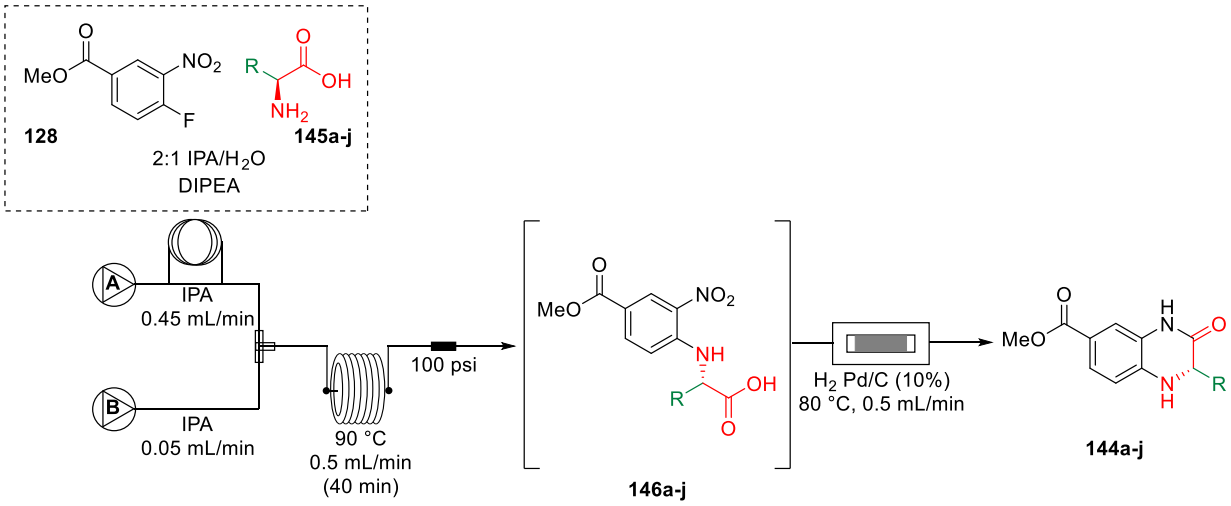

Scheme 88: Combined two step process for the synthesis of quinoxalinone analogues **144a-j** using flow coil and hydrogenation apparatus (H-Cube).

The use of SLA 3D-printing has been studied in detail and stirrer bead devices for batch synthesis applications have also been developed herein. This required the development of a formulation applicable to such a printing method as well as inertness to the reaction the device was to be involved in. The introduction of three different types of catalysts within these devices has been showcased and their efficacy in reactions have been verified through the synthesis of a range of analogues with each of these catalyst containing beads. The first catalyst to be incorporated within these stirrer beads was *p*-TsOH and the utility of such a method has been showcased by the synthesis of Hantzsch polyhydroquinoline analogues. The second catalytic containing device was a transition metal palladium tetrakis(triphenylphosphine) ($Pd(PPh_3)_4$) that was successfully developed into stirrer bead devices for both thermal and microwave reactions. Using such devices, a range of coupling chemistry to form biaryls was performed in a relatively easy manner. The third catalyst used in such systems was a Lewis acid yttrium triflate $Y(OTf)_3$ which was primarily developed into stirrer bead devices for microwave reactions and used for the protection of carbonyl groups in a range of aldehydes and a ketone. A catalytic monolith was also developed and used in the same reaction when repeated under flow conditions.

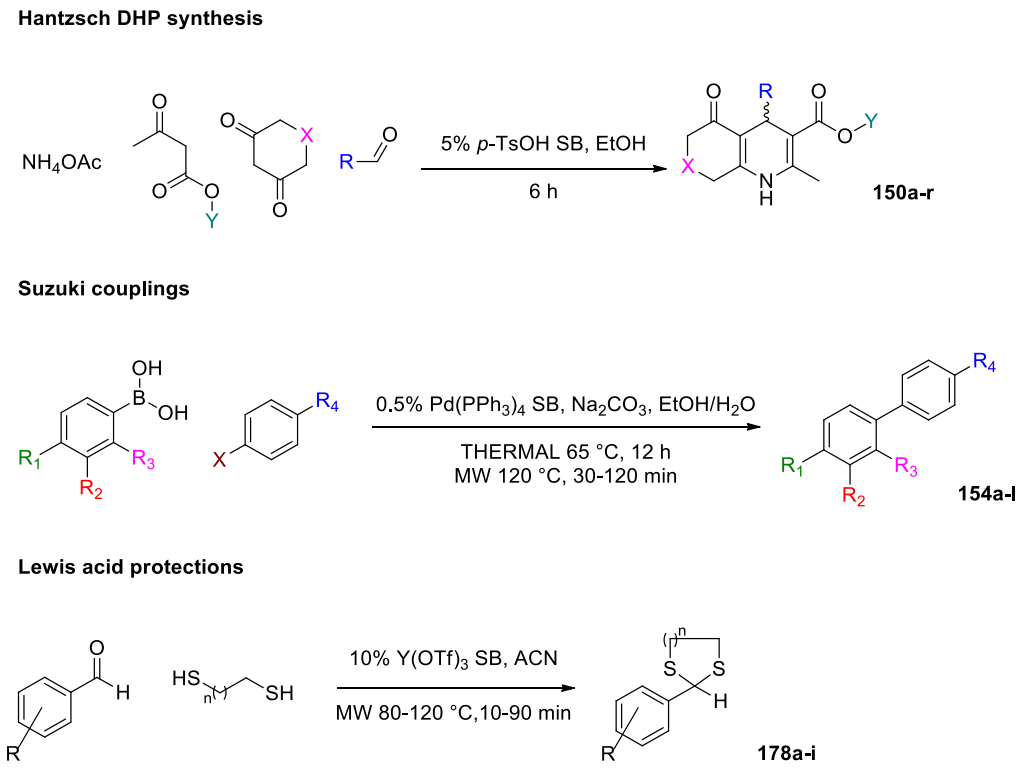

Scheme 89: Reactions using catalytic stirrer beads to perform Hantzsch, Suzuki and Lewis acid protection chemistry.

The concluding work presented in this thesis included the development of an inert flow reactor using SLA 3D-printing and its use in flow photochemistry. The optimisation of the conceptual prototype has been described and the limits of its tolerance have been evaluated through the C-H functionalisation chemistry. Although the reactions with these circular disk reactors proceeded to completion when used with 400 W Actinic bulbs in a flow based protocol, further development on its formulation would be required as the stresses caused by the intense light and heat generated on its surface often caused them to crack. Hence, a revision of the formulation would be necessary to avoid such problems and a significant improvement of the mechanical properties of such a device would be essential.

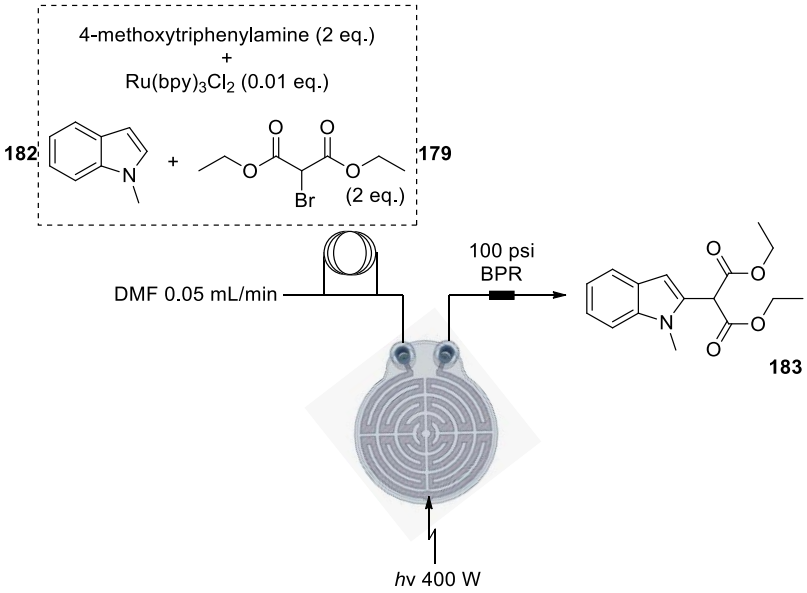

Scheme 90: Reaction between *N*-methyindole **182** and bromomalonate **179** using circular disk reactor CHR12 coupled to Uniqsis FlowSyn and 400W lamp.

A synthetic route towards the *N*-acetyl analogue of antimalarial drug praziquantel was developed in an attempt to utilise the newly designed circular disk reactor in its chemical sequence. *D*/*L*-phenylalanine methyl ester was selected as the starting material for this reaction. The route showcased an acylation and amination reaction followed by a Pictet-Spengler cyclisation, which allowed for a chirality transfer to the cyclised intermediate. The next steps were a simple hydrolysis followed by a decarboxylation reaction which was studied in detail and featured the use of our circular disk reactor. A final acylation of this decarboxylated product would effectively yield the praziquantel analogue however in the sequence which eventually yielded the product, this acylation step was carried out immediately after the cyclisation. Initial attempts were made towards a thermally assisted batch mediated procedure to carry out the decarboxylation as those seen in previous microwave assisted reactions with *N*-methylpyrrolidinone. However, a switch to a radical approach using an acridinium photoredox catalyst (Mes-Acr) was made as it gave us the opportunity to explore the scope of this photoredox reaction in flow and use our disk reactor in the process. Selecting this particular catalyst over phenanthrene systems was advantageous as a lower

energy requirement was necessary to generate the initial radical fragment. Hence a swap from conventional 400W Hg lamps to 8W blue LED's was sufficient to initiate the radical process. We hoped to develop this approach at a later stage by working with chiral starting materials so as to develop a steterocontrolled method for the synthesis of praziquantel.

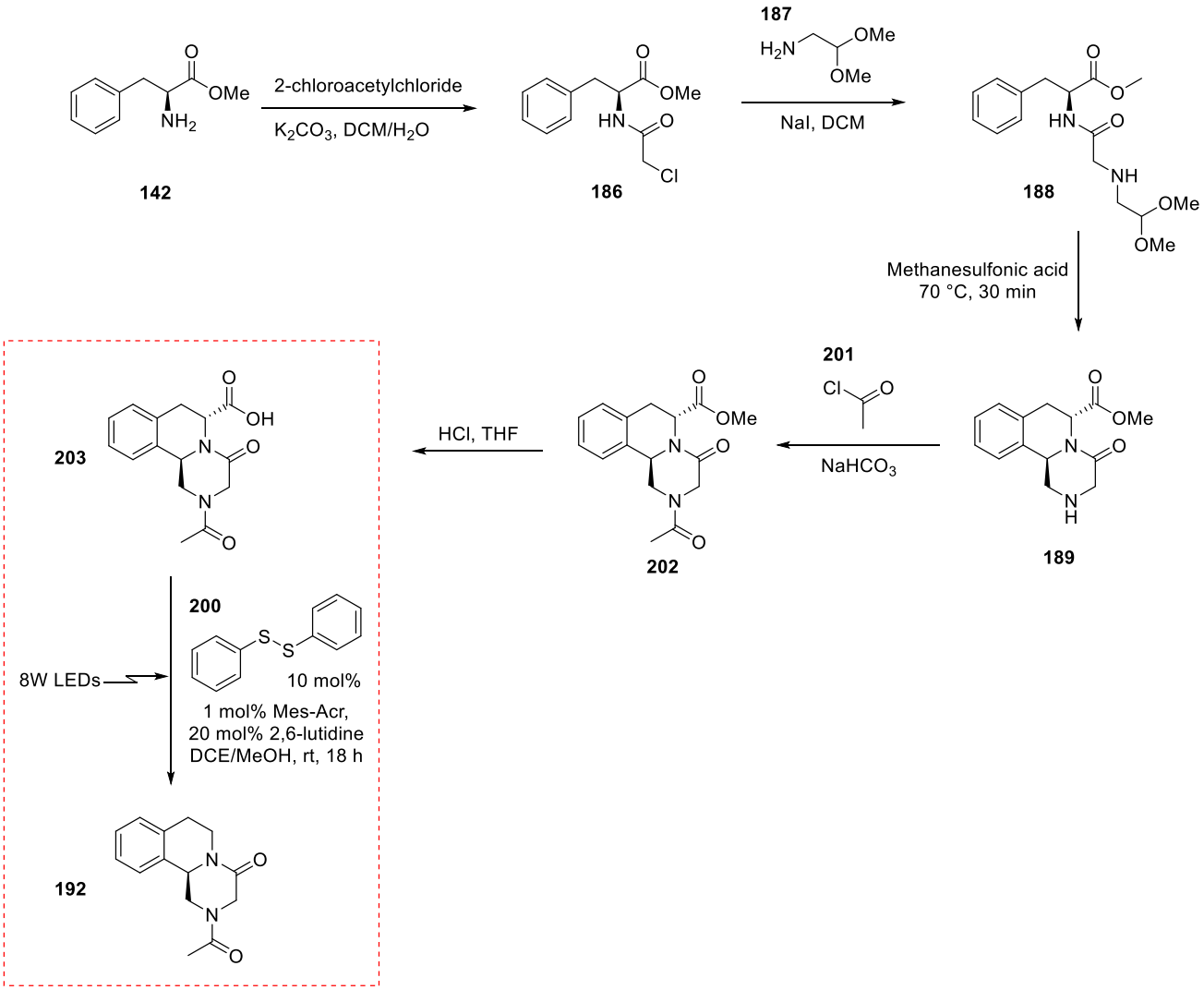

Scheme 91: Six step synthesis of **192** from phenylalanine methyl ester **142** including the light induced photodecarboxylation reaction.

A good endpoint to this research would be using the developed formulation to print a circular hotplate reactor and develop the chemistry of the decarboxylation further such that we could optimize the step for flow

conditions. The acylation step would also involve the use of cyclohexylcarbonyl chloride to produce Praziquantel as seen in **Scheme 92**.

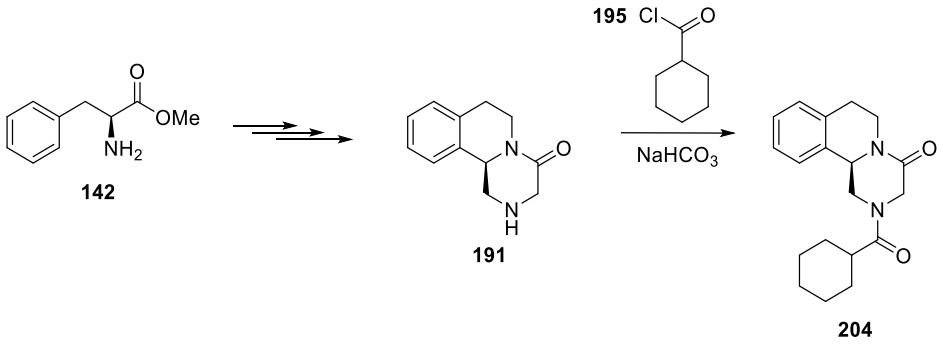

Scheme 92: Extrapolated synthesis of praziquantel **204** from phenylanaline methyl ester **142** showing the use of cyclohexylcarbonyl chloride **195** in the last acylation step.

5.0 Experimental

5.1 General Methods

All reactions requiring the use of dry conditions were carried out under an atmosphere of nitrogen and all glassware was pre-dried in an oven (110 °C) and cooled under nitrogen prior to use. Stirring was by internal magnetic follower unless otherwise stated. All reactions were followed by TLC and organic phases extracted were dried with anhydrous magnesium sulfate. Diethyl ether, tetrahydrofuran, dichloromethane, toluene, methanol, acetonitrile and triethylamine were purchased as anhydrous solvents from Sigma-Aldrich chemical company, UK.

All experiments using a microwave reactor were carried out using Biotage Initiator+ fourth generation microwave synthesizer. Purification was carried out by column chromatography using the flash column chromatography technique reported by Biotage Isolera^{TM} Prime automatic purification. The silica gel used was Merck 60 (230-400 mesh). Thin layer chromatographic analysis was carried out using Merck aluminium-backed plates coated with silica gel 60 F_{254}. Components were visualised using combinations of ultraviolet light and iodine stain.

Infrared spectra were recorded on a Perkin Elmer 1605 FT-IR spectrophotometer. Melting points were determined using open glass capillaries on a Stuart Scientific SMP3 apparatus and are uncorrected. ^{1}H NMR and ^{13}C NMR were recorded on a Bruker AV400, operating at 400 MHz for proton and 101 MHz for carbon, or a Bruker AV500 spectrometer operating at 500 MHz for proton and 126 MHz for carbon.

Chemical shifts (δ_H and δ_C) are quoted as parts per million downfield from 0. The multiplicity of a ^{1}H NMR signal is designated by one of the following abbreviations: s = singlet, d = doublet, t = triplet, q = quartet, quin = quintet, sept = septet, br = broad and m = multiplet. Coupling constants (J) are expressed in Hertz.

High resolution mass spectra were carried out at the UCL School of Pharmacy. Mass spectra carried out at using an Agilent Micromass Q-TOF premier Tandem Mass Spectrometer from Micromass utilising electrospray. All samples were run under Electrospray ionization mode using 50% acetonitrile in water and 0.1% formic acid as solvent.

5.1.1 General procedure A:

A: Synthesis of **133a - 133j**

1-Benzyl-4,5-dihydrocyclopenta[b]pyrrol-2(1H)-one 133a [121]

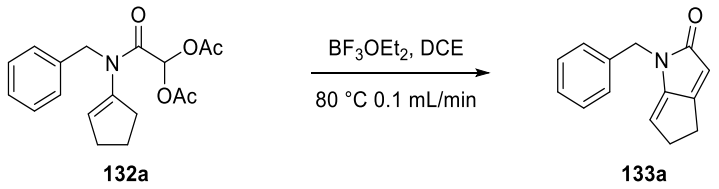

132a

Chemical Formula: $C_{18}H_{21}NO_5$
Molecular Weight: 331.36

133a

Chemical Formula: $C_{14}H_{13}NO$
Molecular Weight: 211.26

Boron trifluoride diethyl etherate (0.10 mL, 0.74 mmol) was added to a mixture of 2-(benzyl(cyclopent-1-en-1-yl)amino)-2-oxoethane-1,1-diyl diacetate (0.05 g, 0.15 mmol) in anhydrous dichloroethane (1.01 mL). The reagents were passed through the flow reactor (0.1 mL/min) at 80 °C. The residue was washed with water (10 mL), extracted with DCM (2 × 10 mL) and dried over Na_2SO_4, filtered and concentrated under reduced pressure to give the crude product. The residue was purified *via* automated flash chromatogrphy (3:1 Hexane : EtOAc; Zip 10 g column) to give 1-benzyl-4,5-dihydrocyclopenta[b]pyrrol-2(1H)-one **133a** (0.011 g, 34%) as a pale yellow semi-solid; ν_{max} (neat) 3032 (C–H), 1699 (C=O), 818 (C=CH); δ_H (500 MHz, $CDCl_3$) 7.29 - 7.35 (3H, m, Ar**H**), 7.22 - 7.27 (2H, m, Ar**H**), 5.73 (1H, s, COC**H**), 5.42 (1H, br.s., NCC**H**), 4.81 (2H, s, NC**H**$_2$), 2.80 (2H, d, J 3.5, NCCHC**H**$_2$), 2.68 - 2.76 (2H, m, NCCC**H**$_2$); δ_C (126 MHz, $CDCl_3$) 175.4 (CO), 161.9 (C), 146.4 (C), 137.3 (C), 128.6 (CH), 127.6 (CH), 127.4 (CH), 113.2 (CH), 109.3 (CH), 44.3 (CH_2), 35.0 (CH_2), 23.9 (CH_2); *m/z* (NSI) Found 212.1070 ($[M+H]^+$ $C_{14}H_{14}NO$ requires 212.1068).

1-Benzyl-5,6-dihydro-1H-indol-2(4H)-one 133b [121]

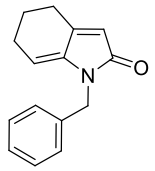

133b
Chemical Formula: $C_{15}H_{15}NO$
Molecular Weight: 225.29

According to general procedure **A** compound **133b** was obtained as a colorless solid (0.035 g, 51%); mp 74 – 75 °C; ν_{max} (neat) 3031, 2924 (C–H), 1677 (C=O), 801 (C=CH); δ_H (500 MHz, $CDCl_3$) 7.28 - 7.34 (2H, m, Ar**H**), 7.20 - 7.28 (3H, m, Ar**H**), 5.82 (1H, s, COC**H**), 5.53 (1H, br. s., NCC**H**), 4.77 (2H, s, NC**H**$_2$), 2.64 (2H, t, J = 6.1 Hz, NCCC**H**$_2$), 2.27 (2H, d, J = 5.4 Hz, NCCHC**H**$_2$), 1.77 - 1.84 (2H, m, CH_2C**H**$_2CH_2$); δ_C (126 MHz, $CDCl_3$) 170.3 (CO), 147.6 (C), 139.7 (C), 137.6 (C), 128.5 (CH), 127.2 (CH), 127.1 (CH), 115.5 (CH), 110.9 (CH), 42.5 (CH_2), 24.3 (CH_2), 24.2 (CH_2), 23.4 (CH_2); *m/z* (NSI) Found 226.1126 ($[M+H]^+$ $C_{15}H_{16}NO$ requires 226.1127).

1-Benzyl-4,5,6,7-tetrahydrocyclohepta[b]pyrrol-2(1H)-one 133c [121]

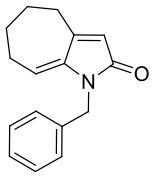

133c
Chemical Formula: $C_{16}H_{17}NO$
Molecular Weight: 239.31

According to general procedure **A** compound **133c** was obtained as an orange oil (0.047 g, 70%); ν_{max} (neat) 3029, 2927 (C–H), 1670 (C=O) δ_H (500 MHz, $CDCl_3$) 7.28 - 7.34 (2H, m, Ar**H**), 7.21 - 7.26 (1H, m, Ar**H**), 7.18 (2H, d, J = 7.6 Hz, Ar**H**), 6.00 (1H, s, COC**H**), 5.60 (1H, t, J = 5.7 Hz, NCC**H**), 4.82 (2H, s, NC**H**$_2$), 2.73 - 2.83 (2H, m, NCCC**H**$_2$), 2.39 (2H, q, J = 5.8 Hz, NCCHC**H**$_2$), 1.73 - 1.83 (4H, m, CH_2C**H**$_2C$**H**$_2CH_2$); δ_C (126 MHz, $CDCl_3$) 175.7 (CO), 151.7 (C), 140.2 (C), 137.7 (C), 128.5 (CH), 127.0 (CH), 126.7 (CH), 120.3 (CH), 117.1 (CH), 42.5 (CH_2), 29.9 (CH_2), 28.2 (CH_2), 27.5 (CH_2), 24.6 (CH_2); *m/z* (NSI) Found 240.1383 ($[M+H]^+$ $C_{16}H_{18}NO$ requires 240.1382).

1-Benzyl-1H-benzo[f]indol-2(4H)-one 133d [121]

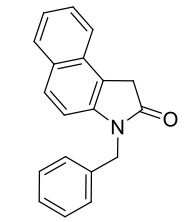

133d

Chemical Formula: $C_{19}H_{15}NO$
Molecular Weight: 273.33

According to general procedure **A** compound **133d** was obtained as an orange solid (0.03 g, 43%); mp 157 - 158 °C; ν_{max} ($CDCl_3$) 3032 (CH), 1707 (C=O),; δ_H (500 MHz, $CDCl_3$) 7.80 (1H, d, J = 8.5 Hz, Ar**H**), 7.73 (1H, d, J = 8.5 Hz, Ar**H**), 7.69 (1H, d, J = 8.2 Hz, Ar**H**), 7.51 (1H, t, J = 7.6 Hz, Ar**H**), 7.34 (5H, quin, J = 7.8 Hz, Ar**H**), 7.24 - 7.30 (1H, m, Ar**H**), 7.05 (1H, d, J = 8.5 Hz, Ar**H**), 5.04 (2H, s, NC**H**$_2$), 3.92 (2H, s, COC**H**$_2$); δ_C (126 MHz, $CDCl_3$) 175.7 (CO), 141.8 (C), 136.0 (C), 129.9 (C), 129.6 (C), 129.0 (CH), 128.8 (CH), 128.7 (CH), 127.6 (CH), 127.3 (CH), 127.2 (CH), 123.9 (CH), 122.5 (CH), 117.8 (C), 110.4 (CH), 43.8 (CH_2), 34.9 (CH_2); *m/z* (NSI) Found 274.1126 ($[M+H]^+$ $C_{19}H_{16}NO$ requires 274.1124).

1-(4-Methoxybenzyl)-4,5-dihydrocyclopenta[b]pyrrol-2(1H)-one 133e [121]

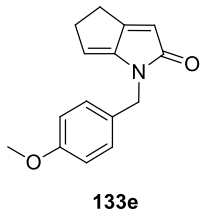

133e

Chemical Formula: $C_{15}H_{15}NO_2$
Molecular Weight: 241.29

According to general procedure **A** compound **133e** was obtained as a dark brown semi-solid (0.013 g, 13%); ν_{max} (neat) 3075 (C–H), 1672 (C=O); δ_H (500 MHz, $CDCl_3$) 7.20 (2H, d, J = 7.9 Hz, Ar**H**), 6.85 (2H, d, J = 7.6 Hz, Ar**H**), 5.71 (1H, br.s, COC**H**), 5.42 (1H, br.s., NCC**H**), 4.74 (2H, s, NC**H**$_2$), 3.79 (3H, s OC**H**$_3$), 2.80 (2H, br.s, NCCHC**H**$_2$), 2.72 (2H, br.s, NCCC**H**$_2$); δ_C (126 MHz, $CDCl_3$) 175.4 (CO), 161.7 (C), 158.9 (C), 146.3 (C), 129.4 (C), 129.1 (CH), 113.9 (CH), 113.2 (CH), 109.3 (CH), 55.2 (CH_3), 43.8 (CH_2), 35.1 (CH_2), 23.8 (CH_2); *m/z* (NSI) Found 242.1176 ($[M+H]^+$ $C_{15}H_{16}NO_2$ requires 242.1173).

1-(4-Methoxybenzyl)-5,6-dihydro-1H-indol-2(4H)-one 133f [121]

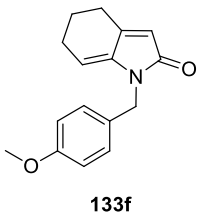

133f

Chemical Formula: $C_{16}H_{17}NO_2$
Molecular Weight: 255.31

According to general procedure **A** compound **133f** was obtained as an orange oil (0.047 g, 61%); ν_{max} (neat) 3005, 2935 (C–H), 1675 (C=O); δ_H (500 MHz, $CDCl_3$) 7.15 (2H, d, J = 8.5 Hz, Ar**H**), 6.83 (2H, d, J = 8.5 Hz, Ar**H**), 5.81 (1H, s, COC**H**), 5.55 (1H, t, J = 4.4 Hz, NCC**H**), 4.69 (2H, s, NC**H**$_2$), 3.78 (3H, s, OC**H**$_3$), 2.61 (2H, t, J = 6.5 Hz, NCCC**H**$_2$), 2.26 (2H, q, J = 5.4 Hz, NCCHC**H**$_2$), 1.79 (2H, quin, J = 6.1 Hz, $CH_2C\mathbf{H}_2CH_2$); δ_C (126 MHz, $CDCl_3$) 170.4 (CO), 158.7 (C), 147.5 (C), 139.6 (C), 129.7 (C), 128.4 (CH), 115.4 (CH), 113.9 (CH), 111.1 (CH), 55.2 (CH_3), 42.0 (CH_2), 24.3 (CH_2), 24.2 (CH_2), 23.4 (CH_2); *m/z* (NSI) Found 256.1332 ($[M+H]^+$ $C_{16}H_{18}NO_2$ requires 256.1335).

1-(4-Methoxybenzyl)-4,5,6,7-tetrahydrocyclohepta[b]pyrrol-2(1H)-one 133g [121]

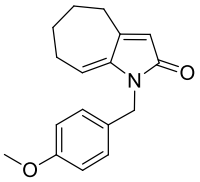

133g

Chemical Formula: $C_{17}H_{19}NO_2$
Molecular Weight: 269.34

According to general procedure **A** compound **133g** was obtained as a dark brown semi-solid (0.056 g, 47%); ν_{max} (neat) 2859 (O–C), 1675 (C=O); δ_H (500 MHz, $CDCl_3$) 7.12 (2H, d, J = 8.5 Hz, Ar**H**), 6.83 (2H, d, J = 8.5 Hz, Ar**H**), 5.96 (1H, s, COC**H**), 5.61 (1H, t, J = 5.7 Hz, NCC**H**), 4.74 (2H, s, NC**H**$_2$), 3.78 (3H, s, OC**H**$_3$), 2.72 - 2.78 (2H, t, J = 5.7 Hz, NCCC**H**$_2$), 2.39 (2H, q, J = 5.7 Hz, NCCHC**H**$_2$), 1.69 - 1.81 (4H, m, NCCHC**H**$_2$C**H**$_2$); δ_C (126 MHz, $CDCl_3$) 169.6 (CO), 158.6 (C), 151.5 (C), 140.2 (C), 129.8 (C), 128.0 (CH), 120.3 (CH), 116.9 (CH), 113.7 (CH), 55.2 (CH_3), 41.9 (CH_2), 29.9 (CH_2), 28.2 (CH_2), 27.5 (CH_2), 24.6 (CH_2); *m/z* (NSI) Found 270.1489 ($[M+H]^+$ $C_{17}H_{20}NO_2$ requires 270.1487).

1-(2-Fluorobenzyl)-5,6-dihydro-1H-indol-2(4H)-one 133h [121]

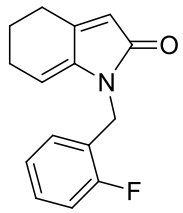

133h

Chemical Formula: $C_{15}H_{14}FNO$
Molecular Weight: 243.28

According to general procedure **A** compound **133h** was obtained as a brown semi-solid (0.045 g, 40%); ν_{max} 3045, 2863 (C–H), 1682 (C=C), 1654 (C=O); δ_H (500 MHz, $CDCl_3$) 7.15 - 7.25 (2H, m, Ar**H**), 7.00 - 7.10 (2H, m, Ar**H**), 5.82 (1H, s, COC**H**), 5.61 (1H, br. s., NCC**H**), 4.82 (2H, s, NC**H**$_2$), 2.64 (2H, t, J = 6.0 Hz, NCCC**H**$_2$), 2.29 (2H, d, J = 4.7 Hz, NCCHC**H**$_2$), 1.75 - 1.86 (2H, m, CH_2C**H**$_2CH_2$); δ_C (101 MHz, $CDCl_3$) 170.4 (CO), 160.1 (C, d, J = 243.7 Hz), 147.7 (C), 139.3 (C), 124.5 (C. d, J = 13.7 Hz), 129.4 (CH, d, J = 3.7 Hz), 128.8 (CH, d, J = 7.5 Hz), 124.3 (CH, d, J = 3.7 Hz), 115.1 (CH, d, J = 21.2 Hz), 115.46 (CH), 110.87 (CH), 35.62 (CH_2), 24.31 (CH_2), 24.18 (CH_2), 23.37 (CH_2); *m/z* (ASAP) Found 244.1132 ($[M+H]^+$ $C_{15}H_{15}FNO$ requires 244.1132).

1-(4-Fluorobenzyl)-5,6-dihydro-1H-indol-2(4H)-one 133i [121]

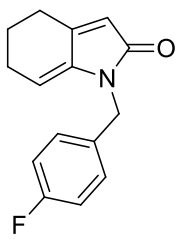

133i

Chemical Formula: $C_{15}H_{14}FNO$
Molecular Weight: 243.28

According to general procedure **A** compound **133i** was obtained as an orange oil (0.051 g, 77%); ν_{max} 2934 (C–H), 1675 (C=C), 1604 (C=O); δ_H (500 MHz, $CDCl_3$) 7.15 - 7.21 (2H, m, Ar**H**), 6.99 (2H, t, J = 8.5 Hz, Ar**H**), 5.81 (1H, s, COC**H**), 5.52 (1H, t, J = 4.6 Hz, NCC**H**), 4.72 (2H, s, NC**H**$_2$), 2.63 (2H, t, J = 6.5 Hz, NCCC**H**$_2$), 2.27 (2H, q, J = 5.4 Hz, NCCHC**H**$_2$), 1.80 (2H, quin, J = 6.1 Hz, CH_2C**H**$_2CH_2$); δ_C (126 MHz, $CDCl_3$) 170.3 (CO), 162.1 (C, d, J = 245.0 Hz), 147.8 (C), 139.6 (C), 133.5 (C, d, J = 2.5 Hz), 128.8 (CH, d, J = 7.9 Hz), 115.6 (CH), 115.4 (CH), 111.0 (CH), 41.9 (CH_2), 24.3 (CH_2), 24.2 (CH_2), 23.4 (CH_2); *m/z* (ASAP) Found 244.1132 ($[M+H]^+$ $C_{15}H_{15}FNO$ requires 244.1135).

1-Phenethyl-5,6-dihydro-1H-indol-2(4H)-one 133j

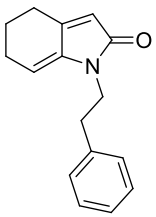

133j

Chemical Formula: $C_{16}H_{17}NO$
Molecular Weight: 239.31

According to general procedure **A** compound **133j** was obtained as a brown semi-solid (0.043 g, 32%); ν_{max} ($CHCl_3$) 3346, 2993 (C–H), 1769 (C=C), 1639 (C=O); δ_H (500 MHz, $CDCl_3$) 7.30 - 7.35 (2H, m, Ar**H**), 7.22 - 7.26 (3H, m, Ar**H**), 5.79 (1H, s, NCOC**H**), 5.52 (1H, t, J = 4.7 Hz, NCC**H**), 3.75 - 3.84 (2H, m, $NCH_2C\mathbf{H}_2$), 2.85 - 2.95 (2H, m, $NC\mathbf{H}_2$), 2.65 (2H, t, J = 6.5 Hz, $NCCC\mathbf{H}_2$), 2.32 (2H, q, J = 5.4 Hz, $NCCHC\mathbf{H}_2$), 1.84 (2H, quin, J = 6.2 Hz, $CH_2C\mathbf{H}_2CH_2$); δ_C (126 MHz, $CDCl_3$) 170.1 (CO), 147.1 (C), 139.7 (C), 138.9 (C), 128.8 (CH), 128.4 (CH), 126.4 (CH), 115.7 (CH), 109.9 (CH), 40.5 (CH_2), 35.2 (CH_2), 24.3 (CH_2), 24.2 (CH_2), 23.4 (CH_2); *m/z* (NSI) Found 240.1383 ($[M+H]^+$ $C_{16}H_{18}NO$ requires 240.1385).

1-(4-(Trifluoromethyl)benzyl)-5,6-dihydro-1H-indol-2(4H)-one 133k [121]

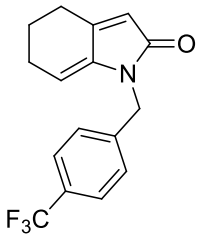

133k

Chemical Formula: $C_{16}H_{14}F_3NO$
Molecular Weight: 293.28

According to general procedure **A** compound **133k** was obtained as an orange oil (0.036 g, 37%); ν_{max} 3042, 2855 (C–H), 1365 (C-F), 1649 (C=O); δ_H (500 MHz, $CDCl_3$) 7.51 - 7.61 (2H, m, ArC**H**), 7.29 - 7.35 (2H, m, ArC**H**), 5.84 (1H, d, J = 1.5 Hz, COC**H**), 5.49 (1H, dt, J = 1.6, 4.6 Hz, NCC**H**), 4.81 (2H, s, $NC\mathbf{H}_2$), 2.60 - 2.71 (2H, m, $NCCC\mathbf{H}_2$), 2.24 - 2.32 (2H, m, $NCCHC\mathbf{H}_2$), 1.76 - 1.88 (2H, m, $CH_2C\mathbf{H}_2CH_2$); δ_C (126 MHz, $CDCl_3$) 170.3 (CO), 147.9 (C), 141.6 (C), 139.4 (C), 129.5 (C, d, J = 25.2 Hz) 127.3 (CH), 125.6 (CH), 124.1 (C, d, J = 219.2 Hz), 115.5 (CH), 111.0 (CH), 42.1 (CH_2), 24.3 (CH_2), 24.2 (CH_2), 23.4 (CH_2); *m/z* (NSI) Found 294.1100 ($[M+H]^+$ $C_{16}H_{15}F_3NO$ requires 294.1099).

1-(Benzo[d][1,3]dioxol-5-ylmethyl)-5,6-dihydro-1H-indol-2(4H)-one 133l

[121]

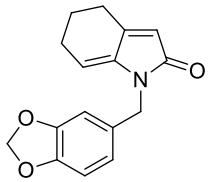

133l

Chemical Formula: $C_{16}H_{15}NO_3$
Molecular Weight: 269.30

According to general procedure **A** compound **133l** was obtained as a colourless solid (0.059 g, 85%); ν_{max} 3080, 2918, 2851, 2788 (CH), 1674 (C=C), 1602 (C=ON)**;** δ_H (400 MHz, $CDCl_3$) 6.67 - 6.78 (m, **3**H, Ar**H**), 5.93 (s, 2H, OC**H**$_2$O), 5.80 (d, J = 1.8 Hz, 1H, NCOC**H**), 5.52 - 5.57 (m, 1H, NCC**H**), 4.67 (s, 2H, NC**H**$_2$), 2.60 - 2.67 (m, 2H, C**H**$_2$CH$_2$CH$_2$C), 2.24 - 2.32 (m, 2H, CH$_2$CH$_2$C**H**$_2$C), 1.76 - 1.85 (m, 2 H, CH$_2$C**H**$_2$CH$_2$C)**;** δ_C (500 MHz, $CDCl_3$) 170.31 (C=O), 148.00 (C), 147.72 (C), 146.81 (C), 139.70 (C), 131.69 (C), 120.43 (CH), 115.58 (CH), 111.08 (CH), 108.25 (CH), 107.91 (CH), 101.10 (CH_2), 42.60 (CH_2), 24.43 (CH_2), 24.33 (CH_2), 23.51 (CH_2); m/z (NSI) 270.1125 ($[M+H]^+$, $C_{16}H_{15}NO_3$ requires 270.1127.

5.1.2 General procedure B:

B: Synthesis of **141a - 141d**

10,11-Dimethoxy-5-oxo-1,2,3,3a,4,5,7,8-octahydrocyclopenta[2,3]pyrrolo[2,1-a]isoquinolin-4-yl acetate 141a [122]

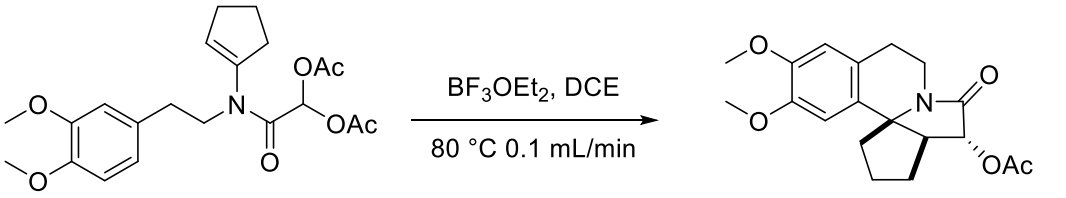

140a

Chemical Formula: $C_{21}H_{27}NO_7$
Molecular Weight: 405.44

141a

Chemical Formula: $C_{19}H_{23}NO_5$
Molecular Weight: 345.39

Boron trifluoride diethyl etherate (0.084 ml, 0.667 mmol) was added to a mixture of 2-(cyclopent-1-en-1-yl(3,4-dimethoxyphenethyl)amino)-2-oxoethane-1,1-diyl diacetate (0.05 g, 0.13 mmol) in anhydrous dichloroethane (0.95 mL) and the reagents were passed through the flow reactor (0.1 mL/min) at 80 °C. The residue was washed with water (10 mL), extracted with DCM (2 × 10 mL), dried over Mg_2SO_4 and filtered. The solution was then concentrated under reduced pressure to give the crude product. The residue was purified *via* automated flash chromatogrphy (3:2 Hexane : EtOAc; Zip 5 g column) togive 10,11-dimethoxy-5-oxo-1,2,3,3a,4,5,7,8-octahydrocyclopenta[2,3]pyrrolo[2,1-a]isoquinolin-4-yl acetate **141a** (0.004 g, 9%) as a brown semi-solid; ν_{max} (neat) 2954, 2921 (C–H), 1718 (C=O); δ_H (500 MHz, $CDCl_3$) 6.60 (0.19H, s, Ar**H**), 6.55 (1H, s, Ar**H**), 6.50 (0.81H, s, Ar**H**), 5.29 (0.19H, d, J = 9.8 Hz, NCOC**H**), 5.06 (0.81H, d, J = 4.1 Hz, NCOC**H**), 4.38 (1H, dd, J = 5.8, 12.5 Hz, 1 × NC$\mathbf{H}_2$), 3.88 (1.14H, s, 2 × OC$\mathbf{H}_3$), 3.86 (4.86H, s, 2 × OC$\mathbf{H}_3$), 2.91 - 3.24 (2H, m, 1 × NC$\mathbf{H}_2$, 1 × $NCH_2C\mathbf{H}_2$), 2.66 (1H, dd, J = 15.3, 3.6 Hz, 1 × $NCH_2C\mathbf{H}_2$), 2.60 (1H, dd, J = 7.7, 4.3 Hz, NCC**H**), 2.31 (1H, dd, J = 12.9, 5.4 Hz, 1 × NCCHC$\mathbf{H}_2$), 2.18 (1H, d, J = 6.3 Hz, 1 × NCC$\mathbf{H}_2$), 2.10 - 2.16 (1H, m, 1 × NCCHC$\mathbf{H}_2$), 2.08 (3H, s, COC$\mathbf{H}_3$), 1.91 - 1.98 (1H, m, 1 × $NCCH_2C\mathbf{H}_2$), 1.77 (1H, m, 1 × NCC$\mathbf{H}_2$), 1.61 - 1.69 (1H, m, 1 × $NCCH_2C\mathbf{H}_2$); δ_C (126 MHz, $CDCl_3$) 170.6 (C=O), 168.2 (C=O), 148.2 (C), 148.0 (C), 133.6 (C), 125.2 (C), 111.2 (CH), 107.4 (CH), 78.6 (CH), 70.9 (C), 56.1 (CH_3), 55.9

(CH_3), 53.5 (CH), 42.4 (CH_2), 36.4 (CH_2), 33.7 (CH_2), 27.5 (CH_2), 25.3 (CH_2), 20.9 (CH_3); *m/z* (NSI) Found 346.1649 ($[M+H]^+$ $C_{19}H_{24}NO_5$ requires 346.1649). Unable to obtain dr for this sample.

11,12-Dimethoxy-6-oxo-2,3,4,4a,5,6,8,9-octahydro-1H-indolo[7a,1-a]isoquinolin-5-yl acetate 141b [122]

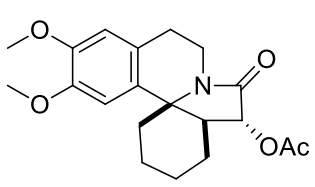

141b

Chemical Formula: $C_{20}H_{25}NO_5$
Molecular Weight: 359.42

According to general procedure **B** compound **141b** was obtained as a colourless solid (0.065 g, 45%); mp 133 - 135 °C; ν_{max} (neat) 3469, 2934 (C–H), 1744 (C=O), 1698 (OC=O); δ_H (500 MHz, $CDCl_3$) 6.94 (1H, s, Ar**H**), 6.63 (1H, s, Ar**H**), 5.68 (1H, d, J = 10.1 Hz, NCOC**H**), 4.01 (1H, td, J = 12.6, 6.0 Hz, 1 × NC**H**$_2$), 3.87 (6H, 2 × s, 2 × OC**H**$_3$), 3.24 - 3.37 (1H, m, 1 × NC**H**$_2$), 2.89 - 3.00 (1H, m, 1 × NCH$_2$C**H**$_2$), 2.76 - 2.87 (1H, m, 1 × NCH$_2$C**H**$_2$), 2.45 - 2.57 (1H, m, NCC**H**), 2.09 - 2.19 (4H, m, 1 × NCCHCH$_2$C**H**$_2$, COC**H**$_3$), 1.96 - 2.09 (2H, m, NCCH$_2$C**H**$_2$), 1.76 - 1.89 (1H, m, 1 × NCC**H**$_2$), 1.60 - 1.75 (3H, m, 1 × NCC**H**$_2$, 1 × NCCHCH$_2$C**H**$_2$, 1 × NCCHC**H**$_2$), 1.47 - 1.60 (1H, m, 1 × NCCHC**H**$_2$); δ_C (126 MHz, $CDCl_3$) 170.6 (C=O), 167.7 (C=O), 147.9 (C), 147.3 (C), 134.1 (C), 125.3 (C), 111.9 (CH), 108.2 (CH), 72.3 (CH), 59.0 (C), 56.1 (CH_3), 55.8 (CH_3), 45.2 (CH), 37.2 (CH_2), 35.5 (CH_2), 27.4 (CH_2), 23.9 (CH_2), 20.9 (CH_3), 20.4 (CH_2), 19.9 (CH_2); *m/z* (NSI) Found 360.1802 ($[M+H]^+$ $C_{20}H_{26}NO_5$ requires 360.1805).

12,13-dimethoxy-7-oxo-1,2,3,4,5,5a,6,7,9,10-decahydrocyclohepta[2,3]pyrrolo[2,1-a]isoquinolin-6-yl acetate 141c [122]

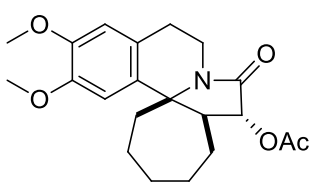

141c

Chemical Formula: $C_{21}H_{27}NO_5$
Molecular Weight: 373.44

According to general procedure **B** compound **141c** was obtained as a colourless solid (0.081 g, 54%); mp 151 - 153 °C; ν_{max} (neat) 3393, 2921 (C–H), 1711 (C=O), 1666 (OC=O); δ_H (500 MHz, $CDCl_3$) 6.73 (1H, s, Ar**H**), 6.52 (1H, s, Ar**H**), 5.84 (1H, d, J = 8.8 Hz, NCOC**H**), 4.28 - 4.41 (1H, m, 1 × NC**H**$_2$), 3.88 (3H, s, OC**H**$_3$), 3.85 (3H, s, OC**H**$_3$), 2.98 - 3.13 (2H, m, 1 × NCH$_2$C**H**$_2$, 1 × NC**H**$_2$), 2.70 (1H, t, J = 7.3 Hz, NCOCHC**H**), 2.59 - 2.66 (1H, m, 1 × NCH$_2$C**H**$_2$), 2.24 (1H, dd, J = 8.5, 15.4 Hz, 1 × NCC**H**$_2$), 2.12 - 2.19 (1H, m, 1 × NCCHC**H**$_2$), 2.10 (3H, s, COC**H**$_3$), 2.02 - 2.09 (1H, m, 1 × NCCHC**H**$_2$), 1.87 - 2.00 (3H, m, 1 × NCCH$_2$CH$_2$C**H**$_2$, 2 × NCCHCH$_2$C**H**$_2$), 1.83 (1H, dd, J = 15.6, 10.9 Hz, 1 × NCC**H**$_2$), 1.61 - 1.72 (1H, m, 1 × NCCH$_2$C**H**$_2$), 1.32 - 1.44 (1H, m, 1 × NCCH$_2$CH$_2$C**H**$_2$), 1.06 - 1.19 (1H, m, 1 × NCCH$_2$C**H**$_2$); δ_C (126 MHz, $CDCl_3$) 170.6 (C=O), 169.4 (C=O), 147.9 (C), 136.5 (C), 124.2 (C), 111.5 (CH), 107.3 (CH), 72.0 (CH), 65.9 (C), 56.1 (CH_3), 55.8 (CH_3), 50.5 (CH), 40.0 (CH_2), 34.4 (CH_2), 31.0 (CH_2), 27.6 (CH_2), 27.3 (CH_2), 24.5 (CH_2), 23.5 (CH_2), 20.9 (CH_3); *m/z* (FTMS + NSI) Found 374.1692 ($[M+H]^+$ $C_{21}H_{28}NO_5$ requires 374.1958).

11,12-Dimethoxy-6-oxo-1,2,4,4a,5,6,8,9-octahydrothiopyrano[4',3':2,3]pyrrolo[2,1-a]isoquinolin-5-yl acetate 141d

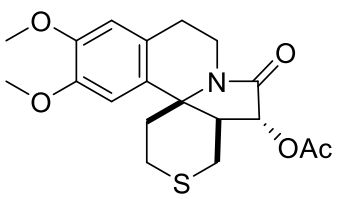

141d

Chemical Formula: $C_{19}H_{23}NO_5S$
Molecular Weight: 377.45

According to general procedure **B** compound **141d** was obtained as a tan solid (0.019 g, 19%); mp 133 - 135 °C; ν_{max} (neat) 3009, 2993 (C–H), 1744 (C=O), 1695 (OC=O); δ_H (500 MHz, $CDCl_3$) 6.79 (1H, s, Ar**H**), 6.59 (1H, s, Ar**H**), 6.07 (1H, d, J = 7.9 Hz, NCOC**H**), 4.27 (1H, dd, J = 6.3, 12.9 Hz, 1 × NC**H**$_2$), 3.88 (6H, 2 × s, 2 × OC**H**$_3$), 3.49 (1H, d, J = 14.2 Hz, 1 × NCCHC**H**$_2$), 3.07 - 3.15 (1H, m, 1 × NC**H**$_2$), 2.97 - 3.07 (1H, m, 1 × NCH$_2$C**H**$_2$), 2.94 (1H, d, J 13.9, 1 ×

NCCHC**H**$_2$), 2.78 - 2.84 (1H, m, NCOCHC**H**), 2.66 - 2.77 (2H, m, 1 × NCCH$_2$C**H**$_2$, 1 × NCH$_2$C**H**$_2$), 2.59 (1H, t, J = 11.2 Hz, 1 × NCCH$_2$C**H**$_2$), 2.30 - 2.40 (1H, m, 1 × NCC**H**$_2$), 2.19 (1H, dd, J = 7.3, 14.5 Hz, 1 × NCC**H**$_2$), 2.12 (3H, s, COC**H**$_3$); δ_C (126 MHz, $CDCl_3$) 170.4 (C=O), 169.1 (C=O), 148.3 (C), 147.9 (C), 133.7 (C), 125.0 (C), 111.9 (CH), 107.5 (CH), 72.8 (CH), 59.2 (C), 56.2 (CH_3), 55.9 (CH_3) 46.6 (CH), 34.85 (CH_2), 34.92 (CH_2), 27.5 (CH_2), 25.2 (CH_2), 20.9 (CH_3), 20.4 (CH_2); *m/z* (NSI) Found 394.1320 ($[M+OH]^+$ $C_{19}H_{24}NO_6S$ requires 394.1319). Unable to obtain dr for this sample.

5.1.3 General procedure C:

C: Synthesis of **146a-146j**

2-((4-(Methoxycarbonyl)-2-nitrophenyl)amino)-3-phenylpropanoic acid 146a

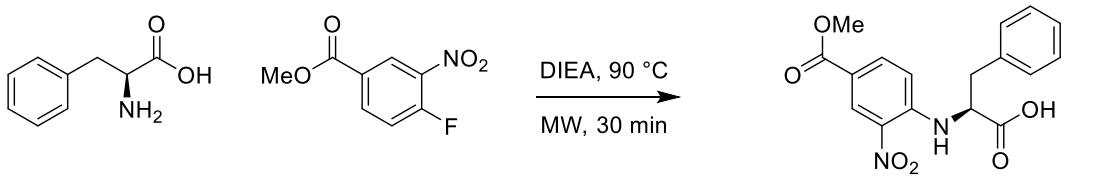

Chemical Formula: $C_{17}H_{16}N_2O_6$
Molecular Weight: 344.32

A solution of (*D*/*L*-phenylalanine) 2-amino-3-phenylpropanoic acid (0.050 g, 0.303 mmol), methyl 4-fluoro-3-nitrobenzoate (0.060 g, 0.303 mmol) and Hünig's Base (0.058 mL, 0.333 mmol) in 2-propanol (1 mL) and water (0.5 mL) was made. It was placed inside a microwave reactor for 30 minutes after which the solution was checked using TLC to indicate disappearance of starting materials. The solution was then concentrated under reduced pressure to give the crude material. This residue was taken up in EtOAc (20 mL), washed with 0.2 M HCl (2 × 10 mL) and brine (10 mL). The organic layers were collected and dried over $MgSO_4$, filtered and concentrated under reduced pressure to give 2-((4-(methoxycarbonyl)-2-nitrophenyl)amino)-3-phenylpropanoic acid (0.106 g, 102 %) as a yellow oil; δ_H (400 MHz, $CDCl_3$) 8.87 (1H, d, J = 2.0 Hz, Ar**H**), 8.66 (1H, d, J = 7.6 Hz, N**H**), 8.02 (1H, dd, J = 1.9, 9.0 Hz, Ar**H**), 7.28 - 7.36 (3H, m, Ar**H**), 7.23 - 7.27 (2H, m, Ar**H**), 6.69 (1H, d, J = 8.8 Hz, Ar**H**), 4.59 (1H, dt, J = 5.1, 7.5 Hz, NHC**H**), 3.90 (3H, s, OC**H**$_3$), 3.41 (1H, dd, J = 4.9, 14.0 Hz, 1 × CHC**H**$_2$), 3.25 (1H, dd, J = 7.6, 13.9 Hz, 1 × CHC**H**$_2$); δ_C (101 MHz, $CDCl_3$) 175.5 (CO), 165.5 (CO), 146.2 (C), 136.4 (CH), 134.8 (C), 132.2 (C), 129.4 (CH), 129.2 (2 × CH), 129.0 (2 × CH), 127.7 (CH), 118.5 (C), 113.5 (CH), 56.9 (CH), 52.2 (CH_3), 38.3 (CH_2); *m/z* (FTMS + NSI) 345.1085 ($[M+H]^+$ $C_{17}H_{17}N_2O_6$ requires 345.1081).

1-(4-(Hydroxy(methoxy)methyl)-2-nitrophenyl)pyrrolidine-2-carboxylic acid 146b

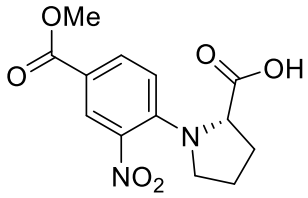

146b

Chemical Formula: $C_{13}H_{14}N_2O_6$
Molecular Weight: 294.26

According to general procedure **C** compound **146b** was isolated as a yellow oil (0.121 g, 94%); δ_H (400 MHz, $CDCl_3$) 8.38 (1H, d, J = 2.3 Hz, Ar**H**), 7.99 (1H, dd, J = 2.1, 9.0 Hz, Ar**H**), 6.83 (1H, d, J = 8.8 Hz, Ar**H**), 4.50 (1H, dd, J = 6.4, 7.7 Hz, NHC**H**), 3.90 (3H, s, OC**H**$_3$), 3.54 (1H, td, J = 7.3, 10.1 Hz, 1 × NC**H**$_2$), 3.17 - 3.28 (1H, m, 1 × NC**H**$_2$), 2.47 - 2.56 (1H, m, 1 × NCHC**H**$_2$), 2.10 - 2.27 (2H, m, 1 × NCHC**H**$_2$, 1 × NCH$_2$C**H**$_2$), 1.92 - 2.06 (1H, m, 1 × NCH$_2$C**H**$_2$); δ_C (101 MHz, $CDCl_3$) 175.9 (CO), 165.5 (CO), 143.9 (C), 133.6 (CH), 128.7 (CH), 118.9 (C), 116.0(CH), 61.8 (CH), 52.2 (CH_3), 51.5 (CH_2), 30.8 (CH_2), 24.6 (CH_2).

2-((4-(Methoxycarbonyl)-2-nitrophenyl)amino)-3-methylpentanoic acid 146d

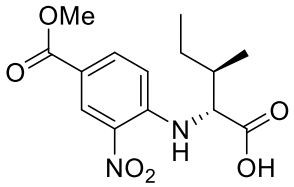

146d

Chemical Formula: $C_{14}H_{18}N_2O_6$
Molecular Weight: 310.31

According to general procedure **C** compound **146d** was isolated as a yellow oil (0.095 g, 80%); δ_H (400 MHz, $CDCl_3$) 8.91 (1H, d, J = 2.0 Hz, Ar**H**), 8.74 (1H, d, J = 7.6 Hz, N**H**), 8.07 (1H, dd, J = 2.0 Hz, 8.8, Ar**H**), 6.78 (1H, d, J = 9.1 Hz, Ar**H**), 4.26 (1H, dd, J = 5.1, 7.8 Hz, NHC**H**), 3.91 (3H, s, OC**H**$_3$), 2.14 (1H, dt, J = 2.1, 4.6 Hz, C**H**CH$_3$), 1.61 - 1.75 (1H, m, J = 4.8, 6.8, 6.8 Hz, 1 × C**H**$_2$CH$_3$), 1.36 - 1.51 (1H, m, 1 × C**H**$_2$CH$_3$), 1.10 (3H, d, J = 6.8 Hz, CHC**H**$_3$), 1.03 (3H, t, J = 7.3 Hz, CH$_2$C**H**$_3$); δ_C (101 MHz, $CDCl_3$) 175.6 (CO), 165.5 (CO), 146.7 (C), 136.6 (CH), 132.2 (C), 129.6 (CH), 118.3 (C), 113.4 (CH), 60.1 (CH), 52.2 (CH_3), 37.7 (CH), 25.4 (CH_2), 15.7 (CH_3), 11.5 (CH_3); *m/z* (FTMS + NSI) 311.1241 ($[M+H]^+$ $C_{14}H_{19}N_2O_6$ requires 311.1238).

2-((4-(Methoxycarbonyl)-2-nitrophenyl)amino)-4-methylpentanoic acid 146e

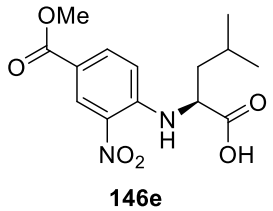

146e

Chemical Formula: $C_{14}H_{18}N_2O_6$
Molecular Weight: 310.31

According to general procedure **C** compound **146e** was isolated as a yellow oil (0.106 g, 90%);

δ_H (400 MHz, $CDCl_3$) 8.91 (1H, d, J = 2.0 Hz, Ar**H**), 8.49 (1H, d, J = 7.3 Hz, N**H**), 8.08 (1H, dd, J = 2.0, 8.8 Hz, Ar**H**), 6.79 (1H, d, J = 8.8 Hz, Ar**H**), 4.28 - 4.35 (1H, m, NHC**H**), 3.92 (3H, s, OC**H**$_3$), 1.83 - 1.95 (3H, m, CH_3C**H**C**H**$_2$), 1.05 (3H, d, J = 6.3 Hz, C**H**$_3$CH), 0.97 (3H, d, J = 6.3 hz, C**H**$_3$CH); δ_C (101 MHz, $CDCl_3$) 177.0 (CO), 165.4 (CO), 146.5 (C), 136.7 (CH), 132.2 (C), 129.5 (CH), 118.5 (C), 113.4 (CH), 54.2 (CH), 52.2 (CH_3), 41.3 (CH_2), 25.0 (CH), 22.7 (CH_3), 21.9 (CH_3); *m/z* (FTMS + NSI) 311.1243 ($[M+H]^+$ $C_{14}H_{19}N_2O_6$ requires 311.1238).

5.1.4 General procedure D:

D: Synthesis of **144a-144j**

Methyl 2-benzyl-3-oxo-1,2,3,4-tetrahydroquinoxaline-6-carboxylate 144a

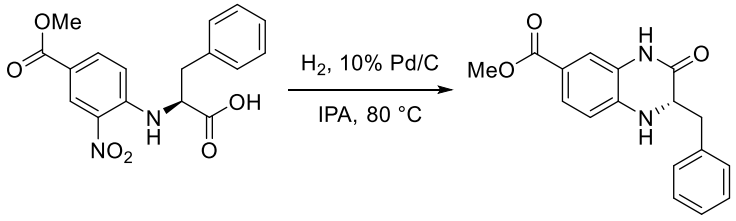

146a

Chemical Formula: $C_{17}H_{16}N_2O_6$
Molecular Weight: 344.32

144a

Chemical Formula: $C_{17}H_{16}N_2O_3$
Molecular Weight: 296.33

A solution of 2-amino-3-phenylpropanoic acid (0.05 g, 0.303 mmol), methyl 4-fluoro-3-nitrobenzoate (0.060 g, 0.303 mmol) and Hunig's Base (0.058 mL, 0.332 mmol) in 2-propanol (1 mL) and water (0.5 mL) was prepared. A 1mL injection was passed through the flow reactor at 90 °C with a flow rate of 0.45 mL/min for 30 minutes. The solution was checked using TLC (disappearance of SM). The total solution was then passed through the H-Cube using a 10% Pd/C cartridge at 80 °C with a flow rate of 0.5 mL/min. The resulting colourless solution was concentrated under reduced pressure. The residue was purified *via* automated flash chromatography (2:1 Hex/EtOAc; Zip 5 g column) to give methyl 2-benzyl-3-oxo-1,2,3,4-tetrahydroquinoxaline-6-carboxylate **144a** (0.042 g, 71%) as a colorless solid; mp (ethyl acetate) 183.5 - 184 °C (lit (methanol) 198 – 201 °C [176]); ν_{max} (neat) 3339 (N–H), 1673 (OC=O), 1613 (NC=O), 1538 (C=C); δ_H (400 MHz, $CDCl_3$) 8.09 (1H, s, N**H**CO), 7.62 (1H, dd, J = 8.2, 1.9 Hz, Ar**H**), 7.45 (1H, d, J = 1.8 Hz, Ar**H**), 7.28 - 7.41 (3H, m, Ar**H**), 7.19 - 7.23 (2H, m, Ar**H**), 6.57 (1H, d, J = 8.1 Hz, Ar**H**), 4.15 - 4.22 (2H, m, ArN**H**, NHC**H**), 3.89 (3H, s, OC**H**$_3$), 3.34 (1H, dd, J = 13.6, 3.0, 1 × ArC**H**$_2$), 2.86 (1H, dd, J = 13.4, 10.9 Hz, 1 × ArC**H**$_2$); δ_C (126 MHz, CDCl3) 167.1 (CO), 166.7 (CO), 136.9 (C), 136.2 (C), 129.4 (CH), 129.1 (CH), 127.3 (CH), 126.4 (CH), 124.4 (C), 120.9 (C), 116.5 (CH), 113.5 (CH), 57.4 (CH), 51.9 (CH_3), 38.4 (CH_2); *m/z* (NSI) Found 297.1234 ($[M+H]^+$ $C_{17}H_{17}N_2O_3$ requires 297.1237).

Methyl 4-oxo-1,2,3,3a,4,5-hexahydropyrrolo[1,2-a]quinoxaline-7-carboxylate 144b

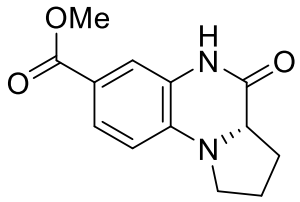

144b

Chemical Formula: $C_{13}H_{14}N_2O_3$
Molecular Weight: 246.27

According to general procedure **D** compound **144b** was obtained as a colourless solid (0.070 g, 99%); mp 183 - 184 °C (lit 182 – 192 °C [176]); ν_{max} (neat) 2977 (C–H), 1703 (OC=O), 1679 (NHC=O), 1535 (C=C); δ_H (400 MHz, $CDCl_3$) 7.70 (1H, dd, J = 8.3, 1.8 Hz, Ar**H**), 7.65 (1H, br.s, N**H**), 7.40 (1H, d, J = 1.8 Hz, Ar**H**), 6.54 (1H, d, J = 8.4 Hz, Ar**H**), 3.97 - 3.84 (1H, m, NHCOC**H**), 3.87 (3H, s, OC**H**$_3$), 3.53 (1H, ddd, J = 9.5, 7.8, 6.1 Hz, 1 × NC**H**$_2$), 3.38 (1H, td, J = 9.5, 4.7 Hz, 1 × NC**H**$_2$), 2.44 - 2.31 (1H, m, 1 × NHCOCHC**H**$_2$), 2.26 - 1.97 (3H, m, 1 × NHCOCHC**H**$_2$, NCH$_2$C**H**$_2$), δ_C (126 MHz, $CDCl_3$) 166.89 (CO), 166.63 (CO), 138.45(C), 126.69 (CH), 125.69 (C), 119.31 (C), 115.80 (CH), 110.81 (CH), 59.86 (CH), 51.86 (CH_3), 46.48 (CH_2), 27.45 (CH_2), 22.37 (CH_2).

Methyl 2-hydroxy-4-oxo-1,2,3,3a,4,5-hexahydropyrrolo[1,2-a]quinoxaline-7-carboxylate 144c

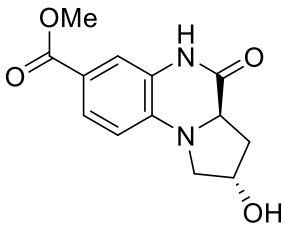

144c

Chemical Formula: $C_{13}H_{14}N_2O_4$
Molecular Weight: 262.26

According to general procedure **D** compound **144c** was obtained as a colourless solid (0.066 g, 99%); mp Decomposed at 197 °C; ν_{max} (neat) 3401 (br, O–H), 2960 (C–H), 1656 (OC=O), 1602 (NHC=O), 1535 (C=C); δ_H (400 MHz, CD_3OD) 7.64 (1H, dd, J = 8.4, 1.9 Hz, Ar**H**), 7.46 (1H, d, J = 1.9 Hz, Ar**H**), 6.60 (1H, d, J = 8.4 Hz, Ar**H**), 4.63 - 4.53 (1H, m, OC**H**), 4.20 (1H, dd, J = 10.8, 5.9 Hz, 1 × NC**H**$_2$), 3.84 (3H, s, OC**H**$_3$), 3.78 (1H, dd, J = 11.0, 5.5 Hz, 1 × NC**H**$_2$), 3.29 (1H, d, J = 1.9 Hz, NHCOC**H**), 2.31 - 2.12 (2H, m, C**H**$_2$); δ_C (101 MHz, CD_3OD) 169.1 (CO), 168.9 (CO), 140.0 (C), 127.9 (C), 127.7 (CH), 120.2 (C), 117.2 (CH), 111.8 (CH), 69.9 (CH), 59.2 (CH), 57.1 (CH_2), 52.4 (CH_3), 39.2 (CH_2); *m/z* (NSI) Found 263.1026 ($[M+H]^+$ $C_{13}H_{15}N_2O_4$ requires 263.1029).

Methyl 2-(sec-butyl)-3-oxo-1,2,3,4-tetrahydroquinoxaline-6-carboxylate 144d

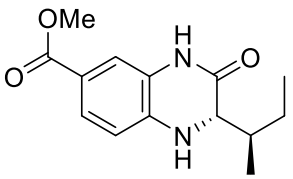

144d

Chemical Formula: $C_{14}H_{18}N_2O_3$
Molecular Weight: 262.31

According to general procedure **D** compound **144d** was obtained as a colourless solid (0.047 g, 71%); mp 227 - 228 °C (lit 225 – 227 °C [176]); ν_{max} (neat) 3340 (N–H), 2960 (C–H), 1698 (OC=O), 1682 (NHC=O), 1500 (C=C); δ_H (400 MHz, CD_3OD) 7.51 (1H, dd, J = 8.4, 1.9 Hz, Ar**H**), 7.36 (1H, d, J = 1.8 Hz, Ar**H**), 6.69 (1H, d, J = 8.4 Hz, Ar**H**), 3.89 (1H, d, J = 4.6 Hz, NHC**H**), 3.82 (3H, s, OC**H**$_3$), 1.86 (1H, m, NHCHC**H**CH_3), 1.54 (1H, m, 1 × CH_3C**H**$_2$), 1.31 - 1.12 (1H, m, 1 × CH_3C**H**$_2$), 0.99 (3H, d, J = 7.0 Hz, NHCHCHC**H**$_3$), 0.89 (3H, t, J = 7.4 Hz, C**H**$_3CH_2$); δ_C (101 MHz, CD_3OD) 173.61 (CO), 172.50 (CO), 168.81 (C), 140.48 (C), 127.43 (CH), 119.37 (C), 117.18 (CH), 112.81 (CH), 61.93 (CH), 52.14 (CH_3), 40.91 (CH), 25.77 (CH_2), 15.58 (CH_3), 11.97 (CH_3); *m/z* (NSI) Found 263.1390 ($[M+H]^+$ $C_{14}H_{19}N_2O_3$ requires 263.1392).

Methyl 2-isobutyl-3-oxo-1,2,3,4-tetrahydroquinoxaline-6-carboxylate 144e

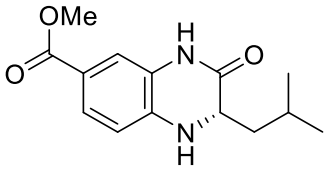

144e

Chemical Formula: $C_{14}H_{18}N_2O_3$
Molecular Weight: 262.31

According to general procedure **D** compound **144e** was obtained as a colourless solid (0.041 g, 63%); mp 214 - 215 °C (lit 212 – 215 °C [176]); ν_{max} (neat) 3345 (N–H), 1649 (OC=O), 1695 (NHC=O), 2921 (C–H); δ_H (400 MHz, $CDCl_3$) 7.61 (1H, dd, J = 8.2, 1.8 Hz, Ar**H**), 7.57 (1H, s, N**H**), 7.37 (1H, d, J = 1.8 Hz, Ar**H**), 6.66 (1H, d, J = 8.3 Hz, Ar**H**), 4.28 (1H, s, N**H**), 4.05 (1H, ddd, J = 9.2, 4.4, 1.8 Hz, NHC**H**), 3.87 (3H, s, OC**H**$_3$), 1.75 (2H, ddd, J = 15.1, 9.4, 4.6 Hz, NHCHC**H**$_2$), 1.68 - 1.59 (1H, m, C**H**$(CH_3)_2$), 1.05 - 0.90 (6H, m, CH(C**H**$_3)_2$); δ_C (126 MHz, $CDCl_3$) 167.85 (CO), 166.80 (CO), 137.21 (C), 126.43 (CH), 124.51 (C), 120.88 (C), 116.51 (CH), 113.31 (CH), 54.58 (CH), 52.05 (CH_3), 41.21 (CH_2), 24.41 (CH_3), 23.32 (CH), 21.66 (CH_3); *m/z* (NSI) Found 263.1390 ($[M+H]^+$ $C_{14}H_{19}N_2O_3$ requires 263.1391).

Methyl 2-((1H-indol-3-yl)methyl)-3-oxo-1,2,3,4-tetrahydroquinoxaline-6-carboxylate 144f

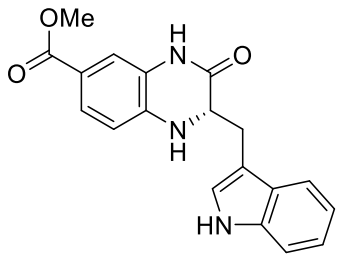

144f

Chemical Formula: $C_{19}H_{17}N_3O_3$
Molecular Weight: 335.36

According to general procedure **D** compound **144f** was obtained as a colourless solid (0.042 g, 77%); mp 119 - 120 °C; ν_{max} (neat) 3443 (N–H), 1694 (OC=O), 1635 (NHC=O), 1521 (C=C); δ_H (400 MHz, CD_3OD) 7.53 (1H, dt, J = 7.9, 1.0 Hz, Ar**H**), 7.43 (1H, dd, J = 8.3, 1.8 Hz, Ar**H**), 7.32 - 7.26 (2H, m, Ar**H**), 7.10 - 6.94 (3H, m, Ar**H**), 6.53 (1H, d, J = 8.3 Hz, Ar**H**), 4.86 - 4.76 (3H, m, OC**H**$_3$), 4.25 (1H, dd, J = 7.9, 4.0 Hz, COC**H**), 3.24 - 3.06 (2H, m, CHC**H**$_2$); δ_C (101 MHz, CD_3OD) 170.1 (CO), 168.9 (CO), 139.8 (C), 138.2 (C), 129.0 (C), 127.3 (CH), 125.6 (C), 125.3 (CH), 122.5 (CH), 120.0 (CH), 119.9 (C), 119.5 (CH), 117.2 (CH), 113.8 (CH), 112.3 (CH), 110.4 (C), 58.4 (CH), 52.3 (CH_3), 30.6 (CH_2); *m/z* (NSI) Found 336.1343 ($[M+H]^+$ $C_{19}H_{18}N_3O_3$ requires 336.1345).

Methyl 3-oxo-2-phenyl-1,2,3,4-tetrahydroquinoxaline-6-carboxylate 144g

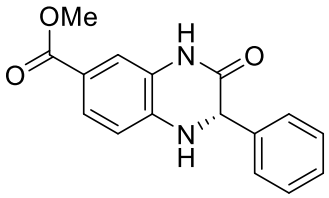

144g

Chemical Formula: $C_{16}H_{14}N_2O_3$
Molecular Weight: 282.30

According to general procedure **D** compound **144g** was obtained as a colourless solid (0.061 g, 99%); mp 207 - 208 °C (lit (racemic) 215 °C [177]); ν_{max} (neat) 3305 (N–H), 1692 (OC=O), 1671 (NHC=O), 1599 (C=C); δ_H (400 MHz, $CDCl_3$) 7.72 (1H, s, N**H**), 7.66 (1H, dd, J = 8.3, 1.8 Hz, Ar**H**), 7.43 - 7.29 (6H, m, Ar**H**), 6.72 (1H, d, J = 8.2 Hz, Ar**H**), 5.17 (1H, d, J = 1.8 Hz, NHC**H**), 4.65 (1H, s, N**H**), 3.88 (3H, s, OC**H**$_3$); δ_C (101 MHz, $CDCl_3$) 166.72 (CO), 165.52 (CO), 138.79 (C), 137.11 (C), 129.16 (CH), 128.96 (CH), 127.12 (CH), 126.73 (CH), 123.88 (C), 120.98 (C), 116.69 (CH), 112.92 (CH), 60.68 (CH), 52.09 (CH_3); *m/z* (NSI) Found 283.1077 ($[M+H]^+$ $C_{16}H_{15}N_2O_3$ requires 283.1079).

Methyl 2-butyl-3-oxo-1,2,3,4-tetrahydroquinoxaline-6-carboxylate 144h

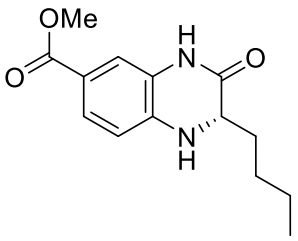

144h

Chemical Formula: $C_{14}H_{18}N_2O_3$
Molecular Weight: 262.31

According to general procedure **D** compound **144h** was obtained as a colourless solid (0.046 g, 69%); mp 197 - 198 °C; ν_{max} (neat) 3351 (N–H), 2934 (C–H), 1681 (OC=O), 1615 (NHC=O),; δ_H (400 MHz, $CDCl_3$) 7.69 (1H, s, N**H**), 7.61 (1H, dd, J = 8.2, 1.8 Hz, Ar**H**), 7.37 (1H, d, J = 1.8 Hz, Ar**H**), 6.65 (1H, d, J = 8.3 Hz, Ar**H**), 4.30 (1H, br.s, N**H**), 4.03 (1H, ddd, J = 7.6, 4.7, 1.8 Hz, NHC**H**), 3.87 (3H, s, OC**H**$_3$), 1.92 - 1.70 (2H, m, NHCHC**H**$_2$), 1.40 (4H, m, $CH_3C\mathbf{H}_2C\mathbf{H}_2$), 0.91 (3H, t, J = 7.1 Hz, C**H**$_3CH_2CH_2$); δ_C (101 MHz, $CDCl_3$) 167.56 (CO), 166.81 (CO), 137.43 (C), 126.49 (CH), 124.28 (CH), 120.68 (C), 116.48 (CH), 113.04 (CH), 56.37 (CH), 52.04 (CH_3), 32.68 (CH_2), 27.33 (CH_2), 22.58 (CH_2), 14.07 (CH_3); *m/z* (NSI) Found 263.1390 ($[M+H]^+$ $C_{14}H_{19}N_2O_3$ requires 263.1394).

Methyl 2-(4-methoxybenzyl)-3-oxo-1,2,3,4-tetrahydroquinoxaline-6-carboxylate 144i

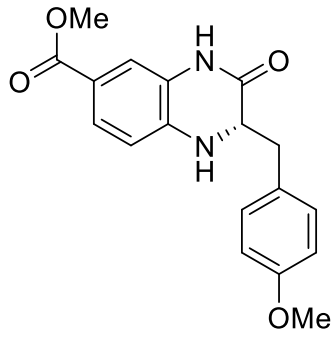

144i

Chemical Formula: $C_{18}H_{18}N_2O_4$
Molecular Weight: 326.35

According to general procedure **D** compound **144i** was obtained as a colourless solid (0.043 g, 77%); mp 176 - 179 °C; ν_{max} (neat) 3323 (N–H), 1682 (OC=O), 1613 (NC=O), 1536 (C=C); δ_H (101 MHz, $CDCl_3$) 7.83 (1H, s, N**H**), 7.61 (1H, dd, J = 8.4, 1.7 Hz, Ar**H**), 7.41 (1H, d, J= 1.6 Hz, Ar**H**), 7.13 - 7.09 (2H, m, Ar**H**), 6.93 - 6.86 (2H, m, Ar**H**), 6.57 (1H, d, J = 8.3 Hz, Ar**H**), 4.20 (1H, s, N**H**), 4.11 (1H, ddd, J = 11.1, 3.2, 1.8 Hz, NHC**H**), 3.88 (3H, s, COOC**H**$_3$), 3.82 (3H, s, ArOC**H**$_3$), 3.26 (1H, dd, J = 13.7, 3.2 Hz, 1 × NHCHC**H**$_2$), 2.79 (1H, dd, J = 13.7, 10.9 Hz, 1 × NHCHC**H**$_2$); δ_C (101 MHz, $CDCl_3$) 167.19 (CO), 166.76 (CO), 159.01 (C), 136.95 (C), 130.53 (CH),

128.16 (C), 126.56 (CH), 124.54 (C), 121.01 (C), 116.56 (CH), 114.63 (CH), 113.62 (CH), 57.73 (CH), 55.48 ($COOCH_3$), 52.08 ($ArOCH_3$), 37.67 (CH_2).

Methyl 2-(2-fluorobenzyl)-3-oxo-1,2,3,4-tetrahydroquinoxaline-6-carboxylate 144j

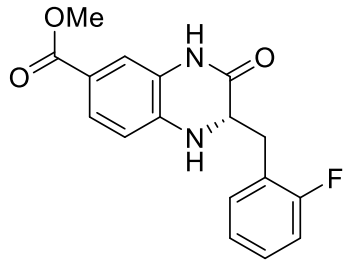

144j

Chemical Formula: $C_{17}H_{15}FN_2O_3$
Molecular Weight: 314.32

According to general procedure **D** compound **144j** was obtained as a colourless solid (0.028 g, 49%); mp 190 - 192 °C; ν_{max} (neat) 3339 (N–H), 1689 (OC=O), 1614 (NHC=O), 1500 (C=C); δ_H (400 MHz, $CDCl_3$) 7.88 (1H, br.s, N**H**), 7.60 (1H, dd, J = 8.3, 1.7 Hz, Ar**H**), 7.37 (1H, d, J = 1.9 Hz, Ar**H**), 7.20 (1H, m, Ar**H**), 7.14 - 7.02 (3H, m, Ar**H**), 6.58 (1H, d, J = 8.3 Hz, Ar**H**), 4.28 (1H, ddd, J = 9.1, 3.8, 1.7 Hz, NHC**H**), 4.23 (1H, s, N**H**), 3.87 (3H, s, OC**H**$_3$), 3.42 - 3.34 (1H, m, 1 × NHCHC**H**$_2$), 2.98 (1H, dd, J = 13.8, 9.2 Hz, 1 × NHCHC**H**$_2$); δ_C (101 MHz, $CDCl_3$) 166.79 (CO), 166.75 (CO), 161.60 (C, d, J = 245.7 Hz), 136.93 (C), 131.97 (CH, d, J = 4.4 Hz), 129.40 (CH, d, J = 8.0 Hz), 126.50 (CH), 124.64 (CH, d, J = 3.4 Hz), 124.33 (C), 123.36 (C, d, J = 15.6 Hz), 120.98 (C), 116.57 (CH), 115.83 (CH, d, J = 21.9 Hz), 113.53 (CH), 56.54 (CH), 52.07 (CH_3), 32.35 (CH_2); *m/z* (NSI) Found 315.1139 ($[M+H]^+$ $C_{17}H_{16}FN_2O_3$ requires 315.1142).

5.1.5 General Procedure E:

E: Synthesis of **150a – 150r**

Ethyl 2,7,7-trimethyl-5-oxo-4-phenyl-1,4,5,6,7,8-hexahydroquinoline-3-carboxylate 150a

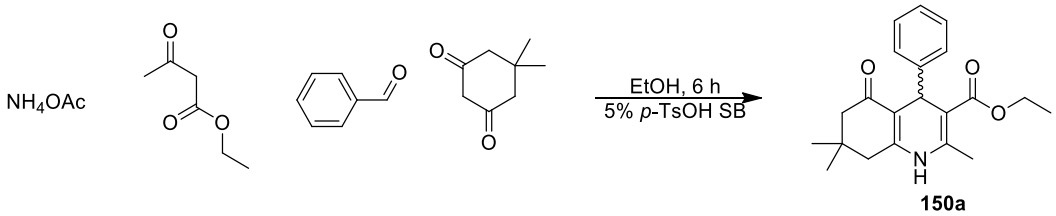

150a

Chemical Formula: $C_{21}H_{25}NO_3$
Molecular Weight: 339.43

Benzaldehyde (0.182 mL, 1.78 mmol), 5,5-dimethylcyclohexane-1,3-dione (0.250 g, 1.78 mmol), ethyl 3-oxobutanoate (0.228 mL, 1.78 mmol), ammonium acetate (0.137 g, 1.78 mmol) and a *p*-TsOH stirrer bead (General Procedure D1) were added to ethanol (6.99 mL). The reaction was stirred for 4 hours then concentrated under reduced pressure.The residue was purified *via* automated flash chromatography (3:2 Hex/EtOAc; Zip 30 g column) to give ethyl 2,7,7-trimethyl-5-oxo-4-phenyl-1,4,5,6,7,8-hexahydroquinoline-3-carboxylate **150a** (0.424 g, 70%) as a yellow solid; mp 212 - 214 °C (lit 217 – 219 °C [178]); ν_{max} (neat) 3286 (N–H), 1691 (C=O), 1651 (OC=O), 1607 (C=C); δ_H (400 MHz, $CDCl_3$) 7.28 - 7.34 (2H, m, Ar**H**), 7.19 (2H, t, J = 7.6 Hz, Ar**H**), 7.06 - 7.12 (1H, m, Ar**H**), 6.81 (1H, br. s., N**H**), 5.06 (1H, s, NHCCC**H**), 4.07 (2H, q, J = 7.1 Hz, OC**H**$_2$CH$_3$), 2.33 (3H, s, C**H**$_3$CNH), 2.11 - 2.32 (4H, m, COC**H**$_2$, NHCC**H**$_2$), 1.20 (3H, t, J = 7.1 Hz, C**H**$_3$CH$_2$O), 1.06 (3H, s, C**H**$_3$CCH$_2$CO), 0.93 (3H, s, C**H**$_3$CCH$_2$CO); δ_C (101 MHz, $CDCl_3$) 195.4 (CO), 167.4 (CO), 147.9 (C), 147.0 (C), 143.3 (C), 128.0 (CH), 127.9 (CH), 126.0 (CH), 112.2 (C), 106.1 (C), 59.8 (CH_2), 50.7 (CH_2), 41.1 (CH_2), 36.5 (CH_3), 32.7 (C), 29.4 (CH_3), 27.1 (CH), 19.4 (CH_3), 14.2 (CH_3); *m/z* (NSI) Found 340.1907 ($[M+H]^+$ $C_{21}H_{26}NO_3$ requires 340.1907).

Ethyl 4-(4-methoxyphenyl)-2,7,7-trimethyl-5-oxo-1,4,5,6,7,8-hexahydroquinoline-3-carboxylate 150b

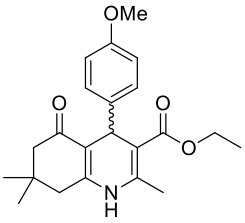

150b

Chemical Formula: $C_{22}H_{27}NO_4$
Molecular Weight: 369.45

According to general procedure **E** compound **150b** was obtained as a colourless solid (0.595 g, 73%); mp 252 - 254 °C (lit 251 – 252 °C [179]), ν_{max} (neat) 3274 (N–H), 1699 (C=O), 1648 (OC=O), 1603 (C=C); δ_H (400 MHz, $CDCl_3$) 7.22 (2H, d, J = 8.8 Hz, Ar**H**), 6.74 (2H, d, J = 8.5 Hz, Ar**H**), 6.21 (1H, s, N**H**), 5.00 (1H, s, NHCCC**H**), 4.07 (2H, q, J = 7.3 Hz, OC**H**$_2$CH$_3$), 3.73 (3H, s, OC**H**$_3$), 2.36 (3H, s, C**H**$_3$CNH), 2.12 - 2.33 (4H, m, COC**H**$_2$, NHCC**H**$_2$), 1.21 (3H, t, J = 7.1 Hz, C**H**$_3$CH$_2$O), 1.07 (3H, s, C**H**$_3$CCH$_2$CO), 0.94 (3H, s, C**H**$_3$CCH$_2$CO); δ_C (101 MHz, $CDCl_3$) 195.6 (CO), 167.5 (CO), 157.7 (C), 148.0 (C), 143.1 (C), 139.6 (C), 128.9 (CH), 113.2 (CH), 112.3 (C), 106.3 (C), 59.8 (CH_2), 55.1 (CH_3), 50.7 (CH_2), 41.0 (CH_2), 35.7 (CH), 32.7 (C), 29.4 (CH_3), 27.1 (CH_3), 19.4 (CH_3), 14.2 (CH_3); *m/z* (NSI) Found 370.1813 ($[M+H]^+$ $C_{22}H_{28}NO_4$ requires 370.2004).

Ethyl 4-(2-bromophenyl)-2,7,7-trimethyl-5-oxo-1,4,5,6,7,8-hexahydroquinoline-3-carboxylate 150c

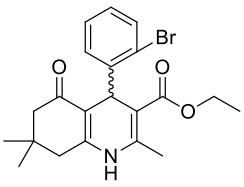

150c

Chemical Formula: $C_{21}H_{24}BrNO_3$
Molecular Weight: 418.32

According to general procedure **E** compound **150c** was obtained as a colourless solid (0.559 g, 75%); mp 205 - 206 °C (lit 209 – 211 °C [180]); ν_{max} (neat) 3277 (N–H), 1695 (C=O), 1607 (C=C); δ_H (400 MHz, $CDCl_3$) 7.45 (1H, dd, J 1.3, 8.1, Ar**H**), 7.37 (1H, dd, J = 7.7,1.6 Hz, Ar**H**), 7.16 (1H, dt, J = 1.3, 7.5 Hz, Ar**H**), 6.90 - 6.99 (1H, m, Ar**H**), 5.63 - 5.72 (1H, br.s, N**H**), 5.38 (1H, s, NHCCC**H**), 4.07 (2H, dd, J = 9.1, 7.1 Hz, OC**H**$_2$CH$_3$), 2.35 (3H, s, C**H**$_3$CNH), 2.13 - 2.32 (4H, m, COC**H**$_2$, NHCC**H**$_2$), 1.18 (3H, t, J = 7.1 Hz, C**H**$_3$CH$_2$O), 1.09 (3H, s, C**H**$_3$CCH$_2$CO), 0.97 (3H, s, C**H**$_3$CCH$_2$CO); δ_C (101 MHz, $CDCl_3$) 195.2 (CO), 167.1 (CO), 147.7 (C), 145.7 (C), 143.1 (C), 133.1 (CH), 132.0 (CH), 127.5 (CH), 126.9 (CH), 123.4 (C), 111.7 (C), 106.0 (C), 59.8 (CH_2), 50.6 (CH_2), 41.4 (CH_2), 38.0 (CH), 32.6 (C), 29.2 (CH_3), 27.4 (CH_3), 19.2 (CH_3), 14.3 (CH_3); *m/z* (NSI) Found 418.1012 ($[M+H]^+$ $C_{21}H_{25}BrNO_3$ requires 418.1009).

Ethyl 4-(4-fluorophenyl)-2,7,7-trimethyl-5-oxo-1,4,5,6,7,8-hexahydroquinoline-3-carboxylate 150d

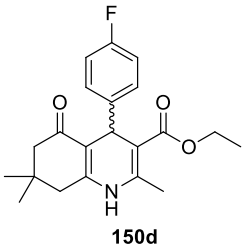

150d

Chemical Formula: $C_{21}H_{24}FNO_3$
Molecular Weight: 357.42

According to general procedure **E** compound **150d** was obtained as a colourless solid (0.417 g, 65%); mp 194 - 195 °C (lit (ethanol) 184 – 187 °C [181]); ν_{max} (neat) 3273 (N–H), 1705 (C=O), 1646 (OC=O), 1601 (C=C); δ_H (400 MHz, $CDCl_3$) 7.44 (1H, s, N**H**), 7.24 - 7.32 (2H, m, Ar**H**), 6.83 - 6.92 (2H, m, Ar**H**), 5.06 (1H, s, NHCCC**H**), 4.04 - 4.16 (2H, m, OC**H**$_2$CH$_3$), 2.34 (3H, s, C**H**$_3$CNH), 2.11 - 2.32 (4H, m, COC**H**$_2$, NHCC**H**$_2$), 1.22 (3H, t, J = 7.2 Hz, C**H**$_3$CH$_2$O), 1.06 (3H, s, C**H**$_3$CCH$_2$CO), 0.93 (3H, s, C**H**$_3$CCH$_2$CO); δ_C (101 MHz, $CDCl_3$) 195.4 (CO), 167.3 (CO), 161.2 (C, d, J = 244.7 Hz), 147.8 (C), 143.3 (C), 142.8 (d, J 3.66, C), 129.4 (CH. d, J = 8.25 Hz), 114.5 (CH, d, J = 21.08 Hz), 112.2 (C), 106.1 (C), 59.8 (CH_2), 50.7 (CH_2), 41.1 (CH_2), 36.0 (CH), 32.7 (C), 29.4 (CH_3), 27.1 (CH_3), 19.4 (CH_3), 14.2 (CH_3); *m/z* (NSI) Found 358.1813 ($[M+H]^+$ $C_{21}H_{25}FNO_3$ requires 358.1813).

Ethyl 2-methyl-5-oxo-4-phenyl-1,4,5,6,7,8-hexahydroquinoline-3-carboxylate 150e

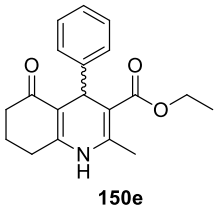

150e

Chemical Formula: $C_{19}H_{21}NO_3$
Molecular Weight: 311.37

According to general procedure **E** compound **150e** was obtained as a colourless solid (0.506 g, 73%); mp 257 - 259 °C (250 – 252 °C [182]); ν_{max} (neat) 3280 (N–H), 1689 (C=O), 1642 (OC=O), 1605 (C=C); δ_H (400 MHz, $CDCl_3$) 7.28 - 7.34 (2H, m, Ar**H**), 7.18 - 7.24 (2H, m, Ar**H**), 7.08 - 7.13 (1H, m, Ar**H**), 5.78 (1H, br. s., N**H**), 5.11 (1H, s, NHCCC**H**), 4.06 (2H, q, J = 7.2 Hz, OC**H**$_2$CH$_3$), 2.41 - 2.48 (2H, m, NCC**H**$_2$), 2.40 (3H, s, C**H**$_3$CNH), 2.30 - 2.38 (2H, m, COC**H**$_2$CH$_2$), 1.89 - 2.05 (2H, m, COCH$_2$C**H**$_2$), 1.19 (3H, t, J = 7.1 Hz, C**H**$_3$CH$_2$O); δ_C (101 MHz, $CDCl_3$) 195.6 (CO), 167.4 (CO), 149.2 (C), 147.1 (C), 143.2 (C), 128.0 (CH), 127.9 (CH), 126.0 (CH), 113.6 (C), 106.1 (C), 59.8 (CH_2), 37.0 (CH_2), 36.4 (CH), 27.6 (CH_2), 21.0 (CH_2), 19.4 (CH_3), 14.2 (CH_3); *m/z* (NSI) Found 312.1594 ($[M+H]^+$ $C_{19}H_{22}NO_3$ requires 312.1595).

Ethyl 4-(4-methoxyphenyl)-2-methyl-5-oxo-1,4,5,6,7,8-hexahydroquinoline-3-carboxylate 150f

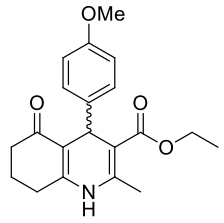

150f
Chemical Formula: $C_{20}H_{23}NO_4$
Molecular Weight: 341.40

According to general procedure **E** compound **150f** was obtained as a colourless solid (0.389 g, 51%); mp (ethyl acetate) 217 - 220 °C (lit (ethanol) 209 – 211 °C [183]); ν_{max} (neat) 3280 (N–H), 1690 (C=O), 1645 (OC=O), 1605 (C=C); δ_H (400 MHz, $CDCl_3$) 7.20 - 7.25 (2H, m, Ar**H**), 6.72 - 6.78 (2H, m, Ar**H**), 5.84 (1H, br. s., N**H**), 5.05 (1H, s. NHCCC**H**), 4.07 (2H, q, J = 7.2 Hz, OC**H**$_2$CH$_3$), 3.75 (3H, s, OC**H**$_3$), 2.40 - 2.50 (2H, m, NCC**H**$_2$), 2.39 (3H, s, C**H**$_3$CNH), 2.29 - 2.38 (2H, m, COC**H**$_2$CH$_2$), 1.89 - 2.04 (2H, m, COCH$_2$C**H**$_2$), 1.20 (3H, t, J = 7.1 Hz, C**H**$_3$CH$_2$O); δ_C (101 MHz, $CDCl_3$) 195.7 (CO), 167.5 (CO), 157.8 (C), 149.1 (C), 142.9 (C), 139.7 (C), 129.0 (CH), 113.7 (C), 113.3 (CH), 106.3 (C), 59.8 (CH_2), 55.1 (CH_2), 37.0 (CH_2), 35.5 (CH), 27.5 (CH_2), 21.0 (CH_2), 19.4 (CH_3), 14.2 (CH_3); *m/z* (NSI) Found 342.1700 ($[M+H]^+$ $C_{20}H_{24}NO_3$ requires 342.1694).

Ethyl 4-(2-bromophenyl)-2-methyl-5-oxo-1,4,5,6,7,8-hexahydroquinoline-3-carboxylate 150g

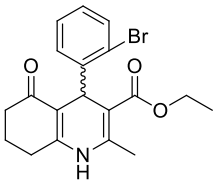

150g
Chemical Formula: $C_{19}H_{20}BrNO_3$
Molecular Weight: 390.27

According to general procedure **E** compound **150g** was obtained as a yellow solid (0.552 g, 63%); mp 206 - 207 °C; ν_{max} (neat) 3300 (N–H), 1693 (C=O), 1608 (C=C); δ_H (400 MHz, $CDCl_3$) 7.45 (1H, dd, J = 8.0, 1.1 Hz, Ar**H**), 7.38 (1H, dd, J = 7.7, 1.6 Hz, Ar**H**), 7.16 (1H, dt, J = 7.5, 1.3 Hz, Ar**H**), 6.95 (1H, m, Ar**H**), 5.95 (1H, br. s., N**H**), 5.39 (1H, s, NHCCC**H**), 4.02 - 4.12 (2H, m, OC**H**$_2$CH$_3$), 2.38 - 2.45 (2H, m, NHCC**H**$_2$), 2.33 (3H, s, C**H**$_3$CNH), 2.27 - 2.32 (2H, m, COC**H**$_2$), 1.87 - 2.03 (2H, m, COCH$_2$C**H**$_2$), 1.18 (3H, t, J = 7.2 Hz, C**H**$_3$CH$_2$O); δ_C (101 MHz, $CDCl_3$) 195.5 (CO), 167.4 (CO), 149.8 (C), 145.9 (C), 143.1 (C), 133.0 (CH), 132.2 (CH), 127.5 (CH), 127.0 (CH), 123.3 (C), 112.8 (C), 105.7 (C), 59.8 (CH_2), 38.0 (CH), 37.0 (CH_2), 27.6 (CH_2), 21.0 (CH_2), 19.4 (CH_3), 14.3 (CH_3); *m/z* (NSI) Found 390.0699 ($[M+H]^+$ $C_{19}H_{21}BrNO_3$ requires 390.0698).

Ethyl 4-(4-fluorophenyl)-2-methyl-5-oxo-1,4,5,6,7,8-hexahydroquinoline-3-carboxylate 150h

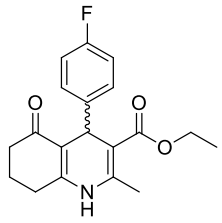

150h

Chemical Formula: $C_{19}H_{20}FNO_3$
Molecular Weight: 329.37

According to general procedure **E** compound **150h** was obtained as a yellow solid (0.368 g, 50%); mp Decomposed at 256 °C; ν_{max} (neat) 3288 (N–H), 1695 (C=O), 1646 (OC=O), 1603 (C=C); δ_H (400 MHz, $CDCl_3$) 7.24-7.29 (2H, m, Ar**H**), 6.84 - 6.92 (2H, m, Ar**H**), 5.73 (1H, br. s., N**H**), 5.08 (1H, s, NHCCC**H**), 4.06 (2H, qd, J 7.2, 1.3 Hz, OC**H**$_2$CH$_3$), 2.41 - 2.49 (2H, m, NCC**H**$_2$), 2.40 (3H, s, C**H**$_3$CNH), 2.30 - 2.39 (2H, m, COC**H**$_2$CH$_2$), 1.88 - 2.07 (2H, m, COCH$_2$C**H**$_2$), 1.18 (3H, t, J 7.1, C**H**$_3$CH$_2$O); δ_C (126 MHz, $CDCl_3$) 195.6 (CO), 167.5 (CO), 160.9 (C, d, J = 243.8 Hz), 149.3 (C), 143.2 (C), 143.0 (C, d, J = 2.8 Hz), 129.4 (CH, d, J = 7.3 Hz), 114.6 (CH, d, J = 20.2 Hz), 113.5 (C), 106.1 (C), 59.8 (CH_2), 37.0 (CH_2), 35.8 (CH), 27.5 (CH_2), 21.0 (CH_2), 19.4 (CH_3), 14.2 (CH_3); *m/z* (NSI) Found 330.1500 ($[M+H]^+$ $C_{19}H_{21}FNO_3$ requires 330.1500).

Ethyl 4-(4-chlorophenyl)-2,7,7-trimethyl-5-oxo-1,4,5,6,7,8-hexahydroquinoline-3-carboxylate 150i

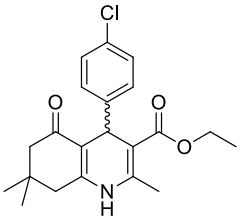

150i

Chemical Formula: $C_{21}H_{24}ClNO_3$
Molecular Weight: 373.87

According to general procedure **E** compound **150i** was obtained as a colourless solid (0.327 g, 49%); mp 241 - 242 °C; ν_{max} (neat) 3272 (N–H), 1704 (C=O), 1647 (OC=O), 1602 (C=C); δ_H (400 MHz, $CDCl_3$) 7.23 - 7.26 (2H, m, Ar**H**), 7.14 - 7.19 (2H, m, Ar**H**), 5.74 (1H, br. s., N**H**), 5.04 (1H, s, NHCCC**H**), 4.06 (2H, q, J = 7.1 Hz, OC**H**$_2$CH$_3$), 2.39 (3H, s, C**H**$_3$CNH), 2.12 - 2.37 (4H, m, COC**H**$_2$, NHCC**H**$_2$), 1.19 (3H, t, J = 7.2 Hz, C**H**$_3$CH$_2$O), 1.09 (3H, s, C**H**$_3$CCH$_2$CO), 0.94 (3H, s, C**H**$_3$CCH$_2$CO); δ_C (101 MHz, $CDCl_3$) 195.3 (CO), 167.2 (CO), 147.8 (C), 145.5 (C), 143.5 (C), 131.6 (C), 129.4 (CH), 128.0 (CH), 112.0 (C), 105.8 (C), 59.9 (CH_2), 50.6 (CH_2), 41.2 (CH_2), 36.2 (CH), 32.7 (C), 29.4 (CH_3), 27.1 (CH_3), 19.5 (CH_3), 14.2 (CH_3); *m/z* (NSI) Found 374.1517 ($[M+H]^+$ $C_{21}H_{25}ClNO_3$ requires 374.1517).

Ethyl 2-methyl-4-(4-nitrophenyl)-5-oxo-1,4,5,6,7,8-hexahydroquinoline-3-carboxylate 150j

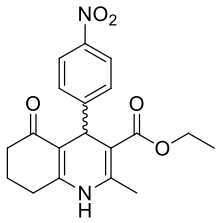

150j

Chemical Formula: $C_{19}H_{20}N_2O_5$
Molecular Weight: 356.37

According to general procedure **E** compound **150j** was obtained as a yellow solid (0.490 g, 62%); mp Decomposed at 218 °C; ν_{max} (neat) 3294 (N–H), 1727 (C=O), 1700 (OC=O), 1648 (C=C), 1517 (NO2); δ_H (400 MHz, $CDCl_3$) 8.07 (2H, d, J = 8.6 Hz, Ar**H**), 7.48 (2H, d, J = 8.8 Hz, Ar**H**), 6.52 (1H, s, N**H**), 5.18 (1H, s. NHCCC**H**), 4.05 (2H, q, J = 7.1 Hz, OC**H**$_2$CH$_3$), 2.42 - 2.49 (2H, m, NHCC**H**$_2$), 2.40 (3H, s, C**H**$_3$CNH), 2.30 - 2.37 (2H, m, COC**H**$_2$), 2.01 (1H, m, 1 × CH_2C**H**$_2$$CH_2$), 1.83 - 1.95 (1H, m, 1 × CH_2C**H**$_2$$CH_2$), 1.17 (3H, t, J = 7.1 Hz, OCH_2C**H**$_3$); δ_C (101 MHz, $CDCl_3$) 195.7 (CO), 166.8 (CO), 154.5 (C), 150.5 (C), 146.1 (C), 144.4 (C), 128.9 (CH), 123.3 (CH), 112.2 (C), 104.8 (C), 60.0 (CH_2), 37.0 (CH), 36.8 (CH_2), 27.3 (CH_2), 20.9 (CH_2), 19.3 (CH_3), 14.1 (CH_3); *m/z* (NSI) Found 357.1445 ($[M+H]^+$ $C_{19}H_{21}N_2O_5$ requires 357.1445).

Ethyl 2,7,7-trimethyl-4-(4-nitrophenyl)-5-oxo-1,4,5,6,7,8-hexahydroquinoline-3-carboxylate 150k

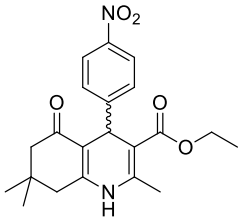

150k

Chemical Formula: $C_{21}H_{24}N_2O_5$
Molecular Weight: 384.43

According to general procedure **E** compound **150k** was obtained as a yellow solid (0.678 g, 99%); mp 239 - 240 °C; ν_{max} (neat) 3274 (N–H), 1701 (C=O), 1648 (OC=O), 1604 (C=C), 1516 (NO_2); δ_H (400 MHz, $CDCl_3$) 8.08 (2H, d, J = 8.8 Hz, Ar**H**), 7.49 (2H, d, J = 8.8 Hz, Ar**H**), 6.09 (1H, s, N**H**), 5.16 (1H, s, NHCCC**H**), 4.05 (2H, qd, J = 7.1, 1.4 Hz, OC**H**$_2$CH$_3$), 2.41 (3H, s, C**H**$_3$CNH), 2.11 - 2.40 (4H, m, COC**H**$_2$, NHCC**H**$_2$), 1.18 (3H, t, J = 7.1 Hz, OCH_2C**H**$_3$), 1.09 (3H, s, C**H**$_3$$CCH_2CO$), 0.91 (3H, s, C**H**$_3$$CCH_2CO$); δ_C (101 MHz, $CDCl_3$) 195.3 (CO), 166.8 (CO), 154.3 (C), 148.4 (C), 146.2 (C), 144.3 (C), 128.9 (CH), 123.3 (CH), 111.2 (C), 105.0 (C), 60.1 (CH_2), 50.5 (CH_2), 41.1 (CH_2), 37.2 (CH), 32.7 (C), 29.3 (CH_3), 27.0 (CH_3), 19.5 (CH_3), 14.2 (CH_3); *m/z* (NSI) Found 385.1758 ($[M+H]^+$ $C_{21}H_{25}N_2O_5$ requires 385.1756).

Isopropyl 2,7,7-trimethyl-5-oxo-4-phenyl-1,4,5,6,7,8-hexahydroquinoline-3-carboxylate 150l

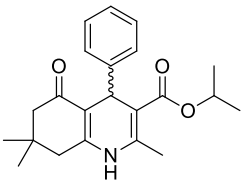

150l

Chemical Formula: $C_{22}H_{27}NO_3$
Molecular Weight: 353.45

According to general procedure **E** compound **150l** was obtained as a colourless solid (0.458 g, 73%); mp 234 - 235 °C; ν_{max} (neat) 3284 (N–H), 1694 (C=O), 1642 (OC=O), 1607 (C=C); δ_H (500 MHz, $CDCl_3$) 7.31 (2H, d, J = 6.9 Hz, Ar**H**), 7.19 (2H, t, J = 7.6 Hz, Ar**H**), 7.07 - 7.11 (1H, m, Ar**H**), 5.95 (1H, br. s., N**H**), 5.04 (1H, s, NHCCC**H**), 4.91 (1H, p, J = 6.2 Hz, OC**H**$(CH_3)_2$), 2.37 (3H, s, C**H**$_3$CNH), 2.13 - 2.35 (4H, m, NHCC**H**$_2$, COC**H**$_2$), 1.23 (3H, d, J = 6.3 Hz, OCHC**H**$_3$), 1.08 (3H, s, C**H**$_3$CCH_2CO), 1.06 (3H, d, J = 6.3 Hz, OCHC**H**$_3$), 0.94 (3H, s, C**H**$_3$CCH_2CO); δ_C (126 MHz, $CDCl_3$) 195.4 (CO), 166.9 (CO), 147.8 (C), 147.1 (C), 143.0 (C), 128.2 (CH), 127.7 (CH), 125.9 (CH), 112.2 (C), 106.6 (C), 67.0 (CH), 50.7 (CH_2), 41.2 (CH_2), 36.7 (CH), 32.7 (C), 29.4 (CH_3), 27.2 (CH_3), 22.1 (CH_3), 21.6 (CH_3), 19.4 (CH_3); *m/z* (NSI) Found 354.2064 ($[M+H]^+$ $C_{22}H_{28}NO_3$ requires 354.2063).

Isopropyl 4-(2-bromophenyl)-2,7,7-trimethyl-5-oxo-1,4,5,6,7,8-hexahydroquinoline-3-carboxylate 150m

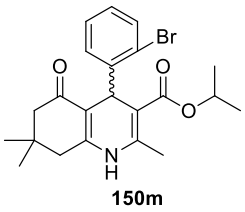

150m

Chemical Formula: $C_{22}H_{26}BrNO_3$
Molecular Weight: 432.35

According to general procedure **E** compound **150m** was obtained as a colourless solid (0.483 g, 63%); mp 215 - 216°C; ν_{max} (neat) 3275 (N–H), 1697 (C=O), 1647 (OC=O), 1602 (C=C); δ_H (500 MHz, $CDCl_3$) 7.43 (1H, dd, J = 8.0, 1.3 Hz, Ar**H**), 7.39 (1H, dd, J = 7.8, 1.7 Hz, Ar**H**), 7.15 (1H, td, J = 7.5, 1.3 Hz, Ar**H**), 6.93 (1H, td, J = 7.7, 1.7 Hz, Ar**H**), 5.73 (1H, s, N**H**), 5.33 (1H, s, NHCCC**H**), 4.95 (1H, m, OC**H**$(CH_3)_2$), 2.33 (3H, s, C**H**$_3$CNH), 2.32 - 2.09 (4H, m, CH_3CC**H**$_2$CO, NHCC**H**$_2$), 1.25 (3H, d, J = 6.2 Hz, OCH(C**H**$_3$)$_2$), 1.07 (3H, s, C**H**$_3$CCH_2CO), 1.00 (3H, d, J = 6.3 Hz, OCH(C**H**$_3$)$_2$), 0.95 (3H, s, C**H**$_3$CCH_2CO); δ_C (126 MHz, $CDCl_3$) 195.42 (CO), 167.07 (CO), 148.05 (C), 145.56 (C), 143.12 (C), 133.26 (CH), 132.69 (CH), 127.60 (CH), 126.91 (CH), 123.49 (C), 111.57 (C), 106.08 (C), 67.34 (CH), 50.82 (CH_2), 41.50 (CH_2), 38.41 (CH), 32.66 (C), 29.35 (CH_3), 27.56 (CH_3), 22.07 (CH_3), 21.66 (CH_3), 19.76 (CH_3); *m/z* (NSI) Found 432.1169 ($[M+H]^+$ $C_{22}H_{27}BrNO_3$ requires 432.1163).

Isopropyl 4-(2-bromophenyl)-2-methyl-5-oxo-1,4,5,6,7,8-hexahydroquinoline-3-carboxylate 150n

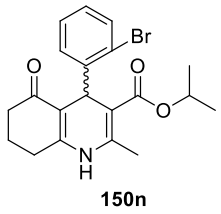

150n

Chemical Formula: $C_{20}H_{22}BrNO_3$
Molecular Weight: 404.30

According to general procedure **E** compound **150n** was obtained as a colourless solid (0.586 g, 65%); mp 246 - 247 °C; ν_{max} (neat) 3273 (N–H), 1695 (C=O), 1645 (OC=O), 1605 (C=C); δ_H (400 MHz, $CDCl_3$) 7.42 (2H, ddd, J = 13.5, 7.9, 1.5 Hz, Ar**H**), 7.16 (1H, m, Ar**H**), 6.95 (1H, m, Ar**H**), 6.21 (1H, br. s., N**H**), 5.36 (1H, s, NHCCC**H**), 4.95 (1H, m, OC**H**$(CH_3)_2$), 2.35 - 2.43 (2H, m, NCC**H**$_2$), 2.25 - 2.33 (5H, m, C**H**$_3$CNH, COC**H**$_2$), 1.84 - 2.01 (2H, m, CH2C**H**$_2$CH$_2$), 1.25 (3H, d, J = 6.3 Hz, OCHC**H**$_3$), 1.01 (3H, d, J = 6.3 Hz, OCHC**H**$_3$); δ_C (101 MHz, $CDCl_3$) 195.6 (CO), 167.0 (CO), 150.3 (C), 145.6 (C), 143.1 (C), 133.1 (CH), 132.7 (CH), 127.4 (CH), 126.8 (CH), 123.3 (C), 112.3 (C), 105.8 (C), 67.1 (CH), 38.3 (CH), 37.1 (CH_2), 27.5 (CH_2), 21.9 (CH_3), 21.5 (CH_3), 20.9 (CH_2), 19.4 (CH_3); *m/z* (NSI) Found 404.0856 ($[M+H]^+$ $C_{20}H_{23}BrNO_3$ requires 404.0864).

Isopropyl 2-methyl-5-oxo-4-phenyl-1,4,5,6,7,8-hexahydroquinoline-3-carboxylate 150o

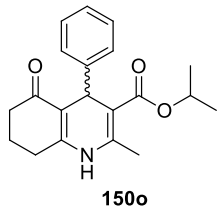

150o

Chemical Formula: $C_{20}H_{23}NO_3$
Molecular Weight: 325.40

According to general procedure **E** compound **150o** was obtained as a yellow solid (0.396 g, 55%); mp Decomposed at 245 °C; ν_{max} (neat) 3289 (N–H), 1693 (C=O), 1645 (OC=O), 1605 (C=C); δ_H (400 MHz, $CDCl_3$) 7.29 - 7.34 (2H, m, Ar**H**), 7.17 - 7.23 (2H, m, Ar**H**), 7.07 - 7.13 (1H, m, Ar**H**), 5.82 (1H, br. s., N**H**), 5.08 (1H, s, NHCCC**H**), 4.93 (1H, m, OC**H**$(CH_3)_2$), 2.40 - 2.50 (2H, m, NCC**H**$_2$), 2.39 (3H, s, C**H**$_3$CNH), 2.26 - 2.38 (2H, m, COC**H**$_2$), 1.88 - 2.04 (2H, m, CH_2C**H**$_2$CH$_2$), 1.23 (3H, d, J = 6.3 Hz, OCHC**H**$_3$), 1.04 (3H, d, J = 6.3 Hz, OCHC**H**$_3$); δ_C (101 MHz, $CDCl_3$) 195.6 (CO), 166.9 (CO), 149.4 (C), 147.2 (C), 142.9 (C), 128.2 (CH), 127.8 (CH), 125.9 (CH), 113.5 (C), 106.5 (C), 67.1 (CH), 37.0 (CH_2), 36.6 (CH), 27.5 (CH_2), 22.1 (CH), 21.6 (CH_3), 21.0 (CH_2), 19.3 (CH_3); *m/z* (NSI) Found 326.1751 ($[M+H]^+$ $C_{20}H_{24}NO_3$ requires 326.1750).

Ethyl 4-(4-chlorophenyl)-2-methyl-5-oxo-1,4,5,6,7,8-hexahydroquinoline-3-carboxylate 150p

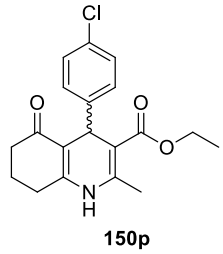

150p

Chemical Formula: $C_{19}H_{20}ClNO_3$
Molecular Weight: 345.82

According to general procedure **E** compound **150p** was obtained as a colourless solid (0.396 g, 55%); mp 226 - 228 °C; ν_{max} (neat) 3279 (N–H), 1696 (C=O), 1646 (OC=O), 1604 (C=C); δ_H (400 MHz, $CDCl_3$) 7.22 - 7.26 (2H, m, Ar**H**), 7.15 - 7.19 (2H, m, Ar**H**), 6.06 (1H, br. s., N**H**), 5.07 (1H, s, NHCCC**H**), 4.03 - 4.10 (2H, m, OC**H**$_2$CH$_3$), 2.40 - 2.46 (2H, m, NCC**H**$_2$), 2.39 (3H, s, C**H**$_3$CNH), 2.29 - 2.37 (2H, m, COC**H**$_2$), 1.86 - 2.06 (2H, m, CH$_2$C**H**$_2$CH$_2$), 1.19 (3H, t, J = 7.2 Hz, OCH$_2$C**H**$_3$); δ_C (101 MHz, $CDCl_3$) 195.6 (CO), 167.2 (CO), 149.5 (C), 145.7 (C), 143.5 (C), 131.6 (C), 129.4 (CH), 128.0 (CH), 113.2 (C), 105.7 (C), 59.9 (CH_2), 37.0 (CH_2), 36.1 (CH), 27.4 (CH_2), 21.0 (CH_2), 19.4 (CH_3), 14.2 (CH_3); *m/z* (NSI) Found 346.1204 ($[M+H]^+$ $C_{19}H_{21}ClNO_3$ requires 346.1202).

Isopropyl 4-(4-fluorophenyl)-2,7,7-trimethyl-5-oxo-1,4,5,6,7,8-hexahydroquinoline-3-carboxylate 150q

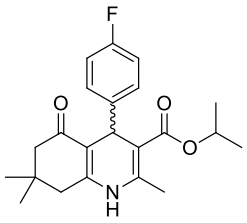

150q

Chemical Formula: $C_{22}H_{26}FNO_3$
Molecular Weight: 371.45

According to general procedure **E** compound **150q** was obtained as a colourless solid (0.399 g, 60%); mp 213 - 214 °C; ν_{max} (neat) 3283 (N–H), 1687 (C=O), 1643 (OC=O), 1606 (C=C); δ_H (400 MHz, $CDCl_3$) 7.24 - 7.30 (2H, m, Ar**H**), 6.87 (2H, t, J = 8.7 Hz, Ar**H**), 6.07 (1H, br. s, N**H**), 5.01 (1H, s, NHCCC**H**), 4.93 (1H, m, OC**H**(CH$_3$)$_2$), 2.37 (3H, s, C**H**$_3$CNH), 2.12 - 2.35 (4H, m, NCC**H**$_2$, COC**H**$_2$), 1.23 (3H, d, J = 6.3 Hz, OCHC**H**$_3$), 1.07 (3H, s, C**H**$_3$CCH$_2$CO), 1.05 (3H, d, J = 6.0 Hz, OCHC**H**$_3$), 0.93 (3H, s, C**H**$_3$CCH$_2$CO); δ_C (101 MHz, $CDCl_3$) 195.5 (CO), 166.8 (CO), 161.2 (C, d, J = 243.7 Hz), 147.8 (C), 143.1 (C), 142.9 (C, d, J = 2.7 Hz), 129.6 (CH, d, J = 8.2 Hz), 114.4 (d, J = 21.1 Hz), 112.0 (C), 106.4 (C), 67.1 (CH), 50.7 (CH_2), 41.0 (CH_2), 36.1 (CH), 32.7 (C), 29.4 (CH_3), 27.1 (CH_3), 22.1 (CH_3), 21.6 (CH_3), 19.3 (CH_3); *m/z* (NSI) Found 372.1969 ($[M+H]^+$ $C_{22}H_{27}FNO_3$ requires 372.1967).

Isopropyl 4-(4-methoxyphenyl)-2,7,7-trimethyl-5-oxo-1,4,5,6,7,8-hexahydroquinoline-3-carboxylate 150r

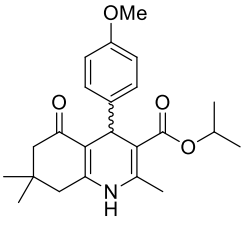

150r

Chemical Formula: $C_{23}H_{29}NO_4$
Molecular Weight: 383.48

According to general procedure **E** compound **150r** was obtained as a colourless solid (0.494 g, 72%); mp 261 - 262 °C; ν_{max} (neat) 3272 (N–H), 1697 (C=O), 1647 (OC=O), 1602 (C=C); δ_H (400 MHz, $CDCl_3$) 7.20 - 7.24 (2H, m, Ar**H**), 6.71 - 6.77 (2H, m, Ar**H**), 6.04 (1H, s, N**H**), 4.98 (1H, s, NHCCC**H**), 4.93 (1H, td, J = 6.3, 12.6 Hz, OC**H**$(CH_3)_2$), 3.74 (3H, s, OC**H**$_3$), 2.36 (3H, s, C**H**$_3$CNH), 2.10 - 2.33 (4H, m, NCC**H**$_2$, COC**H**$_2$CH$_2$), 1.23 (3H, d, J = 6.3 Hz, OCHC**H**$_3$), 1.04 - 1.11 (6H, m, OCHC**H**$_3$, C**H**$_3$CCH$_2$CO), 0.94 (3H, s, C**H**$_3$CCH$_2$CO); δ_C (101 MHz, $CDCl_3$) 195.5 (CO), 167.0 (CO), 157.7 (C), 147.8 (C), 142.7 (C), 139.7 (C), 129.1 (CH), 113.1 (CH), 112.3 (C), 106.7 (C), 67.0 (CH), 55.1 (CH), 50.7 (CH_2), 41.1 (CH_2), 35.8 (CH_3), 32.7 (C), 29.4 (CH_3), 27.2 (CH_3), 22.1 (CH_3), 21.7 (CH_3), 19.3 (CH_3); *m/z* (NSI) Found 384.2169 ($[M+H]^+$ $C_{23}H_{30}NO_4$ requires 384.2169).

5.1.6 General Procedure F:

F: Synthesis of **154a – 154o**

1-([1,1'-Biphenyl]-4-yl)ethanone 154a

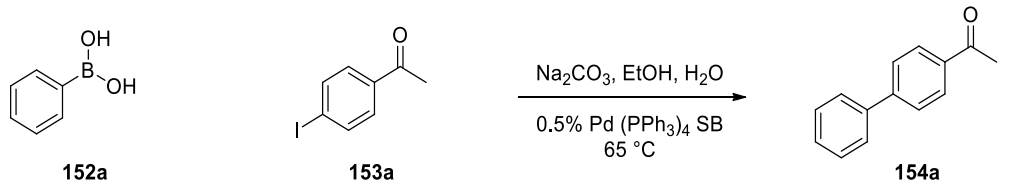

152a **153a** **154a**

Chemical Formula: $C_6H_7BO_2$ Molecular Weight: 121.93

Chemical Formula: C_8H_7IO Molecular Weight: 246.05

Chemical Formula: $C_{14}H_{12}O$ Molecular Weight: 196.24

Phenylboronic acid (0.071 g, 0.586 mmol) and 1-(4-iodophenyl)ethanone (0.131 g, 0.532 mmol) were added to a 0.5% w/w $Pd(PPh_3)_4$ stirrer bead (General Procedure D2A) and a solution of sodium carbonate (0.113 g, 1.065 mmol) in ethanol (8 mL) and water (2 mL) and the resulting mixture heated at 65 °C for 18 hours. The stirrer was washed with DCM and the combined mixture concentrated under reduced pressure. The crude mixture was partitioned between water (15 mL) and DCM (15 mL) and the aqueous phase extracted with DCM (3 × 15 mL) and the combined organic extracts dried ($MgSO_4$), filtered and solvent removed under reduced pressure to give 1-([1,1'-biphenyl]-4-yl)ethanone **154a** (0.101 g, 97%) as a colourless solid; mp 119 - 120 °C (lit 115 - 117 °C [176]); ν_{max} (neat) 3069, 2921 (C–H), 1676 (C=O); δ_H (400 MHz, $CDCl_3$) 8.04 (2H, d, J = 8.4 Hz, Ar**H**), 7.69 (2H, d, J = 8.4 Hz, Ar**H**), 7.65 – 7.62 (2H, m, Ar**H**), 7.48 (2H, t, J = 7.5 Hz, Ar**H**), 7.41 (1H, t, J = 7.4 Hz, Ar**H**), 2.64 (3H, s, COC**H**$_3$); δ_C (101 MHz, $CDCl_3$) 197.80 (CO), 145.87 (C), 139.98 (C), 135.99 (C), 129.06 (CH), 129.01 (CH), 128.34 (CH), 127.37 (CH), 127.32 (CH), 26.73 (CH_3); *m/z* (NSI) Found 197.0961 ($[M+H]^+$ $C_{14}H_{13}O$ requires 197.0960).

1-([1,1'-Biphenyl]-4-yl)ethanone 154a

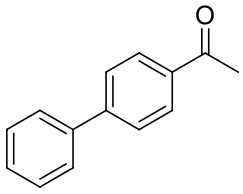

154a

Chemical Formula: $C_{14}H_{12}O$
Molecular Weight: 196.24

According to general procedure **F** compound **154a** was also obtained using 1-(4-bromophenyl)ethanone **153b** (0.105 g, 76%). Identical spectral data to that obtained previously.

1-(4'-Chloro-[1,1'-biphenyl]-4-yl)ethanone 154b

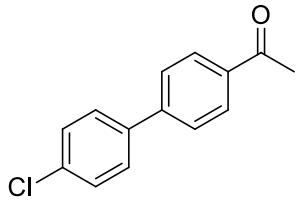

154b

Chemical Formula: $C_{14}H_{11}ClO$
Molecular Weight: 230.69

According to general procedure **F** compound **154b** was obtained as a colourless solid (0.088 g, 85%) as a colourless solid; mp 94 - 95 °C (lit 101 – 102 °C [177]); ν_{max} (neat) 2922 (C–H), 1669 (C=O); δ_H (400 MHz, $CDCl_3$) 8.01 (2H, d, J = 8.3 Hz, Ar**H**), 7.63 (2H, d, J = 8.4 Hz, Ar**H**), 7.53 (2H, d, J = 8.5 Hz, Ar**H**), 7.42 (2H, d, J = 8.5 Hz, Ar**H**), 2.62 (3H, s, COC**H**$_3$); δ_C(101 MHz, $CDCl_3$) 197.63 (CO), 144.47 (C), 138.34 (C), 136.19 (C), 134.52 (C), 129.21 (CH), 129.06 (CH), 128.55 (CH), 127.10 (CH), 26.69 (CH_3); m/z (NSI) Found 231.0571 ($[M+H]^+$ $C_{14}H_{12}ClO$ requires 231.0572).

1-(4'-Chloro-[1,1'-biphenyl]-4-yl)ethanone 154b

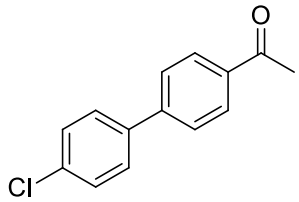

154b

Chemical Formula: $C_{14}H_{11}ClO$
Molecular Weight: 230.69

. According to general procedure **F** compound **154b** was also obtained using 1-(4-bromophenyl)ethanone **153b** (0.076 g, 47%). Identical spectral data to that obtained previously.

1-(4'-Methoxy-[1,1'-biphenyl]-4-yl)ethanone 154c

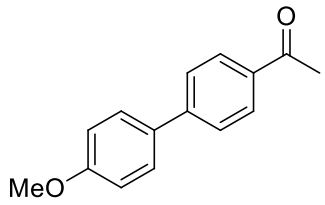

154c

Chemical Formula: $C_{15}H_{14}O_2$
Molecular Weight: 226.27

According to general procedure **F** compound **154c** was obtained as a colourless solid (0.099 g, 98%) as a colourless solid; mp 152 - 153 °C (lit 156 – 158 °C [178]); ν_{max} (neat) 2957 (C–H), 1672 (C=O),; δ_H (400 MHz, $CDCl_3$) 8.00 (2H, d, J = 8.4 Hz, Ar**H**), 7.63 (2H, d, J = 8.4 Hz, Ar**H**), 7.59 – 7.55 (2H, m, Ar**H**), 7.01 – 6.97 (2H, m, Ar**H**), 3.85 (3H, s, OC**H**$_3$), 2.62 (3H, s, COC**H**$_3$); δ_C (101 MHz, $CDCl_3$) 197.74 (CO), 160.03 (C), 145.41 (C), 135.38 (C), 132.29 (C), 129.01 (CH), 128.42 (CH), 126.65 (CH), 114.51 (CH), 55.43 (CH_3), 26.64 (CH_3); *m/z* (NSI) Found 227.1067 ($[M+H]^+$ $C_{15}H_{15}O_2$ requires 227.1068).

1-(3'-Methoxy-[1,1'-biphenyl]-4-yl)ethanone 154d

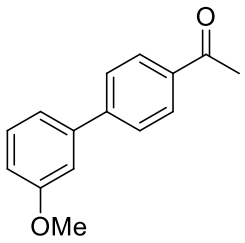

154d

Chemical Formula: $C_{15}H_{14}O_2$
Molecular Weight: 226.27

According to general procedure **F** compound **154d** was obtained as a colourless solid (0.094 g, 93%) as a colourless solid; mp 52 - 53 °C (lit 51 – 52 °C [179]); ν_{max} (neat) 2996 (C–H), 1673 (C=O),; δ_H (500 MHz, $CDCl_3$) 8.03 – 8.00 (2H, m, Ar**H**), 7.68 – 7.65 (2H, m, Ar**H**), 7.38 (1H, t, J = 7.9 Hz, Ar**H**), 7.21 (1H, d, J = 7.7 Hz, Ar**H**), 7.17 – 7.14 (1H, m, Ar**H**), 6.97 – 6.92 (1H, m, Ar**H**), 3.87 (3H, s, OC**H**$_3$), 2.63 (3H, s, COC**H**$_3$); δ_C (126 MHz, $CDCl_3$) 197.76 (CO), 160.16 (C), 145.69 (C), 141.43 (C), 136.08 (C), 130.06 (CH), 128.95 (CH), 127.33 (CH), 119.81 (CH), 113.63 (CH), 113.17 (CH), 55.41 (CH_3), 26.69 (CH_3); *m/z* (NSI) Found 227.1067 ($[M+H]^+$ $C_{15}H_{15}O_2$ requires 227.106).

1-(3'-Methoxy-[1,1'-biphenyl]-4-yl)ethanone 154d

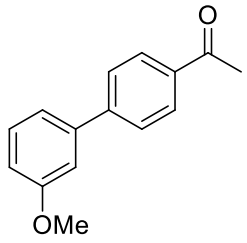

154d

Chemical Formula: $C_{15}H_{14}O_2$
Molecular Weight: 226.27

According to general procedure **F** compound **154d** was also made using 1-(4-bromophenyl)ethanone **153b** (0.11 g, 69%). Identical spectral data to that obtained previously.

1-(4'-(Trifluoromethyl)-[1,1'-biphenyl]-4-yl)ethanone 154e

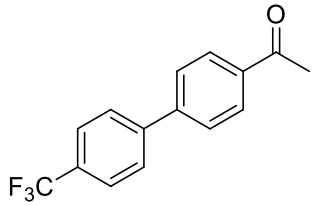

154e

Chemical Formula: $C_{15}H_{11}F_3O$
Molecular Weight: 264.24

According to general procedure **F** compound **154e** was obtained as a colourless solid (0.113 g, 96%) as a colourless solid; mp 119 - 120 °C (lit 118 – 119 °C [180]); ν_{max} (neat) 2924 (C–H), 1683 (C=O),; δ_H (500 MHz, $CDCl_3$) 8.06 (2H, d, J = 8.3 Hz, Ar**H**), 7.72 (4H, s, Ar**H**), 7.69 (2H, d, J = 8.3 Hz, Ar**H**), 2.65 (3H, s, COC**H**$_3$); δ_C (101 MHz, $CDCl_3$) 197.72 (CO), 163.09 (C, d, J = 248.1 Hz), 144.78 (C), 136.07 (C, d, J = 3.1 Hz), 135.95 (C), 129.05 (CH), 128.96 (CH), 127.13 (CH), 115.99 (CH, d, J = 21.4 Hz), 26.68 (CH_3); *m/z* (NSI) Found 265.0840 ($[M+H]^+$ $C_{15}H_{12}F_3O$ requires 265.0845).

1-(4'-(Trifluoromethyl)-[1,1'-biphenyl]-4-yl)ethanone 154e

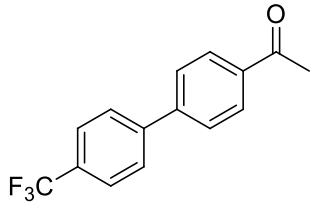

154e

Chemical Formula: $C_{15}H_{11}F_3O$
Molecular Weight: 264.24

According to general procedure **F** compound **154e** was also made using 1-(4-bromophenyl)ethanone **153b** (0.109 g, 58%). Identical spectral data to that obtained previously.

1-(2'-Methoxy-[1,1'-biphenyl]-4-yl)ethanone 154f

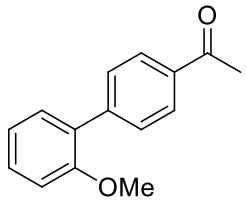

154f

Chemical Formula: $C_{15}H_{14}O_2$
Molecular Weight: 226.27

According to general procedure **F** compound **154f** was obtained as a colourless solid (0.061 g, 60%) as a colourless solid; mp 107 - 108 °C (lit 105 – 106 °C [181]); ν_{max} (neat) 3000 (C–H), 1669 (C=O); δ_H (400 MHz, $CDCl_3$) 8.01 (2H, d, J = 8.3 Hz, Ar**H**), 7.65 (2H, d, J = 8.3 Hz, Ar**H**), 7.40 – 7.32 (2H, m, Ar**H**), 7.06 (1H, t, J = 7.5 Hz, Ar**H**), 7.02 (1H, d, J = 8.2 Hz, Ar**H**), 3.83 (3H, s, OC**H**$_3$), 2.64 (3H, s, COC**H**$_3$); δ_C (101 MHz, $CDCl_3$) 197.90 (CO), 156.58 (C), 143.69 (C), 135.61 (C), 130.79 (CH), 129.81 (CH), 129.58 (CH), 128.15 (CH), 121.06 (CH), 111.48 (CH), 55.64 (CH_3), 26.69 (CH_3); *m/z* (NSI) Found 227.1067 ($[M+H]^+$ $C_{15}H_{15}O_2$ requires 227.1067).

1-(4'-Fluoro-[1,1'-biphenyl]-4-yl)ethanone 154g

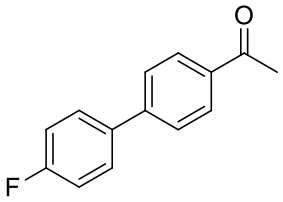

154g

Chemical Formula: $C_{14}H_{11}FO$
Molecular Weight: 214.23

According to general procedure **F** compound **154g** was obtained as a colourless solid (0.061 g, 60%) as a colourless solid; mp 100 - 101 °C (lit 103 – 104 °C [182]); ν_{max} (neat) 2921 (C–H), 1679 (C=O),; δ_H (500 MHz, $CDCl_3$) 8.02 (2H, d, J = 8.3 Hz, Ar**H**), 7.62 (2H, d, J = 8.5 Hz, Ar**H**), 7.60 – 7.56 (2H, m, Ar**H**), 7.18 – 7.12 (2H, m, Ar**H**), 2.63 (3H, s, COC**H**$_3$); δ_C (101 MHz, $CDCl_3$) 197.65 (CO), 163.01 (C, d, J = 248.1 Hz), 144.7 (C), 135.99 (C, d, J = 3.2), 135.87 (C), 128.97 (CH), 128.88 (CH), 127.05 (CH), 115.91 (CH, d, J = 21.5 Hz), 26.60 (CH_3); *m/z* (NSI) Found 215.0872 ($[M+H]^+$ $C_{14}H_{12}FO$ requires 215.0800).

1-(4'-Fluoro-[1,1'-biphenyl]-4-yl)ethanone 154g

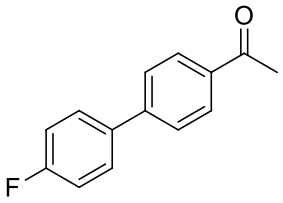

154g
Chemical Formula: $C_{14}H_{11}FO$
Molecular Weight: 214.23

According to general procedure **F** compound **154g** was also made using 1-(4-bromophenyl)ethanone **153b** (0.085 g, 56%). Identical spectral data to that obtained previously.

1-(4'-Nitro-[1,1'-biphenyl]-4-yl)ethanone 154h

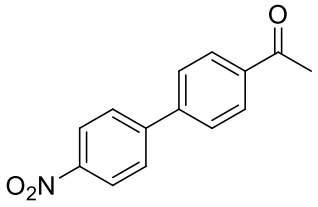

154h
Chemical Formula: $C_{14}H_{11}NO_3$
Molecular Weight: 241.24

According to general procedure **F** compound **154h** was obtained as a colourless solid (0.104 g, 94%) as a colourless solid; mp 151 - 152 °C (lit. 150.2 – 152.1 °C [183]); ν_{max} (neat) 3012 (C–H), 1679 (C=O), 1595 (NO_2); δ_H (400 MHz, $CDCl_3$) 8.31 (2H, d, J = 8.6 Hz, Ar**H**), 8.07 (2H, d, J = 8.2 Hz, Ar**H**), 7.77 (2H, d, J = 8.6 Hz, Ar**H**), 7.71 (2H, d, J = 8.2 Hz, Ar**H**), 2.65 (3H, s, COC**H**$_3$); δ_C (101 MHz, $CDCl_3$) 197.50 (CO), 147.74 (C), 146.30 (C), 143.18 (C), 137.21 (C), 129.22 (CH), 128.18 (CH), 127.72 (CH), 124.30 (CH), 26.79 (CH_3); *m/z* (NSI) Found 242.0817 ($[M+H]^+$ $C_{14}H_{12}NO_3$ requires 242.0817).

4-Methoxy-1,1'-biphenyl 154i

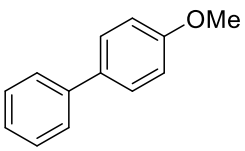

154i
Chemical Formula: $C_{13}H_{12}O$
Molecular Weight: 184.24

According to general procedure **F** and using 1-iodo-4-methoxybenzene **153c** compound **150i** was obtained as a colourless solid (0.078 g, 99%) as a colourless solid; mp 86 - 87 °C (lit. 88 – 89 °C [184]); ν_{max} (neat) 3064 (C–H), 1246 (O–C); δ_H (400 MHz, $CDCl_3$) 7.62 – 7.55 (4H, m, Ar**H**), 7.46 (2H, dd, J = 10.5, 4.8 Hz, Ar**H**), 7.37 – 7.31 (1H, m, Ar**H**), 7.05 – 6.98 (2H, m, Ar**H**), 3.88 (3H, s, OC**H**$_3$); δ_C (101 MHz, $CDCl_3$) 159.30 (C), 140.97 (C), 133.92 (C),

128.85 (CH), 128.27 (CH), 126.86 (CH), 126.78 (CH), 114.35 (CH), 55.45 (CH_3); *m/z* (NSI) Found 185.0966 ($[M+H]^+$ $C_{13}H_{13}O$ requires 185.0958).

4-Chloro-4'-methoxy-1,1'-biphenyl 154j

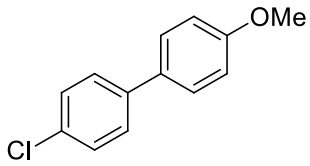

154j

Chemical Formula: $C_{13}H_{11}ClO$
Molecular Weight: 218.68

According to general procedure **F** and using 1-iodo-4-methoxybenzene **153c** compound **154j** was obtained as a colourless solid (0.088 g, 94%) as a colourless solid; mp 108 - 110 °C (lit 109 – 111 °C [185]); ν_{max} (neat) 3010 (C–H), 1287 (O–C); δ_H (400 MHz, $CDCl_3$) 7.53 – 7.46 (4H, m, Ar**H**), 7.42 – 7.37 (2H, m, Ar**H**), 7.01 – 6.96 (2H, m, Ar**H**), 3.86 (3H, s, OC**H**$_3$); δ_C (101 MHz, $CDCl_3$) 159.52 (C), 139.39 (C), 132.80 (C), 132.60 (C), 1128.96 (CH), 128.12 (CH), 128.04 (CH), 114.45 (CH), 55.45 (CH_3); *m/z* (NSI) Found 218.0498 ($[M]^+$ $C_{13}H_{11}OCl$ requires 218.0497).

3,4'-Dimethoxy-1,1'-biphenyl 154k

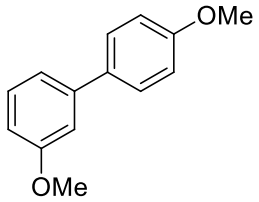

154k

Chemical Formula: $C_{14}H_{14}O_2$
Molecular Weight: 214.26

According to general procedure **F** and using 1-iodo-4-methoxybenzene **153c** compound **154k** was obtained as a colourless solid (0.080 g, 87%) as a colourless solid; mp 56 - 58 °C (lit 59 °C [186]); ν_{max} (neat) 3010 (C–H), 1217 (O–C); δ_H (400 MHz, $CDCl_3$) 7.60 – 7.54 (2H, m, Ar**H**), 7.37 (1H, t, J = 7.9 Hz, Ar**H**), 7.19 (1H, dt, J = 7.7, 1.3 Hz, Ar**H**), 7.14 (1H, t, J = 2.1 Hz, Ar**H**), 7.04 – 6.98 (2H, m, Ar**H**), 6.90 (1H, dd, J = 8.1, 2.5 Hz, Ar**H**), 3.89 (3H, s, OC**H**$_3$), 3.87 (3H, s, OC**H**$_3$); δ_C (101 MHz, $CDCl_3$) 160.08 (C), 159.39 (C), 142.47 (C), 133.72 (C), 129.81 (CH), 128.29 (CH), 119.39 (CH), 114.29 (CH), 112.66 (CH), 112.14 (CH), 55.41 (CH_3), 55.35 (CH_3); *m/z* (NSI) Found 215.1072 ($[M+H]^+$ $C_{14}H_{15}O_2$ requires 215.1070).

4-Methoxy-4'-nitro-1,1'-biphenyl 154l

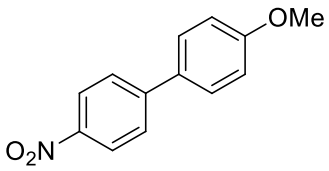

154k
Chemical Formula: $C_{13}H_{11}NO_3$
Molecular Weight: 229.23

According to general procedure **F** and using 1-iodo-4-methoxybenzene **153c** compound **154l** was obtained as a yellow solid (0.030 g, 30%); mp 108 - 109 °C (lit 104 – 105 °C [187]); ν_{max} (neat) 3062 (C–H), 1595 (NO_2); δ_H (400 MHz, $CDCl_3$) 8.29 – 8.24 (2H, m, Ar**H**), 7.72 – 7.66 (2H, m, Ar**H**), 7.61 – 7.55 (2H, m, Ar**H**), 7.04 – 6.99 (2H, m, Ar**H**), 3.88 (3H, s, OC**H**$_3$); δ_C (101 MHz, $CDCl_3$) 160.62 (C), 147.35 (C), 146.72 (C), 131.23 (C), 128.70 (CH), 127.21 (CH), 124.27 (CH), 114.77 (CH), 55.57 (CH_3); *m/z* (NSI) Found 230.0812 ($[M+H]^+$ $C_{13}H_{12}NO_3$ requires 230.0805).

4-Methoxy-4'-nitro-1,1'-biphenyl 154l

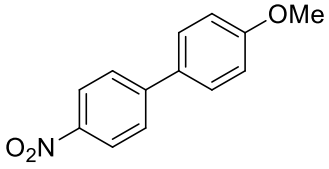

154k
Chemical Formula: $C_{13}H_{11}NO_3$
Molecular Weight: 229.23

According to general procedure **G** and using 1-iodo-4-nitrobenzene **153d** compound **154l** was also obtained as a yellow solid (0.081 g, 83%). Identical spectral data to that obtained previously.

4-Nitro-1,1'-biphenyl 154m

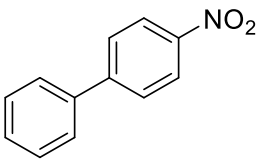

154m
Chemical Formula: $C_{12}H_9NO_2$
Molecular Weight: 199.21

According to general procedure **F** and using 1-iodo-4-nitrobenzene **153d** compound **154m** was obtained as a colourless solid (0.058 g, 73%) as a colourless solid; mp 110 - 112 °C (lit 110 – 111 °C [188]); ν_{max} (neat) 3074 (C–H), 1592 (NO_2); δ_H (400 MHz, $CDCl_3$) 8.32 – 8.26 (2H, m, Ar**H**), 7.77 – 7.70 (2H, m, Ar**H**), 7.66 – 7.60 (2H, m, Ar**H**), 7.54 – 7.42 (3H, m, OC**H**$_3$); δ_C (101 MHz, $CDCl_3$) 147.73 (C), 147.23 (C), 138.88 (C), 129.27 (CH), 129.04 (CH), 127.90 (CH), 127.49 (CH), 124.20 (CH); *m/z* (NSI) Found 200.0712 ($[M+H]^+$ $C_{12}H_{10}NO_2$ requires 200.0715).

4-Fluoro-4'-nitro-1,1'-biphenyl 154n

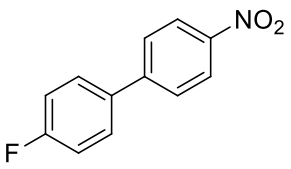

154n

Chemical Formula: $C_{12}H_8FNO_2$
Molecular Weight: 217.20

According to general procedure **F** and using 1-iodo-4-nitrobenzene **153d** compound **154n** was obtained as a colourless solid (0.070 g, 81%) as a colourless solid; mp 125 - 126 °C (lit 122 – 124 °C [189]); ν_{max} (neat) 3074 (C–H), 1592 (NO_2); δ_H (400 MHz, $CDCl_3$) 8.32 – 8.26 (2H, m, Ar**H**), 7.72 – 7.66 (2H, m, Ar**H**), 7.63 – 7.56 (2H, m, Ar**H**), 7.22 – 7.15 (2H, m, Ar**H**); δ_C (101 MHz, $CDCl_3$) 147.73 (C), 147.23 (C), 138.88 (C), 129.27 (CH), 129.04 (CH), 127.90 (CH), 127.49 (CH), 124.20 (CH); *m/z* (NSI) Found 218.0617 ($[M+H]^+$ $C_{12}H_9FNO_2$ requires 218.0623).

5.1.7 General Procedure G:

G: Synthesis of **156a – 156d**

3-Phenylpyridine 156a

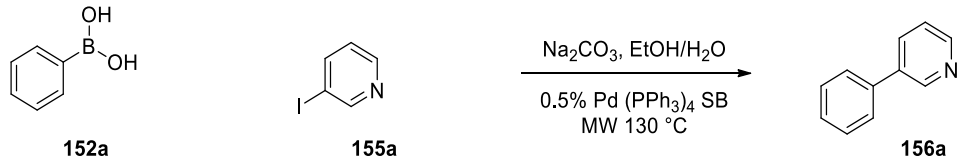

152a **155a** **156a**

Chemical Formula: $C_6H_7BO_2$
Molecular Weight: 121.93

Chemical Formula: C_5H_4IN
Molecular Weight: 205.00

Chemical Formula: $C_{11}H_{9N}$
Molecular Weight: 155.20

Phenylboronic acid (0.065 g, 0.537 mmol) and 3-iodopyridine (0.1 g, 0.488 mmol) were taken in a reaction vial containing a 0.5% w/w $Pd(PPH_3)_4$ stirrer bead (General Procedure D2A) adapted for microwave reactions. Ethanol (2 mL) was added to it and lastly a solution of sodium carbonate (0.103 g, 0.976 mmol) in water (1 mL). The resulting mixture was heated at 130 °C for 20 minutes in the microwave. The stirrer was washed with DCM and the residue was concentrated under reduced pressure. The crude mixture was partitioned between water (15 mL) and DCM (15 mL) and the aqueous phase extracted with DCM (3 x 15 mL). The combined organic extracts dried ($MgSO_4$), filtered and solvent removed under reduced pressure to give the crude material. The residue was purified *via* automated flash chromatography (9:1 Hex/EtOAc; Zip 10 g column) to give 3-phenylpyridine **156a** (0.052 g, 69 %) as a colourless oil; ν_{max} (neat) 3030 (C–H), 1336 (C–N); δ_H (500 MHz, $CDCl_3$) 8.85 (1H, d, J = 2.3 Hz, NC**H**), 8.59 (1H, dd, J = 4.8, 1.6 Hz, NC**H**), 7.87 (1H, dt, J = 7.9, 2.0 Hz, Ar**H**), 7.60 - 7.55 (2H, m, Ar**H**), 7.48 (2H, dd, J = 8.4, 6.9 Hz, Ar**H**), 7.43 - 7.38 (1H, m, Ar**H**), 7.36 (1H, dd, J = 7.9, 4.8 Hz, Ar**H**); δ_C (126 MHz, $CDCl_3$) 148.57 (CH), 148.43 (CH), 137.92 (C), 136.71 (C), 134.43 (CH), 129.16 (CH), 128.18 (CH), 127.24 (CH), 123.63 (CH); *m/z* (NSI) Found 156.0808 ($[M+H]^+$ $C_{11}H_{10}N$ requires 156.0811).

3-Phenylpyridine 156a

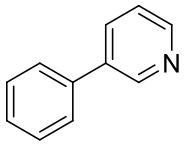

156a

Chemical Formula: $C_{11}H_9N$
Molecular Weight: 155.20

According to general procedure **G** compound **156a** was also obtained using 3-bromopyridine **155b** in 120 minutes (0.32 g, 33%). Identical spectroscopic data to that obtained previously.

3-(4-Methoxyphenyl)pyridine 156b

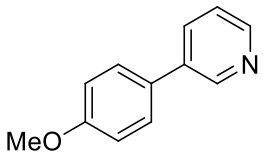

156b

Chemical Formula: $C_{12}H_{11}NO$
Molecular Weight: 185.22

According to general procedure **G** compound **156b** was obtained in 20 minutes as a colourless semi-solid (0.062 g, 69%); ν_{max} (neat) 3008 (C–H), 1281 (C–N); δ_H (500 MHz, $CDCl_3$) 8.81 (1H, d, J = 2.5 Hz, NC**H**), 8.54 (1H, dd, J = 4.8, 1.7 Hz, NC**H**), 7.81 (1H, dt, J = 7.9, 2.0 Hz, Ar**H**), 7.56 - 7.45 (2H, m, Ar**H**), 7.32 (1H, dd, J = 7.9, 4.8 Hz, Ar**H**), 7.04 - 6.95 (2H, m, Ar**H**), 3.85 (3H, s, OC**H**$_3$); δ_C (126 MHz, $CDCl_3$) 159.83 (C), 148.07 (CH), 147.96 (CH), 136.31 (C), 133.91 (CH), 130.31 (C), 128.29 (CH), 123.58 (CH), 114.62 (CH), 55.45 (CH_3); *m/z* (NSI) Found 186.0913 ($[M+H]^+$ $C_{12}H_{12}NO$ requires 186.0910).

3-(4-Fluorophenyl)pyridine 156c

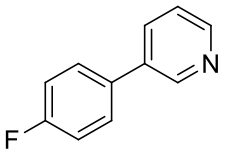

156c

Chemical Formula: $C_{11}H_8FN$
Molecular Weight: 173.19

According to general procedure **G** compound **156c** was obtained in 20 minutes as a colourless oil (0.062 g, 73%); ν_{max} (neat) 3043 (C–H), 1336 (C–N); δ_H (500 MHz, $CDCl_3$) 8.80 (1H, d, J 2.3, NC**H**), 8.58 (1H, dd, J = 4.8, 1.6 Hz, NC**H**), 7.82 (1H, dt, J = 7.9, 2.0 Hz, Ar**H**), 7.57 - 7.49 (2H, m, Ar**H**), 7.35 (1H, dd, J = 8.0 Hz, 4.9, Ar**H**), 7.16 (2H, t, J = 8.6 Hz, Ar**H**); δ_C (126 MHz, $CDCl_3$) 163.01 (C, d, J = 247.7 Hz), 148.43 (CH, d, J = 43.9 Hz), 135.82 (C), 134.33 (CH), 134.04 (C, d, J = 3.3 Hz), 128.92 (CH, d, J = 8.2 Hz), 123.68 (CH), 116.26 (CH), 116.09 (CH); *m/z* (NSI) Found 174.0714 ($[M+H]^+$ $C_{11}H_9FN$ requires 174.0710);

3-(3-Methoxyphenyl)pyridine 156d

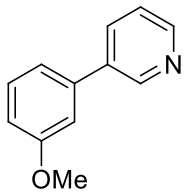

156d

Chemical Formula: $C_{12}H_{11}NO$
Molecular Weight: 185.22

According to general procedure **G** compound **156d** was obtained in 20 minutes as a colourless oil (0.070 g, 77%); ν_{max} (neat) 3031 (C–H), 1299 (C–N); δ_H (500 MHz, $CDCl_3$) 8.84 (1H, d, J = 2.3 , NC**H**), 8.59 (1H, dd, J = 4.9, 1.6 Hz, NC**H**), 7.88 - 7.78 (1H, m, Ar**H**), 7.39 (1H, t, J = 8.0 Hz, Ar**H**), 7.35 (1H, dd, J = 7.9, 4.8 Hz, Ar**H**), 7.16 (1H, dt, J = 7.6, 1.2 Hz, Ar**H**), 7.10 (1H, t, J = 2.1 Hz, Ar**H**), 6.94 (1H, dd, J = 8.2, 2.5 Hz, Ar**H**), 3.86 (3H, s, OC**H**$_3$); δ_C (126 MHz, $CDCl_3$) 160.20 (C), 148.69 (CH), 148.44 (CH), 139.37 (C), 136.59 (C), 134.48 (CH), 130.22 (CH), 123.61 (CH), 119.66 (CH), 113.47 (CH), 113.02 (CH), 55.42 (CH_3); *m/z* (NSI) Found 186.0913 ($[M+H]^+$ $C_{12}H_{12}NO$ requires 186.0909).

1-([1,1'-Biphenyl]-4-yl)ethanone 154a

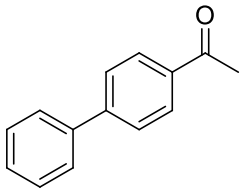

154a

Chemical Formula: $C_{14}H_{12}O$
Molecular Weight: 196.24

According to general procedure **G** compound **154a** was also obtained using 1-(4-bromophenyl)ethanone **153b** by heating in a microwave at 120 °C for 30 minutes (0.80 g, 99%). Identical spectroscopic data to that obtained previously.

1-(4'-Chloro-[1,1'-biphenyl]-4-yl)ethanone 154b

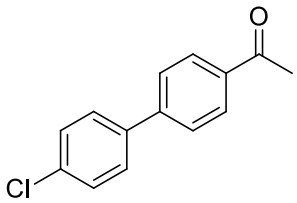

154b

Chemical Formula: $C_{14}H_{11}ClO$
Molecular Weight: 230.69

According to general procedure **G** compound **154b** was also obtained using 1-(4-bromophenyl)ethanone **153b** by heating in a microwave at 120 °C for 60 minutes (0.112 g, 97%). Identical spectroscopic data to that obtained previously.

1-(4'-Fluoro-[1,1'-biphenyl]-4-yl)ethanone 154g

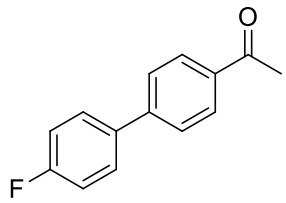

154g

Chemical Formula: $C_{14}H_{11}FO$
Molecular Weight: 214.23

According to general procedure **G** compound **154g** was also obtained using 1-(4-bromophenyl)ethanone **153b** by heating in a microwave at 120 °C for 60 minutes (0.100 g, 93%). Identical spectroscopic data to that obtained previously.

4-Methoxy-4'-nitro-1,1'-biphenyl 154l

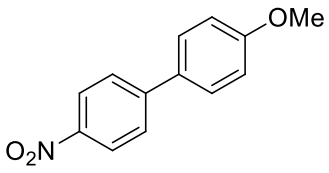

154k

Chemical Formula: $C_{13}H_{11}NO_3$
Molecular Weight: 229.23

According to general procedure **G** compound **154l** was also obtained using 1-iodo-4-methoxybenzene **153c** by heating in the microwave at 120 °C for 40 minutes (0.081 g, 83%) as a yellow solid. Identical spectroscopic data to that obtained previously.

5.1.8 General Procedure H:

H: Synthesis of **178a – 178i**

2-Phenyl-1,3-dithiane 178a

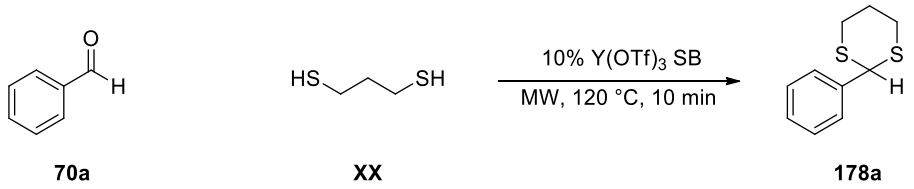

70a **XX** **178a**

Chemical Formula: $C_{10}H_{12}S_2$
Molecular Weight: 196.33

A solution of benzaldehyde (0.481 ml, 4.71 mmol) and propane-1,3-dithiol (0.567 ml, 5.65 mmol) in acetonitrile (4.34 mL) was prepared. The solution was heated in a microwave reactor at 120 °C for 10 min with a 10% $Y(OTf)_3$ stirrer bead (General Procedure D2B). The reaction was monitored *via* TLC. After completion, the solution was concentrated under reduced pressure. The residue was taken up in DCM (20 mL). This was washed with a solution of 0.1M NaOH (20 mL) and dried over Na_2SO_4, filtered and concentrated under reduced pressure to give 2-phenyl-1,3-dithiane **178a** as a colourless solid (0.843 g, 91%); mp 72 - 73 °C (lit 72 – 74 °C [190]); ν_{max} (neat) 2947, 2890 (C–H); δ_H (500 MHz, $CDCl_3$) 7.47 (2H, dd, J = 7.3, 1.7 Hz, Ar**H**), 7.37 - 7.27 (3H, m, Ar**H**), 5.17 (1H, s, SC**H**S), 3.07 (2H, ddd, J = 14.8, 12.5, 2.4 Hz, SC**H**$_2$CH$_2$CH$_2$S), 2.91 (2H, dt, J = 14.2, 3.9 Hz, SCH$_2$CH$_2$C**H**$_2$S), 2.17 (1H, dtt, J = 14.0, 4.6, 2.4 Hz, 1 × SCH$_2$C**H**$_2$CH$_2$S), 2.01 - 1.87 (1H, m, 1 × SCH$_2$C**H**$_2$CH$_2$S); δ_C (126 MHz, $CDCl_3$) 139.22 (C), 128.86 (CH), 128.57 (CH), 127.87 (CH), 51.61 (CH), 32.23 (CH_2), 25.23 (CH_2); *m/z* (NSI) Found 197.0459 ($[M+H]^+$ $C_{10}H_{13}S_2$ requires 197.0459).

2-(4-Bromophenyl)-2-methyl-1,3-dithiane 178b

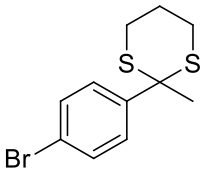

178b

Chemical Formula: $C_{11}H_{13}BrS_2$
Molecular Weight: 289.25

According to general procedure **H** compound **178b** was obtained using 1-(4-bromophenyl)ethanone **70b** after heating in the microwave at 120 °C for 90 minutes as a colourless solid (0.262 g, 36%); mp 84 - 85 °C; ν_{max} (neat) 2963, 2897 (C–H); δ_H (500 MHz, $CDCl_3$) 7.86 - 7.80 (2H, m, Ar**H**), 7.51 - 7.46 (2H, m, Ar**H**), 2.77 - 2.62 (4H, m, SC**H**$_2$CH$_2$C**H**$_2$S), 1.94 (2H, m, SCH$_2$C**H**$_2$CH$_2$S), 1.75 (3H, s, SCC**H**$_3$S); δ_C (126 MHz, $CDCl_3$) 143.27 (C), 131.77 (CH), 129.98 (CH), 121.33 (C), 53.71 (C), 32.99 (CH_3), 28.19 (CH_2), 24.64 (CH_2); *m/z* (NSI) Found 288.9712 ($[M+H]^+$ $C_{11}H_{14}BrS_2$ requires 288.9720).

2-(4-Fluorophenyl)-1,3-dithiane 178c

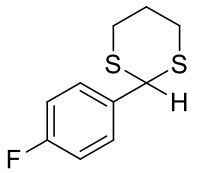

178c

Chemical Formula: $C_{10}H_{11}FS_2$
Molecular Weight: 214.32

According to general procedure **H** compound **178c** was obtained after heating in the microwave at 100 °C for 10 minutes as a colourless solid (0.860 g, 99%); mp 100 - 103 °C (lit. 102 – 104 °C [191]); ν_{max} (neat) 3051, 2903 (C–H), 1220 (C–F); δ_H (500 MHz, $CDCl_3$) 7.44 (2H, dd, J = 8.6, 5.4 Hz, Ar**H**), 7.02 (2H, t, J = 8.6 Hz, Ar**H**), 5.14 (1H, s, SC**H**S), 3.05 (2H, ddd, J 14.7, 12.5, 2.4, 1 × CH$_2$C**H**$_2$CH$_2$, 1 × SC**H**$_2$), 2.90 (2H, m, 1 × CH$_2$C**H**$_2$CH$_2$, 1 × SC**H**$_2$), 2.16 (1H, ddt, J 11.5, 4.4, 2.3, 1 × SC**H**$_2$), 1.97 - 1.89 (1H, m, 1 × SC**H**$_2$); δ_C (126 MHz, $CDCl_3$) 162.61 (C, d, J = 247.3 Hz), 135.11 (C, d, J = 3.6 Hz), 129.63 (CH, d, J = 8.3 Hz), 115.75 (CH, d, J = 22.0 Hz), 50.58 (CH), 32.17 (CH_2), 25.07 (CH_2); *m/z* (NSI) Found 215.0364 ($[M+H]^+$ $C_{10}H_{12}FS_2$ requires 215.0367).

2-(4-Methoxyphenyl)-1,3-dithiane 178d

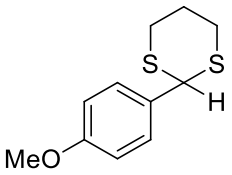

178d

Chemical Formula: $C_{11}H_{14}OS_2$
Molecular Weight: 226.36

According to general procedure **H** compound **178d** was obtained after heating in the microwave at 80 °C for 30 minutes as a colourless solid (0.835 g, 99%); mp 116 - 117 °C (lit 118 – 120 °C [190]); ν_{max} (neat) 3005, 2901 (C–H), 1246 (C–O); δ_H (500 MHz, $CDCl_3$) 7.40 (2H, d, J = 8.6 Hz, Ar**H**), 6.86 (2H, d, J = 8.7 Hz, Ar**H**), 5.13 (1H, s, SC**H**S), 3.78 (3H, s, OC**H**$_3$), 3.04 (2H, ddd, J = 14.8, 12.5, 2.5 Hz, SC**H**$_2$CH$_2$CH$_2$S), 2.88 (2H, ddd, J = 14.3, 4.3, 2.9 Hz, SCH$_2$CH$_2$C**H**$_2$S), 2.21 - 2.09 (1H, m, 1 × SCH$_2$C**H**$_2$CH$_2$S), 1.98 - 1.84 (1H, m, 1 × SCH$_2$C**H**$_2$CH$_2$S); δ_C (126 MHz, $CDCl_3$) 159.60 (C), 131.36 (C), 128.98 (CH), 114.13 (CH), 55.35 (CH_3), 50.78 (CH), 32.24 (CH_2), 25.12 (CH_2); *m/z* (NSI) Found 227.0564 ($[M+H]^+$ $C_{11}H_{15}OS_2$ requires 227.0568).

2-Phenyl-1,3-dithiolane 178e

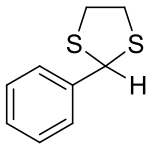

178e

Chemical Formula: C_{9H10S2}
Molecular Weight: 182.31

According to general procedure **H** compound **178e** was obtained after heating in the microwave at 120 °C for 60 minutes as a colourless oil (0.606 g, 93%); δ_H (400 MHz, $CDCl_3$) 7.56 - 7.50 (2H, m, Ar**H**), 7.36 - 7.26 (3H, m, Ar**H**), 5.65 (1H, s, SC**H**S), 3.55 - 3.47 (2H, m, SC**H**$_2$CH$_2$S), 3.41 - 3.32 (2H, m, SCH$_2$C**H**$_2$S); *m/z* (NSI) Found 181.0146 ($[M-H]^-$ $C_9H_9S_2$ requires 181.0150).

2-(2-Bromophenyl)-1,3-dithiolane 178f

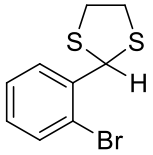

178f

Chemical Formula: $C_{9H9Br}S_2$
Molecular Weight: 261.20

According to general procedure **H** compound **178f** was obtained after heating in the microwave at 120 °C for 20 minutes as a colourless oil (0.89 g, 99%); ν_{max} (neat) 3055, 2919 (C–H); δ_H (400 MHz, $CDCl_3$) 7.85 (1H, dd, J = 7.9, 1.7 Hz, Ar**H**), 7.53 (1H, dd, J = 7.9, 1.2 Hz, Ar**H**), 7.31 (1H, td, J = 7.6, 1.3 Hz, Ar**H**), 7.11 (1H, td, J = 7.6, 1.7 Hz, Ar**H**), 6.06 (1H, s, SC**H**S), 3.50 - 3.42 (2H, m, SC**H**$_2$CH$_2$S), 3.42 - 3.33 (2H, m, SCH$_2$C**H**$_2$S); δ_C (101 MHz, $CDCl_3$) 140.46 (C), 132.92 (CH), 129.54 (CH), 129.29 (CH), 127.86 (CH), 124.10 (C), 55.17 (CH), 39.90 (CH_2); *m/z* (NSI) Found 260.9402 ($[M+H]^+$ $C_9H_{10}BrS_2$ requires 260.9407).

2-(2-Bromophenyl)-1,3-dithiolane 178f

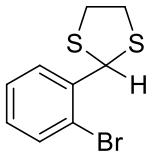

178f

Chemical Formula: $C_{9H9Br}S_2$
Molecular Weight: 261.20

According to general procedure **H** compound **178e** was also obtained after heating in the microwave at 80 °C for 10 minutes as a colourless oil (0.677 g, 76%). Identical spectroscopic data to that obtained previously.

2-(4-Fluorophenyl)-1,3-dithiolane 178g

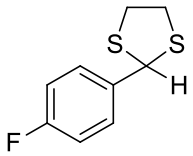

178g

Chemical Formula: $C_9H_9FS_2$
Molecular Weight: 200.30

According to general procedure **H** compound **178g** was obtained after heating in the microwave at 100 °C for 50 minutes as a colourless oil (0.606 g, 94%); ν_{max} (neat) 3067, 2923 (C–H), 1220 (C–F); δ_H (400 MHz, $CDCl_3$) 7.55 - 7.44 (2H, m, Ar**H**), 7.04 - 6.95 (2H, m, Ar**H**), 5.62 (1H, s, SC**H**S), 3.55 - 3.45 (2H, m, SC**H**$_2$CH$_2$S), 3.40 - 3.31 (2H, m, SCH$_2$C**H**$_2$S); δ_C (126 MHz, $CDCl_3$) 162.51 (C, d, J = 247.0 Hz), 136.08 (C, d, J = 2.8 Hz), 129.81 (CH, d, J = 8.3 Hz), 115.49 (CH, d, J = 21.6 Hz), 55.72 (CH), 40.41 (CH_2); *m/z* (NSI) Found 199.0051 ($[M-H]^-$ $C_9H_8FS_2$ requires 199.0056).

2-(4-Methoxyphenyl)-1,3-dithiolane 178h

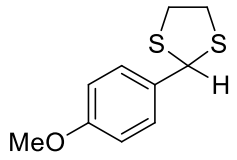

178h

Chemical Formula: $C_{10}H_{12}OS_2$
Molecular Weight: 212.33

According to general procedure **H** compound **178h** was obtained after heating in the microwave at 100 °C for 50 minutes as a colourless solid (0.700 g, 99%); mp 63 - 64 °C (60 – 61 °C [192]); ν_{max} (neat) 3000, 2917 (C–H), 1028 (C–O); δ_H (400 MHz, $CDCl_3$) 7.48 - 7.42 (2H, m, Ar**H**), 6.88 - 6.81 (2H, m, Ar**H**), 5.64 (1H, s, SC**H**S), 3.80 (3H, s, OC**H**$_3$), 3.55 - 3.46 (2H, m, SC**H**$_2$CH$_2$S), 3.39 - 3.29 (2H, m, SCH$_2$C**H**$_2$S); δ_C (126 MHz, $CDCl_3$) 159.53 (C), 131.93 (C), 129.29 (CH), 114.00 (CH), 56.19 (CH), 55.47 (CH_3), 40.36 (CH_2); *m/z* (NSI) Found 213.0408 ($[M+H]^+$ $C_{10}H_{13}OS_2$ requires 213.0408).

2-(4-Nitrophenyl)-1,3-dithiolane 178i

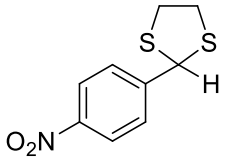

178i

Chemical Formula: $C_9H_9NO_2S_2$
Molecular Weight: 227.30

According to general procedure **H** compound **178i** was obtained after heating in the microwave at 100 °C for 50 minutes as a yellow soild (0.559 g, 74%); mp 80 - 81 °C (lit 78 – 79 °C [193]); ν_{max} (neat) 3011, 2918 (C–H), 1514 (N–O); δ_H (500 MHz, $CDCl_3$) 8.16 (2H, d, J = 8.8 Hz, Ar**H**), 7.77 - 7.57 (2H, m, Ar**H**), 5.65 (1H, s, SC**H**S), 3.57 - 3.48 (2H, m, SC**H**$_2$CH$_2$S), 3.44 - 3.36 (2H, m, SCH$_2$C**H**$_2$S); δ_C (126 MHz, $CDCl_3$) 148.68 (C), 147.43 (C), 128.87 (CH), 123.78 (CH), 54.93 (CH), 40.53 (CH_2); *m/z* (NSI) Found 228.0153 ($[M+H]^+$ $C_9H_{10}NO_2S_2$ requires 228.0156).

5.1.9 Synthesis of 183 and 185

Diethyl 2-(1-methyl-1H-indol-2-yl)malonate 183 [170]

182
Chemical Formula: C_9H_9N
Molecular Weight: 131.17

179

183
Chemical Formula: $C_{16}H_{19}NO_4$
Molecular Weight: 289.33

1-Methyl-1H-indole (0.019 mL, 0.152 mmol), tris(2,2′-bipyridyl)dichlororuthenium(II) hexahydrate (1.140 mg, 1.52 µmol), 4-methoxy-*N*,*N*-diphenylaniline (0.084 g, 0.30 mmol) and diethyl 2-bromomalonate (0.051 mL, 0.30 mmol) were added to a oven dried round bottom flask. DMF (1.5 mL) was added to the mixture and the resulting solution was degassed *via* three repeated cycles of freezing the flask with liquid nitrogen and allowing the frozen reaction mixture to thaw under vacuum. The solution was injected into a 2 mL injection loop of Pump B of the Uniqsis FlowSyn previously flushed with anhydrous DMF. The solution was passed through the CHR12 and irradiated with blue LEDs (400W A160 Actinic bulbs) at 0.05 mL/min. A tube with compressed air was directed at the reactor to allow for the heat to dissipate. The product solution was collected and checked for completion *via* TLC. It was then poured into ethyl acetate (10 mL) and water (10 mL). The layers were separated and the aqueous layer was extracted with ethyl acetate (3 × 10 mL). The combined organic extracts were washed with water (25 mL) and brine (25 mL) and dried over Na_2SO_4, after which it was filtered and concentrated under reduced pressure to give the crude. This residue was purified *via* automated flash chromatography (95:5 Hex/EtOAc; Zip 10 g column) to give diethyl 2-(1-methyl-1H-indol-2-yl)malonate (0.119 g, 78%) as a colourless oil; ν_{max} ($CDCl_3$) 2958, 2928 (C–H), 1731 (C=O), 1367 (C–N); δ_H (500 MHz, $CDCl_3$) 7.60 (1H, d, J = 7.9 Hz Hz, Ar**H**), 7.32 (1H, d, J = 8.4 Hz, Ar**H**), 7.26 - 7.21 (1H, m, Ar**H**), 7.11 (1H, t, J = 7.4 Hz, Ar**H**), 6.60 (1H, s, OCOC**H**), 4.94 (1H, s, NCC**H**), 4.35 - 4.22 (4H, m, 2 × COOC**H**$_2$CH$_3$), 3.73 (3H, s, NC**H**$_3$), 1.30 (6H, t, J = 7.1 Hz, 2 × COOCH$_2$C**H**$_3$); *m/z* (NSI) Found 290.1387 ([M+H]+ $C_{16}H_{20}NO_4$ requires 290.1387)

Diethyl 2-(3-acetyl-1-methyl-1H-pyrrol-2-yl)malonate 185 [170]

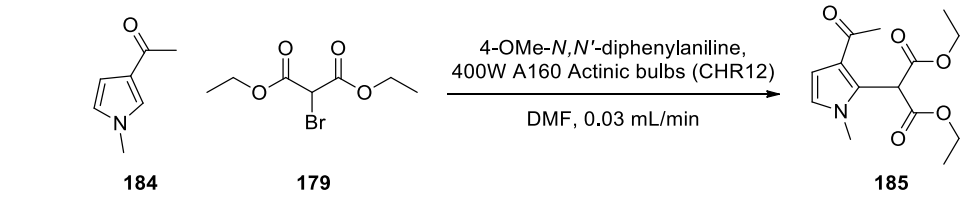

184 **179** **185**

Chemical Formula: C_7H_9NO
Molecular Weight: 123.15

Chemical Formula: $C_{14}H_{19}NO_5$
Molecular Weight: 281.30

1-(1-Methyl-1H-pyrrol-3-yl)ethanone (0.038 mL, 0.406 mmol), Tris(2,2′-bipyridyl)dichlororuthenium(II) hexahydrate (3.04 mg, 4.06 µmol), 4-methoxy-*N*,*N*-diphenylaniline (0.224 g, 0.812 mmol) and diethyl 2-bromomalonate (0.138 ml, 0.81 mmol) were added to a oven dried round bottom flask. DMF (1.5 mL) was added to the mixture and the resulting solution was degassed *via* three repeated cycles of freezing the flask with liquid nitrogen and allowing the frozen reaction mixture to thaw under vacuum. The solution was injected into a 2 mL injection loop of Pump B previously flushed with anhydrous DMF. The solution was passed through the CHR12 and irradiated with blue LEDs (400W A160 Actinic bulbs) at 0.03 mL/min. A tube with compressed air was directed at the reactor to allow for the heat to dissipate. The solution was poured into ethyl acetate (10 mL) and water (10 mL). The layers were separated and the aqueous layer was extracted with ethyl acetate (3 × 10mL). The combined organic extracts were washed with water (25 mL) and brine (25mL) and dried over Na_2SO_4, after which it was filtered and concentrated. This residue was purified *via* automated flash chromatography (95:5 Hex/EtOAc; Zip 10 g column) to give diethyl 2-(3-acetyl-1-methyl-1H-pyrrol-2-yl)malonate (0.047 g, 41%) as a colourless solid; ν_{max} (neat) 2982, 2928 (C–H), 1734 (C=O), 1363 (C–N); δ_H (500 MHz, $CDCl_3$) 6.62 (1H, s, NCC**H**), 6.56 (1H, d, J = 3.0 Hz, Ar**H**), 6.51 (1H, d, J = 3.0 Hz, Ar**H**), 4.30 - 4.16 (4H, m, 2 × OC**H**$_2$CH$_3$), 3.64 (3H, s, NC**H**$_3$), 2.41 (3H, s, COC**H**$_3$), 1.28 (6H, t, J = 7.1 Hz, 2 × OCH$_2$C**H**$_3$); δ_C (126 MHz, $CDCl_3$) 195.70 (CO), 167.73 (CO), 127.96 (C), 123.84 (CH), 122.66 (C), 110.54 (CH), 62.12 (CH_2), 48.63 (CH_3), 35.43 (CH_3), 28.60 (CH), 14.18 (CH_3); *m/z* (NSI) Found 282.1336 ($[M+H]^+$ $C_{14}H_{20}NO_5$ requires 282.1335).

5.1.10 Synthesis of 192

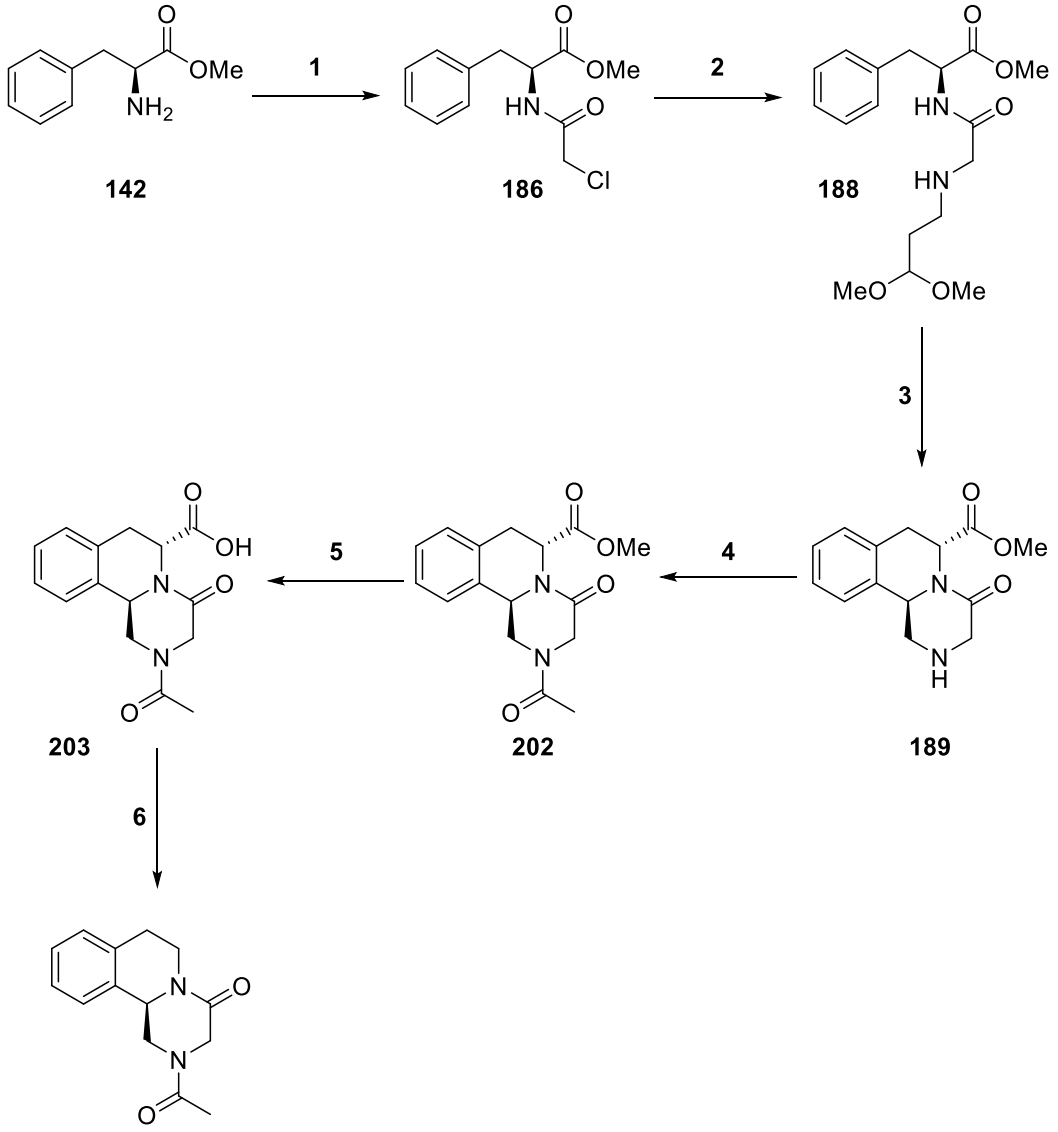

142 186 188 189 202 203

6

192 przaiquantel Analogue

Methyl 2-(2-chloroacetamido)-3-phenylpropanoate 186 [171]

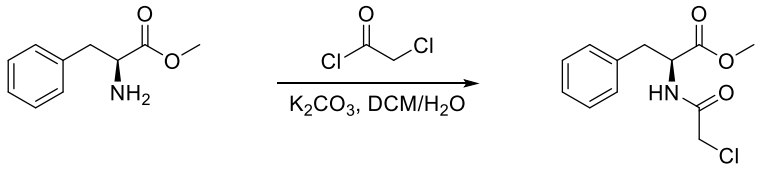

142

Chemical Formula: $C_{10}H_{13}NO_2$
Molecular Weight: 179.22

186

Chemical Formula: $C_{12}H_{14}ClNO_3$
Molecular Weight: 255.70

A solution of *D*-methyl 2-amino-3-phenylpropanoate (0.5 g, 2.79 mmol) in DCM (20 mL) and water (20 mL) was placed in a separating funnel and potassium carbonate (1.157 g, 8.37 mmol) added and shaken for 5 minutes. A solution of 2-chloroacetyl chloride (0.22 mL, 2.79 mmol) in DCM (5 mL) was added to the separating funnel and it was shaken for an additional 10 minutes. The layers were separated and the organic layer was washed with 0.2M HCl (50 mL). The organic layer was separated, dried over Na_2SO_4, filtered and concentrated under reduced pressure to give methyl 2-(2-chloroacetamido)-3-phenylpropanoate (0.61 g, 86%) as a colourless solid. The crude mixture was used in the following step without further purification; δ_H (400 MHz, $CDCl_3$) 7.24 - 7.35 (3H, m, Ar**H**), 7.12 - 7.16 (2H, m, Ar**H**), 7.08 (1H, d, J = 8.0 Hz, N**H**), 4.89 (1H, dt, J = 8.0, 6.0 Hz, NHC**H**), 4.01 (2H, s, C**H**$_2$Cl), 3.74 (3H, s, OC**H**$_3$), 3.08 – 3.26 (2H, m, ArC**H**$_2$); *m/z* (NSI) Found 256.0735 ($[M+H]^+$ $C_{12}H_{15}ClNO_3$ requires 256.0738).

Methyl 2-(2-((2,2-dimethoxyethyl)amino)acetamido)-3-phenylpropanoate 188 [171]

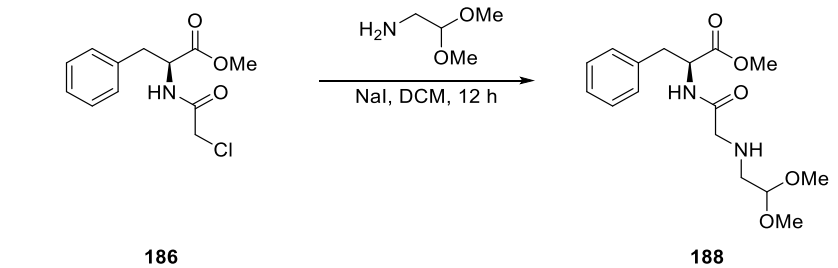

186

Chemical Formula: $C_{12}H_{14}ClNO_3$
Molecular Weight: 255.70

188

Chemical Formula: $C_{16}H_{24}N_2O_5$
Molecular Weight: 324.38

A solution of methyl 2-(2-chloroacetamido)-3-phenylpropanoate (0.610 g, 2.39 mmol) and sodium iodide (0.358 g, 2.39 mmol) in DCM (50 mL) was prepared and 2,2-dimethoxyethanamine (0.780 mL, 7.16 mmol) was added dropwise to it. The reaction mixture was stirred at room temperature for 12 hours. The solution was washed with H_2O (1 × 30 mL), and extracted with DCM (2 × 20 mL). The combined organic layers were dried over Na_2SO_4, filtered and concentrated under reduced pressure to give methyl 2-(2-((2,2-dimethoxyethyl)amino)acetamido)-3-phenylpropanoate (0.764 g, 99%) as a colourless oil. The crude mixture was used in the following step without further purification; δ_H (400 MHz, $CDCl_3$) 7.62 (1H, d, J = 8.4 Hz, N**H**CO), 7.28 - 7.33 (2H, m, Ar**H**), 7.26 (1H, d, J = 5.6 Hz, Ar**H**), 7.12 - 7.16 (2H, m, Ar**H**), 4.89 (1H, td, J = 8.3, 6.1 Hz, NHC**H**CH_2), 4.32 (1H, t, J = 5.3 Hz, NHC**H**$_2$CH), 3.73 (3H, s, COOC**H**$_3$), 3.35 (3H, s, OC**H**$_3$), 3.34 (3H, s, OC**H**$_3$) 3.27 (2H, d, J = 5.3 Hz, NHC**H**$_2$CH), 3.07 - 3.23 (2H, m, NHCOC**H**$_2$), 2.58 - 2.70 (2H, m, ArC**H**$_2$); *m/z* (NSI) Found 325.1758 ($[M+H]^+$ $C_{16}H_{25}N_2O_5$ requires 325.1761).

Methyl 4-oxo-2,3,4,6,7,11b-hexahydro-1H-pyrazino[2,1-a]isoquinoline-6-carboxylate 189 [171]

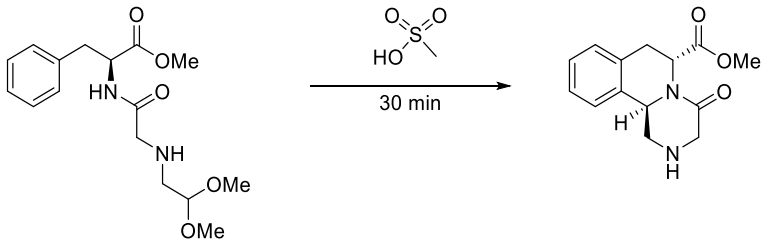

188

Chemical Formula: $C_{16}H_{24}N_2O_5$
Molecular Weight: 324.38

189

Chemical Formula: $C_{14}H_{16}N_2O_3$
Molecular Weight: 260.29

Methyl 2-(2-((2,2-dimethoxyethyl)amino)acetamido)-3-phenylpropanoate (0.1 g, 0.31 mmol) in methanesulfonic acid (1.5 mL, 23.10 mmol) was stirred at 70 °C for 30 minutes. The reaction mixture was quenched with a solution of 1M NaOH. The neutral solution was extracted with DCM (2 × 20 mL), dried over Na_2SO_4, filtered and concentrated under reduced pressure to give methyl 4-oxo-2,3,4,6,7,11b-hexahydro-1H-pyrazino[2,1-a]isoquinoline-6-carboxylate (0.053 g, 66%) as a brown solid. The crude mixture was used in the following step without further purification; δ_H (400 MHz, $CDCl_3$) 7.25 - 7.11 (4H, m, Ar**H**), 5.73 (1H, dd, J = 3.6, 6.2 Hz, NC**H**$COOCH_3$), 5.01 (1H, dd, J = 10.2, 4.2 Hz, NC**H**CH_2NH), 3.82 - 3.70 (2H, m, 1 × NCOC**H**$_2$NH, 1 × NCHC**H**$_2$NH), 3.66 (3H, s, OC**H**$_3$), 3.62 (1H, d, J = 17.6 Hz, 1 × NCOC**H**$_2$NH), 3.30 - 3.12 (2H, m, 1 × ArC**H**$_2$, 1 × NCHC**H**$_2$NH), 3.00 - 2.91 (1H, m, 1 × ArC**H**$_2$); *m/z* (NSI) Found 261.1234 ($[M+H]^+$ $C_{14}H_{17}N_2O_3$ requires 261.1237).

Methyl 2-acetyl-4-oxo-2,3,4,6,7,11b-hexahydro-1H-pyrazino[2,1-a]isoquinoline-6-carboxylate 202

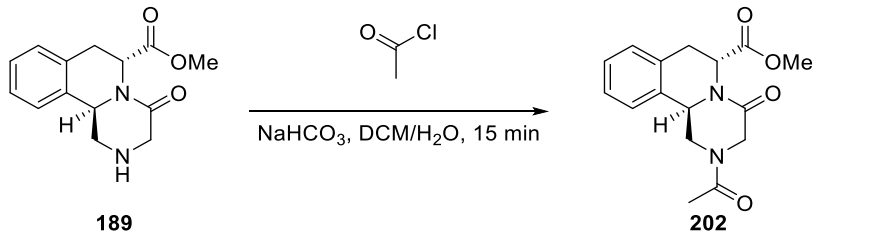

189

Chemical Formula: $C_{14}H_{16}N_2O_3$
Molecular Weight: 260.29

202

Chemical Formula: $C_{16}H_{18}N_2O_4$
Molecular Weight: 302.33

Methyl 4-oxo-2,3,4,6,7,11b-hexahydro-1H-pyrazino[2,1-a]isoquinoline-6-carboxylate (0.786 g, 3.02 mmol) in DCM (13 mL) and sodium bicarbonate (0.761 g, 9.06 mmol) in water (10 mL) were stirred for 10 minutes. A solution of acetyl chloride (0.237 mL, 3.32 mmol) in DCM (5 mL) was added to the reaction mixture and the solution was stirred for 15 minutes. The layers were separated and the organic layer was washed with a saturated solution of sodium bicarbonate (5 × 25 mL). The combined organic layers were dried over Na_2SO_4, filtered and concentrated under reduced pressure to give the methyl 2-acetyl-4-oxo-2,3,4,6,7,11b-hexahydro-1H-pyrazino[2,1-a]isoquinoline-6-carboxylate (0.726 g, 80%); The crude mixture was used in the following step without further purification; δ_H (101 MHz, CD_3OD) 7.43 - 7.19 (4H, m, Ar**H**), 5.58 (1H, ddd, J = 13.3, 5.7, 3.1Hz, N**H**COO), 5.19 (0.5H, ddd, J = 11.3, 3.6 Hz, NC**H**CH_2N), 5.01 (0.5H, dd, J = 10.7, 3.5 Hz), 4.75 (0.5H, d, J = 3.7 Hz) 4.33 (0.5H, dd, J = 12.7, 3.8 Hz), 3.60 (3H, s 1.5H × COOC**H**$_3$, s 1.5H × COOC**H**$_3$), 3.46 - 3.01 (4H, m,), 2.19 (3H, s 1.5H × NCOC**H**$_3$, s 1.5H × NCOC**H**$_3$).

2-Acetyl-4-oxo-2,3,4,6,7,11b-hexahydro-1H-pyrazino[2,1-a]isoquinoline-6-carboxylic acid 203

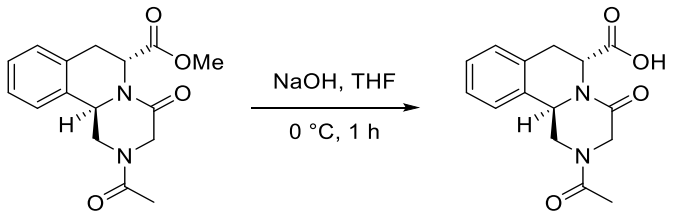

202

Chemical Formula: $C_{16}H_{18}N_2O_4$
Molecular Weight: 302.33

203

Chemical Formula: $C_{15}H_{16}N_2O_4$
Molecular Weight: 288.30

Sodium hydroxide (4.66 ml, 4.66 mmol) was added to a mixture of methyl 2-acetyl-4-oxo-2,3,4,6,7,11b-hexahydro-1H-pyrazino[2,1-a]isoquinoline-6-carboxylate (0.612 g, 2.02 mmol) in THF (20.24 mL) and the reaction mixture was stirred at 0 °C for one hour. The mixture was made acidic (pH 4) with 1M HCl. A precipitate was obtained and the product was extracted with DCM (2 × 20 mL). The precipitate was dissolved in MeOH and concentrated under reduced pressure to give the first fraction (0.091 g).The organic extract was dried over Na_2SO4, filtered and concentrated under reduced pressure to give second fraction (0.131 g). The aqueous fraction was acidified with 1M HCl until the precipitation stopped and this was filtered to give the third fraction (0.021 g). The fractions were combined to give 2-acetyl-4-oxo-2,3,4,6,7,11b-hexahydro-1H-pyrazino[2,1-a]isoquinoline-6-carboxylic acid (0.243 g, 42%). The crude mixture was used in the following step without further purification; δ_H (400 MHz, CD_3OD) 7.43 – 7.17 (4H, m, Ar**H**), 5.57 (1H, ddd, *J* 9.0, 5.9, 3.0, NC**H**COO), 5.12 (1H, ddd, J= 7.6, 11.0, 3.7 Hz, NC**H**CH_2N), 4.79 – 4.69 (m, 1H), 4.57 – 4.18 (m, 2H), 3.51 – 2.97 (m, 6H), 2.19 (3H, s 1.5H × NCOC**H**$_3$ s 1.5H × NCOC**H**3); *m/z* (NSI) Found 287.1037 ($[M-H]^-$ $C_{15}H_{15}N_2O_4$ requires 287.1037).

2-Acetyl-2,3,6,7-tetrahydro-1H-pyrazino[2,1-a]isoquinolin-4(11bH)-one 192

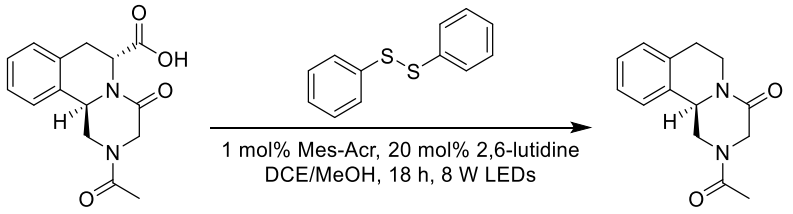

203 **192**

Chemical Formula: $C_{15}H_{16}N_2O_4$
Molecular Weight: 288.30

Chemical Formula: $C_{14}H_{16}N_2O_2$
Molecular Weight: 244.29

2-Acetyl-4-oxo-2,3,4,6,7,11b-hexahydro-1H-pyrazino[2,1-a]isoquinoline-6-carboxylic acid (0.114 g, 0.40 mmol), 1,2-diphenyldisulfane (8.63 mg, 0.04 mmol), 9-mesityl-10-methylacridin-10-ium tetrafluoroborate (3.16 mg, 7.91 µmol) and 2,6-dimethylpyridine (9.21 µl, 0.08 mmol) were added to an oven-dried round bottom flask. The internal atmosphere was exchanged with nitrogen *via* three repeated cycles of vacuum-refill. Anhydrous DCE (7.9 mL) and methanol (7.9 mL) were added and the reaction mixture was sparged with nitrogen for 20 minutes. This was then irradiated with 8W GU10 blue light lamps for 18 hours. The solution was concentrated under reduced pressure. The residue was taken up in DCM (50 mL), washed with 0.1M NaOH (2 × 50 mL) and 0.5M HCl (2 × 50mL). The organic extracts were separated, dried over Na_2SO_4, filtered and concentrated under reduced pressure. The crude residue was purified *via* automated flash chromatography (1:1 Pet-Ether : EtOAc and then 10% DCM : MeOH ; Zip 10 g column) to give 2-acetyl-2,3,6,7-tetrahydro-1H-pyrazino[2,1-a]isoquinolin-4(11bH)-one (0.025 g, 26%) as an orange oil; δ_H (500 MHz, CD_3OD) 7.19 - 7.40 (4H, m, Ar**H**), 5.04 (0.5H, dd, J = 10.6, 3.8 Hz, NC**H**), 4.97 (0.5H, dd, J = 13.3, 3.9, 1 × COC**H**$_2$), 4.87 (0.5H, dd, J = 10.5, 3.9 Hz, NC**H**), 4.67 - 4.74 (1H, m, 1 × NCH$_2$C**H**$_2$), 4.64 (0.5H, d, J = 18.4 Hz, 1 × COC**H**$_2$), 4.48 (0.5H, d, J = 3.8 Hz,1 × NCHC**H**$_2$), 4.43 (0.5H, d, J = 18.2 Hz, 1 × NCHC**H**$_2$), 4.17 (0.5H, d, J = 17.4 Hz, 1 × NCHC**H**$_2$), 3.88 (0.5H, d, J = 18.2 Hz, 1 × COC**H**$_2$), 3.33 - 3.41 (0.5H, m, 1 × NCHC**H**$_2$), 2.91 - 2.99 (2.5H, m, 1 × COC**H**$_2$, 1 × NCH$_2$C**H**$_2$, 1 × CONC**H**$_2$), 2.78 - 2.87 (1H, m, 1 × CONC**H**$_2$), 2.25 (1.5H, s, COC**H**$_3$), 2.16 (1.5H, s, COC**H**$_3$); δ_C (126 MHz, CD_3OD) 172.1 (CO), 172.0 (CO), 167.7 (CO), 166.8 (CO), 136.7 (C), 136.5

(C), 134.2 (C), 133.9 (C), 130.4 (CH), 128.7 (CH), 128.2 (CH), 127.0 (CH), 126.7 (CH), 56.6 (CH), 56.2 (CH), 51.1 (CH_2), 50.4 (CH_2), 46.9 (CH_2), 46.2 (CH_2), 40.5 (CH_2), 40.4 (CH_2), 29.8 (CH_2), 29.7 (CH_2), 21.4 (CH_3), 21.2 (CH_3); *m/z* (NSI) Found 245.1285 ($[M+H]^+$ $C_{14}H_{17}N_2O_2$ requires 245.1287.

5.1.11 3D-Printing: Catalytic Stirrer Bead Development

P1: Preparation of 1st generation catalytically active 3D-printed objects

Design Software: The device was designed using the freeware web-based application - Tinkercad (Autodesk) software (Supp. Fig. 1), exported as an STL (standard tessellation language) file and uploaded to FormLabs PreForm Software 2.10.3 before printing. Support structures to aid printing were automatically generated by PreForm Software 2.10.3.

Stirrer Bead Design: The stirrer bar holder design was based upon a commercial overhead stirrer[176] with a large surface area which, when spun at high speeds, would cause 1) a high flow of liquid over the surface of the stirrer and 2) high turbulence to ensure efficient mixing. A slot to hold a 10 mm x 3 mm magnetic flea was added.

Preparation of *p*-TsOH-doped photopolymerizable resin: Freshly ground *p*-toluene sulfonic acid monohydrate (5% w/w) and diphenyl(2,4,6-trimethylbenzoyl)phosphine oxide (1.9% w/w) were dissolved in isobornyl acrylate (31.35% w/w) in the absence of light with the aid of sonication. Trimethylolpropane triacrylate (14.25% w/w) and bisphenol A ethoxylate diacrylate (47.5% w/w) were added and the mixture stirred for 15 h. The photopolymerizable resin was poured into the tray of a Formlabs Form 1+ SLA 3D-printer.

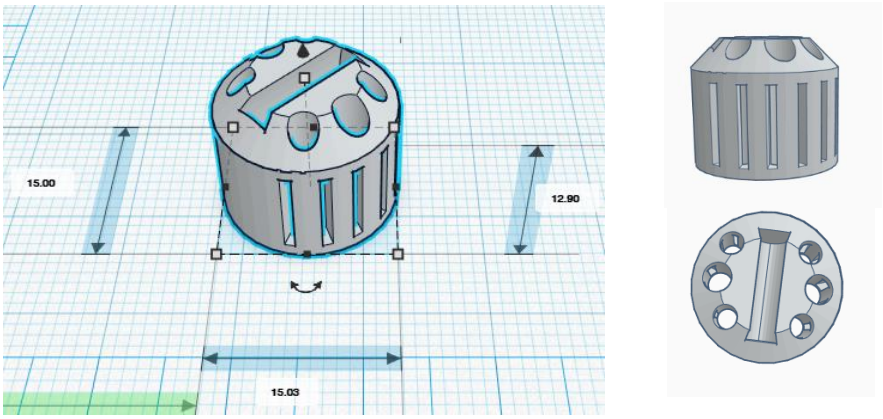

Figure 79: Design and shape of 1st generation RBF stirrer beads.

Device Fabrication: The photopolymerizable resin was poured into the tray of the Formlabs Form 1+ SLA 3D-printer. The .STL file of the model was loaded

using the PreForm software for use with a Formlabs 3D-printer. The stirrer bar holders were printed with a layer height of 0.1 mm using the Clear02 resin setting. The print time for an individual object was approximately 35 minutes (120 layers). After printing, the objects were removed, soaked in isopropanol for 10 minutes and left to dry and cured in natural light for 24 hours. A magnetic flea (10 mm x 3 mm) was added and to secure it, additional catalyst-doped photopolymerizable resin was added and the objects placed in natural sunlight for 24 hours to cure the resin. The objects were finally rinsed with isopropanol and dried.

P2: Preparation of 2nd generation catalytically active 3D-printed objects

A. Preparation of $Pd(PPh_3)_4$-doped photopolymerizable resin: Palladium tetrakis(triphenylphosphine) $Pd(PPh_3)_4$ (0.5% w/w) and diphenyl(2,4,6-trimethylbenzoyl) phosphine oxide (1.463% w/w) were dissolved in poly(ethylene glycol) diacrylate (Mn 250) (98.03%) in the absence of light. When dissolution was complete the photopolymerizable resin was poured into the tray of a Formlabs Form 1+ SLA 3D-printer. The devices were fabricated as discussed in earlier examples and fitted with the appropriate magnetic stirrer.

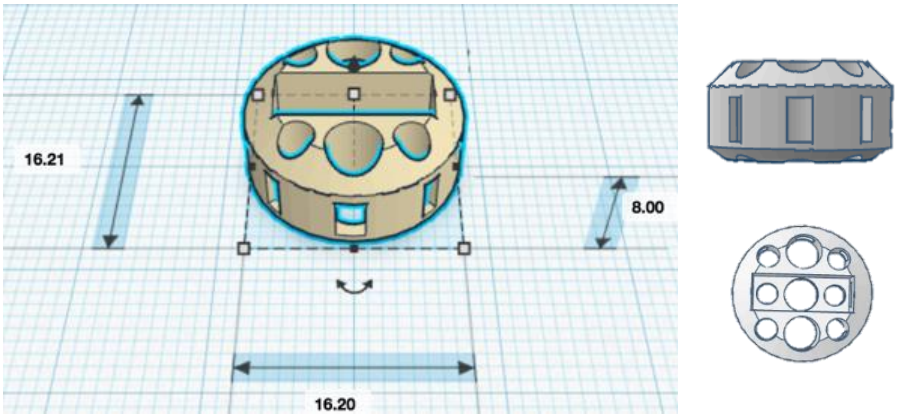

Figure 80: Design and shape of 2nd generation RBF stirrer beads.

Device Fabrication: The photopolymerizable resin was poured into the tray of the Formlabs Form 1+ SLA 3D-printer. The .STL file of the model was loaded using the PreForm software for use with a Formlabs 3D-printer. The stirrer bar holders were printed with a layer height of 0.1 mm using the Black01 resin setting. The print time for an individual object was approximately 30 minutes (100 layers). After printing, the objects were removed, rinsed with isopropanol and left to dry and cured in the Form Cure UV curing oven for 20 minutes after which the supports were removed and the 10 mm magnetic flea was fitted into the cavity.

B. Preparation of $Y(OTf)_3$-doped photopolymerizable resin: Yttrium triflate $Y(OTf)_3$ (10% w/w) and diphenyl(2,4,6-trimethylbenzoyl) phosphine oxide (1.323% w/w) were dissolved in poly(ethylene glycol) diacrylate (Mn 250) (88.677%) in the absence of light. When dissolution was complete the photopolymerizable resin was poured into the tray of a Formlabs Form 1+ SLA 3D-printer. The devices were fabricated as discussed in earlier examples and fitted with the appropriate magnetic stirrer.

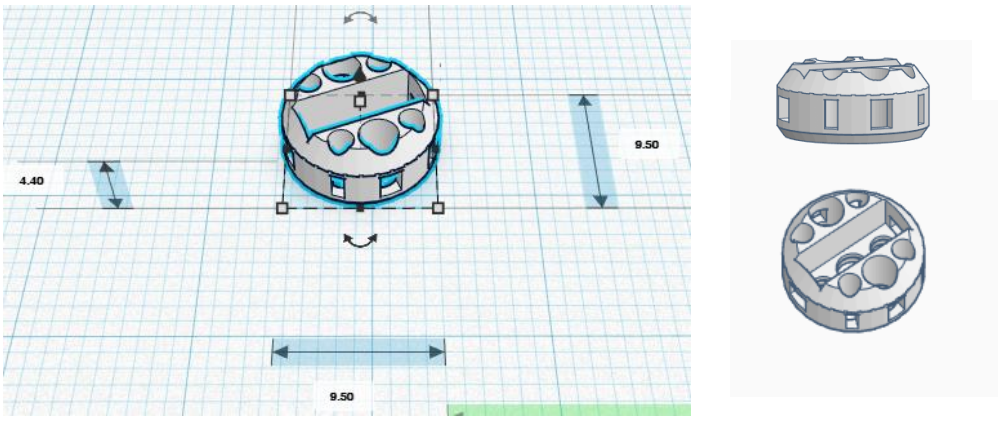

Figure 81: Design and shape of 2nd generation microwave stirrer beads.

Device Fabrication: The photopolymerizable resin was poured into the tray of the Formlabs Form 1+ SLA 3D-printer. The .STL file of the model was loaded using the PreForm software for use with a Formlabs 3D-printer. The stirrer bar holders were printed with a layer height of 0.1 mm using the Clear01 resin setting. After printing, the objects were removed, rinsed with isopropanol and left to dry and cured in the Form Cure UV curing oven for 30 minutes after which the supports were removed and the 8 mm magnetic flea was fitted into the cavity.

All designs were uploaded on the PreForm software and printed in groups of 16 or 9 depending on the size of the object.

Figure 82: Design on the FormLabs software, printed on the build plate and with support and removed support showing.

5.1.12 3D-Printing: Reactor Development

3D-Printing of Reactor Design CHR1

The device was designed using the freeware web-based application - Tinkercad (Autodesk) software (Supp. Fig. 1), exported as an STL (standard tessellation language) file and uploaded to FormLabs PreForm Software 2.10.3 before printing. Support structures to aid printing were automatically generated by PreForm Software 2.10.3.

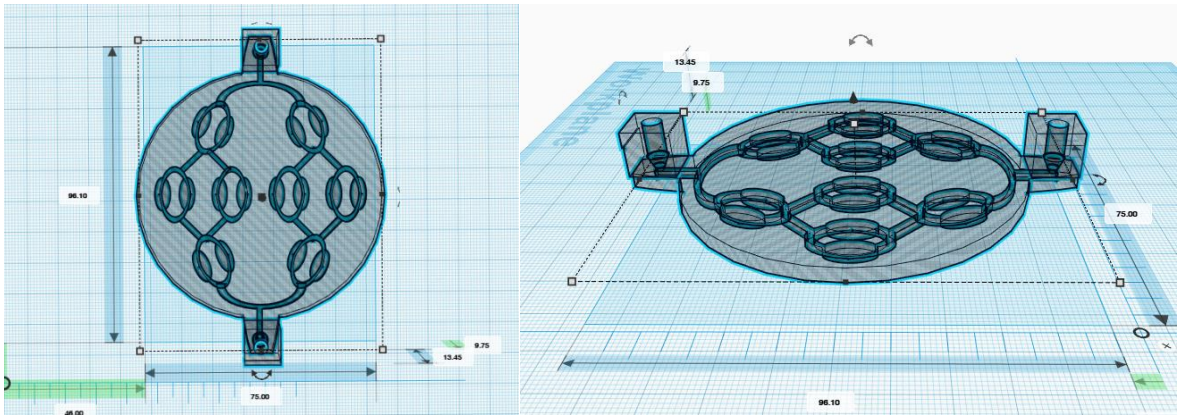

Figure 83: Design size and shape of CHR1.

3D-Printing of the device

Poly(ethylene glycol) diacrylate (PEGDA) Mn 250 98.53% (33.3 g) and diphenyl(2,4,6-trimethylbenzoyl) phosphine oxide (TPO) 1.47% (0.5 g) were dissolved at room temperature and transferred to a Form1+ 3D Printer. The device design was uploaded and printed using the Clear 01 setting at a 45 degree angle with the supports attached to it's rear face. The layer height was adjusted to 100-micron layer height with a print time of approximately 2 hours and 30 minutes (777 layers) giving the object a total volume of 27.19 mL.

Figure 84: Printing of CHRs in FormLabs Form 1+ printer.

Following printing, designs were removed, washed (isopropanol), and post-cured under UV light *in vacuo*. Following curing, supports were removed from each object and devices stored at room temperature.

3D-Printing of Reactor Design CHR2

The device was designed using the freeware web-based application - Tinkercad (Autodesk) software (Supp. Fig. 1), exported as an STL (standard tessellation language) file and uploaded to FormLabs PreForm Software 2.10.3 before printing. Support structures to aid printing were automatically generated by PreForm Software 2.10.3.

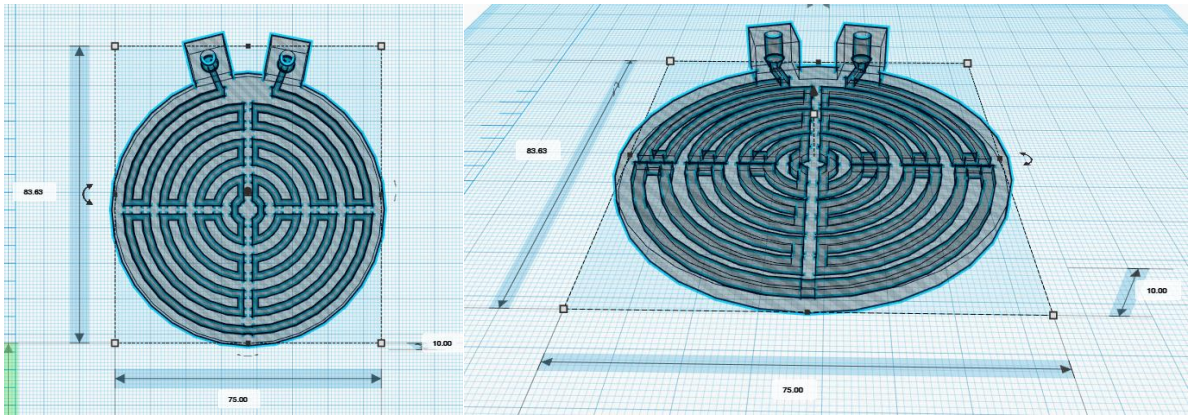

Figure 85: Design size and shape of CHR2.

3D-Printing of the device

Poly(ethylene glycol) diacrylate (PEGDA) Mn 250 98.53% (33.3 g) and diphenyl(2,4,6-trimethylbenzoyl) phosphine oxide (TPO) 1.47% (0.5 g) were dissolved at room temperature and transferred to a Form1+ 3D Printer. The device design was uploaded and printed using the Clear 01 setting at a 45 degree angle with the supports attached to it's rear face. The layer height was adjusted to 100-micron layer height with a print time of approximately 2 hours and 30 minutes (641 layers) giving the object a total volume of 27.68 mL.

Following printing, designs were removed, washed (isopropanol), and post-cured under UV light *in vacuo*. Following curing, supports were removed from each object and devices stored at room temperature.

3D-Printing of Reactor Design CHR3

The device was designed using the freeware web-based application - Tinkercad (Autodesk) software (Supp. Fig. 1), exported as an STL (standard tessellation language) file and uploaded to FormLabs PreForm Software 2.10.3 before printing. Support structures to aid printing were automatically generated by PreForm Software 2.10.3.

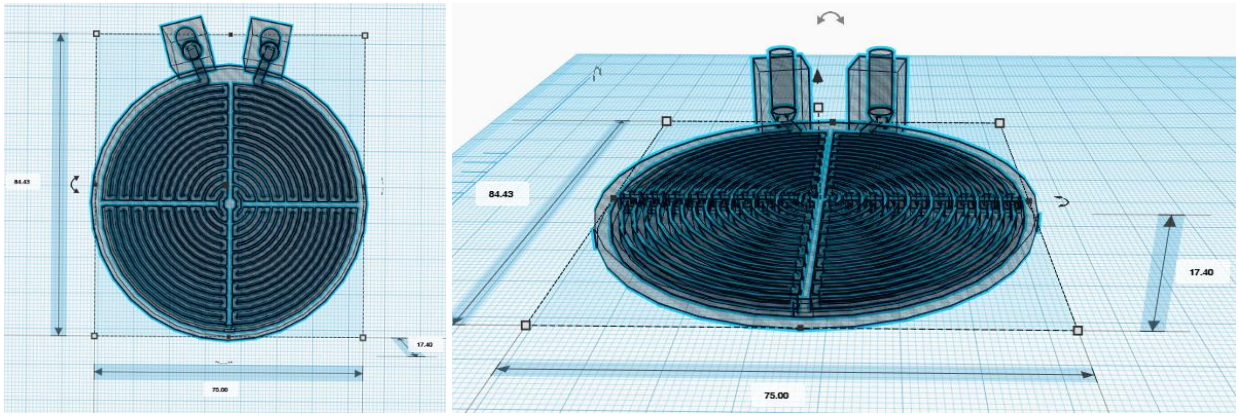

Figure 86: Design size and shape of CHR3.

3D-Printing of the device

Poly(ethylene glycol) diacrylate (PEGDA) Mn 250 98.53% (33.3 g) and diphenyl(2,4,6-trimethylbenzoyl) phosphine oxide (TPO) 1.47% (0.5 g) were dissolved at room temperature and transferred to a Form1+ 3D Printer. The device design was uploaded and printed using the Clear 01 setting at a 45 degree angle with the supports attached to it's rear face. The layer height was adjusted to 100-micron layer height with a print time of approximately 2 hours and 30 minutes (669 layers) giving the object a total volume of 29.78 mL.

Following printing, designs were removed, washed (isopropanol), and post-cured under UV light *in vacuo*. Following curing, supports were removed from each object and devices stored at room temperature.

3D-Printing of Reactor Design CHR4

The device was designed using the freeware web-based application - Tinkercad (Autodesk) software (Supp. Fig. 1), exported as an STL (standard tessellation language) file and uploaded to FormLabs PreForm Software 2.10.3 before printing. Support structures to aid printing were automatically generated by PreForm Software 2.10.3.

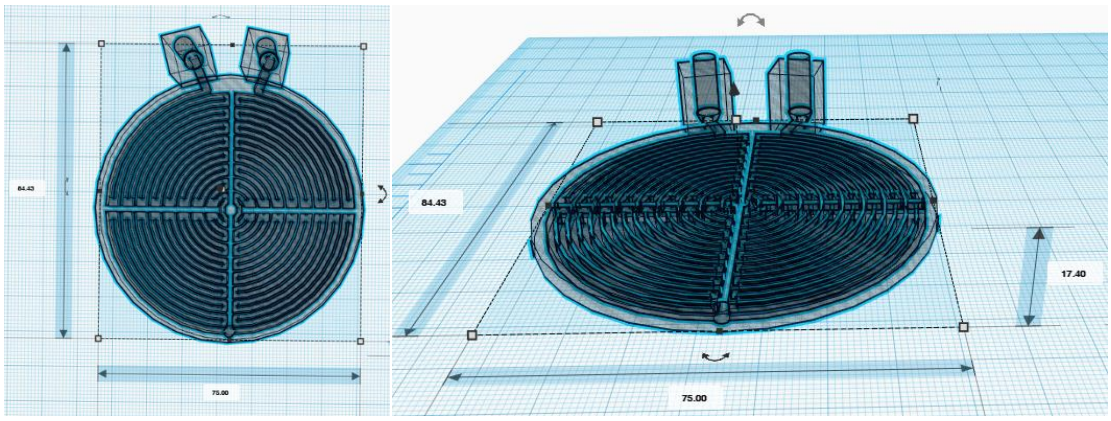

Figure 87: Design size and shape of CHR4.

3D-Printing of the device

Poly(ethylene glycol) diacrylate (PEGDA) Mn 250 98.53% (33.3 g) and diphenyl(2,4,6-trimethylbenzoyl) phosphine oxide (TPO) 1.47% (0.5 g) were dissolved at room temperature and transferred to a Form1+ 3D Printer. The device design was uploaded and printed using the Clear 01 setting at a 45 degree angle with the supports attached to it's rear face. The layer height was adjusted to 100-micron layer height with a print time of approximately 2 hours and 30 minutes (738 layers) giving the object a total volume of 27.56 mL.

Following printing, designs were removed, washed (isopropanol), and post-cured under UV light *in vacuo*. Following curing, supports were removed from each object and devices stored at room temperature.

3D-Printing of Reactor Design CHR5

The device was designed using the freeware web-based application - Tinkercad (Autodesk) software (Supp. Fig. 1), exported as an STL (standard tessellation language) file and uploaded to FormLabs PreForm Software 2.10.3 before printing. Support structures to aid printing were automatically generated by PreForm Software 2.10.3.

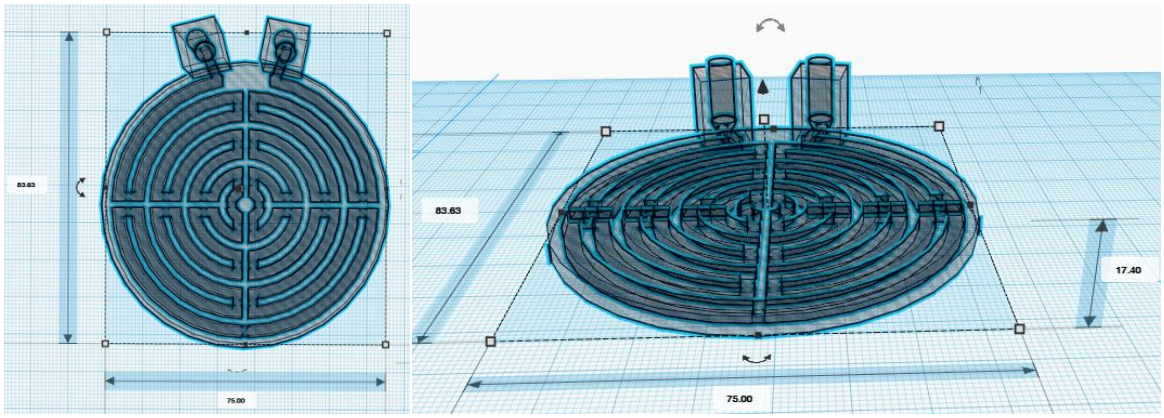

Figure 88: Design size and shape of CHR5.

3D-Printing of the device

Poly(ethylene glycol) diacrylate (PEGDA) Mn 250 98.53% (33.3 g) and diphenyl(2,4,6-trimethylbenzoyl) phosphine oxide (TPO) 1.47% (0.5 g) were dissolved at room temperature and transferred to a Form1+ 3D Printer. The device design was uploaded and printed using the Clear 01 setting at a 45 degree angle with the supports attached to it's rear face. The layer height was adjusted to 100-micron layer height with a print time of approximately 2 hours and 30 minutes (777 layers) giving the object a total volume of 26.36 mL.

Following printing, designs were removed, washed (isopropanol), and post-cured under UV light *in vacuo*. Following curing, supports were removed from each object and devices stored at room temperature.

3D-Printing of Reactor Design CHR6

The device was designed using the freeware web-based application - Tinkercad (Autodesk) software (Supp. Fig. 1), exported as an STL (standard tessellation language) file and uploaded to FormLabs PreForm Software 2.10.3 before printing. Support structures to aid printing were automatically generated by PreForm Software 2.10.3.

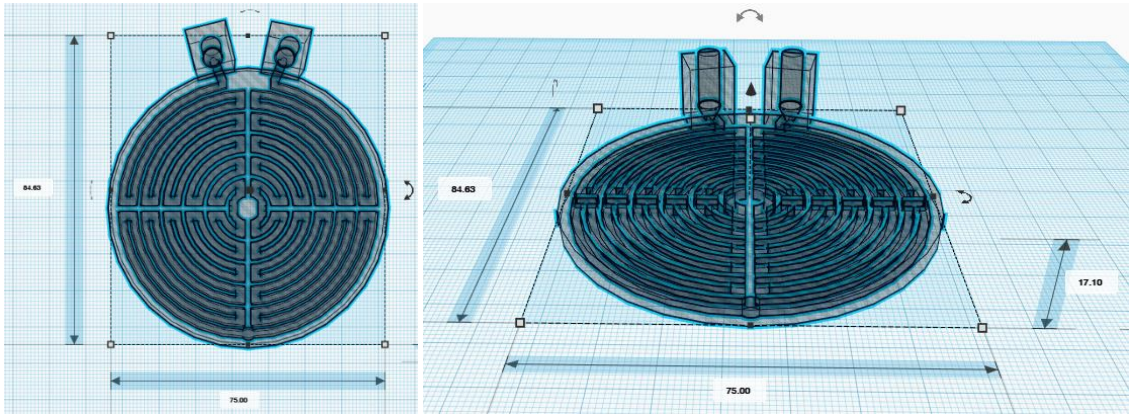

Figure 89: Design size and shape of CHR6.

3D-Printing of the device

Poly(ethylene glycol) diacrylate (PEGDA) Mn 250 98.53% (33.3 g) and diphenyl(2,4,6-trimethylbenzoyl) phosphine oxide (TPO) 1.47% (0.5 g) were dissolved at room temperature and transferred to a Form1+ 3D Printer. The device design was uploaded and printed using the Clear 01 setting at a 45 degree angle with the supports attached to it's rear face. The layer height was adjusted to 100-micron layer height with a print time of approximately 2 hours and 30 minutes (646 layers) giving the object a total volume of 27.50 mL.

Following printing, designs were removed, washed (isopropanol), and post-cured under UV light *in vacuo*. Following curing, supports were removed from each object and devices stored at room temperature.

3D-Printing of Reactor Design CHR7

The device was designed using the freeware web-based application - Tinkercad (Autodesk) software (Supp. Fig. 1), exported as an STL (standard tessellation language) file and uploaded to FormLabs PreForm Software 2.10.3 before printing. Support structures to aid printing were automatically generated by PreForm Software 2.10.3.

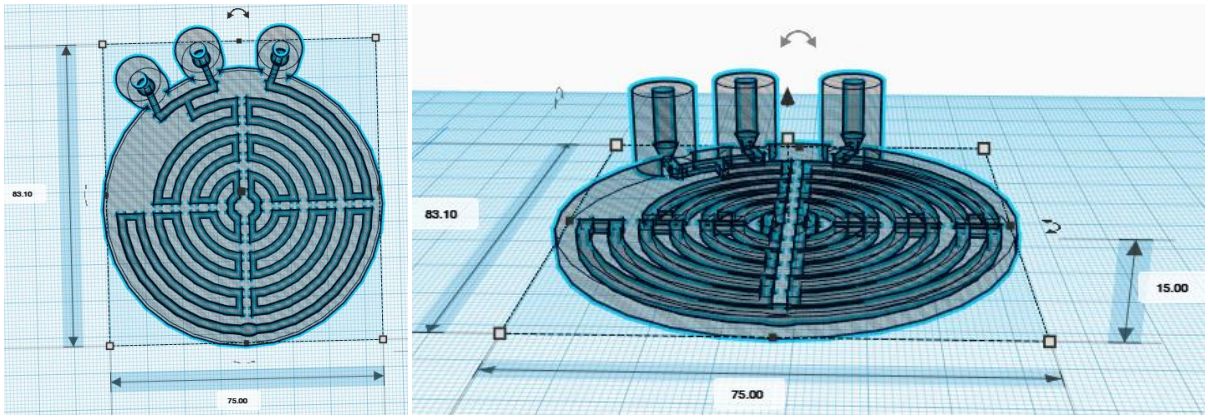

Figure 90: Design size and shape of CHR7.

3D-Printing of the device

Poly(ethylene glycol) diacrylate (PEGDA) Mn 250 98.53% (33.3 g) and diphenyl(2,4,6-trimethylbenzoyl) phosphine oxide (TPO) 1.47% (0.5 g) were dissolved at room temperature and transferred to a Form1+ 3D Printer. The device design was uploaded and printed using the Clear 01 setting at a 45 degree angle with the supports attached to it's rear face. The layer height was adjusted to 100-micron layer height with a print time of approximately 2 hours and 30 minutes (735 layers) giving the object a total volume of 29.61 mL.

Following printing, designs were removed, washed (isopropanol), and post-cured under UV light *in vacuo*. Following curing, supports were removed from each object and devices stored at room temperature.

3D-Printing of Reactor Design CHR8

The device was designed using the freeware web-based application - Tinkercad (Autodesk) software (Supp. Fig. 1), exported as an STL (standard tessellation language) file and uploaded to FormLabs PreForm Software 2.10.3 before printing. Support structures to aid printing were automatically generated by PreForm Software 2.10.3.

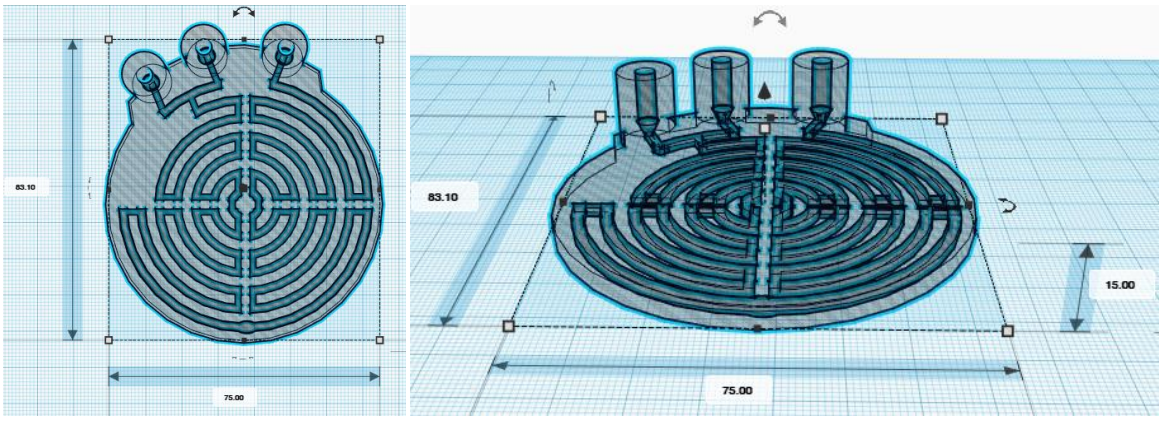

Figure 91: Design size and shape of CHR8.

3D-Printing of the device

Poly(ethylene glycol) diacrylate (PEGDA) Mn 250 98.53% (33.3 g) and diphenyl(2,4,6-trimethylbenzoyl) phosphine oxide (TPO) 1.47% (0.5 g) were dissolved at room temperature and transferred to a Form1+ 3D Printer. The device design was uploaded and printed using the Clear 01 setting at a 45 degree angle with the supports attached to it's rear face. The layer height was adjusted to 100-micron layer height with a print time of approximately 2 hours and 30 minutes (718 layers) giving the object a total volume of 29.55 mL.

Following printing, designs were removed, washed (isopropanol), and post-cured under UV light *in vacuo*. Following curing, supports were removed from each object and devices stored at room temperature.

3D-Printing of Reactor Design CHR9

The device was designed using the freeware web-based application - Tinkercad (Autodesk) software (Supp. Fig. 1), exported as an STL (standard tessellation language) file and uploaded to FormLabs PreForm Software 2.10.3 before printing. Support structures to aid printing were automatically generated by PreForm Software 2.10.3.

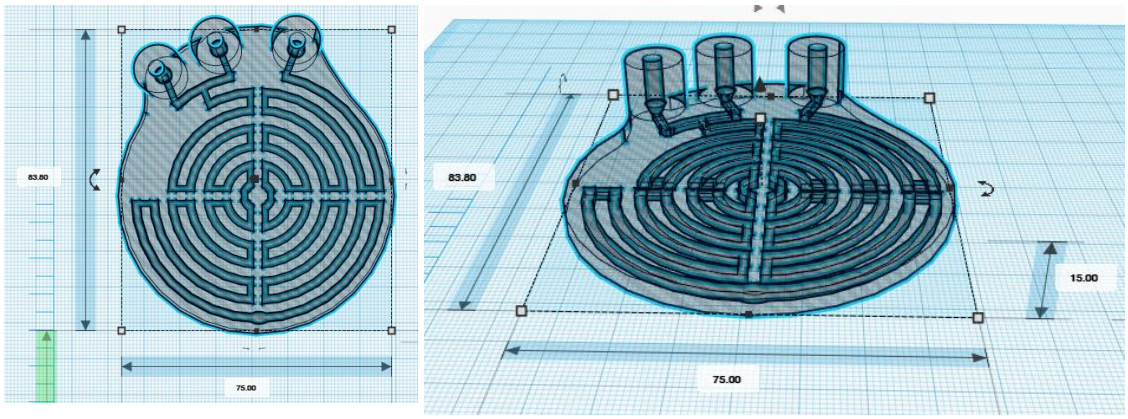

Figure 92: Design size and shape of CHR9.

3D-Printing of the device

Poly(ethylene glycol) diacrylate (PEGDA) Mn 250 98.53% (33.3 g) and diphenyl(2,4,6-trimethylbenzoyl) phosphine oxide (TPO) 1.47% (0.5 g) were dissolved at room temperature and transferred to a Form1+ 3D Printer. The device design was uploaded and printed using the Clear 01 setting at a 45 degree angle with the supports attached to it's rear face. The layer height was adjusted to 100-micron layer height with a print time of approximately 2 hours and 30 minutes (726 layers) giving the object a total volume of 29.53 mL.

Following printing, designs were removed, washed (isopropanol), and post-cured under UV light *in vacuo*. Following curing, supports were removed from each object and devices stored at room temperature.

3D-Printing of Reactor Design CHR10

The device was designed using the freeware web-based application - Tinkercad (Autodesk) software (Supp. Fig. 1), exported as an STL (standard tessellation language) file and uploaded to FormLabs PreForm Software 2.10.3 before printing. Support structures to aid printing were automatically generated by PreForm Software 2.10.3.

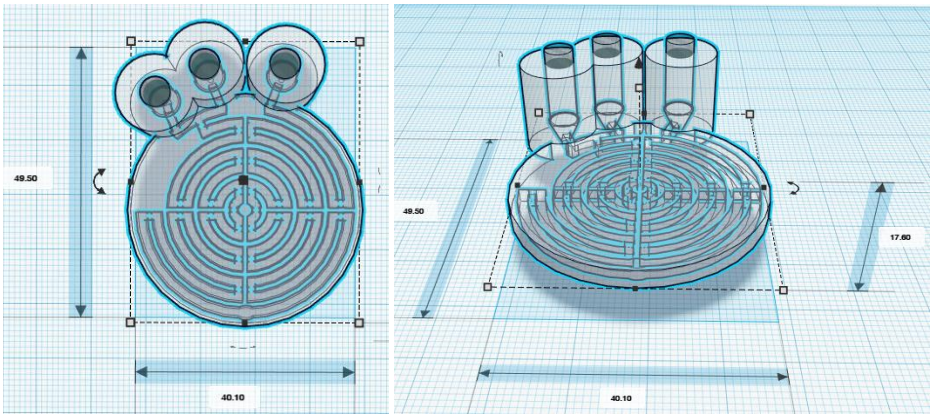

Figure 93: Design size and shape of CHR10.

3D-Printing of the device

Poly(ethylene glycol) diacrylate (PEGDA) Mn 250 98.53% (33.3 g) and diphenyl(2,4,6-trimethylbenzoyl) phosphine oxide (TPO) 1.47% (0.5 g) were dissolved at room temperature and transferred to a Form1+ 3D Printer. The device design was uploaded and printed using the Clear 01 setting at a 45 degree angle with the supports attached to it's rear face. The layer height was adjusted to 100-micron layer height with a print time of approximately 1 hours and 15 minutes (448 layers) giving the object a total volume of 14.08 mL.

Following printing, designs were removed, washed (isopropanol), and post-cured under UV light *in vacuo*. Following curing, supports were removed from each object and devices stored at room temperature.

3D-Printing of Reactor Design CHR11

The device was designed using the freeware web-based application - Tinkercad (Autodesk) software (Supp. Fig. 1), exported as an STL (standard tessellation language) file and uploaded to FormLabs PreForm Software 2.10.3 before printing. Support structures to aid printing were automatically generated by PreForm Software 2.10.3.

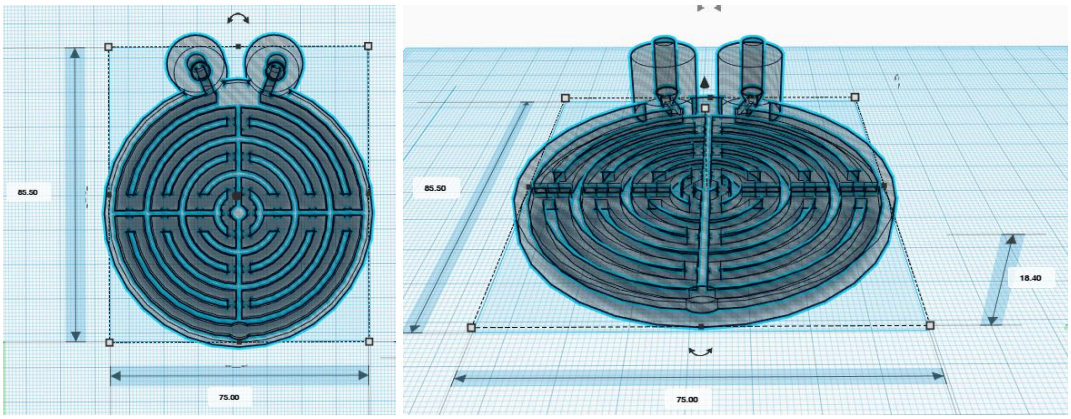

Figure 94: Design size and shape of CHR11.

3D-Printing of the device

Poly(ethylene glycol) diacrylate (PEGDA) Mn 250 98.53% (33.3 g) and diphenyl(2,4,6-trimethylbenzoyl) phosphine oxide (TPO) 1.47% (0.5 g) were dissolved at room temperature and transferred to a Form1+ 3D Printer. The device design was uploaded and printed using the Clear 01 setting at a 45 degree angle with the supports attached to it's rear face. The layer height was adjusted to 100-micron layer height with a print time of approximately 2 hours and 30 minutes (706 layers) giving the object a total volume of 39.37 mL.

Following printing, designs were removed, washed (isopropanol), and post-cured under UV light *in vacuo*. Following curing, supports were removed from each object and devices stored at room temperature.

3D-Printing of Reactor Design CHR12

The device was designed using the freeware web-based application - Tinkercad (Autodesk) software (Supp. Fig. 1), exported as an STL (standard tessellation language) file and uploaded to FormLabs PreForm Software 2.10.3 before printing. Support structures to aid printing were automatically generated by PreForm Software 2.10.3.

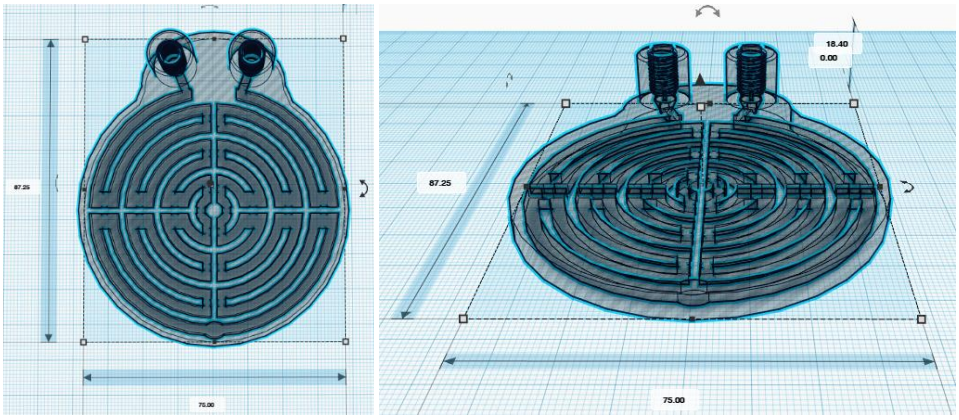

Figure 95: Design size and shape of CHR12.

3D-Printing of the device

Poly(ethylene glycol) diacrylate (PEGDA) Mn 250 98.53% (33.3 g) and diphenyl(2,4,6-trimethylbenzoyl) phosphine oxide (TPO) 1.47% (0.5 g) were dissolved at room temperature and transferred to a Form1+ 3D Printer. The device design was uploaded and printed using the Clear 01 setting at a 45 degree angle with the supports attached to it's rear face. The layer height was adjusted to 100-micron layer height with a print time of approximately 2 hours and 30 minutes (668 layers) giving the object a total volume of 39.91 mL.

Following printing, designs were removed, washed (isopropanol), and post-cured under UV light *in vacuo*. Following curing, supports were removed from each object and devices stored at room temperature.

3D-Printing of Glass Chip Reactor

The device was designed using the freeware web-based application - Tinkercad (Autodesk) software (Supp. Fig. 1), exported as an STL (standard tessellation language) file and uploaded to FormLabs PreForm Software 2.10.3 before printing. Support structures to aid printing were automatically generated by PreForm Software 2.10.3.

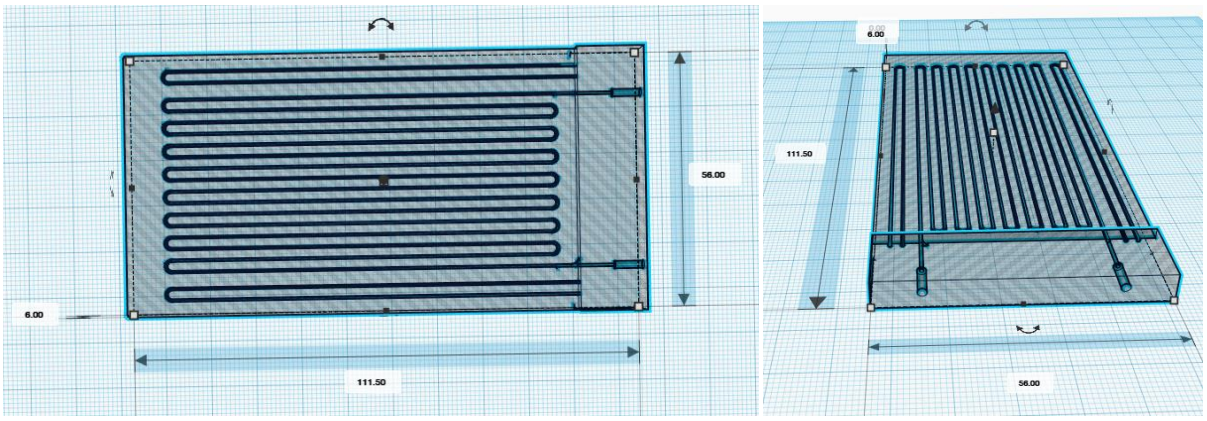

Figure 96: Design size and shape of Chip Reactor.

3D-Printing of the device

Poly(ethylene glycol) diacrylate (PEGDA) Mn 250 99.5% (30 g) and diphenyl(2,4,6-trimethylbenzoyl) phosphine oxide (TPO) 0.5% (0.15 g) were dissolved at room temperature and transferred to a Form1+ 3D Printer. The device design was uploaded and printed using the Clear 01 setting at a 45 degree angle with the supports attached to it's rear face. The layer height was adjusted to 100-micron layer height with a print time of approximately 3 hours (784 layers) giving the object a total volume of 47.63 mL.

Following printing, designs were removed, washed (isopropanol), and post-cured under UV light *in vacuo*. Following curing, supports were removed from each object and devices stored at room temperature.

5.1.13 3D-Printing: Catalytic Monolith Development

3D-Printing of Monoliths

The device was designed using the freeware web-based application - Tinkercad (Autodesk) software (Supp. Fig. 1), exported as an STL (standard tessellation language) file and uploaded to FormLabs PreForm Software 2.10.3 before printing. Support structures to aid printing were automatically generated by PreForm Software 2.10.3.

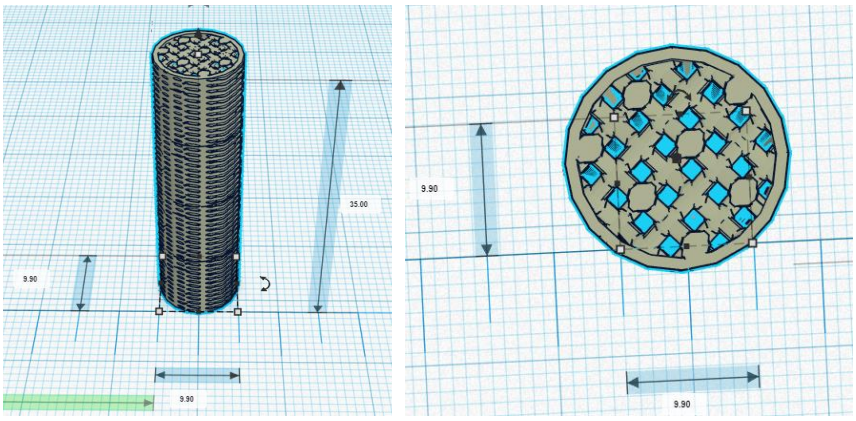

Figure 97: Design size and shape of Monolith.

3D-Printing of $Pd(PPh_3)_4$-doped device

Poly(ethylene glycol) diacrylate (PEGDA) Mn 250 99.09% (49.95 g), diphenyl(2,4,6-trimethylbenzoyl) phosphine oxide (TPO) 0.4% (0.2 g), 2,5-*bis*-(5-*tert*-butyl-benzoxazole-2-yl)thiophene (BBT) 0.01% (0.005 g) and Pd Tetrakis(triphenylphosphine) 0.5% (0.25 g) were dissolved at room temperature and transferred to a Form1+ 3D Printer. The device design was uploaded and printed vertically using the Black 01 setting with the supports attached on the upper edge of the device. The resolution was adjusted to 0.025 mm with a print time of approximately 3 and a half hours (1486 layers) giving the final object a total volume of 0.82 mL.

Following printing, designs were removed, washed (isopropanol), and post-cured under UV light *in vacuo*. Following curing, supports were removed from each object and devices stored at room temperature.

3D-Printing of $Y(OTf)_3$- doped device

Poly(ethylene glycol) diacrylate (PEGDA) Mn 250 89.19% (44.59 g), diphenyl(2,4,6-trimethylbenzoyl) phosphine oxide (TPO) 0.8% (0.4 g), 2,5-*bis*-(5-*tert*-butyl-benzoxazole-2-yl)thiophene (BBT) 0.01% (0.005 g) and yttrium triflate 10% (5.0 g) were dissolved at room temperature and transferred to a Form1+ 3D Printer. The device design was uploaded and printed vertically using the Clear 01 setting with the supports attached on the upper edge of the device. The resolution was adjusted to 0.025 mm with a print time of approximately 3 and a half hours (1486 layers) giving the final object a total volume of 0.82 mL.

Following printing, designs were removed, washed (isopropanol), and post-cured under UV light *in vacuo*. Following curing, supports were removed from each object and devices stored at room temperature.

6.0 References

[1] Uniqsis, “Uniqsis Accessable Flow Chemistry” 2018. [Online]. Available: http://www.uniqsis.com/paProducts.aspx. [Accessed 9 October 2018].

[2] Vapourtec, “ The R-Series modular flow chemistry system” 2018. [Online]. Available: https://www.vapourtec.com/products/r-series-flow-chemistry-system-overview/. [Accessed 9 October 2018].

[3] Syrris, “Asia-Award Einning Lab Scale Flow Chemistry by Syrris” 2018. [Online]. Available: https://syrris.com/product/asia-flow-chemistry/. [Accessed 9 October 2018].

[4] S. V. Ley, I. R. Baxendale, R. N. Bream, P. S. Jackson, A. G. Leach, D. A. Longbottom, M. Nesi, J. S. Scott, R. I. Stroter and S. J. Taylor, "Multi-step organic synthesis using solid-supported reagents and scavengers : a new paradigm in chemical library generation" *J. Chem. Soc., Perkin Trans.,* vol. 1, pp. 3815-4195, 2000.

[5] M. D. Hopkin, I. R. Baxendale and S. V. Ley, "A flow-based synthesis of Imatinib: the API of Gleevec," *Chem. Commun.,* vol. 46, pp. 2450-2452, 2010.

[6] B. J. Deadman, C. Battilocchio, E. Sliwinski and S. V. Ley, "A prototype device for evaporation in batch and flow," *Green Chem.,* vol. 15, pp. 2050-2055, 2013.

[7] C. F. Carter, I. R. Baxendale, M. O'Brien, J. B. J. Pavey and S. V. Ley, "Synthesis of acetal protected building blocks using flow chemistry with flow," *Org. Biomol. Chem.,* vol. 7, pp. 4594-4597, 2009.

[8] H. Lange, C. F. Carter, M. D. Hopkin, A. Burke, J. G. Goode, I. R. Baxendale and S. V. Ley, "A breakthrough method for the accurate addition of reagents in multi-step segmented flow processing," *Chem. Sci.,* vol. 2, pp. 765-769, 2011.

[9] D. L. Browne, S. Wright, B. J. Deadman, S. Dunnage, I. R. Baxendale, R. M. Turner and S. V. Ley, "Continuous flow reaction monitoring using an on-line miniaturemass spectrometer," *Rapid Commun. Mass Spectrom.,* vol. 26, pp. 1999-2010, 2012.

[10] J. Wenger, S. Ceylan and A. Kirschning, "Ten key issues in modern flow chemistry," *ChemComm,* pp. 4583-4592, 2011.

[11] M. Baumann, I. R. Baxendale, S. V. Ley, N. Nikbin and C. D. Smith, "Azide monoliths as convenient flow reactors for efficient Curtius Rearrangement," *Org. Biomol. Chem,* vol. 6, pp. 1587-1593, 2008.

[12] V. Hessel, D. Kralisch and U. Krtschil, "Sustainability through green processing – novel process windows intensify micro and milli processing technologies" *Energy Environ. Sci.,* vol. 1, pp. 467-478, 2008.

[13] D. M. Roberge, M. Gottsponer, M. Eyholzer and N. Kockmann, "Industrial design, scale-up, and use of microreators," *Chemistry Today,* vol. 27, pp. 8-11, 2009.

[14] T. Gustaffson, F. Ponten and P. H. Seeberger, "Trimethylaluminium mediated amide bond formation in a continuous flow microreactor as key to the synthesis of rimonabant and efaproxiral," *Chem. Commun.,* pp. 1100-1102, 2008.

[15] F. Levesque and P. H. Seeberger, "Continuous-Flow Synthesis of the Anti-Malaria Drug Artemisinin," *Angew. Chem., Int. Ed.,* vol. 51, pp. 1706-1709, 2012.

[16] D. Kopetzki, F. Levesque and P. H. Seeberger, "A Continuous-Flow Process for the Synthesis of Artemisinin," *Chem. Eur. J.,* vol. 19, pp. 5450-5456, 2013.

[17] A. R. Bogdan, S. L. Poe, D. C. Kubis, S. J. Broadwater and D. T. McQuade, "The Continuous-Flow Synthesis of Ibuprofen," *Angew. Chem. Int. Ed.,* vol. 48, pp. 8547-8550, 2009.

[18] M. Baumann and I. R. Baxendale, "Continuous photochemistry: the flow synthesis of ibuprofen via a photo-Favorski rearrangement," *React. Chem. Eng.,* vol. 1, pp. 147-150, 2016.

[19] D. R. Snead and T. F. Jamison, "A Three-Minute Synthesis andd Purification of Ibuprofen: Pushing the Limits of Continuous Flow Processing," *Angew. Chem. Int. Ed.,* vol. 54, pp. 983-987, 2015.

[20] M. B. Plutschack, B. Pieber, K. Gilmore and P. H. Seeberger, "The Hitchhiker's Guide to Flow Chemistry," *Chem. Rev. ,* vol. 117, pp. 11796-11893, 2017.

[21] S. N. Oka, Fluidized Bed Combustion, CRC Press, 2003.

[22] E. L. Paul, V. A. Atiemo-Obeng and S. M. Kresta, Handbook of Industrial Mixing: Science and Practice, John Wiley & Sons, 2004.

[23] C. Yan, J. Fraga-Dubreuil, E. Garcia-Verdugo, P. A. Hamley and M. Poliakoff, "The continuous synthesis of ε-caprolactam from 6-aminocapronitrile in high-temperature water," *Green Chem.,* vol. 10, pp. 98-103, 2008.

[24] N. S. Wilson, C. R. Sarko and G. p. Roth, "Development and Applications of a Practical Continuous Flow Microwave Cell," *Org. Process. Res. Dev.,* vol. 8, pp. 535-538, 2004.

[25] W. Shieh, S. Dell and O. Repic, "1,8-Diazabicyclo[5.4.0]undec-7-ene (DBU) and Microwave-Accelerated Green Chemistry in Methylation of Phenols, Indoles, and Benzimidazoles with Dimethyl Carbonate," *Org. Lett.,* vol. 3, pp. 4279-4281, 2001.

[26] T. Fukuyama, Y. Hino, N. Kamata and I. Ryu, "Quick Execution of [2+2] Type Photochemical Cycloaddition Reaction by Continuous Flow System using Glass-made Microreactor," *Chem. Lett.,* vol. 33, pp. 1430-1431, 2004.

[27] J. P. Knowles, L. D. Elliott and K. I. Booker-Milburn, "Flow photochemistry: Old light through new windows," *Beilstein J. Org. Chem.,* vol. 8, pp. 2025-2052, 2012.

[28] C.-L. Li and B. M. Trost, "Green chemistry for chemical synthesis," *Proc. Natl. Acad. Sci. U. S. A.,* vol. 105, pp. 13197-13202, 2008.

[29] P. T. Anastas and M. M. Kirchhoff, "Origins, Current Status, and Future Challenges of Green Chemistry," *Acc. CHem. Res.,* vol. 35, pp. 686-694, 2002.

[30] G. Kaupp, "Waste-free large-scale syntheses without auxiliaries for sustainable production omitting purifying workup," *CrystEngComm.,* vol. 8, pp. 794-804, 2006.

[31] T. Schwalbe, V. Autze, M. Hohmann and W. Stirner, "Novel Innovation Systems for a Cellular Approach to Continuous Process Chemistry from Discovery to Market," *Org. Proc. Res. Dev.,* vol. 8, pp. 440-454, 2004.

[32] C. Wiles and P. Watts, "Continuous flow reactors: a perspective," *Green Chem.,* vol. 14, pp. 38-54, 2012.

[33] T. Razzaq, T. N. Glaznov and C. O. Kappe, "Continuous-Flow Microreactor Chemistry under High-Temperature/Pressure Conditions," *Eur. J. Org. Chem.,* pp. 1321-1325, 2009.

[34] J. P. McMullen and K. F. Jensen, "Rapid Determination of Reaction Kinetics with an Automated Microfluidic System," *Org. Proc. Res. Dev.,* vol. 15, pp. 398-407, 2011.

[35] B. Ahmed-Omer and A. J. Sanderson, "Preparation of fluoxetine by multiple flow processing steps," *Org. Biomol. Chem.,* vol. 9, pp. 3854-3862, 2011.

[36] C. Capello, U. Fischer and K. Hungerbuhler, "What is a green solvent? A comprehensive framework for the environmental assessment of solvents," *Green Chem.,* vol. 9, pp. 927-934, 2007.

[37] K. Mikami, M. Yamanaka, M. N. Islam, K. Kudo, N. Seino and M. Shinoda, "Fluorous nanoflow' system for the Mukaiyama aldol reaction catalyzed by the lowest concentration of the lanthanide complex with bis(perfluorooctanesulfonyl)amide ponytail," *Tetrahedron,* vol. 59, pp. 10593-10597, 2003.

[38] J. D. Moseley and C. O. Kappe, "A critical assessment of the greenness and energy efficiency of microwave-assisted organic synthesis," *Green Chem.,* vol. 13, pp. 794-806, 2011.

[39] S. Ceyla, L. Coutable, J. Wegner and A. Kirschning, "Inductive Heating with Magnetic Materials inside Flow Reactors," *Chem. Eur. J.,* vol. 17, pp. 1884-1893, 2011.

[40] A. Nagaki, S. Yamada, M. Doi, Y. Tomida, N. Takabayashi and J. Yoshida, "Flow microreactor synthesis of disubstituted pyridines from dibromopyridines via Br/Li exchange without using cryogenic conditions," *Green Chem.,* vol. 13, pp. 1100-1113, 2011.

[41] G. P. Wild, C. Wiles, P. Watts and S. J. Haswell, "The use of immobilized crown ethers as in-situ N-protecting groups in organic synthesis and their application under continuous flow," *Tetrahedron,* vol. 65, pp. 1618-1629, 2009.

[42] J. W. Swarts, R. C. Kolfschoten, M. C. A. A. Jansen, A. E. M. Janssen and R. M. Boom, "Effect of diffusion on enzyme activity in a microreactor," *Chem. Eng. J.,* vol. 162, pp. 301-306, 2010.

[43] M. Tarleton and A. McCluskey, "A flow chemistry route to 2-phenyl-3-(1H-pyrrol-2-yl)propan-1-amines," *Tett. Lett.,* vol. 52, pp. 1583-1586, 2011.

[44] M. Irfan, T. N. Glasnov and C. O. Kappe, "Heterogeneous Catalytic Hydrogenation Reactions in Continuous-Flow Reactors," *ChemSusChem.,* vol. 4, pp. 300-316, 2011.

[45] J. Yoshida, Y. Takahashi and A. Nagaki, "Flash Chemistry: Flow Chemistry that cannot be done in Batch," *Chem. Commun.,* vol. 49, pp. 9896-9904, 2013.

[46] C. J. Mallia and I. R. Baxendale, "The Use of Gases in Flow Synthesis," *Org. Process Res. Dev.,* vol. 20, pp. 327-360, 2016.

[47] K. F. Jensen, B. J. Reizman and S. G. Newman, "Tools for chemical synthesis in microsystems," *Lab Chip,* vol. 14, pp. 3206-3212, 2014.

[48] V. Hessel, A. Renken, J. C. Schouten and J. Yoshida, Handbook of Micro Process Technology, Weinheim, Germany: Wiley-VCH, 2009.

[49] M. D. Symes, P. J. Kitson, J. Yan, C. J. Richmond, G. J. T. Cooper, R. W. Bowman, T. Vilbrandt and L. Cronin, "Integrated 3D-printed reactionware for chemical synthesis and analysis," *Nat. Chem.,* vol. 4, pp. 349-354, 2012.

[50] E. K. Lumley, C. E. Dyer, N. Pamme and R. W. Boyle, "Comparison of Photo-oxidation Reactions and a New Photosensitizer-Immobalized Microfluidic Device," *Org. Lett.,* vol. 14, pp. 5724-5727, 2012.

[51] D. Cambie, C. Bottecchia, N. J. W. Straathof, V. Hessel and T. Noel, "Applications of Continuous-Flow Photochemistry in Organic Synthesis, Material Science and Water treatment," *Chem. Rev.,* vol. 116, pp. 10276-10341, 2016.

[52] M. Baumann, I. R. Baxendale, L. J. Martin and S. V. Ley, "Development of fluorination methods using continuous-flow microreactors," *Tetrahedron,* vol. 65, pp. 6611-6625, 2009.

[53] P. A. Messina, K. C. Magne and W. J. Middleton, "Aminosulfur trifluorides: relative thermal stability," *J. Fluorine Chem.,* vol. 42, pp. 137-143, 1989.

[54] D. Cantillo and C. O. Kappe, "Immobilized Transition Metals as Catalysts for Cross-Couplings in Continuous Flow—A Critical Assessment ofthe Reaction Mechanism and Metal Leaching," *ChemCatChem,* vol. 6, pp. 3286-3305, 2014.

[55] T. N. Glasnov, S. Findenig and C. O. Kappe, "Heterogeneous Versus Homogeneous Palladium Catalysts for LigandlessMizoroki–Heck Reactions: A Comparison of Batch/Microwave andContinuous-Flow Processing," *Chem. Eur. J.,* vol. 15, pp. 1001-1010, 2009.

[56] E. Alza, C. Rodrigues-Escrich, S. Sayalero, A. Bastero and M. A. Pericas, "A Solid-Supported Organo catalyst for Highly Stereoselective, Batch, andContinuous-Flow Mannich Reactions," *Chem. Eur. J.,* vol. 15, pp. 10167-10172, 2009.

[57] S. Rossi, M. Bengalia, D. Brenna, R. Porta and M. Orlandi, "Three Dimensional (3D) Printing: A Straightforward, User-Friendly Protocol To Convert Virtual Chemical Models to Real-Life Objects," *J. Chem. Educ.,* vol. 92, pp. 1398-1401, 2015.

[58] M. R. Penny, Z. J. Cao, B. Patel, B. Sil dos Santos, C. R. M. Asquith, B. R. Szulc, Z. X. Rao, Z. Muwaffak, J. P. Malkinson and S. T. Hilton, "Three-Dimensional Printing of a Scalable Molecular Model and Orbit Kit for Organic Chemistry Teaching and Learning," *J. Chem. Educ.,* vol. 94, pp. 1265-1271, 2017.

[59] M. J. Robertson and W. L. Jorgensen, "Illustrating Concepts in Physical Organic Chemistry with 3D Printed Objects," *J. Chem. Educ. ,* vol. 92, pp. 2113-2116, 2015.

[60] B. C. Gross, J. L. Erkal, S. Y. Lockwood, C. Chen and D. M. Spence, "Evaluation of 3D Printing and Its Potential Impact on Biotechnology and the Chemical Sciences," *Anal. Chem.,* vol. 86, pp. 3240-3253, 2014.

[61] F. P. Melchels, J. Feijen and D. W. Grijpma, "A review on stereolithography and its applications in biomedical engineering," *Biomaterials,* vol. 31, pp. 6121-6130, 2010.

[62] A. J. Capel, S. Edmondson, S. D. Christie, R. D. Goodridge, R. J. Bibb and M. Thurstans, "Design and additive manufacture for flow chemistry," *Lab Chip,* vol. 13, pp. 4583-4590, 2013.

[63] A. K. Au, W. Huynh, L. F. Horowitz and A. Folch, "3D-Printed Microfluidics," *Angew. Chem. Int. Ed.,* vol. 128, pp. 3926-3946, 2016.

[64] J. Sun, W. Zhou, D. Huang, J. Y. H. Fuh and G. S. Hong, "An Overview of 3D Printing Technologies for Food Fabrication," *Food. Bioproc. Tech.,* vol. 8, pp. 1605-1615, 2015.

[65] B. Redwood, F. Schoffer and B. Garret, The 3D Printing Handbook Technologies, design and applications, Amsterdam: Coers & Roest, 2017.

[66] S. S. Crump.Patent US5121329, 9 June 1992.

[67] M. R. Penny, Z. J. Cao, B. Patel, B. S. Santos, C. R. M. Asquith, B. R. Szulc, Z. X. Rao, Z. Muwaffak, J. P. Milkinson and S. T. Hilton, "Three-Dimensional Printing of a Scalable Molecular Model and Orbital Kit for Organic Chemistry Teaching and Learning," *J. Chem. Educ.,* vol. 94, pp. 1265-1271, 2017.

[68] D. T. Pham and R. S. Gault, "A comparison of rapid prototyping technologies," *Int. J. Machine Tools Manuf.,* vol. 38, pp. 1257-1287, 1998.

[69] A. Goyanes, J. Wang, A. Buanz, R. Martinez-Pacheco, R. Telford, S. Gaisford and A. W. Basit, "3D Printing of Medicines: Engineering Novel Oral Devices with Unique Design and Drug Release Characteristics," *Mol. Pharmaceutics,* vol. 12, pp. 4077-4084, 2015.

[70] D. Goldberg, "The History of 3D Printing," Chilton's PD & D : Product Design & Development; Radnor, 2014.

[71] L. Hornback, W. E. Nelson and J. Carlo.Patent US4571603, 1986.

[72] L. Hornback and W. E. Nelson.Patent EP0417523, 1991.

[73] Waldbaur, H., H. Rapp, K. Lange and B. E. Rapp, "Let there be chip—towards rapid prototyping of microfluidic devices: one-step manufacturing process," *Anal. Methods,* vol. 3, pp. 2681-2716, 2011.

[74] S. C. Ligon, R. Liska, J. Stampfl, M. Gurr and R. Mulhaupt, "Polymers for 3D Printing qnd Customized Qdditive Manufacturing," *Chem. Rev.,* vol. 117, pp. 10212-10290, 2017.

[75] C. Deckard.Patent U. S. Patent 4863538, 1989.

[76] J. J. Beaman and C. R. Reckard.Patent U. S. Patent 4938816, 3 July 1990.

[77] R. Rossi, A. Puglisi and M. Benaglia, "Additive Manufactuering Technologies: 3D Printing in Organic Synthesis," *Cat. Chem. Cat.,* vol. 10, pp. 1-15, 2018.

[78] G. P. Manogharan, A. N. Martof, L. M. Rodomsky, C. M. Rodomsky, D. C. Jordan, J. W. Limperos and B. P. Conner, "Makind sense of 3-D

printing: Creating a map of additive manufacturing products and services," *Additive Manufacturing,* Vols. 1-4, pp. 64-76, 2014.

[79] S. F. S. Shirazi, S. Gharehkhani, M. Mehrali, H. Yarmand, H. S. C. Metselaar, N. A. Kadri and N. A. A. Osman, "A review on powder-based additive manufacturing for tissue engineering: selective laser sintering and inkjet 3D printing," *Sci. Technol. Adv. Mater.,* vol. 16, p. 033502, 2015.

[80] L. E. Murr, E. V. Esquivel, S. A. Quinones, S. M. Gaytan, M. I. Lopez, E. Y. Martinez, Medina, F., D. H. Hernandez, E. Martinez, J. L. Martinez, S. W. Stafford, D. K. Brown, T. Hoppe, W. Meyers, U. Lindhe and R. B. Wicker, "Microstructures and mechanical properties of electron beam-rapid manufactured Ti–6Al–4V biomedical prototypes compared to wrought Ti–6Al–4V," *Mater. Charact.,* vol. 60, pp. 96-105, 2009.

[81] R. A. Sheldon, "The E Factor: fifteen years on," *Green Chem.,* vol. 9, pp. 1273-1283, 2007.

[82] C. R. Tubío, J. Azuaje, L. Escalante, A. Coelho, F. Guitián and E. Sotelo, "3D printing of a heterogeneous copper-based catalyst," *J. Catal.,* vol. 334, pp. 110-115, 2016.

[83] J. Azuaje, C. R. Tubío, L. Escalante, Gómez, M., F. Guitián, A. Coelho, O. Caamano, A. Gil and E. Sotelo, "An efficient and recyclable 3D printed -Al2O3 catalyst for the multicomponent assembly of bioactive heterocycles," *Appl. Catal. A,* vol. 530, pp. 203-210, 2017.

[84] J. M. Pearce, "Building Research Equipment with Free, Open-Source Hardware," *Science,* vol. 337, pp. 1303-1304, 2012.

[85] E. G. Gordeev, E. S. Degtyareva and V. P. Ananikov, "Analysis of 3D printing possibilities for the development of practical applications in synthetic organic chemistry," *Russ. Chem. Bull.,* vol. 65, pp. 1637-1643, 2016.

[86] R. D. Johnson, "Chemical creativity with 3D printing," *Nat. Chem. ,* vol. 4, pp. 338-339, 2012.

[87] "Combining 3D printing and liquid handling to produce user-friendly reactionware for chemical synthesis and purification," *Chem. Sci.,* vol. 4, pp. 3099-3103, 2013.

[88] P. J. Kitson, S. Glatzel, W. Chen, C.-G. Lin, Y.-F. Song and L. Cronin, "3D printing of versatile reactionware for chemical synthesis," *Nat. Protoc.,* vol. 11, pp. 920-936, 2016.

[89] T. Loiseau, L. Lecroq, C. Volkringer, J. Marrot, G. Ferey, M. Haouas, F. Taulelle, S. Bourrelly, P. L. Llewellyn and M. Latroche, "MIL-96, a Porous Aluminum Trimesate 3D Structure Constructed from a Hexagonal Network of 18-Membered Rings and μ3-Oxo-Centered Trinuclear Units," *J. Am. Chem. Soc.,* vol. 128, pp. 10223-10230, 2006.

[90] S. S.-Y. Chui, S. M.-F. Lo, J. P. H. Charmant, A. G. Orpen and I. D. Williams, "A Chemically Functionalizable Nanoporous Material [Cu3(TMA)2(H2O)3]n," *Science,* vol. 283, pp. 1148-1150, 1999.

[91] P. J. Kitson, Marshall, R. J., D. Long, R. S. Forgan and L. Cronin, "3D Printed High-Throughput Hydrothermal Reactionware for Discovery, Optimization, and Scale-Up," *Angew. Chem. Int. Ed.,* vol. 53, pp. 12723-12728, 2014.

[92] I. D. Williams, "3D frameworks from 3D printers," *Nat. Chem. ,* vol. 6, pp. 953-954, 2014.

[93] P. J. Kitson, S. Glatzel and L. Cronin, "The digital code driven autonomous synthesis of ibuprofen automated in a 3D-printer-based robot," *Beilstein J. Org. Chem.,* vol. 12, pp. 2776-2783, 2016.

[94] S. S. Zalesskiy, N. S. Shlapakov and V. P. Ananikov, "Visible light mediated metal-free thiol–yne click reaction," *Chem. Sci.,* vol. 7, pp. 6740-6745, 2016.

[95] F. Lederle, F. Meyer, C. Kaldun, J. C. Namyslo and E. G. Hubner, "Sonogashira coupling in 3D-printed NMR cuvettes: synthesis and properties of arylnaphthylalkynes," *New J. Chem.,* vol. 41, pp. 1925-1932, 2017.

[96] S. K. Anciaux, M. Geiger and M. T. Bowser, "3D Printed Micro Free-Flow Electrophoresis Device," *Anal. Chem. ,* vol. 88, pp. 7975-7682, 2016.

[97] G. Scotti, S. M. E. Nilsson, M. Haapala, P. Pöhö, G. Boije af Gennäs, J. Yli-Kauhaluoma and T. Kotiaho, "A miniaturised 3D printed polypropylene reactor for online reaction analysis by mass spectrometry," *React. Chem. Eng.,* vol. 2, pp. 299-303, 2017.

[98] G. W. Bishop, J. E. Satterwhite, S. Bhakta, K. Kadimisetty, K. M. Gillette, E. Chen and J. F. Rusling, "3D-Printed Fluidic Devices for Nanoparticle Preparation and Flow-Injection Amperometry Using Integrated Prussian Blue Nanoparticle-Modified Electrodes," *Anal. Chem.,* vol. 87, pp. 5437-5443, 2015.

[99] J. S. Mathieson, M. H. Rosnes, V. Sans, P. J. Kitson, Cronin and L., "Continuous parallel ESI-MS analysis of reactions carried out in a bespoke 3D printed device," *Beilstein J. Nanotechnol. ,* vol. 4, pp. 285-291, 2013.

[100] P. J. Kitson, M. H. Rosnes, V. Sans, V. Dragone and L. Cronin, "Configurable 3D-Printed millifluidic and microfluidic 'lab on a chip' reactionware devices," *Lab Chip,* vol. 12, pp. 3267-3271, 2012.

[101] V. Dragone, V. Sans, M. H. Rosnes, P. J. Kitson and L. Cronin, "3D-printed devices for continuous-flow organic chemistry," *Beilstein J. Org. Chem.,* vol. 9, pp. 951-959, 2013.

[102] Y. Elias, P. R. von Rohr, W. Bonrath, J. Medlock and A. Buss, "A porous structured reactor for hydrogenation reactions," *Chem. Eng. Process,* vol. 95, pp. 175-185, 2015.

[103] A. Avril, C. H. Hornung, A. Urban, D. Fraser, M. Horne, J.-P. Veder, J. Tsanaktsidis, T. Rodopoulos, C. Henry and D. R. Gunasegaram, "Continuous flow hydrogenations using novel catalytic static mixers inside a tubular reactor," *React. Chem. Eng.,* vol. 2, pp. 180-188, 2017.

[104] C. H. Hornung, X. Nguyen, A. Carafa, J. Gardiner, A. Urban, D. Fraser, M. D. Horne, D. R. Gunasegaram and J. Tsanaktsidis, "Use of Catalytic Static Mixers for Continuous Flow Gas−Liquid and Transfer Hydrogenations in Organic Synthesis," *Org. Process Res. Dev.,* vol. 21, pp. 1311-1319, 2017.

[105] A. J. Capel, A. Wright, M. J. Harding, G. W. Weaver, Y. Li, R. A. Harris, S. Edmondson, R. D. Goodridge and C. S. D. R., "3D printed fluidics with embedded analytic functionality for automated reaction optimisation," *Beilstein J. Org. Chem.,* vol. 13, pp. 111-119, 2017.

[106] S. Rossi, R. Porta, D. Brenna, A. Puglisi and M. Benaglia, "StereoselectiveCatalytic SynthesisofActivePharmaceutical Ingredients in Homemade3D-Printed Mesoreactors," *Angew. Chem. Int. Ed. ,* vol. 56, pp. 4290-4294, 2017.

[107] A. J. Clark, "Atom transfer radical cyclisation reactions mediated by copper," *Chem. Soc. Rev. ,* vol. 31, pp. 1-11, 2002.

[108] D. O'Hagan, "Pyrrole, pyrrolidine, pyridine, piperidine and tropane alkaloids," *Nat. Prod. Rep.,* vol. 17, pp. 435-446, 2000.

[109] A. R. Katritsky, C. A. Ramsden, S. E. F. V. and R. J. K. Taylor, Comprehensive Heterocyclic Chemistry III, Oxford: Elsivier, 2008.

[110] J. Cassayre, D. Dauge and S. Z. Zard, "Influence of Copper(II) Acetate on Ni/AcOH-promoted 5-endo and 5-exo Radical Cyclisations of Trichloroacetamides," *Synlett,* pp. 471-474, 2000.

[111] W. K. Goh, D. S. Black and K. N., "Synthesis of novel 7-substituted 5, 6-dihydroindol-2-ones via a Suzuki–Miyaura cross-coupling strategy," *Tetrahedron,* vol. 48, pp. 9008-9011, 2007.

[112] J. K. A. Balzarini, C. Meichsner, A. Paessens, G. Riess, E. DeClercq and J.-P. Kleim, "Resistance Pattern of Human Immunodeficiency Virus Type 1 Reverse Transcriptase to Quinoxaline S-2720," *Journal of Virology,* vol. 68, pp. 7986-7992, 1994.

[113] X. Luo, E. Chenard, P. martens, Y.-X. Cheng and M. J. Tomaszewski, "Practical Synthesis of Quinoxalinones via Palladium-Catalyzed Intramolecular N-Arylations," *Org. Lett.,* vol. 12, pp. 3574-3577, 2010.

[114] A. N. Acharya, J. M. Ostresh and R. A. Houghten, "Solid-phase parallel synthesis of trisubstituted dihydroimidazolyl dihydroquinoxalin-2(1H)-ones," *Tetrahedron,* vol. 58, pp. 221-225, 2002.

[115] C.-H. Shen, C.-C. Tseng, C.-H. Tasi, S. A. Shintre, L.-H. Chen and C.-M. Sun, "Traceless polymer-supported divergent synthesis of quinoxalinones by microwave irradiation," *Tetrahedron,* vol. 68, pp. 3532-3540, 2012.

[116] X. Wu and A. E. V. Gorden, "An Efficient Method for Solution-Phase Parallel Synthesis of 2-Quinoxalinol Salen Schiff-Base Ligands," *Journal of Combinatorial Chemistry,* vol. 9, pp. 601-608, 7 2007.

[117] F. Varano, D. Catarzi, V. Colotta, L. Cecchi, G. Filacchiono, A. Galli and C. Costagli, "Synthesis of a set of ethyl 1-carbamoyl-3-oxoquinoxaline-2-carboxylates and of their constrained analogue imidazo[1,5-a]quinoxaline-1,3,4-triones as glycine/NMDA receptor antagonists," *Eur. J. Med Chem.,* vol. 36, pp. 203-209, 2001.

[118] A. Huang, F. Liu, C. Zhan, Y. Liu and C. Ma, "One-pot synthesis of pyrrolo[1,2-a]quinoxalines," *Org. Biomol. Chem.,* vol. 9, pp. 7351-7357, 2011.

[119] "Autodesk Tinkercad," [Online]. Available: https://www.tinkercad.com/#/. [Accessed 19 November 2018].

[120] BGB, “Fitting, PEEK, Hex Head Standard, No-Twist-One-Piece, 10-32 thread, 1/16" OD Tubing (max. 350 bar), pk.5” [Online]. Available: https://www.bgb-info.com/product.php?productid=1215676. [Accessed 24 November 2018].

[121] A. Monaco, B. R. Szulc, Z. X. Rao, M. Barniol-Xicota, M. Sehailia, B. M. A. Borges and S. T. Hilton, "ShortTotal Synthesis of (+-)-y-Lycorane by a Sequential Intramolecular Acylal Cyclisation (IAC) and Intramolecular Heck Addition Reaction," *Chem. Eur. J.,* vol. 23, pp. 4750-4755, 2017.

[122] A. Monaco, A. E. Aliev and S. T. Hilton, "Intramolecular Acylal Cyclisation (IAC) as an Efficient Synthetic Strategy towards the Total Synthesis of Erythrina Alkaloid Derivatives," *Chem. Eur. J.,* vol. 21, pp. 13909-13912, 2015.

[123] B. R. Szulc, B. C. Sil, A. Ruiz and S. T. Hilton, "A Common Precursor Approach to Structurally Diverse Natural Products: The Synthesis of the Core Structure of (±)-Clausenamide and the Total Synthesis of (±)-Hyalodendrin," *Eur. J. Org. Chem.,* vol. 34, pp. 7438-7442, 2015.

[124] B. C. Sil and S. T. Hilton, "A Mild and Convenient Base-Catalysed Approach to Disubstituted Epidithiodiketopiperazines," *Synlett,* vol. 24, pp. 2563-2566, 2013.

[125] K. M. Cook, S. T. Hilton, J. Mecinovic, W. B. Motherwell, W. D. Figg and C. J. Schofield, "Epidithiodiketopiperazines Block the Interaction between Hypoxia-inducible Factor-1α (HIF-1α) and p300 by a Zinc Ejection Mechanism," *J. Biol. Chem.,* vol. 284, pp. 26831-26838, 2009.

[126] Z. X. Rao, B. Patel, A. Monaco, Z. J. Cao, M. Barniol-Xicota, E. Pichon, M. Ladlow and S. T. Hilton, "3D-Printed Polypropylene Continuous-Flow Column Reactors: Exploration of Reactor Utility in SNAr Reactions and the Synthesis of Bicyclic and Tetracyclic Heterocycles," *Eur. J. Org. Chem.,* pp. 6499-6504, 2017.

[127] T. N. Glasnov and C. O. Kappe, "The Microwave-to-Flow Paradigm: Translating High-Temperature Batch Microwave Chemistry to Scalable Continuous-Flow Processes," *Chem. Eur. J.,* vol. 17, pp. 11956-11968, 2011.

[128] C. Wiles and P. Watts, "Translation of microwave methodology to continuous flow for the efficient synthesis of diaryl ethers via a base-mediated SNAr reaction," *Beilstein J. Org. Chem.,* vol. 7, pp. 1360-1371, 2011.

[129] M. Penny, B. C. Sil, B. Patel and S. T. Hilton, "Three-dimensional printing of impregnated plastics for chemical reactions.". United Kingdom Patent PCT/GB2017/050685, December 2017.

[130] W. A. Green, Industrial Photoinitiators: A Technical Guide, Florida: CRC Press: Boca Raton, 2010.

[131] D. G. Leppard, M. Kohler and L. (.-G. C. Misev, "Photopolymerizable Composites Containing an Alkylbisacylphosphine Oxide.". Patent U. S. Patent 5472992, 1995.

[132] A. L. Coats, J. P. Harriston, J. S. Hay and M. J. (. B. I. Ramos, "Stereolithography Resin and Methods.". Patent U.S. Patent 7211368, 2007.

[133] L. U. Kim, J. W. Kim and C. K. Kim, "Effects of Molecular Structure of the Resins on the Volumetric Shrinkage and the Mechanical Strength of Dental Restorative Composites.," *Biomacromolecules,* vol. 7, pp. 2680-2687, 2006.

[134] C. J. Kloxin, T. F. Scott and C. N. Bowman, "Stress Relaxation via Addition-Fragmentation Chain transfer in a Thiol-Ene Photopolymerization.," *Macromolecules,* vol. 42, pp. 2551-2556, 2009.

[135] R. Patel, M. Rhodes and Y. (. S. I. Zhao, "Photocurable Compositions.". Patent U.S. Patent 8097399, 2012.

[136] C. Grosche, T. Koch, N. Moszner and R. Liska, "Exploring the Benefits of B-Allyl Sulfones for More Homogeneous Dimethacrylate Photopolymer Networks.," *Polym. Chem.,* vol. 6, pp. 2038-2047, 20151.

[137] J. V. Crivello and K. Dietliker, Photoinitiators for Free Radical Cationic and Anionic Photopolymerisation, Chichester: John Wiley & Sons Ltd., 1998.

[138] S. C. Lapin, J. R. Snyder, E. V. Sitzmann, D. K. Barnes and G. D. (. I. Green, "Stereolithography Using Vinyl Ether-Epoxide Polymers.". Patent U.S. Patent 5437964, 1995.

[139] T. Yamamura, T. Watanabe, A. Takeuchi, T. (. Ukachi and J. F. C. C. L. JSR Corporation, "Photo-Curable Resin Composition Used for Photo Fabrication of Three-Dimensional Objects.". Patent U.S. Patent 5981616, 1997.

[140] L. Messe and C. (. S. I. Chapelat, "Curable Composition". Patent U.S. Patent 8362148, 2013.

[141] A. P. Melisaris, R. Wang and T. H. (. I. Pang, "Liquid, Radiation-Curable Composition, Especially for Producing Flexible Cured Articles by Stereolithography.". Patent U.S. Patent 6136497, 1998.

[142] E. V. Sitzmann, R. F. Anderson, D. K. Barnes and A. B. (. I. Patel, "Increasing the Useful Range of Cationic Photoinitiators in Stereolithography.". Patent U.S. Patent 5705116, 1998.

[143] D. T. Belmont and L. A. Paquette, "Synthetic Studies Aimed at the Dolastanes. An Attempted A + C - ABC Approach," *J. Org. Chem.,* vol. 50, pp. 4102-4107, 1985.

[144] S. Takano, M. Yonaga, M. Morimoto and K. Ogasawara, "Chiral synthesis of (+)-eburnamine, (–)-eburnamenine, and (–)-eburnamonine," *J. Chem. Soc. Perkin. Trans. 1,* vol. 0, pp. 305-309, 1985.

[145] Y. Oikawa, T. Nishi and O. Yonemitsu, "Chiral synthesis of polyketide-derived natural products. Part 4. Synthesis of a left-hand segment with six consecutive chiral centres of dihydroerythronolide A for the total synthesis of erythromycin A from D-glucose," *J. Chem. Soc. Perkin. Trans. 1,* vol. 0, pp. 7-17, 1985.

[146] A. C. Cope, E. C. Herrick, C. C. Price and G. A. Cypher, "Diethyl cis-Δ4-Tetrahydrophthalate and Diethyl cis-Hexahydrophthalate," *Org. Synth., Coll. Vol.,* vol. 4, p. 304, 1963.

[147] H. Suemune, K. Oda, S. Saeki and K. Sakai, "A New Conversion Method from (-)-Limonene to Nepetalactones," *Chem. Pharm. Bull.,* vol. 36, pp. 172-177, 1988.

[148] F. Sondheimer, R. Mechoulam and M. Sprecher, "The synthesis of 10-hydroxy-10α-testosterone," *Tetrahedron,* vol. 20, pp. 2473-2485, 1964.

[149] N. P. Peet, R. L. Cargill and D. F. Bushey, "Synthesis and Acid-Catalyzed Rearrangements of Tricyclo[4.S.2.0]undecanones," *J. Org. Chem.,* vol. 38, pp. 1218-1221, 1973.

[150] P. Z. Bedoukian, "Synthesis of a-Bromoketones," *J. Am. Chem. Soc.,* vol. 67, pp. 1430-1431, 1945.

[151] J. Goodacre, H. J. Ponsford and I. Stirling, "Selective removal of the t-butyloxycarbonyl protecting group in the presence of t-butyl and p-methoxybenzyl esters," *Tett. Lett.,* vol. 16, pp. 3609-3612, 1975.

[152] B. Loev and K. M. Snader, "The Hantzsch Reaction. I. Oxidative Dealkylation of Certain Dihydropyridines," *J. Org. Chem.,* vol. 30, pp. 1914-1916, 1965.

[153] J. Smidt, W. Hafnew, R. Jira, J. Sedlmeier, R. Sieber, R. Ruttinger and H. Kojer, "Katalytische Umsetzungen von Olefinen an Platinmetall-Verbindungen Das Consortium-Verfahren zur Herstellung von Acetaldehyd," *Angew. Chem.,* vol. 71, pp. 176-182, 1959.

[154] R. F. Heck, "Acylation, methylation, and carboxyalkylation of olefins by Group VIII metal derivatives," *J. Am. Chem. Soc.,* vol. 90, pp. 5518-5526, 1968.

[155] R. F. Heck, "The palladium-catalyzed arylation of enol esters, ethers, and halides. A new synthesis of 2-aryl aldehydes and ketones," *J. Am. Chem. Soc.,* vol. 90, pp. 5535-5538, 1968.

[156] R. F. Heck, "A synthesis of diaryl ketones from arylmercuric salts," *J. Am. Chem. Soc.,* vol. 90, pp. 5546-5548, 1968.

[157] T. Mizoroki, K. Mori and A. Ozaki, "Arylation of Olefin with Aryl Iodide Catalyzed by Palladium," *Bull. Chem. Soc. Jpn.,* vol. 46, pp. 1505-1508, 1973.

[158] K. Mori, T. Mizoroki and A. Ozaki, "Arylation of Olefin with Iodobenzene Catalyzed by Palladium," *Bull. Chem. Soc. Jpn.,* vol. 44, pp. 581-581, 1971.

[159] R. F. Heck and J. P. Nolley, "Palladium-catalyzed vinylic hydrogen substitution reactions with aryl, benzyl, and styryl halides," *J. Org. Chem.,* vol. 37, pp. 2320-2322, 1972.

[160] H. A. Dieck and R. F. Heck, "Organophosphinepalladium complexes as catalysts for vinylic hydrogen substitution reactions," *J. Am. Chem. Soc.,* vol. 96, pp. 1133-1136, 1974.

[161] C. C. C. J. Seechurn, M. O. Kitching, T. J. Colacot and V. Snieckus, "Palladium-Catalyzed Cross-Coupling: A HistoricalContextual Perspective to the 2010 Nobel Prize," *Angew. Chem. Int. Ed.,* vol. 51, pp. 5062-5085, 2012.

[162] N. T. S. Phan, M. Van Der Slus and C. Jones, "On the Nature of the Active Species in Palladium Catalyzed Mizoroki–Heck and Suzuki–Miyaura Couplings – Homogeneous or Heterogeneous Catalysis, A Critical Review," *Adv. Synth. Catal.,* vol. 348, pp. 609-679, 2006.

[163] S.-I. Fukuzawa, T. Tsuchimoto and T. Kanai, "Ytterbium Trifluoromethanesulfonate Mediated Cross-Aldol Reaction between Ketones and Aldehydes," *Bull. Chem. Soc. Jpn.,* vol. 67, pp. 2227-2232, 1994.

[164] S. Kobayashi, M. Araki, H. Ishitani, S. Nagayama and I. Hachiya, "Activation of Imines by Rare Earth Metal Triflates. Ln(OTf)3- or Sc(OTf)3-Catalyzed Reactions of Imines with Silyl Enolates and Diels-Alder Reactions of Imines," *Synlett,* pp. 233-234, 1995.

[165] L. Sun, C. Gao, W. Zhou and Y. Wei, "Yttrium triflate-catalyzed reactions of indoles with electron-deficient olefins," *Indian J. Chem.,* vol. 47B, pp. 481-484, 2008.

[166] I. Komoto, J.-I. Matsuo and S. Kobayashi, "Catalytic Friedel–Crafts acylation of heteroaromatics," *Top. Catal.,* vol. 19, pp. 43-47, 2002.

[167] S. Kobayashi, H. Ishitani and S. Nagayama, "Lanthanide Triflate Catalyzed Imino Diels-Alder Reactions; Convenient Syntheses of Pyridine and Quinoline Derivatives," *Synthesis,* pp. 1195-1202, 1995.

[168] S. K. De, "Yttrium triflate as an efficient and useful catalyst for chemoselective protection of carbonyl compounds," *Tett. Lett.,* vol. 45, pp. 2339-2341, 2004.

[169] A. K. Au, A. M. Gonzalez-Suarez, U. Nallapati, N. Bhattacharjee, A. Karkamkar, C. A. DeFrost, J. L. Garcia-Cordero and A. Folch, "Biocompatible 3D-Printed PEG-Diacrylate Microfluidics," *MicroTAS 2015 - 19th International Conference on Miniaturized Systems for Chemistry and Life Sciences. Chemical and Biological Microsystems Society,* pp. 1548-1550, 2015.

[170] L. Furst, B. S. Matsuuram, J. M. R. Narayanam, J. W. Tucker and C. R. J. Stephenson, "Visible Light-Mediated Intermolecular C-H Functionalization of Electron-Rich Heterocycles with Malonates," *Org. Lett.,* vol. 12, pp. 3104-3107, 2010.

[171] M. Seki and T. Ogiku, "A diastereoselective construction of pyrazinoisoquinoline skeletons via tandem cyclization of phenylalanine derivatives: a facile synthesis of optically active pyrazinoisoquinolines," *Tetrahedron,* vol. 70, pp. 3864-3870, 2014.

[172] V. Aberg, F. Norman, E. Chorell, A. Westermark, A. Olofsson, A. E. Sauer-Eriksson and F. Almqvist, "Microwave-assisted decarboxylation of bicyclic 2-pyridone scaffolds and identification of Aβ-peptide aggregation inhibitors," *Org. Biomol. Chem.,* vol. 3, pp. 2817-2823, 2005.

[173] Y. Yoshimi, T. Itou and M. Hatanaka, "Decarboxylative reduction of free aliphatic carboxylic acids by photogenerated cation radical," *Chem. Commun.,* pp. 5244-5246, 2007.

[174] D. H. R. Barton, D. Crich and W. B. Motherwell, "New and Improved Methods for the Radical Decarboxylation of Acids," *J. Chem. Soc., Chem. Commun.,* pp. 939-941, 1983.

[175] C. Cassani, G. Bergonzini and C.-J. Wallentin, "Photocatalytic Decarboxylative Reduction of Carboxylic Acids and Its Application in Asymmetric Synthesis," *Org. Lett.,* vol. 16, pp. 4228-4231, 2016.

[176] R. W. Holley and A. D. Holley, "A New Stepwise Degradation of Peptides," *J. Am. Chem. Soc.,* vol. 74, pp. 5545-5548, 1952.

[177] M. Johnson, "Epi-6-aminopenicillanic acid and epipenicillin G.," *Tetrahedron,* vol. 4, pp. 267-270, 1969.

[178] A. Ghorbani-Choghamarani and B. Tahmasbi, "The first report on the preparation of boehmite silica sulfuric acid and its applications in some multicomponent organic reactions," *New Journal of Chemistry,* vol. 40, pp. 1205-1212, 2016.

[179] S. Phukan, M. Saha, A. K. Pal and S. Mitra, "Synthesis and fluorescence behavior of photoactive polyhydroquinoline derivatives: A combined experimental and DFT study," *Journal of Molecular Structure,* vol. 1039, pp. 119-129, 2013.

[180] A. Ghorbani-Choghamarani, Z. Heidarnezhad, B. Tahmasbi and G. Azadi, "TEDETA@BNPs as a basic and metal free nanocatalyst for Knoevenagel condensation and Hantzsch reaction," *J. Ir. Chem. Soc.,* vol. 15, pp. 2281-2293, 2018.

[181] A. Ghorbani-Choghamarani, P. Moradi and B. Thmasbi, "Nickel(II) immobilized on dithizone–boehmite nanoparticles: as a highly efficient and recyclable nanocatalyst for the synthesis of polyhydroquinolines and sulfoxidation reaction," *J. Ir. Chem. Soc.,* vol. 16, pp. 511-512, 2019.

[182] O. Goli-Jolodar, F. Shirini and M. Seddighi, "Introduction of a novel nanosized N-sulfonated Brönsted acidic catalyst for the promotion of the synthesis of polyhydroquinoline derivatives via Hantzsch condensation under solvent-free conditions," *RSC Advances,* vol. 6, pp. 26026-26037, 20416.

[183] K. Mohammadi, F. Shirini and A. Yahyazadeh, "1, 3-Disulfonic acid imidazolium hydrogen sulphate as an efficient and reusable ionic liquid for the multicomponent synthesis of polyhydroquinoline derivatives

under solvent-free conditions," *Research on Chemical Intermediates,* vol. 42, pp. 2047-2054, 2016.

[184] R. A. Fernandes and D. A. Chaudhari, "Iron(III) sulfate as terminal oxidant in the synthesis of methyl ketones via wacker oxidation," *J. Org. Chem.,* vol. 79, pp. 5787-5793, 2014.

[185] C. Xu, L. Yin, B. Huang, H. Liu and M. Cai, "A phosphine-free, atom-efficient cross-coupling of aryl iodides with triarylindiums or trialkynylindiums catalyzed by immobilization of palladium(0) in MCM-41," *Tetrahedron,* vol. 72, pp. 2065-2071, 2016.

[186] W. Liu, D. Xiong, P. Huo and G. Mei, "Highly active palladium catalysts with bisacetylacetonate ligands for suzuki miyaura cross-coupling reactions in mild conditions," *Chem. Lett.,* vol. 46, pp. 1550-1552, 2017.

[187] C. K. Bradsher, F. C. Brown and H. K. Porter, "Synthesis and Fungistatic Activity of Some 3-Hydroxybiphenyl Derivatives," *J. Am. Chem. Soc.,* vol. 76, pp. 2357-2362, 1954.

[188] G. A. Edwards, M. A. Trafford, A. E. Hamilton, A. M. Buxton, M. C. Bardeaux and J. M. Chalker, "Melamine and melamine-formaldehyde polymers as ligands for palladium and application to Suzuki-Miyaura cross-coupling reactions in sustainable solvents," *J. Org. Chem.,* vol. 79, pp. 2094-2104, 2014.

[189] H. Ke, X. Chen and G. Zou, "N-heterocyclic carbene-assisted, Bis(phosphine)nickel-catalyzed cross-couplings of diarylborinic acids with aryl chlorides, tosylates, and sulfamates," *J. Org. Chem.,* vol. 79, pp. 7132-7140, 2014.

[190] W.-Y. Wu, L.-J. Liu, F.-P. Chang, Y.-L. Cheng and F.-Y. Tsai, "A highly efficient and reusable palladium(II)/cationic 2,2′-bipyridyl-catalyzed stille coupling in water," *Molecules,* vol. 21, p. 1205, 2016.

[191] Z.-J. Jiang, Z.-H. Li, J.-B. Yu and W.-K. Su, "Liquid-Assisted Grinding Accelerating: Suzuki-Miyaura Reaction of Aryl Chlorides under High-Speed Ball-Milling Conditions," *J. Org. Chem.,* vol. 81, pp. 10049-10055, 2016.

[192] L. Zhang, Z. Su, F. Jiang, Y. Zhou, W. Xu and M. Hong, "Catalytic palladium nanoparticles supported on nanoscale MOFs: A highly active catalyst for Suzuki-Miyaura cross-coupling reaction," *Tetrahedron,* vol. 69, pp. 9237-9244, 2013.

[193] A. Fiebor, R. Tia, B. C. E. Makhubela and H. H. Kinfe, "Water-soluble SNS cationic palladium(II) complexes and their Suzuki–Miyaura cross-coupling reactions in aqueous medium," *B. J. Org. Chem.,* vol. 14, pp. 1859-1870, 2018.

[194] B. Schmidt and M. Riemer, "uzuki-Miyaura coupling of halophenols and phenol boronic acids: Systematic investigation of positional isomer effects and conclusions for the synthesis of phytoalexins from pyrinae," *J. Org. Chem.,* Vols. 4104-4118, p. 79, 2014.

[195] S. Bunda, A. Udvardy, K. Voronova and F. Joo, "Organic Solvent-Free, Pd(II)-Salan Complex-Catalyzed Synthesis of Biaryls via Suzuki-Miyaura Cross-Coupling in Water and Air," *J. Org. Chem.,* vol. 83, pp. 15486-15492, 2018.

[196] S.-L. Mao, Y. Sun, G.-A. Yu, C. Zhao, Z.-J. Han, J. Yuan, X. Zhu, Q. Yang and S.-H. Liu, "A green and cost-effective approach for the production of gold nanoparticles using corn silk extract: A recoverable catalyst for Suzuki–Miyaura reaction and adsorbent for removing of dye pollutants," *Org. and Biomol. Chem.,* vol. 10, pp. 9410-9417, 2012.

[197] Na, J. L. asivam and R. A. Fernandes, "Development of unimolecular tetrakis(piperidin-4-ol) as a ligand for Suzuki-Miyaura cross-coupling reactions: Synthesis of incrustoporin and preclamol," *Eur. J. Org. Chem,* vol. 2015, pp. 3558-3567, 2015.

[198] Z. Xing, M. Yang, H. Sun, Z. Wang, P. Chen, L. Liu, X. Wang, X. Xie and S. She, "Visible-light promoted dithioacetalization of aldehydes with thiols under aerobic and photocatalyst-free conditions," *Green Chem.,* vol. 20, pp. 5117-5122, 2018.

[199] K. Ishida, F. Tobita and H. Kusama, "Lewis Acid-Assisted Photoinduced Intermolecular Coupling between Acylsilanes and Aldehydes: A Formal Cross Benzoin-Type Condensation," *Chemistry- A European Journal,* vol. 24, pp. 543-546, 2018.

[200] K. Nishino, K. Minato, T. Miyazaki, Y. Ogiwara and N. Sakai, "Indium-Catalyzed Reductive Dithioacetalization of Carboxylic Acids with Dithiols: Scope, Limitations, and Application to Oxidative Desulfurization," *J. Org. Chem.,* vol. 82, pp. 3659-3665, 2017.

[201] S. C. Sondej and J. A. Katzenellenbogen, "gem-Difluoro Compounds: A Convenient Preparation from Ketones and Aldehydes by Halogen Fluoride Treatment of 1,3-Dithiolanes," *J. Org. Chem.,* vol. 51, pp. 3508-3513, 1986.

[202] B. Hallmark, M. R. Mackley and F. Ga dala-Maria, "Hollow Microcapillary Arrays in Thin Plastic Films," *Adv. Eng. Mater.,* vol. 7, pp. 545-547, 2005.

[203] Y. Tsuda and T. Sano, The Alkalloids, New York: Academic Press, 1996.

[204] B. Deng, L. Ye, H. Yin, Y. Lui, S. Hu and B. Li, "Determination of pseudolycorine in the bulb of lycoris radiata by capillary electrophoresis combined with online electrochemiluminescence using ultrasonic-assisted extraction," *J. Chromatography B,* vol. 879, pp. 927-932, 2011.

[205] G. Li, J. Xie, J. Hou, S. Zhu and Q. Zhou, "Catalytic Asymmetric Hydrogenation of α-Arylcyclohexanones and Total Synthesis of (−)-α-

Lycorane," *Advanced Synthesis & Catalysis,* vol. 355, pp. 1597-1604, 17 5 2013.

[206] W. Wu, Y. Zhu, H. Li, H. Yu, P. Zhang and R. H. Pi, "Two new alkaloids from the bulbs of Lycoris sprengeri," *J. Asian Nat. Prod. Res.,* vol. 16, pp. 192-199, 2013.

[207] G. M. Onusic, R. L. Nogueira, A. M. S. Pereira and M. B. Viana, "Effect of acute treatment with a water-alcohol extract of *Erythrina mulungu* on anxiety-related responses in rats," *Braz. J. Med. Biol. Res,* vol. 35, pp. 473-477, 2002.

[208] S. M. M. Vasconcelos, N. M. Lima, G. T. M. Sales, G. M. A. Cunha, L. M. V. Aguiar, E. R. Silveira, A. C. P. Rodrigues, D. S. Macedo, M. M. F. Fonteles, F. C. F. Sousa and G. S. B. Viana, "Aiconvulsant activity of hydroalcoholic extracts from Erythrina velutina and Erythrina mulungu," *Journal of Ethnopharmacology,* vol. 110, pp. 271-274, 2007.

[209] O. A. Flausino, A. M. Pereira, V. S. Bolzani and R. L. N. De Sounza, "Effects of Erythrinian Alkaloids Isolated from *Erythrina mulungu* (*Papilionaceae*) in Mice Submitted to Animal Models of Anxiety," *Biol. Pharm. Bull.,* vol. 30, pp. 375-378, 2007.

[210] P. Setti-Perdigao, M. A. R. Serrano, O. A. Flausino, V. S. Bolzani, M. Z. P. Guimaraes and N. G. Castro, "*Erythrina mulungu* Alkaloids Are Potent Inhibitors of Neuronal Nicotinic Receptor Currents in Mammalian Cells," *Plos One,* vol. 8, p. e82726, 2013.

[211] J. Sarris, E. McIntyre and D. A. Camfield, "Plant-Based Medicines for Anxiety Disorders, Part 1," *CNS Drugs,* vol. 27, pp. 207-219, 2013.

[212] Z. Liu, X. Huang, M. Cui, X. Zhang, Z. Chen, B. Yang and X. Zhao, "Amaryllidaceae alkaloids from the bulbs of Lycoris radiata with cytotoxic and anti-inflammatory activities," *Fitoterapia,* vol. 101, pp. 188-193, 2015.

[213] B. Hao, S. Shen and Q. Zhao, "Cytotoxic and Antimalarial Amaryllidaceae Alkaloids from the Bulbs of Lycoris radiata," *Molecules,* pp. 2458-2468, 2013.

[214] J. McNulty, J. J. Nair, J. R. L. Little, J. D. Brennan and J. Bastida, "Structure–activity studies on acetylcholinesterase inhibition in the lycorine series of Amaryllidaceae alkaloids," *Bioorg. Med. Chem. Lett.,* vol. 20, pp. 5290-5294, 2010.

[215] M. R. Herrera, A. K. Machocho, R. Brun, F. Viladomat, C. Codina and J. Bastida, "Crinane and Lycorane Type Alkaloids from *Zephyranthes citrina*," *Planta. Med.,* vol. 67, pp. 191-193, 2001.

[216] D. Lamoral-Theys, A. Andolfi, G. V. Goietsenoven, A. Cimmino, B. Le Calve, N. Wauthoz, V. Megalizzi, T. Gras, C. Bruyere, J. Dubois, V. Mathieu, A. Kornienko, R. Kiss and A. Evidente, "Lycorine, the Main Phenanthridine Amaryllidaceae Alkaloid, Exhibits Significant Antitumor Activity in Cancer Cells That Display Resistance to Proapoptotic Stimuli: An Investigation of Structure-Activity Relationship and Mechanistic Insight," *J. Med. Chem.,* vol. 52, pp. 6244-6256, 2009.

[217] W. E. Campbell, J. J. Nair, D. W. Gammon, C. Codina, J. Bastida, F. Viladomat, P. J. Smith and C. F. Albrecht, "Bioactive alkaloids from *Brunsvigia radulosa*," *Phytochemistry,* vol. 53, pp. 587-591, 2000.

[218] P. Wang, H. Yuan, X. Zhang, Y. Li, L. Shang and Z. Yin, "Novel Lycorine Derivatives as Anticancer Agents Synthesis and In Vitro Biological Evaluation," *Molecules,* vol. 19, pp. 2469-2480, 2014.

[219] M. Jokhadze, L. Eristavi, J. Kutchukhidze, A. Chariot, L. Angenot, M. Tits, O. Jansen and M. Frederich, "In Vitro Cytotoxicity of some Medicinal Plants from Georgian Amaryllidaceae," *Phytotherapy Research,* vol. 21, pp. 622-624, 2007.

[220] J. J. Nair, J. Van Staden and J. Bastida, "Apoptosis-Inducing Effects of Amaryllidaceae Alkaloids," *Current Medicinal Chemistry,* vol. 23, pp. 913-919, 2016.

[221] Z. Jin, "Amaryllidaceae and Sceletiumalkaloids," *Nat. Prod. Res.,* vol. 22, pp. 111-126, 2005.

[222] A. Padwa, H. I. Lee, P. Rashatasakhon and M. Rose, "Electrophilic-Induced Cyclization Reaction of Hexahydroindolinone Derivatives and Its Application toward the Synthesis of (±)-Erysotramidine," *J. Org. Chem.,* vol. 69, pp. 8209-8218, 11 2004.

[223] M. A. Le Dreau, D. Desmaele, F. Dumas and J. d'Angelo, "A new access to homoerythrina alkaloids," *J. Org. Chem.,* vol. 58, pp. 2933-2935, 5 1993.

[224] J. M. Joo, R. A. David, Y. Yuan and C. Lee, "Concise Synthesis of the Erythrina Alkaloid 3-Demethoxyerythratidinone via Combined Rhodium Catalysis," *Org. Lett.,* vol. 12, pp. 5704-5707, 17 12 2010.

[225] J. Liang, J. Chen, J. Liu, L. Li, H. Z. -. C. Communications and u. 2010, "Oxidative dearomatization in the synthesis of erythrina, oxindole and hexahydropyrrolo[2,3-b]indole skeletons," *Chem. Commun.,* vol. 46, pp. 3666-3688, 2010.

[226] T. Onoda, Y. Takikawa, T. Fujimoto, Y. Yasui, K. Suzuki and T. Matsumoto, "First Total Synthesis of (+)-11-Hydroxyerythratidine," *Synlett,* vol. 2009, pp. 1041-1046, 26 4 2009.

[227] Y. Yoshida, K. Mohri, K. Isobe, T. Itoh and K. Yamamoto, "Biomimetic Total Synthesis of (±)-8-Oxoerymelanthine," *The J. Org. Chem.,* vol. 74, pp. 6010-6015, 21 8 2009.

[228] P. C. Stanislawski, A. C. Willis and M. G. Banwell, "New Protocols for the Assembly of the Tetracyclic Framework Associated with the Aromatic Erythrina Alkaloids," *Org. Lett.,* vol. 8, pp. 2143-2146, 5 2006.

[229] G. Kim, J. H. Kim and K. Lee, "New Palladium-Catalyzed Reaction Pathway to the Erythrina Skeleton," *J. Org. Chem.,* vol. 71, pp. 2185-2187, 3 2006.

[230] Y. Yasui, K. Suzuki and T. Matsumoto, "Transmission of Axial Chirality to Spiro Center Chirality, Enabling Enantiospecific Access to Erythrinan Alkaloids," *Synlett,* vol. 2004, pp. 619-622, 10 2 2004.

[231] S. Ogawa, N. Iida, E. Tokunaga, M. S. and N. Shibata, "Cinchona Alkaloid/Ti IV-Catalyzed Enantioselective Enamine-Trifluoropyruvate Condensation-Cyclization Reaction and Its Application to Drug-like Heterocycles," *Chemistry - A European Journal,* vol. 16, pp. 7090-7095, 25 6 2010.

[232] L. F. Tietze, N. Tölle, D. Kratzert and D. Stalke, "Efficient Formal Total Synthesis of the Erythrina Alkaloid (+)-Erysotramidine, Using a Domino Process," *Org. Lett.,* vol. 11, pp. 5230-5233, 19 11 2009.

[233] F. Zhang, N. S. Simpkins and A. J. Blake, "New approaches for the synthesis of erythrinan alkaloids," *Org. Biomol. Chem.,* vol. 7, pp. 1963-1979, 2009.

[234] A. Padwa and Q. Wang, "Synthesis of the Tetracyclic Framework of the Erythrina Alkaloids Using a [4 + 2]-Cycloaddition/Rh(I)-Catalyzed Cascade of 2-Imidofurans," *J. Org. Chem.,* vol. 71, pp. 7391-7402, 9 2006.

[235] H. Ishibashi, K. Sato, M. Lkeda, H. Maeda, S. Akai and Y. Tamura, "One-step synthesis of the erythrinane skeleton by acid-promoted double cyclization of N-(cyclohex-1-enyl)-N-[2-(3,4-dimethoxyphenyl)ethyl]-α-(methylsulphinyl)acetamide and its derivatives," *J. Chem. Soc., Perkin Trans. 1,* pp. 605-609, 1 1 1985.

[236] Y. Zhao, P. Gu, Y. Tu, H. Zhang, Q. Zhang and C. Fan, "One-Pot Synthesis of Aminoenone via Direct Reaction of the Chloroalkyl Enone

with NaN ₃ : Rapid Access to Polycyclic Alkaloids," *J. Org. Chem.,* vol. 75, pp. 5289-5295, 6 8 2010.

[237] S. R. Angle and J. P. Boyce, "A stereoselective formal synthesis of (±)-(γ)-lycorane," *Tet. Lett.,* vol. 36, pp. 6185-6188, 1995.

[238] Y. Wang, H. Lu and P. Xu, "Asymmetric Catalytic Cascade Reactions for Constructing Diverse Scaffolds and Complex Molecules," *Accounts of Chemical Research,* vol. 48, pp. 1832-1844, 21 7 2015.

[239] K. Nishimura, N. Fukuyama, T. Yasuhara, M. Yamashita, T. Sumiyoshi, Y. Yamamoto, K. Yamada and K. Tomioka, "A short synthesis of (+)-β-lycorane by asymmetric conjugate addition cascade," *Tetrahedron,* vol. 71, pp. 7222-7226, 2015.

[240] I. A. Andreev, N. K. Ratmanova, A. M. Novoselov, D. S. Belov, I. F. Seregina and A. V. Kurkin, "Oxidative Dearomatization of 4,5,6,7-Tetrahydro-1 H-indoles Obtained by Metal- and Solvent-Free Thermal 5- endo- dig Cyclization: The Route to Erythrina and Lycorine Alkaloids," *Chemistry - A European Journal,* vol. 22, , pp. 7262-7267, 17 5 2016.

[241] Z. Sun, M. Zhou, X. Li, X. Meng, F. Peng, H. Zhang and Z. Shao, "Catalytic Asymmetric Assembly of Octahydroindolones: Divergent Synthesis of Lycorine-type Amaryllidaceae Alkaloids (+)-α-Lycorane and (+)-Lycorine," *Chemistry - A European Journal,* vol. 20, pp. 6112-6119, 12 5 2014.

[242] Y. Jung, S. C. Lee, H. Cho, N. B. Darvatkar, J. Y. Song and C. Cho, "Total Syntheses of (±)-α-Lycorane and (±)-1-Deoxylycorine," *Org. Lett.,* vol. 15, pp. 132-135, 4 1 2013.

[243] D. Liu, A. Long, L. F., A. Zhao, J. Chen, H. Zhang and J. Liu, "Total synthesis of lycorine-type alkaloids by cyclopropyl ring-opening rearrangement," *Org. Biomol. Chem.,* vol. 12, pp. 3191-3200, 2014.

[244] E. S. Conner, K. E. Crocker, R. G. Fernando, F. R. Fronczek, G. G. Stanley and J. R. Ragains, "Visible-Light-Promoted Selenofunctionalization of Alkenes," *Org. Lett.,* vol. 15, pp. 5558-5561, 17 11 2013.

[245] C. Liu, J. Xie, Y. Li, J. Chen and Q. Zhou, "Asymmetric Hydrogenation of α,α′-Disubstituted Cycloketones through Dynamic Kinetic Resolution: An Efficient Construction of Chiral Diols with Three Contiguous Stereocenters," *Angewandte Chemie International Edition,* vol. 52, pp. 593-596, 7 1 2013.

[246] Y. Wang, Y. C. Luo, H. B. Zhang and P. F. Xu, "Concise construction of the tetracyclic core of lycorine-type alkaloids and the formal synthesis of α-lycorane based on asymmetric bifunctional thiourea-catalyzed," *Biomol. Chem.,* vol. 10, pp. 8211-8215, 2012.

[247] S. Rajkumar, K. Shankland and G. D. Brown, "Organocatalytic enantioselective construction of nitrocyclohexanes containing multiple chiral centres via a cascade reaction," *Science,* vol. 3, pp. 584-588, 2012.

[248] R. J. Huntley and R. L. Funk, "Total synthesis of (±)-γ-lycorane via the electrocyclic ring closure of a divinylpyrroline," *Tetrahedron,* vol. 52, pp. 6671-6674, 2011.

[249] K. Tomooka, M. Suzuki, K. Uehara, M. Shimada and T. Akiyama, "Novel Synthetic Approach to Nine-Membered Diallylic Amides: Stereochemical Behavior and Utility as Chiral Building Block," *Synlett,* vol. 2008, pp. 2518-2522, 22 8 2008.

[250] B. Hong, R. Y. Nimje, M. Wu and A. A. Sadani, "Organocatalytic Double Michael Reaction of 7-Oxohept-2-enoates and Nitrostyrene – Formal Synthesis of (–)-α- and (–)-β-Lycorane," *Eur. J. Org. Chem.,* vol. 2008, pp. 1449-1457, 3 2008.

[251] L. Dong, Y. Xu, W. Yuan, X. Cui, L. Cun and L. Gong, "Rhodium-Catalyzed Asymmetric Nitroallylation of Arylmetallics with Cyclic Nitroallyl Acetates and Applications in Organic Synthesis," *Eur. J. Org. Chem.,* vol. 2006, pp. 4093-4105, 9 2006.

[252] B. D. Chapsal and I. Ojima, "Total Synthesis of Enantiopure (+)-γ-Lycorane Using Highly Efficient Pd-Catalyzed Asymmetric Allylic Alkylation," *Org. Lett.,* vol. 8, pp. 1395-1398, 3 2006.

[253] H. Fujioka, K. Murai, Y. Ohba, H. Hirose and Y. Kita, "Intramolecular bromo-amination of 1, 4-cyclohexadiene aminal: one-pot discrimination of two olefins and concise asymmetric synthesis of (−)-γ-lycorane," *Chem. Commun.,* pp. 832-834, 2006.

[254] S. Gao, Y. Q. Tu, Z. Song, A. Wang, X. Fan and Y. Jiang, "A General and Efficient Strategy for 7-Aryloctahydroindole and cis-3a-Aryloctahydroindole Alkaloids: Total Syntheses of (±)-γ-Lycorane and (±)-Crinane," *J. Org. Chem.,* vol. 70, pp. 6523-6525, 8 2005.

[255] T. Yasuhara, E. Osafune, K. Nishimura, M. Yamashita, K. Yamada, O. Muraoka and K. Tomioka, "Efficient synthesis of (±)-γ-lycorane employing stereoselective conjugate addition to nitroolefin," *Tet. Lett.,* vol. 45, pp. 3043-3045, 5 4 2004.

[256] A. Padwa, J. D. Ginn, S. K. E. C. K. Bur and S. M. Lynch, "Synthesis of Azapolycyclic Systems via the Intramolecular [4 + 2] Cycloaddition Chemistry of 2-(Alkylthio)-5-amidofurans," *J. Org. Chem.,* vol. 66, pp. 1716-1724, 2002.

[257] A. Padwa, M. A. Brodney and S. M. Lynch, "Formal Total Synthesis of (±)-γ-Lycorane and (±)-1-Deoxylycorine Using the [4+2]-Cycloaddition/Rearrangement Cascade of Furanyl Carbamates," *J. Org. Chem.,* vol. 66, pp. 1716-1724, 3 2001.

[258] M. G. Banwell, J. E. Harvey, D. C. R. Hockless and A. W. Wu, "Electrocyclic Ring-Opening/π-Allyl Cation Cyclization Reaction

Sequences Involving gem-Dihalocyclopropanes as Substrates: Application to Syntheses of (±)-, (+)-, and (−)-γ-Lycorane," *J. Org. Chem.,* vol. 65, pp. 4241-4250, 2000.

[259] A. Padwa, M. A. Brodney and D. Martin, "A New Method for the Formation of Octahydroindole Alkaloids via the Intramolecular Diels−Alder Reaction of 2-Amidofurans," *J. Org. Chem.,* vol. 62, pp. 5304-5305, 1998.

[260] M. G. Banwell and A. W. Wu, "A stereoselective total synthesis of (±)-γ-lycorane," *J. Chem. Soc. Perkin. Trans I,* pp. 2671-2672, 1994.

[261] D. B. Grotjahn and K. P. C. Vollhardt, "Cobalt-Mediated [2+2+2] Cycloaddition of Alkynes to the Enamine Double Bond: A Formal Total Synthesis of γ-Lycorane," *Synthesis,* vol. 1993, pp. 579-605, 1993.

[262] P. Magnus, J. M. Bailey and M. J. Porter, "Application of the β-azidonation reaction to the enantioselective synthesis of the lycorane Amaryllidaceae alkaloids," *Tetrahedron,* vol. 55, pp. 13927-13936, 1999.

[263] H. Rudler, A. Parlier, M. Rudler, J. Vaissermann, "Reaction of aminocarbene complexes of chromium with alkynes 9.: From nitrogen ylid complexes toward alkaloid frameworks," *Journal of Organometallic Chemistry,* vol. 561, pp. 101-117, 1998.

[264] H. Yoshizaki, H. Satoh, Y. Sato, S. Nukui, M. Shibasaki and M. Mori, "Palladium-Mediated Asymmetric Synthesis of Cis-3,6-Disubstituted Cyclohexenes. A Short Total Synthesis of Optically Active (+)-.gamma.-Lycorane," *J. Org. Chem.,* vol. 60, pp. 2016-2021, 4 1995.

[265] W. H. Pearson and J. M. Schkeryantz, "Synthesis of (.+-.)-.gamma.-lycorane by the intramolecular cycloaddition of an azide with an .omega.-chloroalkene," *The J. Org. Chem.,* vol. 57, pp. 6783-6789, 12 1992.

[266] D. Pérez, E. Guitián and L. Castedo, "A new approach to the synthesis of antitumoralkaloids with the lycorane skeleton," *Tetrahedron,* vol. 33, pp. 2407-2408, 1992.

[267] C. J. Wang, W. C. Ripka and P. Confalone, "A short and stereospecific synthesis of (±)-α-lycorane," *Tet. Lett.,* vol. 25, pp. 4613-4616, 1 1 1984.

[268] J. E. Baeckvall, P. G. Andersson, G. B. Stone and A. Gogoll, "Synthesis of (.+-.)-.alpha.- and (.+-.)-.gamma.-lycorane via a stereocontrolled organopalladium route," *J. Org. Chem.,* vol. 56, pp. 2988-2993, 4 1991.

[269] H. Higashiyama, T. Honda, H. Otomasu and T. Kametani, "Aziridines in Alkaloid Synthesis. IV. A Formal Synthesis of α-Dihydrocaranone and γ-Lycorane," *Planta Medica,* vol. 48, pp. 268-271, 26 8 1983.

[270] H. Iida, Y. Yuasa and C. Kibayashi, "An intramolecular cyclization of enaminones involving benzyne intermediates and application to the synthesis of .gamma.-lycorane and related compounds," *Journal of the American Chemical Society,* vol. 100, pp. 3598-3599, 5 1978.

[271] K. Kotera, "γ-And δ-lycorane," *Tetrahedron,* vol. 12, pp. 248-261, 1961.

[272] J. Cossy, L. Tresnard, J. Pardo., "Radical Cyclizations–Synthesis of γ-Lycorane," *Eur. J. Org. Chem.,* pp. 1925-1933, 1999.

[273] J. Cassayre and S. Z. Zard, "A Short Synthesis of γ-Lycorane using Ni/AcOH Mediated Radical Cyclisation," *Synlett,* vol. 1999, pp. 501-503, 4 1999.

[274] E. Bialy and A. A. Serry, "Efficient synthesis of (−)-γ-lycorane alkaloid by two Bu ₃ SnH-mediated radical cyclisations," *Natural Product Research,* vol. 22, pp. 1176-1188, 10 9 2008.

[275] M. Ikeda, S. Ohtani, T. Sato and H. Ishibashi, "Total Synthesis of (-)-γ-Lycorane Using Diastereoselective 5-endo-trig Radical Cyclization of N-Vinylic α-Halo Amides.," *Synthesis,* pp. 1803-1806, 17 6 1998.

[276] L. D. Miranda and S. Z. Zard, "A Short Synthesis of the Erythrina Skeleton and of (±)-α-Lycorane," *Org. Lett.,* vol. 4, pp. 1135-1138, 4 2002.

[277] A. F. Parsons and D. A. J. Williams, "Radical cyclisation reactions leading to polycyclics related to the Amaryllidaceae and Erythrina alkaloids," *Tetrahedron,* vol. 56, pp. 7217-7228, 2000.

[278] H. Ishibashi, K. Kodama, M. Higuchi and O. Muraoka, "Regiochemistry in radical cyclizations (5-endo versus 4-exo) of N-(2-phenylthio- and 2-phenylcyclohex-1-enyl)-α-halo amides," *Tetrahedron,* vol. 57, pp. 7629-7637, 2001.

[279] M. Harnik and E. Margoliash, "Synthesis of N-α-(2,4-dinitrophenyl)-D,L-Histidine," *J. Org. Chem.,* vol. 20, pp. 1650-1653, 1995.

[280] M. Baumann and I. R. Baxendale, "An overview of the synthetic routes to the best selling drugs containing 6-membered heterocycles," *Beilstein J. Org. Chem.,* vol. 9, pp. 2265-2319, 2013.

[281] J. Spencer, "Research Spotlight: Microwave chemistry enabling the synthesis of biologically relevant amines," *Future Medicinal Chemistry,* vol. 2, pp. 161-168, 2010.

[282] C. Zhang, Z. Wang, L. Tan, T.-L. Zhai, S. Wang, B. Tan, Y.-S. Zheng, X.-L. Yang and H.-B. Xu, "A Porous Tricyclooxacalixarene Cage Based on Tetraphenylethylene," *Angew. Chem. Int. Ed.,* vol. 54, pp. 9244-9248, 2015.

[283] L. Zhang, N. He and C. Lu, "Aggregation-Induced Emission: A Simple Strategy to Improve Chemiluminescence Resonance Energy Transfer," *Anal. Chem.,* vol. 87, pp. 1351-1357, 2015.

[284] Z. Xu, J. Ge, T. Wang, T. Luo and L. Y. X. Hongwei, "Highly Stereoselective Synthesis of 2-Aminobenzylidene Derivatives by a

Convergent 3-Component Approach," *Synlett,* vol. 25, pp. 2913-2917, 2013.

[285] J. W. Walton and J. M. J. Williams, "Catalytic SNAr of unactivated aryl chlorides," *Chem. Commun.,* vol. 51, pp. 2786-2789, 2015.

[286] U. P. De Albuquerque, P. M. De Medeiros, A. L. S. De Almeida, J. M. Monteiro, E. M. F. L. Neto, J. G. De Melo and J. P. Dos Saantos, "Medicinal plants of the caatinga (semi-arid) vegetation of NE Brazil: A quantitative approach," *Journal of Ethnopharmacology,* vol. 114, pp. 325-354, 2007.

[287] X. Li, H. Yu, Z. Wang, H. Pi, P. Zhang and H. Ruan, "Neuroprotective compounds from the bulbs of Lycoris radiata," *Fitoterapia,* vol. 88, pp. 82-90, 2013.

[288] X. Liu, J. Jiang, X. Jiao, Y. Wu, J. Lin and Y. Cai, "Lycorine induces apoptosis and down-regulation of Mcl-1 in human leukemia cells," *Cancer Letters,* vol. 274, pp. 16-24, 2009.

[289] C. L'Homme, M. Ménard and S. Canesi, "Synthesis of the Erythrina Alkaloid Erysotramidine," *J. Org. Chem.,* vol. 79, pp. 8481-8485, 5 9 2014.

[290] D. Kalaitzakis, T. Montagnon, E. Antonatou and G. Vassilikogiannakis, "One-pot Synthesis of the Tetracyclic Framework of the Aromatic Erythrina Alkaloids from Simple Furans," *Org. Lett.,* vol. 15, pp. 3714-3717, 19 7 2013.

[291] D. Lin, Y. Xu, L. Cun, X. Cui, A. Mi, J. Y. and L. Gong, "Asymmetric Nitroallylation of Arylboronic Acids with Nitroallyl Acetates Catalyzed by Chiral Rhodium Complexes and Its Application in a Concise Total Synthesis of Optically Pure (+)-γ-Lycorane," *Org. Lett.,* vol. 7, pp. 4285-4288, 2005.

[292] C. H. Shen, C. C. Tseng, C. H. Tasi, S. A. Shintre, L.-H. Chen and C.-M. Sun, "Traceless polymer-supported divergent synthesis of quinoxalinones by microwave irradiation," *Tett. Lett.,* vol. 68, pp. 3532-3540, 2012.

[293] "Autodesk Tinkercad," [Online]. Available: https://www.tinkercad.com/#/. [Accessed 19 November 2018].

[294] Silverson, "Ultramix Mixer from Silverson Mixers" [Online]. Available: www.silverson.com/us/products/ultramix-mixers. [Accessed 18 December 2018].